The Pennsylvania State University

The Graduate School

EXPLORING THE ROOT PHENOME: SIMULATION MODELING WITH A FUNCTIONAL STRUCTURAL PLANT MODEL

A Dissertation in

Horticulture

by

Harini Rangarajan

Submitted in Partial Fulfillment
of the Requirements
for the Degree of

Doctor of Philosophy

May 2021

The dissertation of Harini Rangarajan was reviewed and approved by the following:

Jonathan P. Lynch
Distinguished Professor of Plant Nutrition
Dissertation Advisor
Chair of Committee

Kathleen M. Brown
Professor of Plant Stress Biology

Armen R. Kemanian
Associate Professor of Production Systems and Modeling

Kamesh Madduri
Associate Professor, School of Electrical Engineering and Computer Science

Erin L. Connolly
Professor and Head
Department of Plant Science

ABSTRACT

Root phenomics involves the study of root architecture which is highly complex and multidimensional. Root architectural and anatomical phenotypes determine nutrient uptake from soil and plant productivity. Root phenotypes are comprised of phenes, the states of which determine the utility of a root phene in an environment. Interactions between phenes is non-linear and evaluating the utility of the integrated phenotypes is made easier with *in-silico* methods. In this work I used *SimRoot*, a functional-structural plant model, to evaluate the utility of multiple phenes in contrasting states in common bean root systems. I extended the work to explore the entire phenotypic space of several architectural phenes in all possible states, by linking *SimRoot* to a multiobjective evolutionary algorithm, to identify optimal root phenotypes for nutrient uptake and carbon costs in bean as well as maize root systems. I found that several optimal integrated root phenotypes exist and are specific to target environments.

Selecting robust, stable and reliable phenotyping metrics is an important step towards obtaining relevant data from phenotyping studies to map the phenotype to the genotype, an important goal to explore root phenomics. The complexity and inaccessibility of roots along with the technicalities in image processing make it difficult to evaluate which metrics are most useful and informative. I used *SimRoot* to simulate hundreds of bean and maize root phenotypes, estimated an array of phenotyping metrics and conducted a comparative analysis of the metrics. I found that phenes such as root number, root diameter, lateral root branching density are stable, reliable measures and are not affected by imaging method or plane. Metrics aggregating multiple phenes such as *total length, total volume, convex hull volume, bushiness index* etc. estimate different subsets of the constituent phenes, they however do not provide any information regarding the underlying phene states.

TABLE OF CONTENTS

List of Figures

List of Tables

Acknowledgements

I am thankful to my advisor, Dr. Jonathan Lynch, for his guidance and support over the course of my PhD. Dr. Lynch offered me new and challenging opportunities, and I am indebted to him for appreciating my research strengths and patiently encouraging me when nothing seemed to work. Without his strong support of my research direction and his confidence in my abilities, my doctoral work would not have been possible.

I wish to thank my committee members Dr. Kathleen Brown, Dr. Armen Kemanian and Dr. Kamesh Madduri for their time and helpful and insightful suggestions. I also thank our collaborators, Dr. Patrick Reed and Dr. David Hadka, for their help and suggestions.

I would like to acknowledge my funding support provided by the U.S. Department of Agriculture National Institute of Food and Agriculture Federal Appropriations under Project PEN04732. Even though this research aligns with the research objectives of this organization, the findings and conclusions do not necessarily reflect the views of the funding agency.

Throughout the writing of this dissertation, I have received a great deal of support and assistance in the form of much needed laughter, distractions and encouraging nudges from dear friends and family. My thanks are also due to all my friends and family, whose names are not mentioned here, but who nevertheless contributed to the success of my research at the Pennsylvania State University.

Chapter 1

Introduction

Crop production needs to double by 2050 to provide for the increasing global population (Tilman et al., 2011; Ray et al., 2013; Wise, 2013; FAO, 2017). A major challenge is the identification of efficient crops that cope with climate change and reduce the need for fertilizer and water inputs to make agriculture environmentally sustainable. Root architecture influences water and nutrient uptake, so, selecting and developing efficient crops based on their root system architecture (RSA) has been proposed as a strategy towards a "second green revolution" (Lynch, 2007; Herder et al., 2010; Villordon et al., 2014; Lynch, 2019).

Root phenotypes are avenues to the development of crop cultivars with improved nutrient capture, which is an important goal for global agriculture. Root phenotypes are comprised of phenes, which are elementary units of the phenotype; phenes are related to phenotypes as genes are to genotypes (Lynch and Brown, 2012; York et al., 2013). Phenes exist in several states and may be beneficial in specific scenarios. Fitness tradeoffs for contrasting soil resources, and between abiotic and biotic constraints, determine the utility of phenes (Ho et al., 2005; Hu et al., 2014; Postma et al., 2014; Miguel et al., 2015; Dathe et al., 2016; Galindo-Castañeda et al., 2018; Rangarajan et al., 2018; Yang et al., 2019). The fitness landscape of specific phene states is also dependent on other aspects of the plant phenotype including dynamic constraints such as carbon availability which further add to the complexity of the system. Multiple phenes interact through highly non-linear interaction to impact plant performances. The fitness landscape of root phenotypes is therefore highly complex and multidimensional.

In-silico studies allow evaluation of interaction of several phenes across several environmental scenarios. In the first chapter, I tried to explore how interactions among architectural phenes in common bean determine the acquisition of phosphate and nitrate, two key soil resources contrasting in mobility using the functional-structural plant model (FSPM), *SimRoot*. We evaluated the utility of basal root whorl number (BRWN) when basal root growth angle (BRGA), hypocotyl-borne roots (HBR), and lateral root branching density (LRBD) were varied in the bean root system, under varying availability of phosphate and nitrate. We conclude that the utility of a root architectural phenotype is determined by whether the constituent phenes are synergistic or antagonistic. Competition for internal resources and tradeoffs for external

resources result in multiple phenotypes being optimal under a given nutrient regime. However, there is no single optimal architectural phenotype; there exist multiple co-optimal root architectural phenotypes for a given environment (Rangarajan et al., 2018). This was a study which included contrasting and extreme phene states combined factorially and showed that interactions among phenes in combination with trade-offs due to carbon limitations result in several distinct root architectures with varied fitness in environments varying in nutrient availability.

Considering multiple states for each phene, phene synergisms and antagonisms, acquisition of multiple nutrients simultaneously, multiple soil types, multiple precipitation regimes etc., the number of relevant scenarios is extremely large. Moreover, when evaluating the functional benefits of alternative trait interactions there a large number of conflicting objectives (e.g., maximize biomass production, minimize nutrient requirements, etc.). Therefore, the challenge of mapping and understanding the fitness landscape for root phenotypes (i.e., the relationship of root phenes and root phenotypes to plant performance), is a hugely complex and challenging nonlinear problem. To address this problem, in Chapter 2, we used Borg, multi-objective optimization algorithm, with *SimRoot* to explore the fitness landscape. Evolutionary algorithms in multi-objective search and optimization are effective in their ability to handle complex problems, involving features such as discontinuities, multimodality, disjoint feasible spaces and noisy function evaluations (Fonseca and Fleming, 1995). The parameters explored (also called input variables or decision variables) are states of phenes including angles, number of roots, lateral root branching density. The numerical outputs from *SimRoot* model are used as the objectives subjected to optimization. The constraints on the range of values a decision variable can assume is set based on studies on root trait variations derived from phenotypic studies in published literature and this defines the space to be explored within a given domain of variation. By linking *SimRoot* with Borg we were able to identify optimal integrated common bean and maize root phenotypes, representing a dicot and a monocot species that are both primary global food security crops. The main difference between dicot and monocot root systems is that new roots (laterals) emerge from already existing roots in dicots, whereas in monocots nodal roots continually emerge over time from shoot nodes near or above the soil surface. Using the *SimRoot* – Borg framework, we were able to identify optimal integrated common bean and maize root phenotypes, which have optimal phosphorus and nitrate uptake, representing a mobile

and immobile nutrient in the soil, under a dynamic constraint imposed by carbohydrate availability.

Another challenge in root phenomics is root phenotyping, which is especially challenging because of the complexity, plasticity, and inaccessibility of roots. Phenotyping is a bottleneck for breeding and genetic analysis because it is species-specific, labor intensive and environmentally sensitive, unlike genotyping, which is uniform across organisms, highly automated, and increasingly inexpensive (Furbank and Tester, 2011; Lynch and Brown, 2012; Cobb et al., 2013; Atkinson et al., 2019). In order to develop efficient strategies to explore the phenome, it is important to clarify what constitutes a phenotype, delineate the key components that comprise a phenotype, and determine the level of resolution at which phenotypic data must be collected. Several conventionally measured traits including *total root length, total area, total volume*, as well as novel phenotypic metrics such as *convex hull volume, convex hull area, ellipse major axis, ellipse minor axis, ellipse aspect ratio, volume distribution, solidity, bushiness* (Iyer-Pascuzzi et al., 2010; Clark et al., 2011; Cobb et al., 2013; Topp et al., 2013) and metrics which measure the geometry and complexity of root systems such as *fractal dimension* (FD), *fractal abundance* (FA), and *lacunarity* (Fitter and Stickland, 1992; Nielsen et al., 1999; Walk et al., 2004). Aggregate phenotypic metrics are comprised of phenes, some of these can be measured as a simple aggregate of phenes (e.g. *total length*), some are represented as a function of other aggregates (e.g. *bushiness index, solidity, volume distribution*), some measure shapes resulting from interaction of the constituent phenes (e.g. *Convex hull volume*), and some metrics are complex metrics which measure emergent properties of root architecture and cannot be described as a simple aggregate, shape aggregate or a function of other aggregates (*e.g. Fractal Dimension*). Although an essentially infinite number of measurements may be collected to describe each phenotype, a smaller number of more basic variables may explain most of the important phenotypic variation among genotypes. In Chapter 3, we use *SimRoot* as a tool to generate several hundred phenotypes to evaluate the various phenotyping metrics to identify phenotyping metrics that are sensitive enough to provide information on the constituent root phenes and their states, are stable over time and are independent of the time of phenotyping and are robust to the imaging method *i.e.*, do not vary when measured in the intact 3D root system or when estimated using 2D rotational image series. Our analysis shows that phene aggregates can be explained by phenes. Different phene aggregates capture different combinations of subtending

phenes, but do not provide any information or measure of the phene state of the constituent phenes. Several combinations of phenes in different states can produce phenotypes which have comparable estimates of phene aggregates. Estimates of phene aggregates are not unique representations of the state of the underlying phenes. As the number of phenes captured by an aggregate phenotypic metric increases, the stability of that metric becomes less stable over time.

This work demonstrates the applications of FSPM, *SimRoot* in particular, in exploring the root phenome in terms of identifying optimal integrated phenotypes as well as a tool to evaluate metrics of root phenotyping. The value of FSPM when used with advanced computational methods is exemplified in this study and leads to opening of several possibilities.

REFERENCES

Atkinson JA, Pound MP, Bennett MJ, Wells DM. 2019. Uncovering the hidden half of plants using new advances in root phenotyping. *Current Opinion in Biotechnology* 55: 1–8

Clark RT, MacCurdy RB, Jung JK, Shaff JE, McCouch SR, Aneshansley DJ, Kochian LV. 2011. Three-dimensional root phenotyping with a novel imaging and software platform. *Plant Physiology* 156: 455–465

Cobb JN, DeClerck G, Greenberg A, Clark R, McCouch S. 2013. Next-generation phenotyping: requirements and strategies for enhancing our understanding of genotype–phenotype relationships and its relevance to crop improvement. *Theoretical and Applied Genetics* 126: 867–887

Dathe A, Postma JA, Postma-Blaauw MB, Lynch JP. 2016. Impact of axial root growth angles on nitrogen acquisition in maize depends on environmental conditions. *Annals of Botany* 118: 401–414

FAO. 2015. The future of food and agriculture: Trends and challenges. Rome

Fitter AH, Stickland TR. 1992. Fractal characterization of root system architecture. *Functional Ecology* 6: 632

Fonseca CM, Fleming PJ. 1995. An overview of evolutionary algorithms in multiobjective optimization. *Evolutionary Computation* 3: 1–16

Furbank RT, Tester M. 2011. Phenomics – technologies to relieve the phenotyping bottleneck. *Trends in Plant Science* 16: 635–644

Galindo-Castañeda T, Brown KM, Lynch JP. 2018. Reduced root cortical burden improves

growth and grain yield under low phosphorus availability in maize. Plant, Cell & Environment 41: 1579–1592

Hadka D, Reed P. 2013. Borg: an auto-adaptive many-objective evolutionary computing framework. *Evolutionary Computation* 21: 231–59

Herder GD, Van Isterdael G, Beeckman T, De Smet I . 2010. The roots of a new green revolution. *Trends in Plant Science* 15: 600–607

Ho M, Rosas J, Brown K, Lynch J P. 2005. Root architectural tradeoffs for water and phosphorus acquisition. *Functional Plant Biology* 32: 737–748

Hu B, Henry A, Brown KM, Lynch JP. 2014. Root cortical aerenchyma inhibits radial nutrient transport in maize (*Zea mays*). *Annals of Botany* 113: 181–189

Iyer-Pascuzzi AS, Symonova O, Mileyko Y, Hao Y, Belcher H, Harer J, Weitz JS, Benfey PN. 2010. Imaging and analysis platform for automatic phenotyping and trait ranking of plant root systems. *Plant Physiology* 152: 1148–57

Lynch JP. 2019. Root phenotypes for improved nutrient capture: an underexploited opportunity for global agriculture. *New Phytologist* 223: 548–564

Lynch JP, Brown KM. 2012. New roots for agriculture: exploiting the root phenome. Philosophical transactions of the Royal Society of London. Series B, Biological sciences. 367: 1598–1604

Lynch JP. 2007. Roots of the second green revolution. *Australian Journal of Botany* 55: 493

Miguel MA, Postma JA, Lynch JP. 2015. Phene synergism between root hair length and basal root growth angle for phosphorus acquisition. *Plant Physiology* 167: 1430–1439

Nielsen KL, Lynch JP, Weiss HN. 1997. Fractal geometry of bean root systems: field correlations between spatial and fractal dimension. *American Journal of Botany* 84: 26–33

Postma JA, Dathe A, Lynch J. 2014. The optimal lateral root branching density for maize depends on nitrogen and phosphorus availability. *Plant Physiology* 166: 590-602

Rangarajan H, Postma JA, Lynch JP. 2018. Co-optimization of axial root phenotypes for nitrogen and phosphorus acquisition in common bean. *Annals of Botany* 122: 485-499

Ray DK, Mueller ND, West PC, Foley JA. 2013. Yield trends are insufficient to double global crop production by 2050. *PLoS One* 8: e66428

Tilman D, Balzer C, Hill J, Befort BL. 2011. Global food demand and the sustainable intensification of agriculture. *Proceedings of the National Academy of Sciences*108:

20260–20264

Topp CN, Iyer-Pascuzzi AS, Anderson JT, Lee C-R, Zurek PR, Symonova O, Zheng Y, Bucksch A, Mileyko Y, Galkovskyi T, et al. 2013. 3D phenotyping and quantitative trait locus mapping identify core regions of the rice genome controlling root architecture. *Proceedings of the National Academy of Sciences* 110: 1695–1704

Villordon AQ, Ginzberg I, Firon N. 2014. Root architecture and root and tuber crop productivity. *Trends in Plant Science* 19: 419–427

Walk TC, Van Erp E, Lynch JP. 2004. Modelling applicability of fractal analysis to efficiency of soil exploration by roots. *Annals of Botany* 94: 119–128

Wise TA. 2013. Can we feed the world in 2050? A scoping paper to assess the evidence. GDAE Working paper Np.13-04. Global Development and Environment Institute, Tufts University, Medford, MA, USA. Available at http://www.ase.tufts.edu/gdae/Pubs/wp/113-04WiseFeedWorld2050.pdf

Yang JT, Schneider HM, Brown KM, Lynch JP, Gifford M. 2019. Genotypic variation and nitrogen stress effects on root anatomy in maize are node specific. *Journal of Exerimental Botany* 70: 5311–5325

York LM, Nord EA, Lynch JP. 2013. Integration of root phenes for soil resource acquisition. *Frontiers in Plant Science* 4: 355.

Chapter 2

Co-optimization of axial root phenotypes for nitrogen and phosphorus acquisition in common bean

Harini Rangarajan, Johannes A. Postma and Jonathan P. Lynch

Published in *Annals of Botany*

ABSTRACT

Background and Aims Root architecture is a primary determinant of soil resource acquisition. We hypothesized that root architectural phenes will display both positive and negative interactions with each other for soil resource capture because of competition for internal resources and functional trade-offs in soil exploration.

Methods We employed the functional-structural plant model *SimRoot* to explore how interactions among architectural phenes in common bean determine the acquisition of phosphate and nitrate, two key soil resources contrasting in mobility. We evaluated the utility of basal root whorl number (BRWN) when basal root growth angle (BRGA), hypocotyl-borne roots, and lateral root branching density (LRBD) were varied, under varying availability of phosphate and nitrate.

Key Results Three basal root whorls were optimal in most phenotypes. This optimum shifted towards greater values when LRBD decreased and to smaller numbers when LRBD increased. The maximum biomass accumulated for a given BRWN phenotype in a given limiting nutrient scenario depended upon root growth angle. Under phosphorus stress shallow phenotypes grew best, whereas under nitrate stress fanned phenotypes grew best. The effect of increased hypocotyl-borne roots depended upon BRWN as well as the limiting nutrient. Greater production of axial roots due to BRWN or hypocotyl-borne roots reduced rooting depth, leading to reduced biomass under nitrate-limiting conditions. Increased BRWN as well as greater LRBD increased root carbon consumption, resulting in reduced shoot biomass.

Conclusions We conclude that the utility of a root architectural phenotype is determined by whether the constituent phenes are synergistic or antagonistic. Competition for internal resources and trade-offs for external resources result in multiple phenotypes being optimal under a given nutrient regime. We also find that no single phenotype is optimal across contrasting environments. These results have

implications for understanding plant evolution and also for the breeding of more stress-tolerant crop phenotypes.

Keywords: root architecture, basal root whorl number, common bean, functional structural plant modelling, nitrate, phene integration, phosphorus.

INTRODUCTION

Global population is projected to increase to 9.6 billion by 2050 (United Nations: Department of Social and Economic Affairs, 2013). Agricultural production needs to increase by at least 60% to keep up with the food demand of the increasing population. Limited access to fertilizers by smallholder farmers in developing nations and constraints on the sustainability of intensive fertilization makes it imperative to develop crops and cropping systems capable of sustaining satisfactory yields with reduced fertilizer inputs. An approach towards this goal is the selection of plants with superior root phenotypes (Lynch, 2007).

Root system architecture, the spatial arrangement of a root system, is important for anchorage in the soil (Ennos et al., 1993; Stokes et al., 1996) and for soil resource acquisition by allocating root foraging to soil domains with optimal resource availability (Lynch and Brown, 2012). Root system architecture is composed of architectural phenes ('phene' is to 'phenotype' as 'gene' is to 'genotype' [Serebrovsky, 1925; Lynch, 2011; Pieruschka and Poorter, 2012; Lynch and Brown, 2012; York et al., 2013]), such as number of axial roots, root growth angle (RGA), and lateral root branching density (LRBD) (Lynch, 2011; Pieruschka and Poorter, 2012; Lynch and Brown, 2012; York et al., 2013). The combination of root phenes and phene states produces a wide variety of diverse phenotypes that differ in their ability to acquire nutrients and water and require differing investments of internal resources. The interaction of these phenes can be additive, synergistic or antagonistic (York et al., 2013). In addition to trade-offs due to competition for internal resources, contrasting patterns in the spatiotemporal availability of nutrients lead to trade-offs in resource acquisition when more than one resource is limiting (Ho et al., 2004; Lynch and Ho, 2005). Phenotypes that have superior performance under conditions of low phosphorus, representing immobile resources including ammonium and potassium,

and low nitrate, representing mobile resources including water, are likely to co-optimize acquisition of multiple soil resources of varying mobility.

Extensive study of the common bean (*Phaseolus vulgaris*) root system has led to the identification of several architectural phenes that influence the acquisition of mobile and immobile resources (Bonser et al., 1996; Miller et al., 2003; Lynch and Ho, 2005; Miguel et al., 2013). The bean root system consists of the primary root, hypocotyl-borne roots, basal roots (HBRs), and lateral roots associated with each of these root classes (Zobel, 1986; Lynch and van Beem, 1993; Lynch, 2011). An important feature of the bean root system is the presence of basal roots which form a major portion of the axial root system (Miguel et al., 2013). Basal roots emerge from distinct nodes (whorls) along the base of the hypocotyl (Basu et al., 2007). The number of these whorls, basal root whorl number (BRWN), varies from one to four, with each whorl giving rise to up to four roots. The uppermost whorls produce roots with shallower RGAs and the lower whorls produce steeper angles (Lynch 2011). Basal root gravitropism is regulated by phosphorus availability and is genotype-specific (Bonser et al., 1996; Liao et al., 2001, 2004). Phenotypes with similar RGA have greater competition among roots of the same plant as well as with roots of neighbouring plants (Ge et al., 2000; Rubio et al., 2001). However, phenotypes with greater BRWN and a greater range of growth angles enable a more dispersed root system for greater soil exploration (Basu et al., 2007; Miguel et al., 2013). Basal roots emerge within 2 d of germination (Basu et al., 2007). Initially resources are made available from the large seed reserves, but as the plant grows, competition for internal resources results in trade-offs in resource allocation among different sinks which can limit root elongation and branching (Rubio and Lynch, 2007). This competition becomes more evident under nutrient stress where resource availability is very limited. This suggests that the utility of BRWN depends on the optimal placement of roots in different soil depths as determined by RGAs and by phenes which affect the sink strength of the root system. The optimal number of basal root whorls may therefore depend on nutrient regimes, and specifically the balance of mobile and immobile resources, as well as other architectural phene states.

Most functional studies of root phenes are conducted by comparing genotypes which vary only in the phene of interest, i.e. near-isophenic lines (Lynch, 2011; York et al., 2013). Populations of recombinant inbred lines (RILs) have been used for

comparisons and evaluation of phenes in common bean and maize (Lynch, 2013; Chimungu et al., 2014 a, b; Chimungu et al., 2015; Saengwilai et al., 2014a; Miguel et al., 2015; Zhan and Lynch, 2015; Zhan et al., 2015). A recent study used intensive field phenotyping of maize crown roots to identify phenes and phene integration for nitrogen acquisition (York and Lynch, 2015). Results from simulation studies have successfully predicted the utility of various root phenes as well as phene interactions (Postma and Lynch, 2011a, b; York et al., 2013; Postma et al., 2014). Studies of multiple phene combinations in multiple environmental conditions are a daunting task due to trade-offs among phenes for contrasting soil resources, interaction with other phenes and phene plasticity to environmental conditions (Lynch and Brown, 2012). In such situations, functional-structural plant modelling has proven to be a valuable tool. Simulation models allow the study of functional utility of specific phenes and their interactions with other phenes in different climates, nutrient availability and soil types (York et al., 2013).

In this study, we used the functional-structural plant model *SimRoot* to evaluate the optimal BRWN for soil resource capture and how it is influenced by 1) basal RGA, which influences the depth of the root system 2) basal root lateral branching density, which influences the sink strength and density of the root system or 3) HBR formation, which changes the sink strength of the root system and increases shallow soil exploration (Walk et al., 2006).

METHODS

The functional-structural plant model *SimRoot*, which has been used successfully to simulate the growth of the bean root system (e.g. Lynch et al., 1997; Rubio et al., 2001; Walk et al., 2006; Postma and Lynch, 2011a,2011b; Postma et al., 2014) was used in this study. *SimRoot* is now an open source platform (Postma et al. 2017). *SimRoot* simulates nutrient uptake and resource utilization of a root system in three dimensions over time. The root system simulated by the model comprises roots of distinct root classes. In *SimRoot*, root architecture is discretized into small (~1 cm) connected root segments. Nutrient uptake by the entire root system is estimated by integrating the nutrient uptake over all root segments. We simulated root system development from germination to 40 d after germination.

Carbon module

Carbon required for growth is derived initially from seed reserves. Initial seed dry weight and an on-demand release function determine carbon availability from seed reserves. The shoot is not simulated geometrically, but is represented by two pools: leaves and stems. Leaf photosynthesis, which becomes the dominant source of carbon after the seedling has been established, is simulated in *SimRoot* using techniques similar to LINTUL (Spitters and Schapendonk, 1990, Postma and Lynch, 2011a). Allocation of assimilated carbon to the different pools is based on sink strength and priority. The strength of growth sinks in *SimRoot* is based on potential growth. Maintenance sinks like respiration and root exudates are obligatory costs and prioritised over growth sinks. The shoot has a greater priority over the root for carbon partitioning. In the shoot, leaves and stems receive carbon proportional to their sink strength. Carbon allocated to roots is partitioned between primary and secondary growth. Carbon for primary growth is divided among major axes and fine roots, with the major axes having priority over fine roots. The model includes carbon storage which increases when available carbon is more than that needed for potential growth. When carbon requirements are not met, this storage acts as an added carbon source until depletion of the storage. Root and shoot growth over time lead to changes in sink strength and resource capture, thereby causing positive and negative feedbacks. The model keeps track of the carbon assimilated and utilized.

We simulated single plants as representatives of an individual plant in a monoculture stand. The light interception function assumed a planting density of 15 plants per m^2 and a light extinction coefficient of 0.9. Root competition for soil resources is an emergent property of the model and depends on the placement of roots in different soil domains. In order to simulate root densities relevant to field conditions we used a mirroring boundary condition for the roots at a mid-distance between the simulated and neighbouring plants.

Phosphorus module

Nutrient uptake can be simulated using either the Barber-Cushman (Itoh and Barber, 1993) model or the SWMS3D (Šimůnek et al., 1995) model in *SimRoot*. Previous studies have shown that SWMS3D is better for simulating mobile nutrients while Barber-Cushman model is better for simulation of immobile nutrients (Postma and

Lynch, 2011). Hence, phosphorus uptake was simulated using the Barber-Cushman model. Since Barber-Cushman is a one dimensional radial model, in order to account for inter-root competition, the average mid-distance between roots in the vicinity of each root segment was used as the boundary across which nutrient flux is assumed to be zero. As new roots grow in the neighbourhood of existing roots, this mid-distance is adjusted. The initial concentration of nutrients which is available for the new root is corrected for nutrient extraction by existing roots. The kinetic parameters for nutrient uptake were kept constant over time and phosphorus uptake was a function of root class and development only. Phosphorus availability was vertically stratified with greatest phosphorus availability in the top 10 cm of the soil. In the low phosphorus soil, the top 5 cm of had 15 µM phosphorus and the 5 cm below this had 7.5 µM phosphorus in the soil nutrient solution. At soil depths > 10 cm, 1 µM phosphorus was available. High phosphorus soil had at all depth 10 times as much phosphorus as low phosphorus soil.

Nitrate module

SimRoot coupled to SWMS3D was used for simulation of nitrate uptake (Postma and Lynch, 2011; Dathe et al., 2013). SWMS3D simulates water and solute movement in a variably saturated 3-D medium. This program solves the Richards equation for unsaturated water flow numerically and the advection dispersion equation for solute transport. The flow equation includes a term in the Richards equation to include water uptake by plant roots, while nutrient uptake is introduced as a sink term in the solute transport equations. In our simulations, nitrate is initially in the topsoil but leaches to the deeper strata over time with precipitation events. Phosphorus leaching is, however, negligible in the time span of the simulations.

Nutrient stress module

A stress factor is used to reduce the potential leaf area expansion rate for plants under phosphorus stress (Lynch et al., 1991) and photosynthetic efficiency for plants under nitrogen stress (Sinclair and Horie, 1989). The stress factor is estimated based on the actual uptake and the minimal and optimal nutrient content of the whole plant. The target nutrient content of different plant parts are calculated based on the optimal and minimal ratios of nutrient to dry weight.

Phenotypes

We simulated root phenotypes by varying the number of basal root whorls from one to four. The angles attained by roots of each whorl can range from 0 to 90° (from the soil surface). Simulating all the permutations of all the basal whorls with all possible angles would require numerous simulations and hence three representative angles were selected to parameterise the RGA. The factorial combination of four BRWN and three RGAs resulted in 12 phenotypes (3 angles X 4 whorls) which were considered throughout the studies. The number of basal root whorls and the associated angles are given in Table 1. All the roots in a whorl in a phenotype had the same angle. All of these phenotypes had five HBRs and LRBD of 4 branches cm^{-1}. The simulations included four levels of BRWN, three levels of RGA, two levels of phosphorus and two levels of nitrate in a factorial design. In order to study the effect of increasing HBR, the 12 phenotypes were simulated with 0, 10, 20, 30 and 40 HBRs under two levels of phosphorus and two levels of nitrate (42.6 kg/ha and 213 kg/ha). Two levels of LRBD (2 and 6 branches cm^{-1}) were also included in the study. The 12 phenotypes were also evaluated under low and high leaching scenarios simulated by changes in precipitation.

We repeated the runs 6 times in order to show the variation caused by stochasticity in root growth rates in the model. All simulations were run for 40 d of growth after germination. All simulations were run on the Penn State computational LionXF, LionXG, LionXH or LionXJ clusters (https://rcc.its.psu.edu/resources/hpc/). Visualization toolkit (www.vtk.org) was used for model visualization.

Parameterization

The parameter set, with references, is published in the appendix of Postma and Lynch (2011a). For the present study we used the previously published parameter set, but varied the initial phosphorus and nitrogen availability by varying the initial concentrations. Full parameterization is provided in the Supplementary Data parameterization. Basal whorls emerged within a few hours of germination (Basu et al., 2007). All the basal roots have identical growth parameters. Hypocotyl-borne roots emerged 10 days after germination. Each whorl was assumed to give rise to four roots (Miguel et al., 2013). Full parameterization is provided in the Supplementary Data (Parameterization file).

Validation

To validate the model, we compared the simulated root lengths of six root classes (primary roots, basal roots, HBRs and their respective laterals) of two- and three-whorl phenotypes with measured root lengths of two- and three-whorl genotypes reported by Walk et al. (2006). The measured data was an independent data set, not used for model parameterization.

RESULTS

An illustration of simulated roots with one, two, three and four whorls in plants with deep, fanned and shallow RGAs is shown in Figure 2-1. The accuracy of simulated root growth was verified by comparing the measured lengths of each root type in plants with two and three whorls with simulated roots. This empirical data set was not used for the parameterization of the model. Simulated phenotypes show good agreement with empirical data (Supplementary Data Figure 2-S1).

The distribution of growth among the different root classes in *SimRoot* is determined by carbon availability, which is in turn determined by initial seed reserves and shoot photosynthesis (Postma and Lynch, 2011a). Nutrient deficiency reduces shoot growth and photosynthesis, thereby reducing carbon availability. When nutrients and carbon were non-limiting, root length increased with number of whorls. The four-whorled phenotype had the greatest root length. Light-use efficiency of 3.8×10^{-7} g μmole^{-1} was used in our simulations. At this level of light-use efficiency, root length increased with increased whorl number but was much less than that under non-limiting carbon conditions. At the level of light-use efficiency used for simulations, the genotypes with greater whorl numbers are carbon-limited. This was seen as the difference in root length in plants simulated with greater carbon fixation and default carbon fixation (Figure 2-2). The three- and four- whorl phenotype had no nutrient deficiency under high phosphorus + nitrogen. Phenotypes with one and two whorls had slight phosphorus deficiency, the magnitude of which was dependent on the RGA. The stress levels for low phosphorus, low nitrogen, Low phosphorus + nitrogen as well as high phosphorus + nitrogen are depicted in Supplementary Data Figures 2-S2-2-S4.

Root length in the topsoil increases with increased whorl number (Figure 2-3). This corresponds to greater phosphorus uptake in phenotypes with greater whorl number (Figure 2-4). Hypocotyl-borne-roots and basal roots contributed substantially to the total root length in the top 10 cm of the soil corresponding to the region of greatest phosphorus availability in our simulations (Figure 2-3). Among phenotypes varying in angle under a given stress environment, root length differed by 30-40 m. Shallow-angled phenotypes have greater root length in the topsoil than fanned or deep angled phenotypes (Figure 2-3).

Greater topsoil exploration, however, occurred at the cost of deep soil exploration, resulting in reduced nitrate uptake (Figures 2-5 and 2-6). Leaching was enabled in the simulations. The amount of nitrate at different soil depths changes with precipitation events, resulting in nitrate becoming available in deeper soil strata over time. Greater rooting depth as well as root length in different soil strata therefore determines nitrate capture. Phenotypes with greater whorl number had fewer roots at greater depths as well as reduced rooting depth (Figure 2-5). Deep- and fanned-angle phenotypes have greater rooting depth (Figure 2-5) and so greater nitrate uptake (Figure 2-6) than shallow-angled phenotypes. Among deep-angled phenotypes, phenotypes with fewer whorls had more roots at greater depth than those with more whorls (Figure 2-5). The rate of nitrate uptake was greater for the deep- and the fanned-angled phenotypes compared with the shallow-angled phenotype (Figure 2-7). Nitrate uptake by basal roots was much greater than that of the primary root except in shallow one-whorl phenotypes. When the precipitation was half that of the default precipitation, the trends in biomass accumulation were similar to those of the default precipitation (Supplementary Data Figure 2-S5). The utility of greater rooting depth as caused by deep-angled phenotypes with fewer whorls was even more evident in greater leaching environment (Supplementary Data Figure 2-S6).

Biomass is a result of trade-offs in carbon allocation to different root classes and the resulting uptake of limiting nutrients. Phenotypes that are able to optimally acquire different nutrients perform better under combined stress condition than those that are superior for a single resource acquisition. Deep- and fanned-angle phenotypes with three whorls are able to efficiently explore more soil layers and so have the greatest biomass (Figure 2-8). Further increasing whorl number increases competition for available carbon, resulting in reduced shoot biomass as seen in phenotypes with

four whorls (Figure 2-8). The benefit of BRWN is therefore dependent on the carbon status of the plant. When carbon fixation was increased by 20%, increasing whorl number increased biomass irrespective of RGA. Four-whorled phenotypes had the largest biomass, this optimum reduced to two whorls when the carbon fixation was reduced by 20% (Supplementary Data Figure 2-S7).

Sink strength is sensitive to variation in LRBD. The LRBD was maintained at 4 branches cm^{-1} in the previous simulations. When sink strength was reduced by reducing LRBD to 2 branches cm^{-1}, the biomass in phenotypes under low nitrate availability increased and optimal whorl number increased to four (Supplementary Data Figure 2-S8). When LRBD was increased to 6 branches cm^{-1}, biomass was reduced when compared to the default LRBD (Supplementary Data Figure.2-S9). The four-whorl phenotype was much more carbon-limited than phenotypes with fewer whorls, as seen in a drastic reduction in shoot biomass upon increasing sink strength by increasing LRBD. Increasing HBRs enabled greater topsoil exploration but also increased sink strength. Under low phosphorus, increasing the number of HBRs increased biomass. This increase was greatest for phenotypes with fewer basal roots. Increasing the number of HBRs under conditions of limiting nitrate decreased biomass (Figure 2-9).

We conducted sensitivity analyses to determine whether simulation results were sensitive to planting density (Supplementary Data Figure 2-S10). Increasing planting density from 15 to 25, 40 or 50 plants m^{-2} resulted in plants with reduced biomass even under high nitrogen + phosphorus. Biomass was similar for one-, two- and three-whorl phenotypes when greater planting densities were simulated. Further increase in whorl number reduced plant biomass. A greater whorl number was optimal for plants simulated with reduced planting density.

DISCUSSION

This study investigates the utility of axial root phenotypes, focusing on BRWN, for the acquisition of nitrate, the primary mobile nutrient resource, and phosphate, the primary immobile nutrient resource, in contrasting nutrient regimes. Our results confirm that BRWN has important roles for nutrient acquisition, and indicate that the utility of BRWN is affected by interactions with other architectural

phenes.

Root phenes which enhance topsoil foraging are important for the capture of topsoil resources (Lynch and Brown, 2001; Lynch, 2011). Shallow RGA, greater BRWN, more HBRs, greater LRBD, increased root hair length and density can by themselves increase root exploration of the topsoil and increase the capture of topsoil resources (Lynch and Brown, 2001; Zhu and Lynch, 2004; Zhu et al., 2005). However, when several phenes are co-expressed, the fitness of integrated root phenotypes is determined by phene interactions and trade-offs (York et al., 2013). Shallow BRGA and HBRs explore different regions of soil independently and hence their interaction is synergistic when HBR increased up to 20 (Walk et al., 2006). Shallow BRGA and greater BRWN are also synergistic for phosphorus uptake (Figure 2-4). Trade-offs between basal roots, HBRs and their laterals in phenotypes with greater BRWN, shallow or fanned RGA and greater HBRs result in an increase in total root length in the topsoil, leading to increased P uptake. The result is that, in a low phosphorus environment, the three- and four-whorl shallow-sangled phenotypes and the four-whorl fanned phenotypes are optimal and have similar fitness for phosphorus uptake.

Shallow RGAs and BRWN > 3, however, are antagonistic for biomass accumulation (Figure 2-8). Soil resources are distributed heterogeneously through the soil profile: phosphorus, potassium and ammonium are more abundant in the topsoil and nitrogen can be available in topsoil due to mineralization or continual fertilizer applications or in low-leaching scenarios caused by low precipitation (Dathe et al., 2013). Water and nitrate are mobile soil resources and are eventually available in deep soil domains (Jobbágy and Jackson, 2001; Di and Cameron, 2002; Lynch and Wojciechowski, 2015). As the number of axial roots (basal roots or HBRs) increases, the sink strength of the root system increases. The resulting carbon limitation leads to reduced elongation of axial roots (Walk et al., 2006; Saengwilai et al., 2014 ; Postma et al., 2014). This reduces rooting depth, resulting in trade-offs for nitrate acquisition (Figure 2-6) and growth (Figure 2-8). Reducing root metabolic burden by formation of fewer BRWN, fewer HBRs and/or reduced LRBD can increase root depth and enable better nitrate capture (Figure 2-9; Supplementary Data Figure.2-S8). The benefit of this increased rooting depth becomes more apparent in leaching environments (Supplementary Data Figure.2-S6). Bean can obtain 20-60% of its

nitrogen requirement by symbiotic nitrogen fixation. Root depth is more important for nitrate uptake in maize and other crops which depend on soil nitrate. Deep roots are also important for water uptake, especially under water limitation (Uga et al., 2013; Lynch and Wojciechowski, 2015).

Trade-offs for water and phosphorus acquisition in shallow- and deep- rooted common bean genotypes have been demonstrated by Ho et al. (2004). Use of multilines with contrasting root architectures can co-optimize capture of shallow and deep resource at the stand level (Henry et al., 2010). Root architectural differences among crops in traditional polyculture systems facilitate niche complementarity, enabling better resource acquisition and better yields than component monocultures (Postma and Lynch, 2012; Zhang et al., 2014). Shallow and deep resource capture can also be co-optimized by use of dimorphic architectural phenotypes (Dunbabin et al., 2003, 2004). Phenotypes with greater BRWN are an example of dimorphic phenotypes. In phenotypes with greater BRWN, lower whorls produce deeper roots while upper whorls develop progressively shallower roots (Miguel et al., 2013). This increases the vertical range of soil exploration except when BRGA are shallow. The shallow portions of deep or fanned root systems explore the topsoil, therefore root length in the topsoil increases along with increased whorl number. This improves plant growth under low phosphorus in phenotypes with deep and fanned RGA and greater BRWN (Figure 2-8). Greater BRWN phenotypes with fanned growth angles perform consistently well under all scenarios; this phenotype is important when there are limitations in multiple resources with conflicting spatial availability, as well as for capture of mobile resources whose distribution in the soil profile changes with soil type and precipitation dynamically over time (Figure 2-8). These characteristics are also important in circumstances where roots are lost due to herbivory or disease (Miguel et al., 2013).

The main constraint in maintaining greater BRWN is carbon limitation. Our results show that the three-whorled phenotype is optimal under most conditions. The results of the trade-off between phosphorus and nitrate uptake brought about by the trade-offs in length of basal roots and hypocotyl roots and their laterals, resulted in the three-whorled phenotype having the greatest growth when both N and P were limiting (Figure 2-8). Poorter et al. (2012) in a meta-analyses study showed that around 80% of biomass is allocated to the shoots in herbaceous species. We relaxed these ratios

somewhat as short term allocation patterns may deviate from long term patterns, and set the threshold for carbon allocation to shoot growth to a maximum 85% of the total carbon allocation for growth, while minima were not set, as severe nutrient deficiency may arrest shoot growth completely and seedlings tend to have greater allocation to roots. This threshold means that, even when nutrients do not limit shoot growth, carbon allocation may do so in strongly source-limited scenarios or in sink-limited scenarios in which the sink strength of the root system is <15% of the total sink strength of the plant. Source-limitation of shoot growth occurred in the four-whorl, abundant-nutrient scenarios unless carbon fixation rates were increased (Supplementary Data Figure 2-S7). This, along with the finding that the majority of cultivated beans have two or three whorls (Miguel et al., 2013), suggests that phenotypes with more than three whorls could have better utility when carbon fixation is greater as expected with increased CO_2 in the environment.

Plants initially derive their required carbon from seed reserves. There is a significant positive correlation between seed weight and the number of whorls in bean genotypes (Vieira et al., 2008). Hence larger seeds could provide the required greater carbon reserves in plants with greater BRWN. Carbon made available by reducing metabolic costs can increase axial root length of HBRs or basal roots. However, the relative benefit of carbon allocation to one class over other depends on the limiting nutrient. For example, drought stress results in reduced allocation to adventitious roots (Pardales and Yamauchi, 2003); however, phosphorus stress results in more HBRs (Miller et al., 2003). When both stresses occur together, the optimum allocation is determined by the benefits accrued over costs incurred (Ho et al., 2004).

In our simulations, phenotypes with one shallow whorl performed better under combined phosphorus + nitrogen stress than when only nitrate was limited (Figure 2-8). Phosphorus stress results in increased carbon allocation to roots. In shallow-angled phenotypes this results in improved phosphorus uptake and growth under phosphorus limitation. This is in agreement with the study of (Postma and Lynch, 2011a), who observed a similar response where phosphorus stress developed early, but as the root system developed uptake rates of phosphorus increased and plants eventually grow out of stress.

Intense competition exists among neighbouring plants for soil resources and root architecture is a primary factor affecting root competition among plants (Rubio et

al., 2003). In this study, a single plant was modelled, which represented an individual in a monoculture stand. Modelling predicts that competition is greater among plants with similar root architecture (Rubio et al., 2001; Postma and Lynch, 2012). Relative biomass partitioning to roots may be an expression of a functional equilibrium, and as such may be influenced by competition depending on whether competition for light is greater than that for nutrients. In greenhouse studies with beans, no change in root to shoot ratios was found in response to neighbours (Nord et al., 2011). Competition reduces resource uptake per unit root length and leaf area, i.e., there is less benefit for the same amount of carbon invested. This leads to a decrease in resource capture and reduced relative growth rates in plants grown under greater planting densities. Phenotypes with less BRWN perform better at greater planting densities. Phenotypic plasticity is an important factor in resource capture (Zhu et al., 2010; Lynch and Brown, 2012). Phenotypic plasticity of RGA in response to N and phosphorus availability exists in some genotypes of common bean and maize (Bonser et al., 1996; Trachsel et al., 2013). Phenotypic plasticity is not simulated in our models, but there exist trade-offs to plasticity as evident by the presence of non-plastic genotypes (Bonser et al., 1996; Trachsel et al., 2013).

This study focuses on the common bean root system, but concepts emerging from this study are applicable to root systems of other crops. Basal roots in bean are analogous to crown roots in maize and the mesocotyl-borne roots in maize are homologous with HBRs in dicots (Lynch, 2013). Some dicots do not have basal roots but are dominated by lateral root systems emerging from the primary root. The main difference between bean which is a dicot root system and monocot root systems is that new roots (laterals) emerge from already existing roots in dicots, whereas in monocots, nodal roots continually emerge from shoot nodes near or above the soil surface over time. These differences suggest that the optimal phene state is likely to be different in different species, but the fitness of the resulting phenotype is likely to depend on the outcome of phene interactions among each other and with the environment.

We have used mechanistic simulation modelling to demonstrate the importance of BRWN and phene interactions in determining nutrient capture. Previous studies have considered the interaction of two phenes (Walk et al., 2006; Postma and Lynch, 2011a; York et al., 2013; Miguel et al., 2015). In this study, for

the first time the interaction of more than two phenes has been considered. In-silico studies allow evaluation of interaction of several phenes across several environmental scenarios of interest including scenarios that do not yet exist such as future climate scenarios (Lynch, 2015). These experiments, however, require greater computational power and strategies to analyse the resulting complex fitness landscape. The results will be heuristic; however, they will prove invaluable in identifying subsets of cases that warrant field evaluation (Lynch and Brown, 2012; York et al., 2013; Lynch, 2015).

CONCLUSIONS

Our study indicates that the utility of a root phene is largely dependent on the expression of other root phenes. The fitness landscape of plant performance against the multi-dimensional array of environmental and internal factors is highly complex. Interactions among phenes in combination with trade-offs due to carbon limitations result in several distinct root architectures with varied fitness in environments varying in nutrient availability. However, plants with different phenotypes can have comparable performance. For example, shallow root phenotypes with two or three basal root whorls and tens HBR, one or three whorls and greater LRBD, and four whorls with lower LRBD, had comparable biomass under low phosphorus. Therefore, there is no single optimal architectural phenotype; there exist multiple optimal root architectural phenotypes for a given environment. In an interesting study with shoot architectures optimized for light capture, reproductive success, mechanical stability and minimizing water loss, Niklas (1994) demonstrated that the number of optimal shoot architectures increases with increase in the number of functions they need to perform. In this study we have considered only a few root phenes and have demonstrated that there exists more than one optimal architectural phenotype for a given environment. We hypothesize that when all the identified phenes are considered, under varied environmental condition; the number of optimal phenotypes will be much greater and will provide insight into the mechanisms of phene interactions.

REFERENCES

Basu P, Zhang YJ, Lynch JP, Brown KM. 2007. Ethylene modulates genetic, positional, and nutritional regulation of root plagiogravitropism. *Functional Plant Biology* 34: 41–51.

Bonser AM, Lynch J, Snapp S. 1996. Effect of phosphorus deficiency on growth angle of basal roots in *Phaseolus vulgaris*. *New phytologist* 132: 281–288.

Chimungu JG, Brown KM, Lynch JP. 2014a. Reduced root cortical cell file number improves drought tolerance in maize. *Plant Physiology* 166: 1943–1955.

Chimungu JG, Brown KM, Lynch JP. 2014b. Large root cortical cell size improves drought tolerance in maize. *Plant Physiology* 166: 2166–2178.

Chimungu JG, Maliro MFA, Nalivata PC, Kanyama-Phiri G, Brown KM, Lynch JP. 2015. Utility of root cortical aerenchyma under water limited conditions in tropical maize (*Zea mays* L.). *Field Crops Research* 171: 86–98.

Dathe A, Postma JA, Lynch JP. 2013. Modeling resource interactions under multiple edaphic stresses. In: Timlin D, Ahuja LR, eds. Enhancing understanding and quantification of soil-root interactions. Madison, WI: American Society of Agronomy, Crop Science Society of America, Soil Science Society of America, 273–294.

Di HJ, Cameron KC. 2002. Nitrate leaching in temperate agroecosystems: Sources, factors and mitigating strategies. *Nutrient Cycling in Agroecosystems* 64: 237–256.

Ennos AR, Crook MJ, Grimshaw C. 1993. The anchorage mechanics of maize, *Zea mays*. *Journal of Experimental Botany* 44: 147–153.

Dunbabin V, Diggle AJ, Rengel Z. 2003. Is there an optimal root architecture for nitrate capture in leaching environments? *Plant, Cell & Environment* 26: 835–844.

Dunbabin V, Rengel Z, Diggle AJ. 2004. Simulating form and function of root systems : Efficiency of nitrate uptake is dependent on root system architecture and the spatial and temporal variability of nitrate supply. *Functional Ecology* 18: 204–211.

Ge Z, Rubio G, Lynch JP. 2000. The importance of root gravitropism for inter-root competition and phosphorus acquisition efficiency: results from a geometric simulation model. *Plant and Soil* 218: 159–171.

Henry A, Rosas JC, Beaver JS, Lynch JP. 2010. Multiple stress response and belowground competition in multilines of common bean (*Phaseolus vulgaris* L.). *Field Crops Research* 117: 209–218.

Ho MD, McCannon BC, Lynch JP. 2004. Optimization modeling of plant root architecture for water and phosphorus acquisition. *Journal of Theoretical Biology* 226: 331–340.

Itoh S, Barber SA. 1983. A numerical solution of whole plant nutrient uptake for soil-root systems with root hairs. *Plant and Soil* 70: 403-413.

Jobbágy EG, Jackson RB. 2001. The distribution of soil nutrients with depth: Global patterns and the imprint of plants. *Biogeochemistry* 53: 51–77.

Liao H, Rubio G, Yan X, Cao A, Brown KM, Lynch JP. 2001. Effect of phosphorus availability on basal root shallowness in common bean. *Plant and Soil* 232: 69–79.

Liao H, Yan X, Rubio G, Beebe SE, Blair MW, Lynch JP. 2004. Genetic mapping of basal root gravitropism and phosphorus acquisition efficiency in common bean. *Functional Plant Biology* 31: 959–970.

Lynch JP. 2007. Turner review no. 14. Roots of the second green revolution. *Australian Journal of Botany* 55: 493–512.

Lynch JP. 2011. Root phenes for enhanced soil exploration and phosphorus acquisition: tools for future crops. *Plant Physiology* 156: 1041–1049.

Lynch JP. 2013. Steep, cheap and deep: an ideotype to optimize water and N acquisition by maize root systems. *Annals of Botany* 112: 347–357.

Lynch JP. 2015. Root phenes that reduce the metabolic costs of soil exploration: opportunities for 21st century agriculture. *Plant, Cell & Environment* 38: 1775–1784.

Lynch JP, van Beem JJ. 1993. Growth and architecture of seedling roots of common bean genotypes. *Crop Science* 33: 1253–1257.

Lynch JP, Brown KM. 2001. Topsoil foraging - an architectural adaptation of plants to low phosphorus availability. *Plant and Soil* 237: 225–237.

Lynch JP, Brown KM. 2012. New roots for agriculture: exploiting the root phenome. *Philosophical Transactions of the Royal Society B: Biological Sciences* 367: 1598–1604.

Lynch JP, Ho MD. 2005. Rhizoeconomics: carbon costs of phosphorus acquisition. *Plant and Soil* 269: 45–56.

Lynch J, Läuchli A, Epstein E. 1991. Vegetative growth of the common bean in response to phosphorus nutrition. *Crop Science* 31: 380-387.

Lynch JP, Nielsen KL, Davis RD, Jablokow AG. 1997. *SimRoot*: Modelling and visualization of root systems. *Plant and Soil* 188: 139–151.

Lynch JP, Wojciechowski T. 2015. Opportunities and challenges in the subsoil: pathways to deeper rooted crops. *Journal of Experimental Botany* 66: 2199–2210.

Miguel MA, Postma JA, Lynch JP. 2015. Phene synergism between root hair length and basal root growth angle for phosphorus acquisition. *Plant Physiology* 167: 1430–1439.

Miguel MA, Widrig A, Vieira RF, Brown KM, Lynch JP. 2013. Basal root whorl number: a modulator of phosphorus acquisition in common bean (*Phaseolus vulgaris*). *Annals of Botany* 112: 973–982.

Miller CR, Ochoa I, Nielsen KL, Beck D, Lynch JP. 2003. Genetic variation for adventitious rooting in response to low phosphorus availability: Potential utility for phosphorus acquisition from stratified soils. *Functional Plant Biology* 30: 973–985.

Niklas KJ. 1994. Morphological evolution through complex domains of fitness. *Proceedings of the National Academy of Sciences of the USA* 91: 6772–6779.

Nord EA, Zhang C, Lynch JP. 2011. Root responses to neighboring plants in common bean are mediated by nutrient concentration rather than self/non-self recognition. *Functional Plant Biology* 38: 941-952.

Pardales JR, Yamauchi A. 2003. Regulation of root development in sweetpotato and cassava by soil moisture during their establishment period. *Plant and Soil* 255: 201–208.

Pieruschka R, Poorter H. 2012. Phenotyping plants: genes, phenes and machines. *Functional Plant Biology* 39: 813–820.

Poorter H, Niklas KJ, Reich PB, Oleksyn J, Poot P, Mommer L. 2012. Biomass allocation to leaves, stems and roots: meta-analyses of interspecific variation and environmental control. *New phytologist* 193: 30–50.

Postma JA, Lynch JP. 2011a. Theoretical evidence for the functional benefit of root cortical aerenchyma in soils with low phosphorus availability. *Annals of Botany* 107: 829–841.

Postma JA, Lynch JP. 2011b. Root cortical aerenchyma enhances the growth of maize on soils with suboptimal availability of nitrogen, phosphorus, and potassium. *Plant Physiology* 156: 1190–1201.

Postma JA, Lynch JP. 2012. Complementarity in root architecture for nutrient uptake in ancient maize/bean and maize/bean/squash polycultures. *Annals of Botany* 110: 521–534.

Postma JA, Dathe A, Lynch JP. 2014. The optimal lateral root branching density for maize depends on nitrogen and phosphorus availability. *Plant Physiology* 166:

590-602.

Postma JA, Kuppe C, Owen MR, et al. 2017. Open*SimRoot*: Widening the scope and application of root architectural models. *New Phytologist* 215: 1274-1286.

Rubio G, Lynch JP. 2007. Compensation among root classes in *Phaseolus vulgaris* L. *Plant and Soil* 290: 307–321.

Rubio G, Walk T, Ge Z, Yan X, Liao H, Lynch J. 2001. Root gravitropism and below-ground competition among neighboring plants: a modelling approach. *Annals of Botany* 88: 929–940.

Rubio G, Liao H, Yan X, Lynch JP. 2003. Topsoil foraging and its role in plant competitiveness for phosphorus in common bean. *Crop Science* 43: 598–607.

Saengwilai P, Nord EA, Chimungu JG, Brown KM, Lynch JP. 2014a. Root cortical aerenchyma enhances nitrogen acquisition from low-nitrogen soils in maize. *Plant Physiology* 166: 726–735.

Saengwilai P, Tian X, Lynch JP. 2014b. Low crown root number enhances nitrogen acquisition from low nitrogen soils in maize (*Zea mays* L.). *Plant Physiology* 166: 581-589.

Serebrovsky AS. 1925. “Somatic segregation” in domestic fowl. *Journal of genetics* 16(1): 33-42

Šimůnek J, Huang K, Van Genuchten MT. 1995. The SWMS-3D code for simulating water flow and solute transport in three-dimensional variably-satured media. Riverside, CA: U.S.Salinity Laboratory, USDA.

Sinclair TR, Horie T. 1989. Leaf nitrogen, photosynthesis, and crop radiation use efficiency: A Review. *Crop Science* 29: 90-98.

Spitters CJT, Schapendonk AHCM. 1990. Evaluation of breeding strategies for drought tolerance in potato by means of crop growth simulation. *Plant and Soil* 123: 193–203.

Stokes A, Ball J, Fitter AH, Brain P, Coutts MP. 1996. An experimental investigation of the resistence of model root systems to uprooting. *Annals of Botany* 78: 415–421.

Trachsel S, Kaeppler SM, Brown KM, Lynch JP. 2013. Maize root growth angles become steeper under low N conditions. *Field Crops Research* 140: 18–31.

Uga Y, Sugimoto K, Ogawa S, et al. 2013. Control of root system architecture by DEEPER ROOTING 1 increases rice yield under drought conditions. *Nature Genetics* 45: 1097–1102.

United Nations: Department of Social and Economic Affairs. 2013. World population

prospects: The 2012 revision, Key findings and Advance Tables. Population Division 2013: Working Paper No. ESA/P/WP.227. New York, United Nations.

Vieira RF, Carneiro JES, Lynch JP. 2008. Root traits of common bean genotypes used in breeding programs for disease resistance. *Pesquisa Agropecuária Brasilia* 43: 707–712.

Walk TC, Jaramillo R, Lynch JP. 2006. Architectural tradeoffs between adventitious and basal roots for phosphorus acquisition. *Plant and Soil* 279: 347–366.

York LM, Lynch JP. 2015. Intensive field phenotyping of maize (*Zea mays* L.) root crowns identifies phenes and phene integration associated with plant growth and nitrogen acquisition. *Journal of Experimental Botany* 66: 5493–5505.

York LM, Nord EA, Lynch JP. 2013. Integration of root phenes for soil resource acquisition. *Frontiers in Plant Science* 4: 355.

Zhan A, Lynch JP. 2015. Reduced frequency of lateral root branching improves N capture from low-N soils in maize. *Journal of Experimental Botany* 66: 2055–2065.

Zhan A, Schneider H, Lynch JP. 2015. Reduced lateral root branching density improves drought tolerance in maize. *Plant Physiology* 168: 1603-1615.

Zhang C, Postma JA, York LM, Lynch JP. 2014. Root foraging elicits niche complementarity-dependent yield advantage in the ancient “three sisters” (maize/bean/squash) polyculture. *Annals of Botany* 114: 1719–1733.

Zhu J, Lynch JP. 2004. The contribution of lateral rooting to phosphorus acquisition efficiency in maize (*Zea mays*) seedlings. *Functional Plant Biology* 31: 949-958.

Zhu J, Kaeppler SM, Lynch JP. 2005. Topsoil foraging and phosphorus acquisition efficiency in maize (*Zea mays*). *Functional Plant Biology* 32: 749-762.

Zhu J, Zhang C, Lynch JP. 2010. The utility of phenotypic plasticity of root hair length for phosphorus acquisition. *Functional Plant Biology* 37: 313–322.

Zobel RW. 1986. Rhizogenetics (root genetics) of vegetable crops. *HortScience* 21: 956–959.

FIGURES AND TABLES

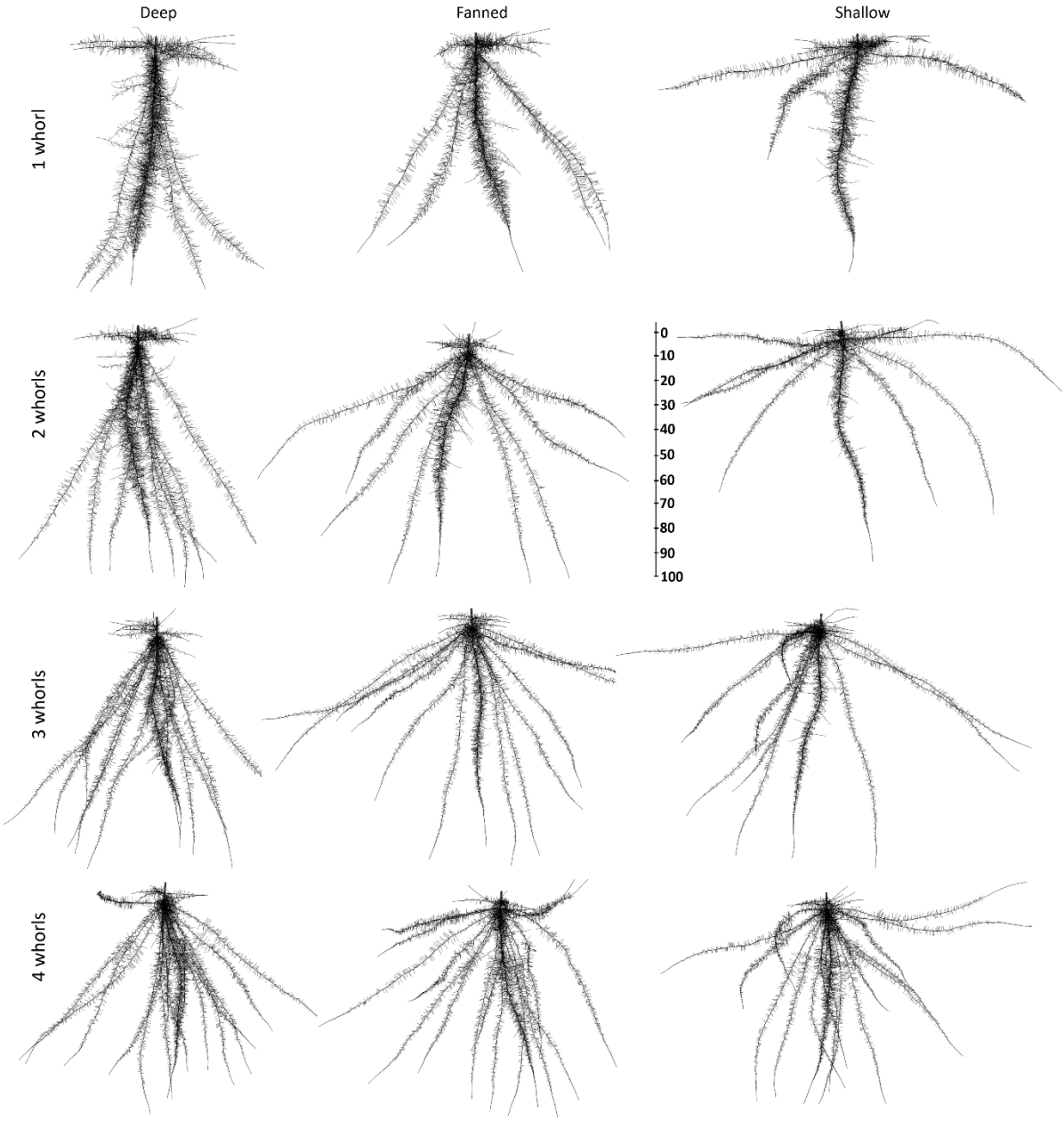

Figure 2-1: Visualization of the simulated root architecture of bean at 40 d after germination. The phenotypes vary in basal root whorl number as well as root growth angle. Units shown are cm.

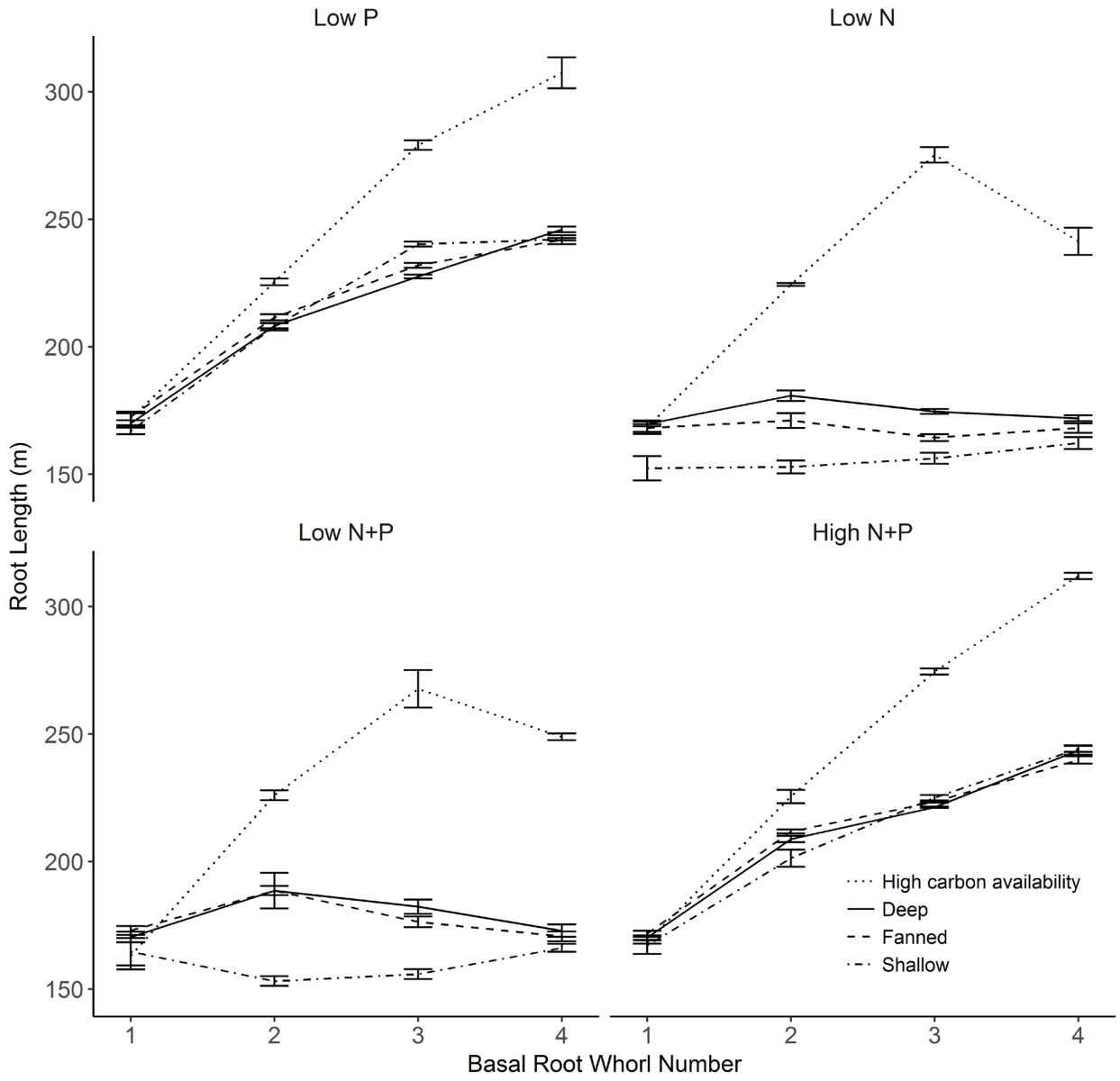

Figure 2-2: Root length 40 d after germination (d.a.g) at low phosphorus, low nitrogen, combined low phosphorus and low nitrogen, and non-limiting nitrogen and phosphorus availability. Lines show results for plants with one, two, three and four whorls with shallow, fanned and deep root growth angles along with plant simulated under high carbon availability. Error bars show the standard error for six repeated runs, with inter-run variation caused by stochasticity in root growth rates and branching frequency.

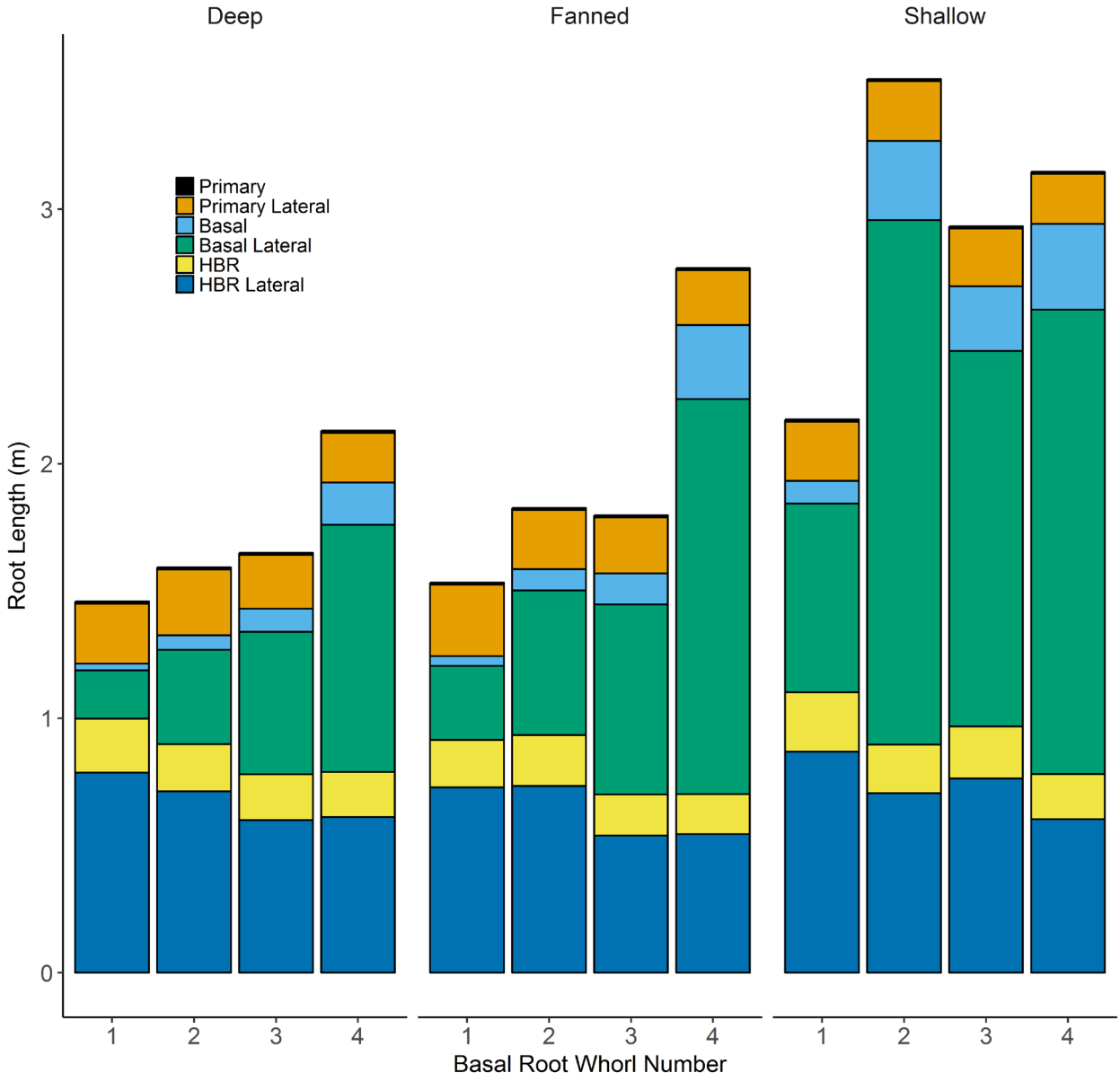

Figure 2-3: Root length in the top 10 cm of soil for plants with one, two, three and four whorls with deep, fanned and shallow root growth angles. The plants are simulated in soil which is low in phosphorus but non-limiting in nitrate availability.

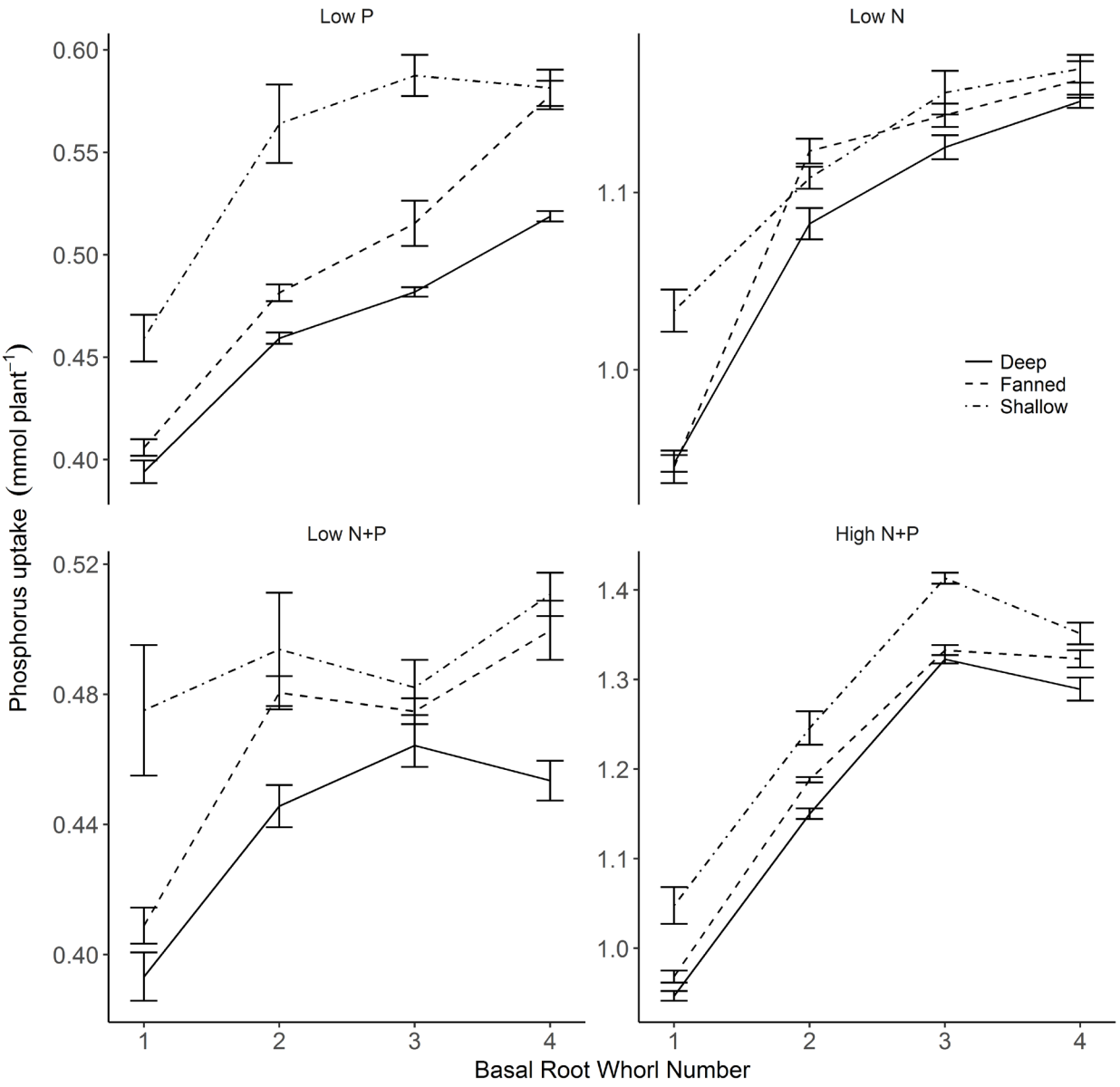

Figure 2-4: Phosphorus acquisition 40 d after germination (d.a.g) at low phosphorus, low nitrogen, combined low phosphorus and low nitrogen, and non-limiting nitrogen and phosphorus availability. Lines show results for plants with one, two, three and four whorls with shallow, fanned and deep root growth angles. Error bars show the standard error for six repeated runs, with inter-run variation caused by stochasticity in root growth rates and branching frequency.

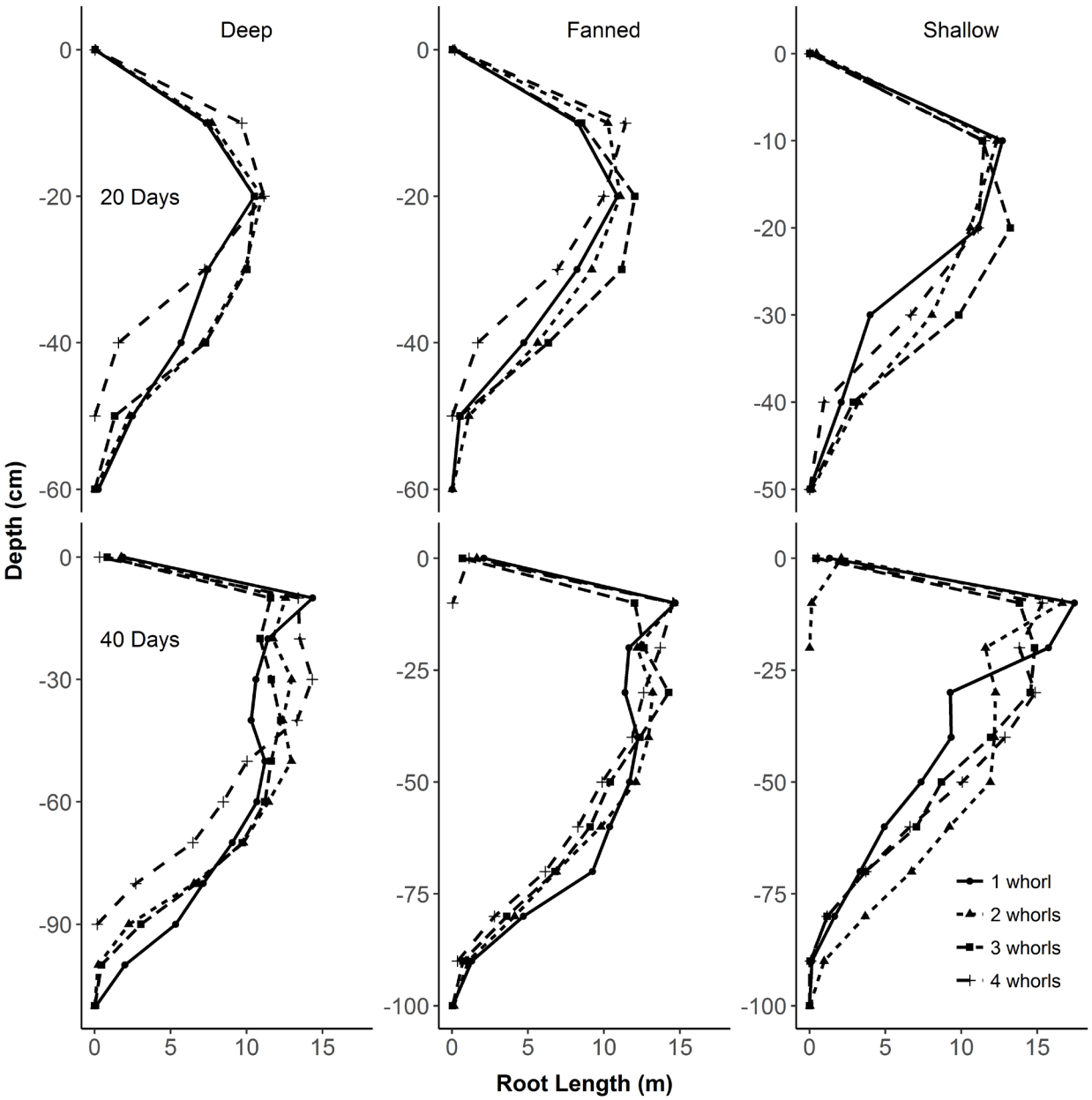

Figure 2-5: Root length distribution for plants with one, two, three and four whorls with deep, fanned and shallow angles at 20 d.a.g (top) and 40 d.a.g (bottom).

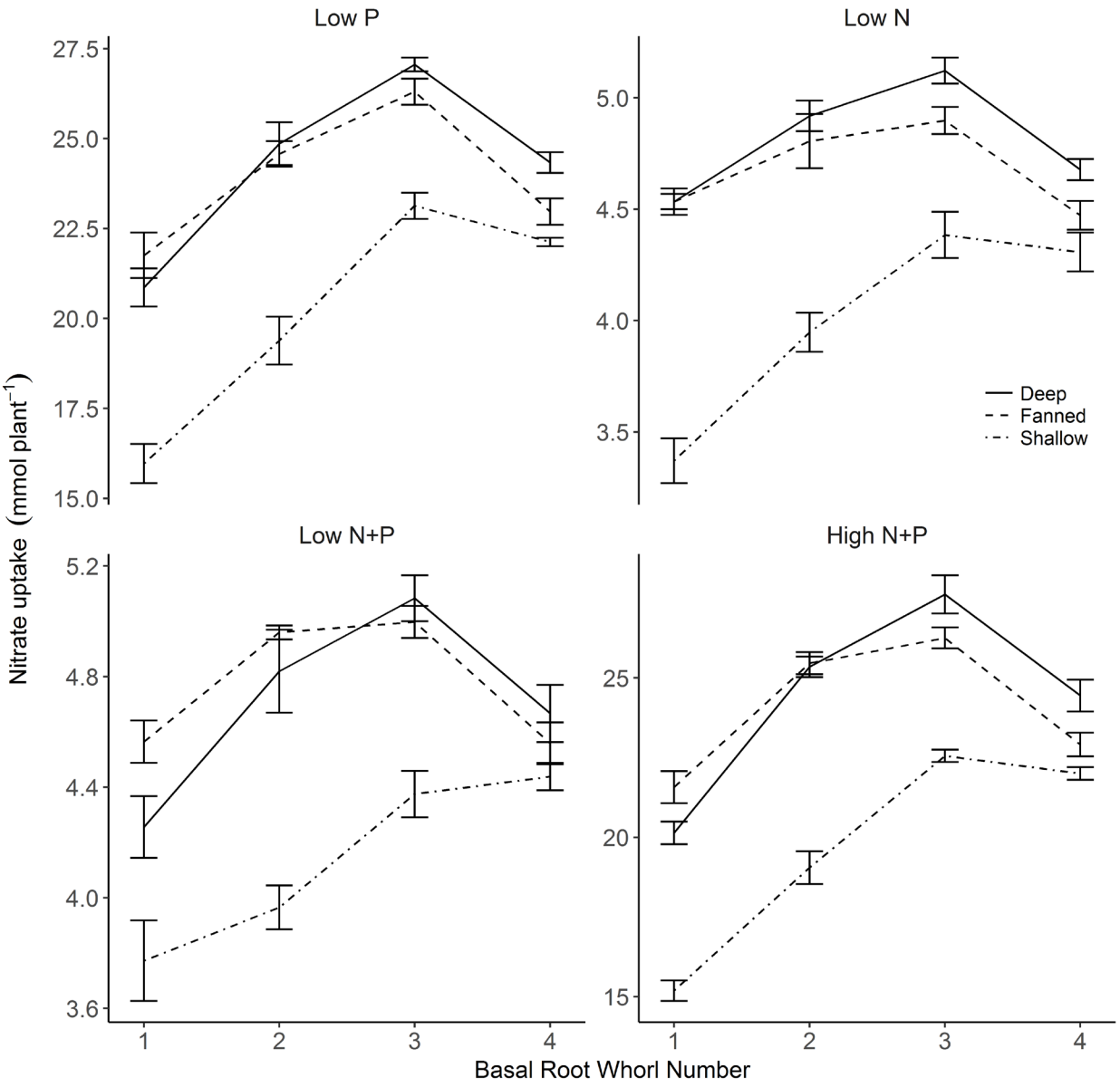

Figure 2-6: Nitrate acquisition 40 d after germination (d.a.g) at low phosphorus, low nitrogen, combined low phosphorus and low nitrogen, and non-limiting nitrogen and phosphorus availability. Lines show results for plants one, two, three and four whorls with shallow, fanned and deep root growth angles. Error bars show the standard error for six repeated runs, with inter-run variation caused by stochasticity in root growth rates and branching frequency.

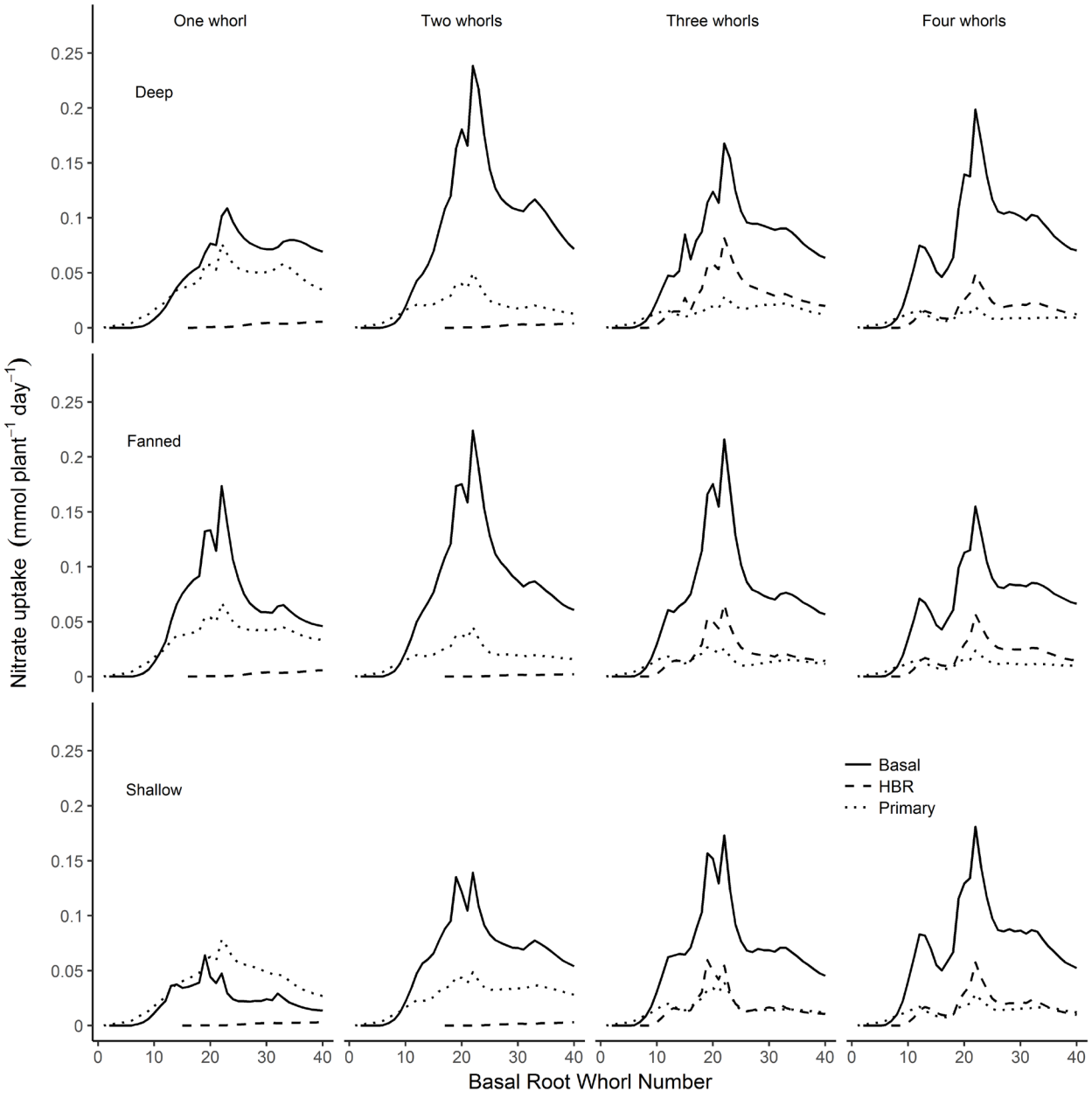

Figure 2-7: Nitrate uptake rate of different root classes for plants with one, two, three and four whorls with deep, fanned and shallow root growth angles. The plants are simulated in soil which is low nitrate but non-limiting in phosphorus availability.

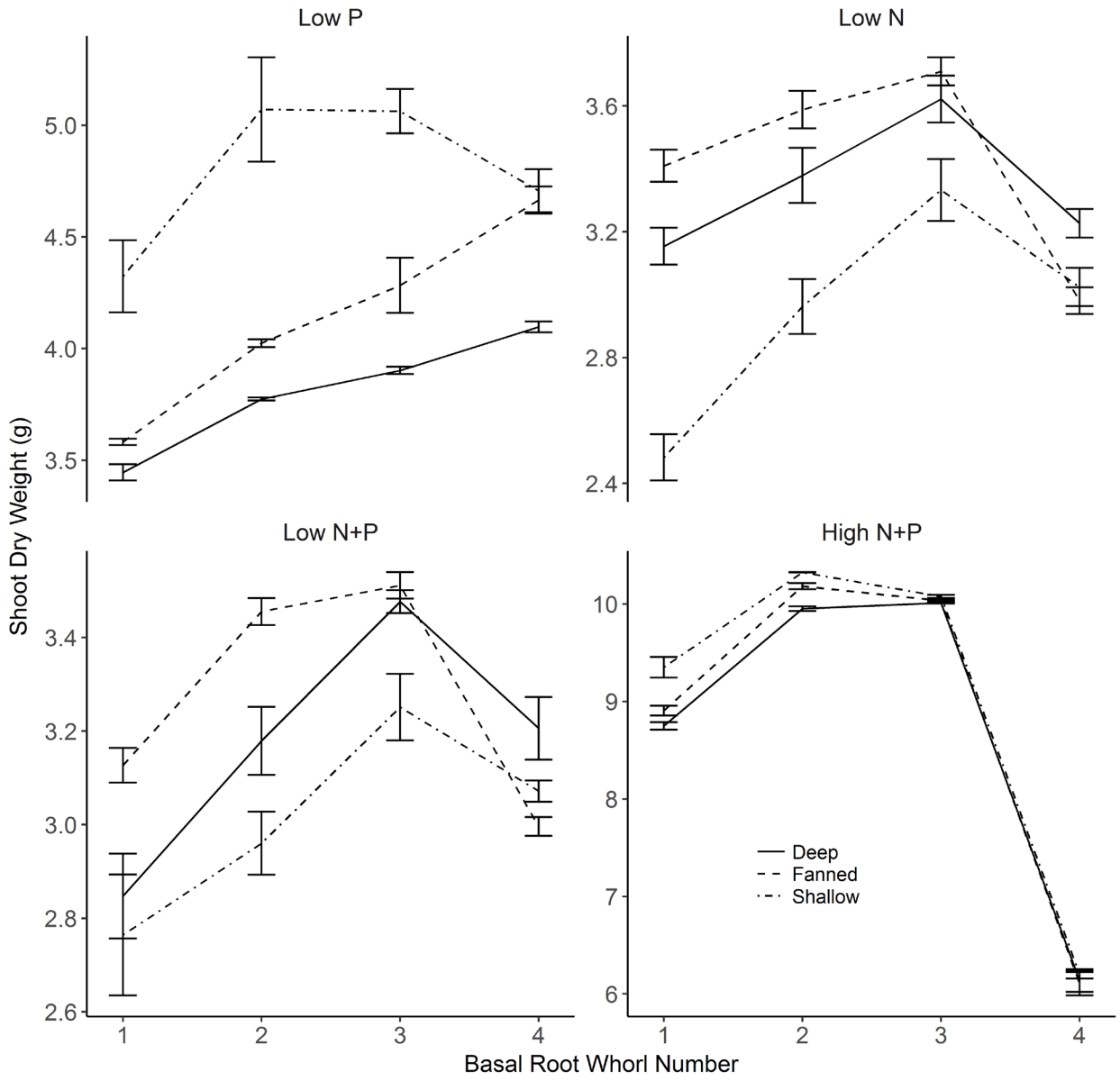

Figure 2-8: Shoot biomass 40 d after germination (d.a.g) at low phosphorus, low nitrogen, combined low phosphorus and low nitrogen, and non-limiting nitrogen and phosphorus availability. Lines show results for plants with one, two, three and four whorls with shallow, fanned and deep root growth angles. Error bars show the standard error for six repeated runs, with inter-run variation caused by stochasticity in root growth rates and branching frequency.

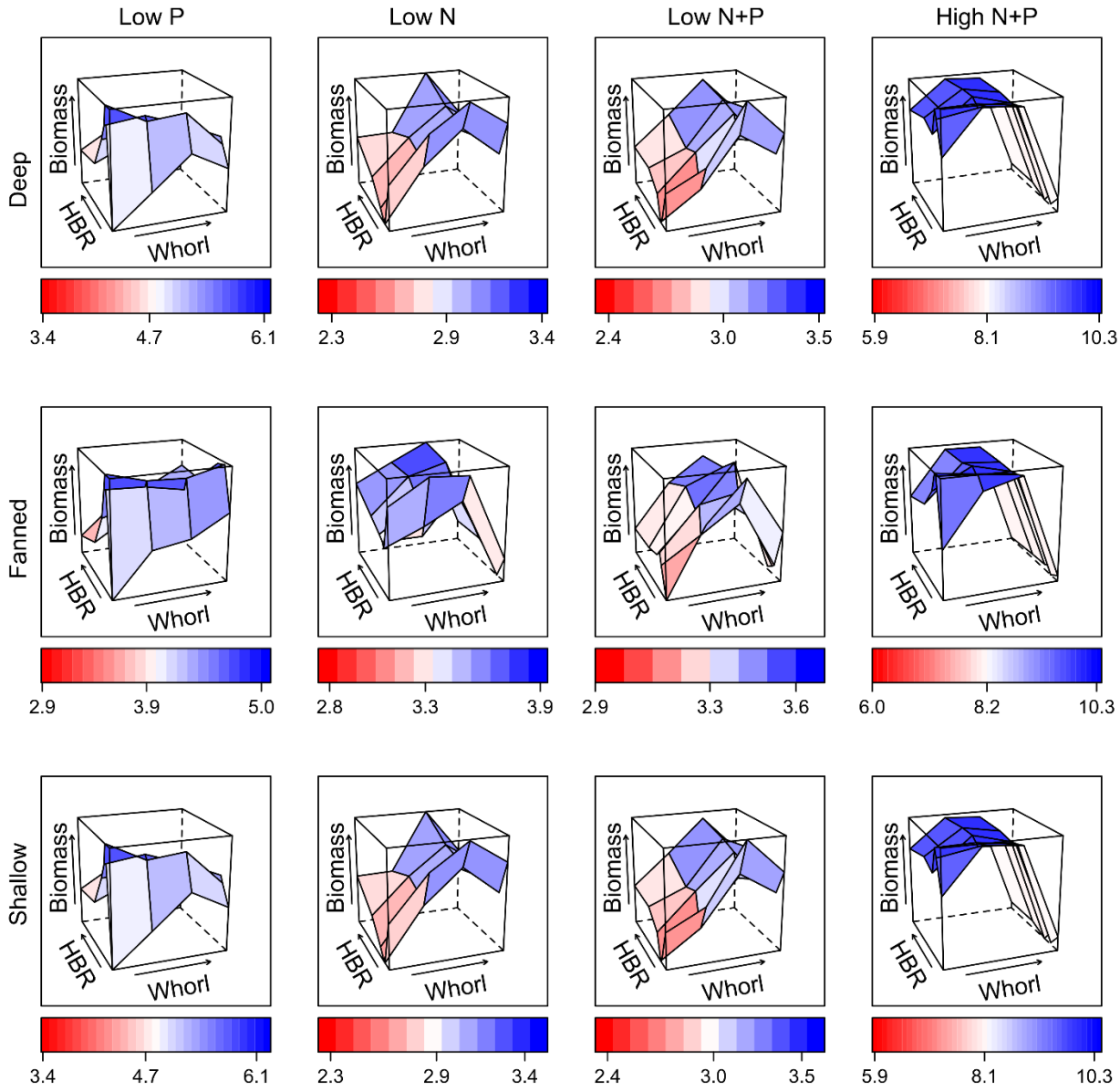

Figure 2-9: Shoot biomass at 40 d after germination in plants with one, two, three and four whorls and different number of hypocotyl-borne roots at low phosphorus, low nitrogen and combined low phosphorus and low nitrogen availability. The color scale represents biomass in g per plant. The arrow in the axes indicated the direction of increasing whorl number, HBR or biomass.

Table 2-1: Root angles and basal root whorl number used in simulation of bean root architecture. *Whorl position was counted from basipetal to acropetal position.

	Whorl Position*	Shallow	Fanned	Deep
One-whorl	Whorl 4	5	45	85
Phenotype	Whorl 3	-	-	--
	Whorl 2	-	-	
	Whorl 1	-	-	
Two-whorl	Whorl 4	5	25	65
phenotype	Whorl 3	25	65	85
	Whorl 2	-	-	-
	Whorl 1	-	-	-
Three-whorl	Whorl 4	5	25	45
phenotype	Whorl 3	25	45	65
	Whorl 2	45	65	85
	Whorl 1	-	-	-
Four-whorl	Whorl 4	5	5	25
phenotype	Whorl 3	25	25	45
	Whorl 2	45	65	65
	Whorl 1	65	85	85
Mean of angles		< 45	45	> 45

Chapter 3

Multi-objective optimization of root phenotypes for nutrient capture using evolutionary algorithms

ABSTRACT

Root phenotypes are avenues to the development of crop cultivars with improved nutrient capture, which is an important goal for global agriculture. The fitness landscape of root phenotypes is highly complex and multidimensional. In this study, we demonstrate the application of a Multi-Objective Optimization Algorithm (MOEA) to find optimal root architectures for the acquisition of N and P by maize and common bean. The three-dimensional structural functional root architectural model, *SimRoot*, was linked to the Borg MOEA, and the optimization runs were evaluated for several generations to find the optimal root phenotype in terms of biomass production, nutrient acquisition and root carbon costs. The solution set identified multiple optimal phenotypes for the objectives. The optimal phenotype was dependent on the limiting nutrient as well as how limiting the nutrient is. Phenotypes were found to co-optimize several objectives but none of the phenotypes performed the best in all the objectives. Optimal phenotypes reflected the trade-offs between objectives. Some trade-offs such as those between root carbon cost and shoot biomass were common in all regions of the landscape whereas others such as between uptake of different nutrients and shoot biomass were specific to specific regions. Several combinations of root phenes generated optimal integrated phenotypes, and such combinations differed for mobile nutrient and non-mobile nutrient and for maize and bean. The number of optimal phenotypes decreased in the order of low N+P, low N, low P. We demonstrate that FSPM can be used with multiobjective optimization to identify optimal root phenotypes under various environments.

INTRODUCTION

Root system architecture (RSA) plays key roles in a range of processes from anchorage to nutrient and water acquisition (Lynch, 1995; Voss-fels et al., 2018). Increased nutrient acquisition can increase fertilizer use efficiency and is critical for crop production. Genotypes

with optimal RSA can be exploited for crop design especially with respect to plant breeding in infertile soils (Kong et al., 2014; Meister et al., 2014; Paez-Garcia et al., 2015; Koevoets et al., 2016; Lynch, 2019). However, an important obstacle to deploying root phenotypes in crop breeding is that we do not understand the utility of specific phenotypes in specific soil environments (Lynch, 2019; Schneider and Lynch, 2020).

Root phenotypes are comprised of phenes which exist in several states, which may be beneficial in specific scenarios. Fitness tradeoffs for contrasting soil resources, and between abiotic and biotic constraints, are important (Ho et al., 2005; Hu et al., 2014; Postma et al., 2014a; Miguel et al., 2015; Dathe et al., 2016; Galindo-Castañeda et al., 2018; Rangarajan et al., 2018; Yang et al., 2019). In addition to tradeoffs for external resources, the fitness landscape of specific phene states is dependent on other aspects of the plant phenotype. Dynamic constraints such as carbon availability further increase the complexity of the system. For example, phosphorus-deficient plants have smaller leaves and slower leaf appearance resulting in reduced sink strength of the shoot, thereby increasing relative allocation of carbon to the root system, whereas nitrogen deficiency slows growth, sometime severely, due to reduction in photosynthetic efficiency, both engendering C limitations, though, in different ways (Sinclair and Horie, 1989; Lynch et al., 1991). Identifying optimal integrated phenotypes is a highly complex, nontrivial challenge.

Considering multiple states for each phene, phene synergisms and antagonisms, acquisition of multiple nutrients simultaneously, multiple soil types, multiple precipitation regimes etc., the number of relevant scenarios is of the order of 6×10^{23}. Moreover, when evaluating the functional benefits of alternative trait interactions there a large number of conflicting objectives (e.g., maximize biomass production, minimize nutrient requirements, etc.). Therefore, the challenge of mapping and understanding the fitness landscape for root phenotypes (i.e., the relationship of root phenes and root phenotypes to plant performance), is a hugely complex and challenging nonlinear problem. In a recent study with three root phenes (BRWN [Basal Root Whorl Number], RGA [Root Growth Angle], and LRBD [Lateral Root Branching Density]) in contrasting and extreme phene states combined factorially, we have shown that interactions among phenes in combination with trade-offs due to carbon limitations result in several distinct root architectures with varied fitness in environments varying in nutrient availability. However, there is no single optimal architectural phenotype; there exist multiple co-

optimal root architectural phenotypes for a given environment (Rangarajan et al., 2018). The findings of multiple optimal integrated phenotypes have been supported by a recent study which identified multiple integrated root phenotypes associated with improved drought tolerance in maize (Klein et al., 2020). These phenotypes were found to co-optimize three strategies; enabling greater root construction and soil exploration by reducing maintenance costs brought about by increase in aerenchyma formation and larger cortical cells; increasing penetrability by formation of thicker roots with larger proportion of stele, and slower water extraction by restricted hydraulic conductance through narrower metaxylem vessels (Klein et al., 2020).

One approach to identify optimal root phenotypes in a varying nutrient landscape is via Multi-Objective Evolutionary Algorithms (Coello Coello et al., 2007). Multi-objective algorithms were chosen over other optimization techniques because there are multiple objectives to optimize, and most of the decision variables (*i.e.* input parameters) are continuous, so by discretizing the decision space, there are an extremely large number of model configurations to evaluate. Inherent trade-offs exist between component of fitness which limits the set of potential phenotypes (Ho et al., 2005), therefore, the integrated phene space is discontinuous. Evolutionary algorithms in multi-objective search and optimization are effective in their ability to handle complex problems, involving features such as discontinuities, multimodality, disjoint feasible spaces and noisy function evaluations (Fonseca and Fleming, 1995). Multi-objective evolutionary algorithm frameworks, particularly Borg (Hadka and Reed, 2013), have been shown to give better solutions than other evolutionary algorithms and random evaluations in several real-world optimization applications. The premise of multi-objective optimization is that the best phenotype for one task is usually not the best for other tasks—resulting in a fitness tradeoff. Tradeoffs occur when the benefit of one trait comes at the cost of allocating resources to a different trait (Kimball et al., 2013). Biomass is the result of trade-offs between uptake of nutrients which require deployment of strategies which are conflicting in functionality. Tradeoffs also exist among different phenes in terms of function as well as carbon investment required. Due to these tradeoffs, different strategies are adapted by different phenotypes to obtain comparable biomass. Addressing the optimization as a single objective problem, i.e. evaluation of the phenotypes based solely on their biomass, will result in a single optimal solution while disregarding a wealth of information regarding comparable phenotypes. The result of the multi-objective optimization is a set of non-dominated solutions (Pareto optimal solutions), which are

points on the pareto–front (Coello Coello et al 2007; Noor and Milo 2012; Shoval et al. 2012). This set comprises phenotypes whose performance in one objective cannot be improved without reducing performance in the other objectives.

SimRoot, a functional-structural plant model has been used extensively for elucidating the functional value of one or more phenes, and to analyze phene interactions (Walk et al., 2006; Lynch, 2007; Postma and Lynch, 2011a; Postma and Lynch, 2011b; Postma et al., 2014; Dathe et al., 2016; Rangarajan et al., 2018). In this study, we use Borg with *SimRoot* to identify optimal root phenotypes of common bean (*Phaseolus vulgaris)* and maize (*Zea mays*), representing a dicot and a monocot species that are both primary global food security crops. The optimizing routine searches the decision space constrained by a range of root phenes while optimizing for several objectives including maximizing phosphorus uptake, nitrate uptake, shoot biomass and rooting depth while minimizing carbon investment in root construction and maintenance including root respiration. Rooting depth was chosen as an objective in the study. Deeper rooting improves water and N capture in many agroecosystems ((Tuberosa, 2012; Wasson et al., 2012; Comas et al., 2013; Lynch, 2013; Maeght et al., 2013; Lynch and Wojciechowski, 2015; Pierret et al., 2016; Lynch, 2019), and increases the stability of plant-derived carbon (C) in the soil. Globally, soil C is estimated to be twice as large as the pool of atmospheric C (Kell, 2011, 2012), and the capacity of soils to retain C has not yet been saturated. Since the depth of C deposited in the soil by root activity is related to its residence time, deeper crop rooting, achieved by genetic selection or agronomic management, has been proposed as a viable option to sequester atmospheric CO_2 and partially mitigate global climate change (Rasse et al., 2005; Gewin, 2010; Kell, 2011; Kell, 2012; Grieder et al., 2014). Numerous combinations of root phenes could generate integrated phenotypes and such combinations differ between monocots and dicots, and among taxa within these groups (Lynch, 2019). Using *SimRoot* with Borg, we are able to identify optimal integrated common bean and maize root phenotypes which have optimal phosphorus and nitrate uptake, representing a mobile and immobile nutrient in the soil, under a dynamic constraint imposed by carbohydrate availability.

METHODS

Description of the model

In this study, the functional-structural plant model *SimRoot* (Lynch et al., 1997; Postma and Lynch, 2011; Rangarajan et al., 2018) was used in conjunction with Borg (Hadka and Reed, 2013), a multi-objective evolutionary algorithm. Evolutionary algorithms are nature inspired heuristic stochastic algorithms. In these algorithms the space of parameters are encoded as strings and the algorithm use these strings to create populations of candidate solutions and the principle of survival of the fittest selects those candidates that are better in terms of objective function (fitness function). The Borg multiobjective evolutionary algorithm (MOEA) is a many objective, multimodal optimization procedure (Hadka and Reed, 2013). It represents a class of algorithms whose operators are adaptively selected based on the problem and combines ε-dominance, ε-progress and randomized restarts (Hadka and Reed, 2013). The algorithm includes an ε-box dominance archive for maintaining convergence and diversity through-out search, use of ε-progress, which is a computationally efficient measure of search progression and stagnation, an adaptive population sizing operator to maintain search diversity and to facilitate escape from local optima, and multiple recombination operators to enhance search in a wide assortment of problem.

Figure 3-1 outlines the functioning of the *SimRoot*-Borg evaluation system. The parameters explored (also called input variables or decision variables) are root phene states including angles, number of roots, lateral root branching density. The numerical outputs from *SimRoot* model are used as the objectives subjected to optimization. The constraints on the range of values a decision variable can assume is set based on studies on root trait variations derived from phenotypic studies in published literature and this defines the space to be explored within a given domain of variation. The input variables for the maize root system and bean root phenotypes included in the study with the constraints on the range of values are presented in Table 3-1 and 3-2 respectively.

Population size and the number of generations were chosen after performing many simulations and taking into account the needs of our case study. Preliminary studies showed that the optimization runs headed towards regions of high nutrient availability. In order to include all regions of the nitrate phosphorus availability landscape, availability was included as an objective

which was minimized. Optimization runs were conducted on Texas Advanced Computing Center's Stampede and Cornell University's The Cube. 50,000 runs corresponding to 500 generations were run with at least 5 random seed resulting in at least 250,000 total evaluations each for the bean system and maize system and the solutions from the end of the run with each seed were used for further analysis. Epsilon values corresponding to 10% of objective values were used. Solutions from specific regions in the nitrate and phosphorus landscape were selected further analysis. The regions included corresponds to regions with low phosphorus and non-limiting nitrate, low nitrate and non-limiting phosphorus and regions where both nitrate and phosphorus were limiting.

Analysis of simulation results

Model outputs and visualization of the objective space

SOM was performed to analyze the objective space within the Pareto-optimal set of solutions. The pareto-optimal solutions consist of a variety of distinct phenotypes which differ in their performances in one or more objectives. Self-organizing maps (SOMs) provide a graphical and qualitative way of extracting knowledge. SOMs result from a process in which neighboring clusters influence each other, resulting in a network topology reminiscent of biological systems (Kohonen, 1997; Wehrens and Buydens, 2007). A SOM allows the projection of information embedded in the multidimensional objective and decision spaces onto a two- dimensional map (Bandaru et al., 2017). All phenotypes, regardless of the region in the nitrate -phosphorus landscape they evolved in, were clustered under a SOM scheme (som function).1000 training iterations were used during clustering, over which the α-learning rate decreased from 0.05 to 0.01. Phenotypes are thus assigned to a node in the SOM grid based on their combined performance in all the objectives. In this way different phenotypes in the pareto front are clustered solely based on their position in the objective space. Phenotypes evolved in different regions of the nitrate/phosphorus landscape having similar performances in all the objectives were clustered on the same or neighboring nodes by this method.

Analysis of optimal phenotypes

Nodes containing phenotypes with greater biomass under each combination of available nitrate and phosphorus was considered for further analysis. The optimal phenotypes resulting from the

optimization procedure are obtained as vectors of numerical values of root traits corresponding to each root type. These values are in a continuous space and to represent them, a heatmap plot was used. The root systems were simulated based on the optimized root phene values and images rendered for visualizing the root phenotype.

Several phenotypes were seen in the optimal set. Three phenotypes were selected for further analysis in each region of the NP landscape (low P, low N, low N+P). A sensitivity analysis was conducted on the phenotypes evolved in low N region by varying the number of nodal roots.

RESULTS

The objective space

2700 maize solutions and 2400 bean solutions corresponding to optimal phenotypes in regions varying in nitrate and phosphorus were obtained. Shoot biomass, phosphorus uptake and nitrate uptake were maximized in the optimization routines. The Pareto solutions were obtained in the multi-dimensional objective function space (5 dimensions for bean root system; biomass, P uptake, N uptake, carbon cost and root respiration and 6 dimensions for the maize root system; biomass, P uptake, N uptake, carbon cost, root respiration and root length at depth). The pareto-front is mapped onto the two-dimensional Self-Organizing Map (SOM) (Kohonen, 1997), according to the scaled objective function values, where trade-offs are successfully visualized. The clustering by SOM can be visualized as fan plots or as SOM heatmaps. The performances of the various phenotypes in different objectives in the optimal solution set of bean and maize root system in a region with low N+P is visualized in Figure 3-2(a) and Figure 3-2(c) respectively. The complete pareto set obtained from the bean and maize optimization routines are shown in Supplementary Figure 3-S1(a) and Supplementary Figure 3-S1(b).

Regions with greatest shoot biomass corresponded to regions with greatest nutrient availability, however, not all phenotypes evolved under greatest nutrient availability had high shoot biomass. Root carbon cost and root respiration were minimized in the optimization routine. The regions with low carbon cost and low respiration typically had low phosphorus uptake, nitrate uptake and so, low biomass also (Figure 3-2(a), Figure 3-2(b) node 9; Figure 3-2(c), Figure 3-2(d) node 7, Supplementary Figure 3-S1(a), Supplementary Figure 3-S1(b) region 1).

Phenotypes with good biomass varied in carbon costs. Few phenotypes had very good nitrate uptake and/or very good phosphorus uptake in every region of the NP landscape. Phenotypes with good biomass had good nitrate and phosphorus uptake but phenotypes with very good nitrate uptake or phosphorus uptake did not necessarily have the greatest shoot biomass and depended upon the carbon invested in the root system (Figure 3-2(c), Figure 3-2(d): node 9). Regions with optimal biomass were regions which had intermediate performances in all other objectives (Figure 3-2(a), Figure 3-2(b): node 4; Figure 3-2(c), Figure 3-2(d): node 3, Supplementary Figure 3-S1(a), Supplementary Figure 3-S1(b) region 2).

Different phenotypes had different performances in different objectives in the same region of the NP landscape. Trade-offs between objectives were seen in different regions of the landscape. The trade-offs in performance in the objective was specific to specific NP regions. For example, phenotypes optimizing for greater P uptake in a low P environment were also the ones which had the greatest biomass (Figure 3-3: Phenotype a1). However, phenotypes optimized for P uptake in a low N environment had less than optimal biomass for that region of the NP landscape (Figure 3-3: Phenotype b2)).

The maize root optimization routine included an objective to find optimal phenotypes which had greatest root length at deeper soil strata, i.e., maximize root length at greater depth. Many phenotypes with the greatest root length in deeper soil strata were also the phenotypes which had good nitrate uptake and consequently good biomass (Supplementary Figure 3-S1(b) region 3). There were also phenotypes which had good root length but not as efficient in accumulating biomass (Figure 3-4).

Different phenotypes had similar performances in at least one of the objectives in the same region of the NP landscape, i.e. multiple optimal phenotypes existed for an objective. For example, the phenotypes evolved in a region of the landscape with suboptimal N and P had less than 10% Coefficient of variation (CV) in all the one of the objectives i.e. shoot biomass whereas they had greater than 10% CV in other objectives. (Supplementary Figure 3-S2, Supplementary Figure 3-S3). Similar trends were seen in other regions of the NP landscape too. In this study we focus on optimal phenotypes for shoot biomass in bean and maize and for greater rooting depth in maize. The data corresponding to these objectives, irrespective of how they performed in the other objectives, in specific regions of NP landscape corresponding to low P, low N and low N+P were further analyzed.

The phenotypic space / Morphospace

Preliminary investigation of the optimal phenotypes suggested that not all combinations of states of different phenes were represented in the final optimal solution set. The phene states of the constituent phenes represented in the optimized phenotypes had very skewed distribution. For better interpretation of the characteristics of the optimal solutions, the phenotypes were analyzed at the root class levels.

Primary root (PR): The primary root phenotype in bean and maize root system is defined by diameter and LRBD. Phenotypes with primary roots differing in both diameter and LRBD were found among the optimal solutions of both bean as well as maize (Supplementary Figure 3-S4(a), Supplementary Figure 3-S4(b)). None of the optimal phenotypes had high values for both diameter and LRBD in bean or maize. Some phenotypes had very large diameter and some very high LRBD (Supplementary Figure 3-S4(a), Supplementary Figure 3-S4(b)). Phenotypes with large diameter primary roots typically had low biomass and also low carbon cost and lower respiration in bean as well as maize. Phenotypes with very high LRBD were seen in phenotypes optimal under low P in bean and in maize root systems. Roots under low P had smaller primary root diameter than under low N or low N+P (Figure 3-5(a), Figure 3-5(b)).

Hypocotyl-borne roots (HBR) in bean: The HBR phenotype is defined by the number of root axes, their diameter and LRBD, and phenotypes differing in all three of these phenes were found among the optimal solutions in bean (Supplementary Figure 3-S5). Phenotypes with more HBR as well as greater LRBD of HBR were found in optimal phenotypes evolved under low P (Figure 3-5(a)). Some phenotypes did not have any HBR and were typically found in regions low in N and under very low P (Supplementary Figure 3-S5).

Seminal roots (SR) in maize: The SR phenotype is defined by the number of root axes, and their angle, diameter and LRBD. Phenotypes differing in all of these phenes were found among the optimal solutions in maize (Figure 3-6). Some optimal phenotypes had no SR whereas some had many SR. Under low P, phenotypes had fewer SR, which were highly branched and had shallow growth angles. Under low N, phenotypes had deep angled SR, with very few lateral roots. Phenotypes under low P had shallow SR, while those under low N had deep angles and those under low N+P had intermediate SR angles. Greatest LRBD in SR was found in regions with low P (Figure 3-5(b)). The seminal root characteristics were dependent on the primary root. For example, if the primary root diameter was larger than 2 mm, there were more constraints on the

possible phene states of SR phenes; there was a constraint on SR LRBD in that high LRBD SR were not found when primary root diameter was large (Figure 3-6).

Basal roots (BR) in bean: The BR phenotype is defined by the number of root axes, and their angle, diameter and LRBD as well as the BRWN. Small diameter, highly branched, shallow basal roots were found almost exclusively in low P regions as well as in low N+P (Figure 3-5(a)). Basal root phenotypes in low N are distinctly different from those expressed in low P conditions and typically had more basal roots with fewer lateral roots (Figure 3-5(a)) and had a wide range of root growth angles. The basal root phenotypes found in the optimal bean phenotypes are presented in Supplementary Figure 3-S6.

Nodal roots (NR) in maize: The NR phenotype is defined by the number of root axes, and their angle and diameter as well as time of emergence. Optimal phenotypes under low P had fewer NR while those under low N had more NR (Figure 3-5(b)). Phenotypes with the greatest NR LRBD were found in the low P region (Figure 3-5(b)). The nodal root phenotypes found in the optimal maize phenotypes are presented in Supplementary Figure 3-S7.

The integrated phenotype

The optimal phenotypes that evolved in different regions of the NP landscape were based on certain root class specific phenotypes. None of the phenotypes had the maximum potential value for all the phenes even under non-limiting nutrient conditions, i.e., huge root systems were not found in the optimal set. Some of the optimal bean and maize root phenotypes in high N+P region are depicted in Supplementary Figure 7. There were differences in root class phenotypes in different regions of the NP landscape. Optimal phenotypes under low P had the greatest LRBD, shallowest angles, greatest number of roots (Figure 3-5(a), 3-5(b)) and whorl occupancy

The characteristics of root classes emerging later in development depended upon the already emerged phenotype as well as nutrient availability in a particular region of the NP landscape. For example, optimal maize roots with very highly branched primary roots were found in regions with suboptimal P, suboptimal N as well as suboptimal N+P regions but with different states of phenes of the SR and NR (Figure 3-7). While phenotypes in suboptimal P had no SR (Figure 3-7: Phenotype a), those under suboptimal N had a large number of SR with steep growth angles (Figure 3-7**:** Phenotype b) and when both P and N were suboptimal, the phenotype with highly branched PR had shallow-angled SR (Figure 3-7**:** Phenotype c).

Optimal bean root phenotypes under low P had highly branched PR with few highly branched, shallow BR and more HBR (Figure 3-8: Phenotype Low P1). Other optimal phenotypes under low P included a phenotype with more BR and greater LRBD and no HBR (Figure 3-8: Phenotype Low P2). A phenotype with more BR with varying number of branches and few HBR was also found to be optimal in low P (Figure 3-8: Phenotype Low P3). Tradeoffs between the number of BR, BR LRBD and number of HBR with shallow angled BR resulted in optimal phenotypes in low P. Optimal bean root phenotypes under low N had slightly larger diameter PR than optimal phenotypes under low P, more basal whorls were occupied with varying number of BR and LRBD and varying RGA (Figure 3-8: Phenotype Low N1). A phenotype with well-developed PR having optimal LRBD and very few BR with intermediate angles, very low BR LRBD, no HBR was also found to be optimal under low N (Figure 3-8: Phenotype Low N2). This phenotype, Phenotype Low N2, had very few axial roots which enabled much greater production of primary and secondary root laterals of PR (Figure 3-8: Phenotype Low N2). The combination of low carbon cost due to very few axial and a well-developed primary root resulted in a phenotype optimal under low N. Another optimal phenotype under low N had greater occupancy at basal whorls, with few roots at each whorl and BR with more branches and intermediate angles (Figure 3-8: Phenotype Low N3). More whorl occupancy with few roots at each whorl, varying number of BR with varying angles and very few LRBD as compared to optimal phenotypes under low P were characteristic of optimal bean root phenotypes under low N. Optimal bean phenotypes under low N+P conditions had phenotypes with few or medium number of lateral roots, intermediate growth angles and few or no HBR (Figure 3-7: Phenotype Low N+P1, Phenotype Low N+P2, Phenotype Low N+P3).

Maize root phenotypes in low P had highly branched primary roots with no SR and few NR (Figure 3-9: Phenotype Low P1), or primary roots with very low LRBD, no SR and highly branched NR (Figure 3-9: Phenotype Low P2) or primary roots with very few branches and highly branched shallow SR with few NR with very low LRBD (Figure 3-9: Phenotype Low P3). Under Low N, one of the optimal maize phenotypes had more SR with intermediate branching (Figure 3-9: Phenotype Low N1) and very few deep NR with very low LRBD. Another optimal phenotype under low N had SR with very few branches and many NR with very low LRBD. This phenotype had more NR with some NR with deep angles and some with shallow angles (Figure 3-9: Phenotype Low N2). A phenotype with more SR with few lateral root branches and few NR

with greater LRBD was also found to be an optimal phenotype under low N (Figure 3-9: Phenotype Low N3). Under low N+P, varying number of SR and SR LRBD as well as varying NR number and NR LRBD with intermediate root growth angles were found among the optimal maize phenotypes (Figure 3-9: Phenotype Low N+P1, Low N+P2, Low N+P3)

Sensitivity analysis

While phenotypes with low P tended towards very high LRBD obtained in terms of high LRBD in PR or SR or NR, those under low N had different phenotypes varying specifically only in SR LRBD and number of nodal roots or NR LRBD and number of nodal roots. Varying all the parameters to perform sensitivity analysis would be computationally very expensive. So, we conducted a sensitivity analysis by varying only the number of nodal roots in the three optimal phenotypes presented under low N. (Figure 3-10). We changed the number of nodal roots in two distinct optimal phenotypes under low N (Phenotype Low N1, Phenotypes Low N2) and analyzed the performance of the phenotypes in various objectives and found that the biomass of several phenotypes with different number of nodal roots were comparable, while the performance in other objectives varied. This suggests that when the state of a single phene is varied, the states a particular phene could occupy to result in optimal biomass is not a single unique value but a range of values, as long as roots are allocated to regions with greater resource availability (Figure 3-10(a), Figure 3-10(b)) and there is balance in the tradeoffs in carbon costs and nutrient acquisition.

DISCUSSION

In this study we used *SimRoot*, a FSPM with Borg, a multi-objective evolutionary algorithm to identify optimal maize and bean root phenotypes in environments with varying availability of N and P. Nutrient uptake and biomass were maximized while root carbon costs were minimized in the routine and the optimal root phenotypes were identified by estimating the performances of various phenotypes generated by varying the states of phenes such as the number of root axes, root growth angle, diameter and branching density of different root classes. Using the Borg-*SimRoot* framework, we were able to obtain optimal root phenotypes under varying levels of N and P in bean and maize root systems. Nitrogen and P are primary limitations to plant growth in

terrestrial environments, and providing an interesting contrast in that N (as nitrate) is highly mobile in soil water whereas as P is highly immobile in soil. These two resources therefore represent two broad classes of resources; mobile (including water and nutrients soluble in water such as nitrate, sulfate, Ca, Mg, silicate) and immobile (remaining nutrients). We analyzed root phenotypes of two species, maize and common bean, representing a monocot and a dicot root architecture. The main difference between dicot and monocot root systems is that new roots (laterals) emerge from already existing roots in dicots, whereas in monocots nodal roots continually emerge over time from shoot nodes near or above the soil surface. Similarities and differences were seen among the optimal phenotypes in the two species. While diameter of all root classes in both species were optimized towards thinner diameters, states of the other phenes varied based on the limiting nutrient. Some strategies for optimal nutrient uptake were similar while others differed between bean and maize. Multiple phenotypes with similar biomass were seen in each region of the NP landscape. The optimal phenotypes were distinct based on trade-offs between root class for optimum nutrient uptake to maximize shoot biomass while being economical in terms carbon invested in the root system.

SimRoot is a FSPM which considers the dynamic feedbacks between function and structure, spatial and temporal heterogeneity in resource distribution and competition and also includes costs and benefits of different root phenes and growth strategies, was used in this study to generate and evaluate various root phenotypes (Lynch et al., 1997). *SimRoot* has been extensively used to evaluate trait utility, estimate process such as competition for soil resources within and among neighboring plants, discover new traits, and to evaluate phenotypes and environments that do not exist in nature (Postma and Lynch, 2011a; Postma and Lynch, 2011b, York and Lynch, 2015; Rangarajan et al., 2018; Strock et al., 2018; Benes et al., 2020). Few studies have attempted to optimize root phenotypes, typically using simple representations of root structure and function and relatively few parameters (Dunbabin et al., 2003; Ho et al., 2004) and fewer studies have used evolutionary algorithms towards attaining this goal. Evolutionary algorithms and plant structural models have been used to explore multicriteria fitness landscapes for shoots (Niklas, 1994). A study by Renton and Poot (2014) used an evolutionary optimization algorithm to simulate the evolution of water foraging strategies using a simple representation of the dynamic root structure. The complexity of both the root phenotype and the soil environment, the large number of parameters involved and their dynamic nature make exploring all possible

parameter combinations to identify optimal phenotypes a nontrivial computational challenge (Lynch and Brown, 2012; Renton and Poot, 2014; Rangarajan et al., 2018).

Optimal root phenotypes in low P

Phenotypes with maximum biomass under low P had the greatest LRBD in both maize and bean. Studies have shown that greater LRBD and more axial roots are independently beneficial for P uptake (Lynch, 2007; Postma et al., 2014a; Jia et al., 2018; Rangarajan et al., 2018; Sun et al., 2018; Lynch, 2019). However, the optimal number of axial roots depends on the LRBD (Rangarajan et al., 2018). The phenotypes optimized under low P prioritized greater LRBD over production of more axial roots in maize as well as bean resulting in root phenotypes with greater soil exploitation, a requirement for the uptake of immobile soil resources such as P. Bean had shallow basal roots with a very narrow range of growth angles; this is in agreement with several studies which show that topsoil foraging is beneficial for P uptake (Liao et al., 2001; Rubio et al., 2003; Ho et al., 2004; Ho et al., 2005; Lynch and Ho, 2005; Zhu et al., 2005; Lynch, 2011; Miguel et al., 2013; Kong et al., 2014; Rangarajan et al., 2018). However, maize did not have very shallow root growth angles. Like other monocots, maize continually forms nodal roots which pass through topsoil as they descend to deeper soil strata (Lynch and Wojciechowski, 2015) and so are not dependent on an exclusively shallow angled root class for topsoil exploration, unlike dicots. The different alternate bean root phenotypes selected as optimal were variation of the same phenotype with occupancy at different whorls. Basal roots emerge around the same time (Basu et al., 2007; Miguel et al., 2013) and since the states of the other basal root phenes were similar except for the whorl position in several of the phenotypes, these phenotypes were not very distinct from each other, resulting in fewer distinct phenotypes under low P. In the case of maize, temporal variation in emergence of different classes of roots (Hoppe et al., 1986) results in more distinct phenotypes for phosphorus uptake as compared to bean. At very low P, optimal maize phenotypes had a highly branched primary root with an absence of seminal roots. The large carbon cost imposed by a highly branched primary root and absence of emerging seminal roots for next few days enabled better primary root, which subsequently supported production of more nodal roots. In bean, the basal roots emerge soon after germination, forming the scaffold of subsequent lateral roots. However, hypocotyl-borne roots emerge much later and are restricted in their root growth angle, growing almost horizontally, exploring almost

exclusively the topsoil(Miller et al., 2003)) unlike nodal roots in maize which have a greater range of growth angles (Trachsel et al., 2011; Trachsel et al., 2013; Wu et al., 2014; Dathe et al., 2016). Hypocotyl-borne roots are therefore well-represented in the optimal phenotypes under low P but not under low N. Hypocotyl-borne roots with greater plagiogravitropism in dicots such as those in cowpea (Burridge et al., 2016) could enable more varied phenotypes under low P similar to those seen in maize. The effects of other complementary traits for phosphorus acquisition such as root hairs, colonization by mycorrhiza, etc. (Zhu et al., 2006; Miguel et al., 2015; Hochholdinger, 2016; Galindo-Castañeda et al., 2018) have not been included in this study and could certainly have a significant influence in determining optimal number of axial and LRBD.

Optimal root phenotypes in low N

Phenotypes evolving in a low N environment have to optimize against another level of complexity as compared to those in low P due to fact that nitrate availability varies spatially and temporally. Nitrate has greater mobility than P and competition for mobile resources is much greater than for immobile resources (Postma and Lynch, 2012; Postma et al., 2014a). The greater number of constraints for N uptake results in a greater number of distinct optimal phenotypes under low N than under low P in both maize and bean. It is well established that the number of optimal phenotypes increases in proportion to the number of biological tasks that must be simultaneously performed (Niklas, 1997). Optimal phenotypes under N-limiting conditions had steep root growth angles or had a wide range of growth angles and low LRBD in both maize and bean. The utility of low LRBD and steep root growth angles for N uptake under low N conditions is well established (Lynch, 2013; Trachsel et al., 2013; Postma et al., 2014a; Lynch and Wojciechowski, 2015; Zhan et al., 2015; Dathe et al., 2016; Rangarajan et al., 2018, Lynch, 2019). We found that optimal phenotypes under low N were those that were able to place roots where nutrient availability was greatest (Dathe et al., 2016) while being economical in carbon investment. By investing in axial roots with low LRBD, the optimal phenotype is able to reduce carbon cost, while the number and angle of axial roots at different nodes/whorls result in a wide range of angles allowing greater soil exploration by optimally placing roots in regions with greater nutrient availability. The performance of the optimal phenotypes was not sensitive to root growth angles as long as the angles were not too deep as roots with very deep angles resulted in

competition between roots (Ge et al., 2000; Rubio et al., 2001, Dathe et al., 2016). The emergence of roots at different nodes sequentially over time enabled maize to adopt other strategies of optimizing nitrate uptake. One strategy was to develop a deep seminal root system with an optimal number of branches, such that the benefit of having more branches outweighs the effect of competition, enabling early vigorous root growth with deep soil exploration. Seminal roots are known to be important for seedling vigor during early development (Hochholdinger et al., 2018, Perkins and Lynch, 2020). In wheat, by the time the nodal roots appear, the seminal root system was found to be up to 40 cm deep in the soil. Increasing root length contributed by seminal roots is thought to increase water extraction from deeper soil layers (Richards, 2008). An added advantage of vigor during early development is that greater root and shoot development earlier during the season could synchronize with availability of N in the topsoil while reducing loss of nitrogen especially in soils prone to leaching. The phenotypes in the optimal set varied in the number of crown roots. While previous studies have shown that fewer crown roots are efficient for N capture (Saengwilai et al., 2014), our study shows that the optimal nodal root number depends on LRBD of nodal roots as well as the branching frequency and number of seminal roots. Phenotypes with fewer nodal roots with very low LRBD were beneficial when expressed with a well-developed seminal root system, and phenotypes with fewer nodal roots with relatively greater LRBD were beneficial when the seminal LRBD was low. A highly branched seminal or nodal root system had better nutrient acquisition with a large carbon cost associated with the greater LRBD of the seminal roots or nodal roots. In contrast, a phenotype with more nodal roots with very low LRBD was beneficial when the seminal roots had very fewer branches. In the low LRBD phenotype with more nodal roots, the root system did not acquire as much nutrients as the well branched phenotype, but since the carbon cost of the root system was much lower in comparison to the well branched seminal roots and few nodal roots phenotype or the well branched few nodal root phenotype, all three phenotypes varying in the number of nodal roots had comparable biomass. With an increased number of nodal roots, the length of the lateral roots is reduced, however, the resulting phenotypes will still have comparable biomass as long as roots coincide with regions of high nutrient availability in time and space and, tradeoffs in the different root classes do not result in phenotypes with vastly different total carbon cost or resource acquisition.

Optimal root phenotypes in low N+P

The importance of colocalizing root foraging and nutrient availability becomes evident when multiple nutrients are limited. Optimal phenotypes in low N+P had integrated strategies optimized for uptake of both N and P. The phenotypes were found to have roots with more node/whorl occupancy and a wide range of growth angles as were seen in optimal phenotypes in low N. The LRBD was intermediate between those in low P and low N, with shallower roots having more branches than deep roots. This ensured that efficient soil exploitation could occur in regions with greatest availability of phosphorus while exploring for nitrate in subsoil. Even though the number of whorls occupied were more in the optimal phenotypes under low N+P, the number of roots per node was low. The different states of the number, growth angle and LRBD of roots at different whorls in bean ensured that the root system had a wide range of angles for exploring maximum soil volume. Another strategy was to have roots that were neither deep nor shallow but intermediate angled roots. Basal roots in bean and nodal roots in maize with optimal number of branching were found to assume intermediate angles when both N and P were limiting. Dimorphic root architectures with axial roots with greater range of growth angles, or comprising of specific combinations of topsoil foraging such as HBR with traits for subsoil foraging such as steep axial growth angles are thought to be efficient for uptake of P and N (Miller et al., 2003; Miguel et al., 2013). Maize roots with early shallow and late deep rooting are dimorphic (Postma et al., 2014b; Lynch, 2019). Dimorphic root systems (Burridge et al., 2020; Lynch, 2019) with shallow and deep roots are also efficient for uptake of mineralized and leached N (Ho et al., 2005). A phenotype with greater LRBD in the topsoil and fewer LRBD in the subsoil along the same axial root is thought to be an important (Kong et al., 2014), however, such phenotypes were not seen in our simulations because plasticity was not included in out simulations. The utility of plasticity varies depending on the environment and is poorly understood (Schneider and Lynch, 2020). Under low N+P, several phenotypes were found to be optimal. The phene states occupied by the various phenes were intermediate in terms of LRBD as well as angles. This along with more whorl/ node occupancy and fewer roots resulted in many combinations of phenes resulting in greater number of optimal phenotypes than in low P or low N.

Phenotypes with large diameter / low carbon cost

Optimal phenotypes had small root diameter with those under low N having slightly larger diameter than those in low P. While small diameter roots are cheaper to construct and maintain, large diameter roots may have better penetrability and are useful under drought stress (Wu et al., 2016; Klein et al., 2020). Larger diameter roots are also better for mycorrhizal colonization (Reinhardt and Miller, 1990). Some of the phenotypes in the optimized set had larger diameter. These phenotypes, while not having as much biomass as those with smaller diameter, had lower carbon costs. Development of a strong, large diameter primary root imposed carbon constraints such that only roots with low LRBD could have enough growth to efficiently explore and exploit nutrient resources needed to accumulate optimal biomass. Investing in axial roots rather than high LRBD thereby reduced carbon requirement of the total root system, while at the same time enabling much better development of the primary root and more seminal and/or nodal axes tending towards greater soil exploration. Root diameter is an aggregate trait by itself, comprised of several anatomical phenes which can further be optimized to reduce the carbon cost including root cortical aerenchyma, living cortical area, cortical cell file number, cortical cell size many of which have tradeoffs between nutrient and water acquisition, mechanical strength of root structure and susceptibility to microbial colonization (Galindo-Castañeda et al., 2019; Lynch, 2015; Lynch, 2018). In dicots like bean which undergo radial growth, large diameter phenotypes can benefit by phenes such as root etiolation (reduced secondary growth) which reduces root metabolic costs (Lynch, 2007; Strock et al., 2018).

Phenotypes with greater root length at depth

Our optimization included maximizing root length deeper than 1 meter as one of the objectives. The phenotypes were evaluated after 40 days of growth. At 40 days all optimal phenotypes except those with large diameter primary roots had roots beyond 1 meter; however, only phenotypes that had greater primary or seminal root LRBD had more root length beyond 1 meter. Nodal roots of phenotypes with low LRBD of nodal roots and steep growth angles were found at depths greater than 70 cm, suggesting these roots could contribute to deep soil exploration over time. Early fast root proliferation could improve nutrient capture and vigorous growth during early development helps better establishment of the plant. Phenotypes with deeper roots are better for capturing deeper soil resources (Lynch, 2013; Lynch and Wojciechowski, 2015; Lynch, 2019). Roots contribute to soil organic carbon in the form of exudates, mucilage and also,

since fine root turnover decreases with soil depth, deeper roots can contribute to carbon sequestration as well (Pierret el al., 2016; Kell, 2011; Kell, 2012).

Complexity of the landscape

In this study, we focused only on a small subset of data corresponding to regions low in N, P and low N+P, as N and P limitations are ubiquitous in natural soils, are primary constraints to food production in low-input systems, and are primary causes of environmental pollution in high-input systems (Lynch 2019). However, the ultimate landscape of all possible constraints faced by a plant in an environment is highly complex and multidimensional. Optimal phenotypes will be different for different soil types / precipitation scenarios as the utility of root traits are dependent on the pattern of water availability in the target environment (Dathe et al., 2016) seasonal rainfall distribution, soil type, crop management, *etc*. (Lilley and Kirkegaard, 2011). Optimal phenotypes also depend on biotic factors, root loss as well as competition among plants of same species as well as other species. Many chemical and physical constraints occur in the subsoil which effectively reduce rooting depth, water use and nutrient acquisition. These include mechanical impedance, hypoxia, soil temperature, changes in physical and chemical characteristics of the rhizosphere brought out by the release of protons and exudates. Occurrence of several constraints simultaneously requires the integration of several distinct phene states in one optimal phenotype specific to the target environment. The use of FSPM with MOEA provides a valuable tool to identify phenotypes specific to target environments.

Future directions

Understanding the root phenome is a bottleneck to breeding crops with improved nutrient efficiency and stress tolerance. The complexity of fitness landscapes and inability of plant biologists and crop breeders to explore the phenotypic space through empirical experimentation is a major constraint to the design of breeding strategies for complex phenotypes. The focus on identifying useful phenotypes has been limited to evaluating a specific phene or small set of phenes rather than a large number of phene combinations. Because of their complexity, the large number of parameters and their dynamic nature, exploring all possible parameter combinations to identify optimal growth strategies is a computational challenge. Our approach of combining a mechanistic model of root architecture with an evolutionary algorithm can be very useful in

providing information for selecting and breeding for a limited number of distinct root phenotypes. These results identify phenotypes that have specific elements of ideotypes confirmed to have utility for improved P acquisition or N capture. These phenotypes warrant empirical validation. Spatial arrangement of roots for competition between species is also an optimization problem (Postma et al., 2014b). *SimRoot* can simulate a single plant or a plant in a crop stand and so can also be used to include to optimize overall system benefits in cropping systems. Scenarios of future climate scenarios can also be conveniently included and tested in our Borg-*SimRoot* framework

CONCLUSIONS

Many optimal phenotypes identified by the optimization algorithm are phenotypes integrating specific nutrient acquisition strategies previously identified empirically. The algorithm results in several alternate phenotypes cross the NP landscape, all of which have not been included in this study. A wealth of information is made available by the MOEA which can be further used to study integrated phenotypes across different regions of the NP landscape as well get insights into the mechanisms of phene interactions. Including several other parameters of agronomical interests can expand the utility of the framework to identify optimal phenotypes across various constraints.

REFERENCES

Bandaru S, Ng AH, Deb K (2017) Data mining methods for knowledge discovery in multi-objective optimization: Part A - Survey. *Expert Systems with Applications* 70: 139–159

Basu P, Zhang YJ, Lynch JP, Brown KM (2007) Ethylene modulates genetic, positional, and nutritional regulation of root plagiogravitropism. *Functional Plant Biology* 34: 41–51

Benes B, Guan K, Lang M, Long SP, Lynch JP, Marshall-Colón A, Peng B, Schnable J, Sweetlove LJ, Turk MJ (2020) Multiscale computational models can guide experimentation and targeted measurements for crop improvement. *The Plant Journal* 103: 21-31

Burridge JD, Rangarajan H, Lynch JP (2020) Comparative phenomics of annual grain legume root architecture. *Crop Science* 60: 2574–2593

Burridge J, Jochua CN, Bucksch A, Lynch JP (2016) Legume shovelomics : High — Throughput phenotyping of common bean (Phaseolus vulgaris L .) and cowpea (Vigna unguiculata subsp , unguiculata) root architecture in the field. *Field Crop Research* 192: 21–32

Burton AL, Johnson JM, Foerster JM, Hirsch CN, Buell CR, Hanlon MT, Kaeppler SM, Brown KM, Lynch JP (2014) QTL mapping and phenotypic variation for root architectural traits in maize (Zea mays L.). *Theoretical and Applied Genetics* 127: 2293-2311

Burton AL, Brown KM, Lynch JP (2013) Phenotypic diversity of root anatomical and architectural traits in species. *Crop Science* 53: 1042

Coello Coello CA, Lamont GB, Van Veldhuizen DA (2007) Evolutionary Algorithms for Solving Multi-Objective Problems Second Edition.

Comas LH, Becker SR, Cruz VMV, Byrne PF, Dierig DA (2013) Root traits contributing to plant productivity under drought. *Frontiers in Plant Science* 4: 442

Dathe A, Postma JA, Postma-Blaauw MB, Lynch JP (2016) Impact of axial root growth angles on nitrogen acquisition in maize depends on environmental conditions. *Annals of Botany* 118: 401–414

Dunbabin V, Diggle A, Rengel Z (2003) Is there an optimal root architecture for nitrate capture in leaching environments? *Plant Cell & Environment* 26: 835–844

Fonseca CM, Fleming PJ (1995) An Overview of Evolutionary Algorithms in Multiobjective Optimization. *Evolutionary Computation* 3: 1–16

Galindo-Castañeda T, Brown KM, Lynch JP (2018) Reduced root cortical burden improves growth and grain yield under low phosphorus availability in maize. *Plant Cell & Environment* 41: 1579–1592

Ge Z, Rubio G, Lynch JP (2000) The importance of root gravitropism for inter-root competition and phosphorus acquisition efficiency: results from a geometric simulation model. *Plant and Soil* 218: 159–171

Gewin V (2010) Food: An underground revolution. *Nature* 466: 552–553

Grieder C, Trachsel S, Hund A (2014) Early vertical distribution of roots and its association with drought tolerance in tropical maize. *Plant and Soil* 377: 295–308

Hadka D, Reed P (2013) Borg: an auto-adaptive many-objective evolutionary computing framework. *Evolutionary Computation* 21: 231–59

Henry A, Kleinman PJA, Lynch JP (2009) Phosphorus runoff from a phosphorus deficient soil under common bean (Phaseolus vulgaris L.) and soybean (Glycine max L.) genotypes with contrasting root architecture. *Plant and Soil* 317: 1-16

Ho M, Rosas J, Brown K, Lynch JP (2005) Root architectural tradeoffs for water and phosphorus acquisition. *Functional Plant Biology* 32: 737–748

Ho MD, McCannon BC, Lynch JP (2004) Optimization modeling of plant root architecture for water and phosphorus acquisition. *Journal of Theoretical Biology* 226: 331–340

Hochholdinger F, Yu P, Marcon C (2018) Genetic Control of Root System Development in Maize. *Trends in Plant Science* 23: 79–88

Hochholdinger F (2016) Untapping root system architecture for crop improvement. *Journal of Experimental Botany* 67: 4431–4433

Hochholdinger F, Tuberosa R (2009) Genetic and genomic dissection of maize root development and architecture. *Current Opinion in Plant Biology* 12: 172-177

Hoppe DC, Mccully ME, Wenzel CL (1986) The nodal roots of Zea : their development in relation to structural features of the stem. Canadian Journal of Botany 64: 2524-2537

Hu B, Henry A, Brown KM, Lynch JP (2014) Root cortical aerenchyma inhibits radial nutrient transport in maize (Zea mays). *Annals of Botany* 113: 181–189

Jia X, Liu P, Lynch JP (2018) Greater lateral root branching density in maize improves phosphorus acquisition from low phosphorus soil. *Journal of Experimental Botany* 69: 4961–4790

Liao H, Yan X, Rubio G, Beebe SE, Blair MW, Lynch JP (2004) Genetic mapping of basal root gravitropism and phosphorus acquisition efficiency in common bean. *Functional Plant Biology* 31: 959-970

Kell DB (2012) Large-scale sequestration of atmospheric carbon via plant roots in natural and agricultural ecosystems: Why and how. *Philosophical Transactions of the Royal Society of London. Series B, Biological Sciences* 367: 1589–1597

Kell DB (2011) Breeding crop plants with deep roots : their role in sustainable carbon , nutrient and water sequestration. *Annals of Botany* 108: 407–418

Kimball S, Gremer JR, Huxman TE, Lawrence Venable D, Angert AL (2013) Phenotypic selection favors missing trait combinations in coexisting annual plants. *The American Naturalist* 182: 191–207

Klein SP, Schneider HM, Perkins AC, Brown KM, Lynch JP (2020) Multiple integrated root phenotypes are associated with improved drought tolerance. *Plant Physiology* 183: 1011-1025

Koevoets IT, Venema JH, Elzenga JT, Testerink C (2016) Roots withstanding their environment:

exploiting root system architecture responses to abiotic stress to improve crop tolerance. *Frontiers in Plant Science* 7: 1335

Kohonen T (1998) "The self-organizing map," *Neurocomputing* 21: 1-6

Kong X, Zhang M, De Smet I, Ding Z (2014) Designer crops: optimal root system architecture for nutrient acquisition. *Trends in Biotechnology* 32: 597–598

Liao H, Rubio G, Yan X, Cao A, Brown KM, Lynch JP (2001) Effect of phosphorus availability on basal root shallowness in common bean. *Plant and Soil* 232: 69–79

Lilley JM, Kirkegaard JA (2011) Benefits of increased soil exploration by wheat roots. *Field Crops Research* 122: 118–130

Lynch J, Lauchli A, Epstein E (1991) Vegetative Growth of the Common Bean in Response to Phosphorus-Nutrition. *Crop Science* 31: 380–387

Lynch JP (2019) Root phenotypes for improved nutrient capture: an underexploited opportunity for global agriculture. *New Phytologist* 223: 548–564

Lynch JP (2013) Steep, cheap and deep: an ideotype to optimize water and N acquisition by maize root systems. *Annals of Botany* 112: 347–357

Lynch JP (2011) Root phenes for enhanced soil exploration and phosphorus acquisition: tools for future crops. *Plant Physiology* 156: 1041–1049

Lynch JP, Brown KM (2012) New roots for agriculture: exploiting the root phenome. *Philosophical Transactions of the Royal Society of London. Series B, Biological Sciences* 367: 1598–1604

Lynch JP (2007) Turner review no. 14. Roots of the second green revolution. *Australian Journal of Botany* 55: 493–512

Lynch JP, Ho MD (2005) Rhizoeconomics: Carbon costs of phosphorus acquisition. *Plant and Soil* 269: 45-56

Lynch JP, Nielsen KL, Davis RD, Jablokow AG (1997) SimRoot : Modelling and visualization of root systems. *Plant and Soil* 188: 139–151

Lynch J (1995) Root Architecture and Plant Productivity. *Plant Physiology* 109: 7–13

Lynch JP, Wojciechowski T (2015) Opportunities and challenges in the subsoil: pathways to deeper rooted crops. *Journal of Experimental Botany* 66: 2199–2210

Maeght JL, Rewald B, Pierret A (2013) How to study deep roots—and why it matters. *Frontiers in Plant Science* 4: 299

Meister R, Rajani MS, Ruzicka D, Schachtman DP (2014) Challenges of modifying root traits in crops for agriculture. *Trends in Plant Science* 19: 779–788

Miguel MA, Widrig A, Vieira RF, Brown KM, Lynch JP (2013) Basal root whorl number: a modulator of phosphorus acquisition in common bean (Phaseolus vulgaris). *Annals of Botany* 112: 973–982

Miguel MA, Postma JA, Lynch JP (2015) Phene synergism between root hair length and basal root growth angle for phosphorus acquisition. *Plant Physiology* 167: 1430–1439

Miller CR, Ochoa I, Nielsen KL, Beck D, Lynch JP (2003) Genetic variation for adventitious rooting in response to low phosphorus availability: Potential utility for phosphorus acquisition from stratified soils. *Functional Plant Biology* 30: 973–985

Niklas KJ (1997) Adaptive walks through fitness landscapes for early vascular land plants. *American Journal of Botany* 84: 16–25

Niklas KJ. 1994. Morphological evolution through complex domains of fitness. *Proceedings of the National Academy of Sciences of the USA* 91: 6772–6779.

Noor E, Milo R (2012) Evolution. Efficiency in evolutionary trade-offs. *Science* 336: 1114–1115

Paez-Garcia A, Motes CM, Scheible WR, Chen R, Blancaflor EB, Monteros MJ (2015) Root Traits and Phenotyping Strategies for Plant Improvement. *Plants* 4: 334–355

Perkins A, Lynch JP (2020) Increased seed carbohydrate reserves associated with domestication influence the optimal number of seminal root number of Zea mays. doi: https://doi.org/10.1101/2020.12.09.417691

Pierret A, Maeght JL, Clément C, Montoroi JP, Hartmann C, Gonkhamdee S (2016) Understanding deep roots and their functions in ecosystems: An advocacy for more unconventional research. *Annals of Botany* 118: 621–635

Postma JA, Lynch JP (2011a) Theoretical evidence for the functional benefit of root cortical aerenchyma in soils with low phosphorus availability. *Annals of Botany* 107: 829–841

Postma JA, Lynch JP (2011b) Root Cortical Aerenchyma Enhances the Growth of Maize on Soils with Suboptimal Availability of Nitrogen, Phosphorus, and Potassium. *Plant Physiology* 156: 1190–1201

Postma JA, Dathe A, Lynch JP (2014a) The optimal lateral root branching density for maize depends on nitrogen and phosphorus availability. *Plant Physiology* 166: 590-602

Postma JA, Schurr U, Fiorani F (2014b) Dynamic root growth and architecture responses to limiting nutrient availability: linking physiological models and experimentation.

Biotechnology Advances 32: 53–65

Rangarajan H, Postma JA, Lynch JP (2018) Co-optimization of axial root phenotypes for nitrogen and phosphorus acquisition in common bean. *Annals of Botany* 122: 485-499

Rasse DP, Rumpel C, Dignac M (2005) Is soil carbon mostly root carbon ? Mechanisms for a specific stabilisation. *Plant and Soil* 269: 341–356

Renton M, Poot P (2014) Simulation of the evolution of root water foraging strategies in dry and shallow soils. *Annals of Botany* 114: 763–778

Richards RA (2008) Genetic opportunities to improve cereal root systems for dryland agriculture. Plant Production *Science* 11: 12–16

Rubio G, Liao H, Yan X, Lynch JP (2003) Topsoil foraging and its role in plant competitiveness for phosphorus in Common Bean. *Crop Science* 43: 598–607

Saengwilai P, Tian X, Lynch JP (2014a) Low crown root number enhances nitrogen acquisition from low nitrogen soils in maize (Zea mays L.). *Plant Physiology* 166: 581-589

Saengwilai P, Nord EA, Chimungu JG, Brown KM, Lynch JP (2014b) Root cortical aerenchyma enhances nitrogen acquisition from low-nitrogen soils in maize (Zea mays L.). *Plant Physiol* 166: 726-735

Schneider HM, Lynch JP (2020) Should Root Plasticity Be a Crop Breeding Target ? *Frontiers in Plant Science* 11: 546

Shoval O, Sheftel H, Shinar G, Hart Y, Ramote O, Mayo A, Dekel E, Kavanagh K, Alon U (2012) Evolutionary Trade-Offs, Pareto Optimality, and the Geometry of Phenotype Space. *Science* 336: 1157–1160

Sinclair TR, Horie T (1989) Leaf Nitrogen, Photosynthesis, and Crop Radiation Use Efficiency: A Review. *Crop Science* 29: 90-98

Strock CF, De La Riva LM, Lynch JP (2018) Reduction in root secondary growth as a strategy for phosphorus acquisition. *Plant Physiology* 176: 691–703

Sun B, Gao Y, Lynch JP (2018) Large crown root number improves topsoil foraging and phosphorus acquisition. *Plant Physiology* 177: 90-104

Trachsel S, Kaeppler SM, Brown KM, Lynch JP (2013) Maize root growth angles become steeper under low N conditions. *Field Crops Research* 140: 18–31

Trachsel S, Kaeppler SM, Brown KM, Lynch JP (2011) Shovelomics: High throughput phenotyping of maize (Zea mays L.) root architecture in the field. *Plant and Soil* 341: 75–87

Tuberosa R (2012) Phenotyping for drought tolerance of crops in the genomics era. *Frontiers in Physiology* 3: 347

Uga Y, Okuno K, Yano M (2011) Dro1, a major QTL involved in deep rooting of rice under upland field conditions. *Journal of Experimental Botany* 62: 2485–2494

Voss-fels KP, Snowdon RJ, Hickey LT (2018) Designer Roots for Future Crops. *Trends in Plant Science* 23: 957–960

Walk TC, Jaramillo R, Lynch JP (2006) Architectural tradeoffs between adventitious and basal roots for phosphorus acquisition. *Plant and Soil* 279: 347–366

Wasson AP, Richards RA, Chatrath R, Misra SC, Prasad SV, Rebetzke GJ, Kirkegaard JA, Christopher J, Watt M (2012) Traits and selection strategies to improve root systems and water uptake in water-limited wheat crops. *Journal of Experimental Botany* 63: 3485–3498

Wehrens R, Buydens LMC (2007) Self-and super-organizing maps in R: the Kohonen package. *Journal of Statistical Software* 21: 1-19

Yang JT, Schneider HM, Brown KM, Lynch JP, Gifford M (2019) Genotypic variation and nitrogen stress effects on root anatomy in maize are node specific. *Journal of Experimental Botany* 70: 5311–5325

York LM, Lynch JP (2015) Intensive field phenotyping of maize (Zea mays L.) root crowns identifies phenes and phene integration associated with plant growth and nitrogen acquisition. *Journal of Experimental Botany* 66: 5493–5505

Zhan A, Schneider H, Lynch JP (2015) Reduced lateral root branching density improves drought tolerance in maize. *Plant Physiology* 168: 1603–1615

Zhu J, Kaeppler SM, Lynch JP (2005) Topsoil foraging and phosphorus acquisition efficiency in maize (Zea mays). *Functional Plant Biology* 32: 749-762

Zhu J, Mickelson SM, Kaeppler SM, Lynch JP (2006) Detection of quantitative trait loci for seminal root traits in maize (Zea mays L.) seedlings grown under differential phosphorus levels. *Theoretical and Applied Genetics* 113: 1–10

Table 3-1: Decision variables, root phenes, with constraints for the maize root system.

		Units	Min	Max	References
Number of roots	Seminal Roots; Nodal Roots at position 1 to 4	Number	0	12	Hochholdinger and Tuberosa, 2009; Burton et al., 2013; York and Lynch, 2015
Angle	Nodal Roots 1 to 4	Degree from horizontal	0	90	Liao et al., 2004; Zhu et al., 2005
Lateral root density	Primary Roots, Seminal Roots; Nodal roots at position 1 to 4	lateral roots per cm	1	30	Postma et al., 2014; York and Lynch, 2015
Diameter	Primary Roots; Seminal Roots; Nodal roots at position 1 to 4	mm	0.5	6	Burton et al., 2013, 2014; York and Lynch, 2015
Aerenchyma	Primary Roots; Seminal Roots; Nodal roots at position 1 to 4	Percent of cross-sectional area	0	40	Postma and Lynch, 2011b; Hu et al., 2014; Saengwilai et al., 2014

Table 3-2: Decision variables, root phenes, with constraints for the bean root system.

		Units	Min	Max	References
Number of Whorls	Basal root	Number	0	5	Miguel et al., 2013
Number of roots	Basal Roots; HBR	Number	0	4 (Basal roots)	Miller et al., 2003
Angle	Basal roots	Degree from horizontal	0	90	Miguel et al., 2013
Lateral root density	Primary Roots, Basal Roots, HBR	lateral roots per cm	1	30	Miller et al., 2003
Diameter	Primary Roots; Basal Roots whorl 1 to 5; HBR	mm	0.6	5	Henry et al., 2009
Aerenchyma	Primary Roots; Basal Roots whorl 1 to 5 ;HBR	Percent of cross sectional area	0	40	Postma and Lynch, 2011a

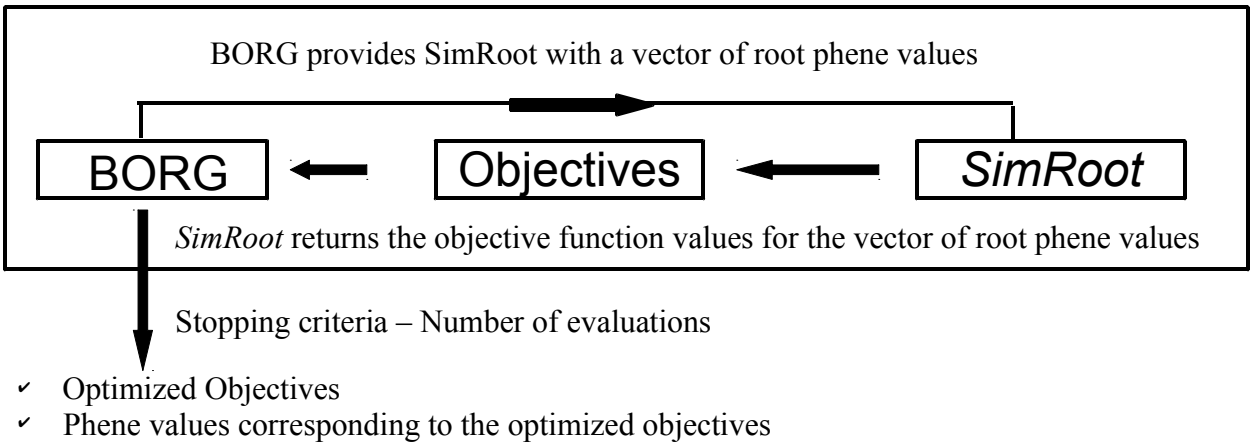

Figure 3-1: Flow chart of the SimRoot-Borg loop. Vector of phene values is provided by Borg to *SimRoot* as *SimRoot* inputs. The root architecture model is generated based on the input values by *SimRoot* and outputs obtained at the end of the model run are provided as objective function values to Borg for evaluation.

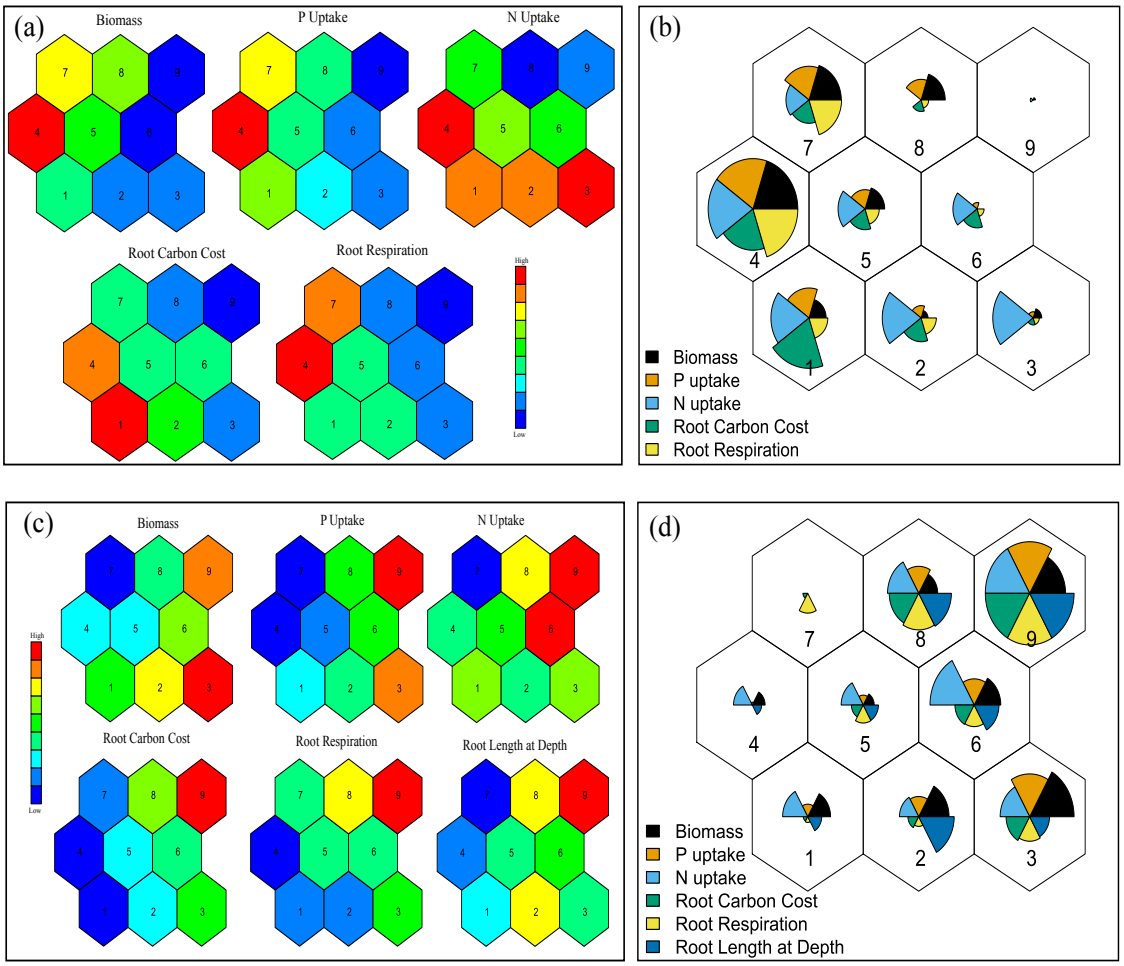

Figure 3-2: Self organizing map (SOM) heatmap of performance of phenotypes in different objectives in a region with low N+P. The objectives are clustered by SOM. Each cluster (node) in the heatmap has phenotypes with similar performance in all objectives. (a) and (c) presents the average value of the objective in bean and maize root systems respectively in that node. (b) and (d) show the relative performances of phenotypes in all the objectives in bean and maize root systems respectively in that node

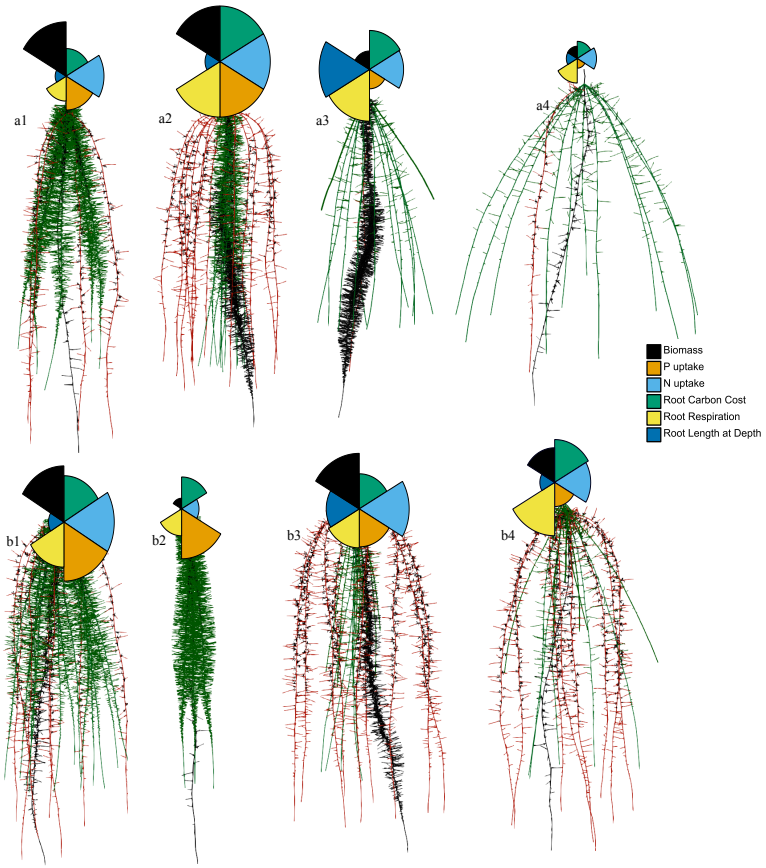

Figure 3-3: Tradeoffs in performance in different objectives. Representative optimal phenotypes in low P (a1-a4). Representative optimal phenotypes in low N (b1-b4). The fan plots show the relative performance of the different phenotypes in different objectives. Primary roots are in black; Seminal roots in red; Nodal roots in green.

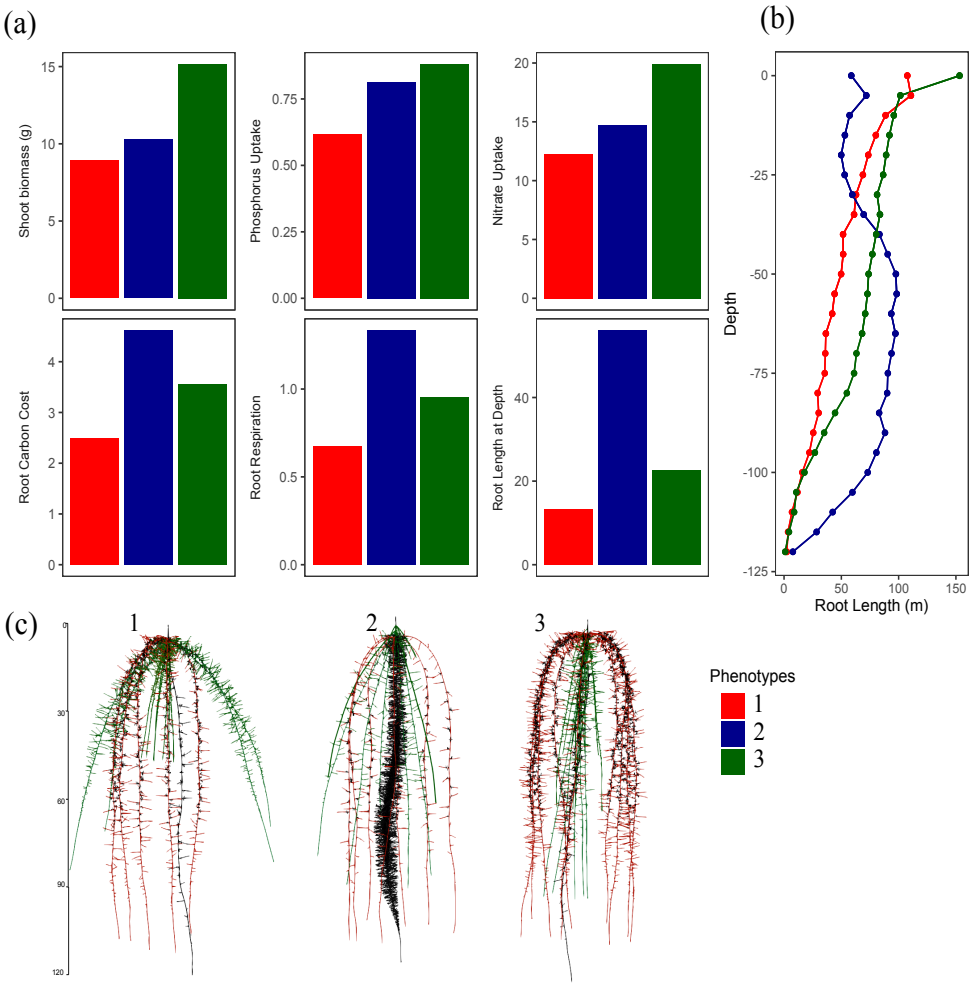

Figure 3-4: Performance of optimal maize phenotypes varying in root length at depth in different objectives (a). Distribution of root length with depth for the phenotypes (b). Visualization of the phenotypes (c). Primary roots are in black; Seminal roots are in red; Nodal roots are in green

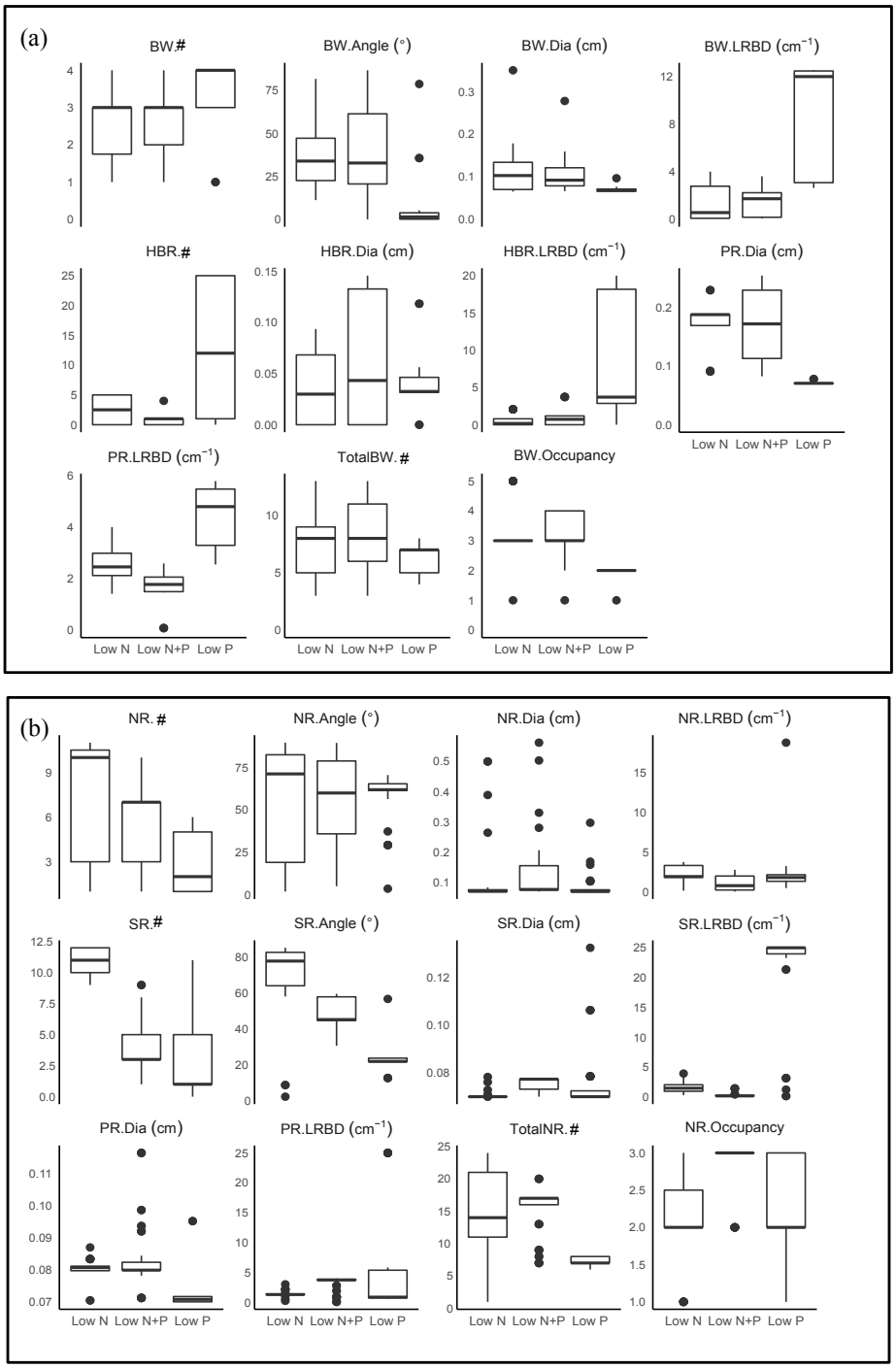

Figure 3-5: Distribution of phene states of bean root phenes in optimal bean phenotypes in low N, low P and low N+P regions of the landscape (a). Distribution of phene states of maize root phenes in optimal maize phenotypes in low N, low P and low N+P regions of the landscape (b).

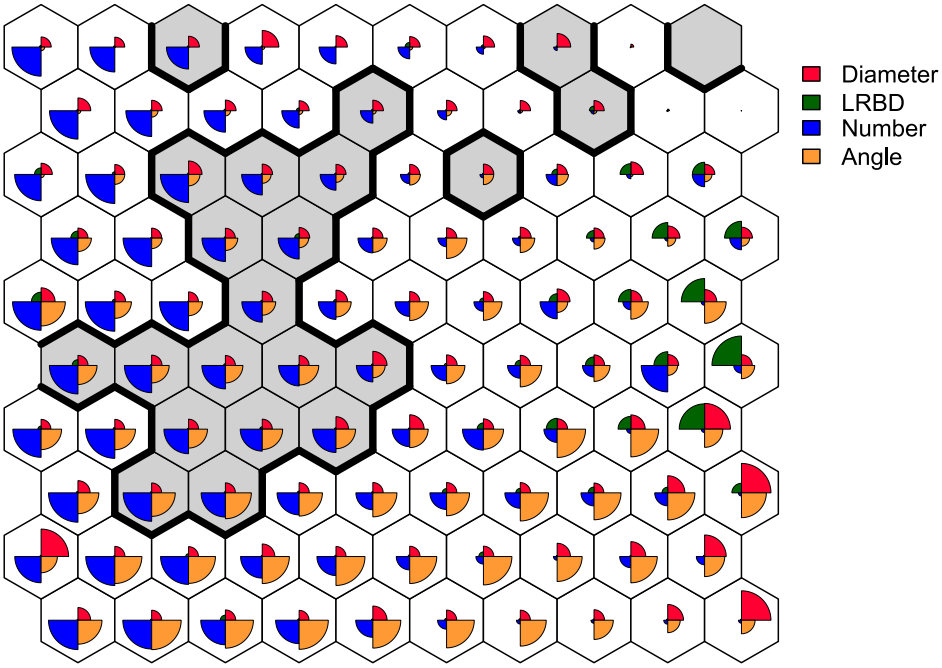

Figure 3-6: Different seminal root phenotypes found in the optimal maize phenotypes. The nodes shaded in grey contain the phenotypes that are seen when primary roots have larger diameter.

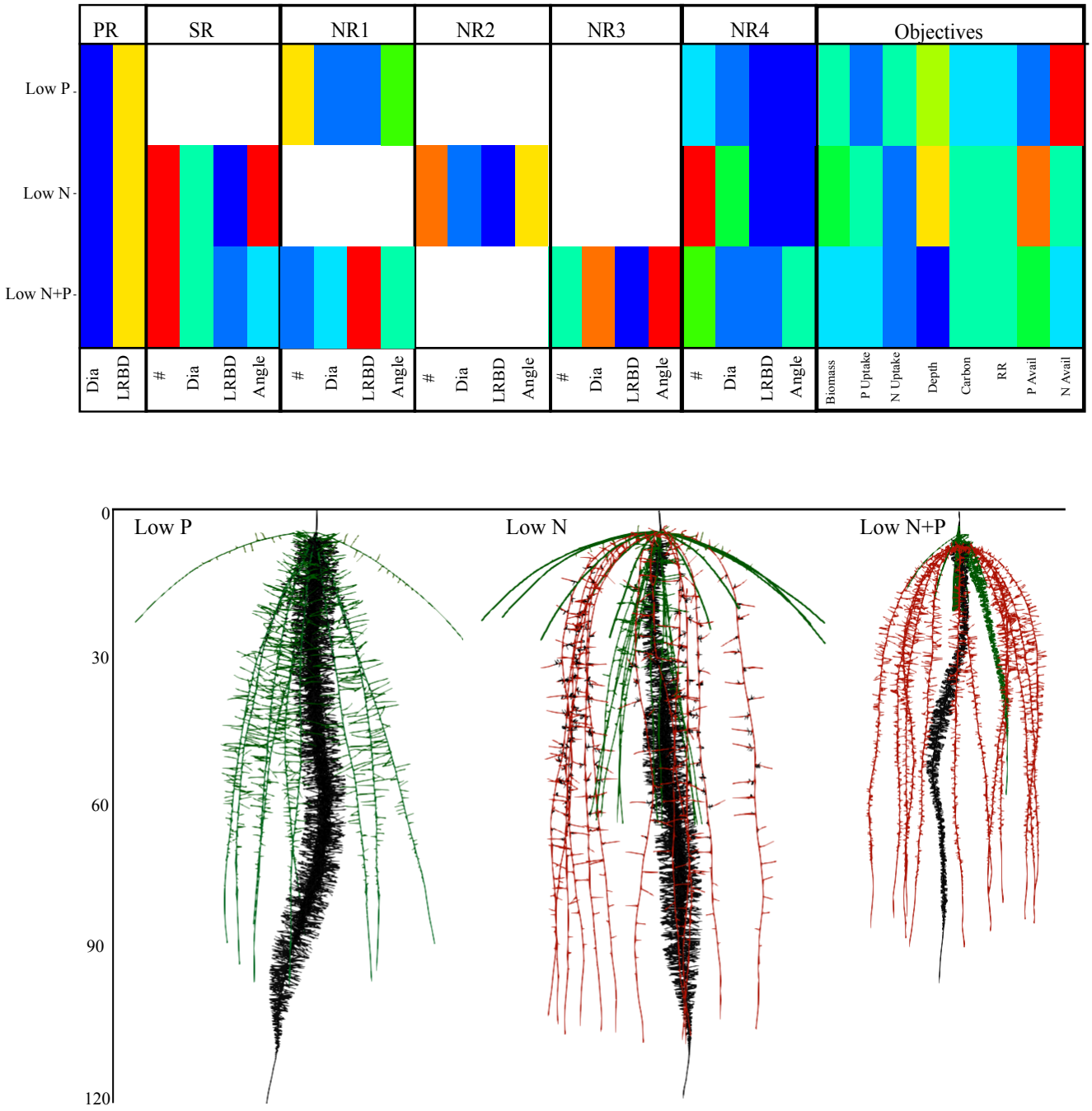

Figure 3-7: Phenotypes with similar primary root ideotypes and different SR and NR ideotypes in optimal maize phenotypes in regions with low P, low N and low N+P.

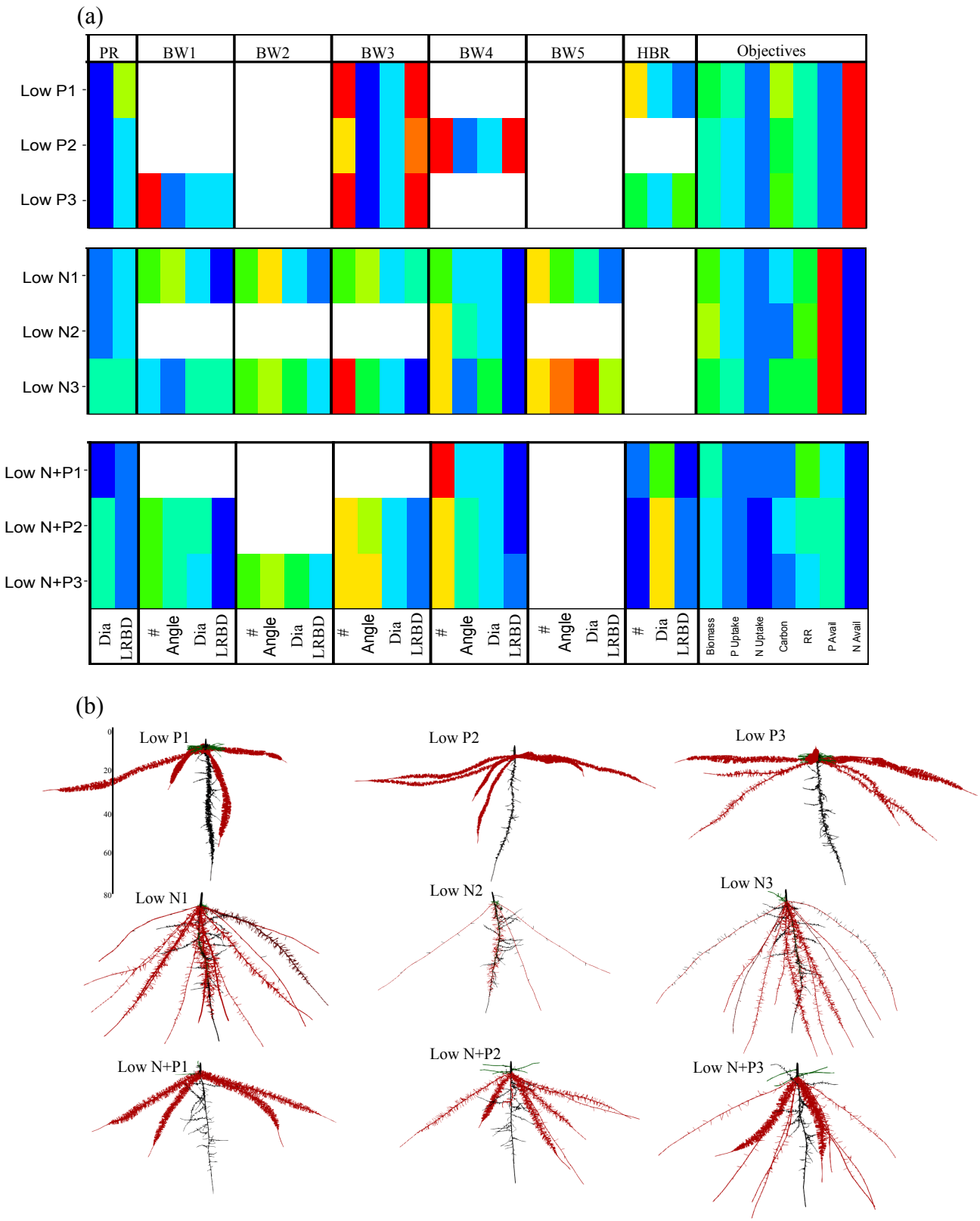

Figure 3-8: Heatmap showing the phene states of different phenes of optimal bean root system low P, low N and low N+P (a). The respective phenotypes are visualized in (b). Primary roots are in black; Basal roots in red; Hypocotyl-borne roots in green.

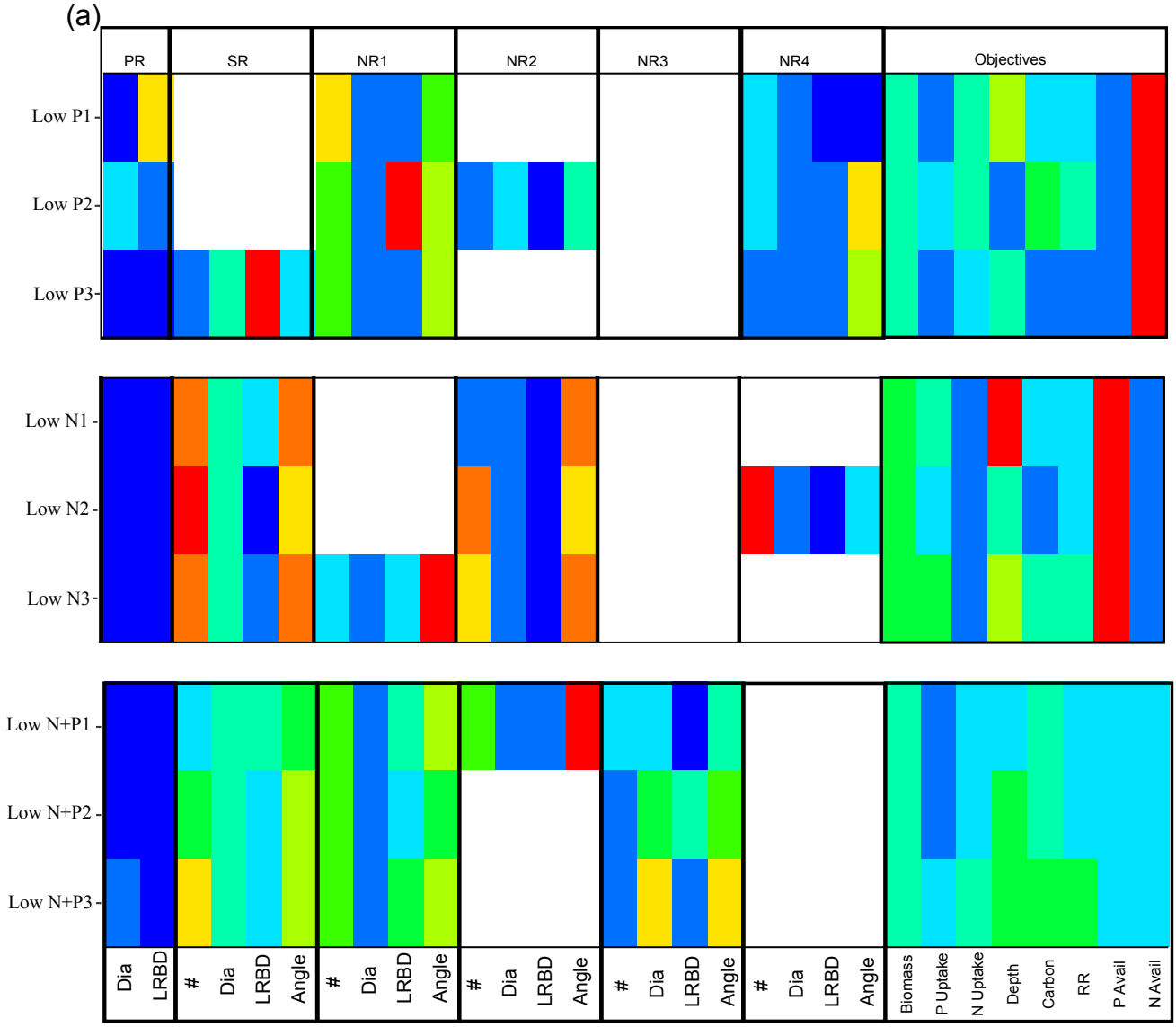
(a)
PR
SR
NR1
NR2
NR3
NR4
Objectives
Low P1
Low P2
Low P3
Low N1
Low N2
Low N3
Low N+P1
Low N+P2
Low N+P3
Dia
LRBD
#
Dia
LRBD
Angle
Biomass
P Uptake
N Uptake
Depth
Carbon
RR
P Avail
N Avail

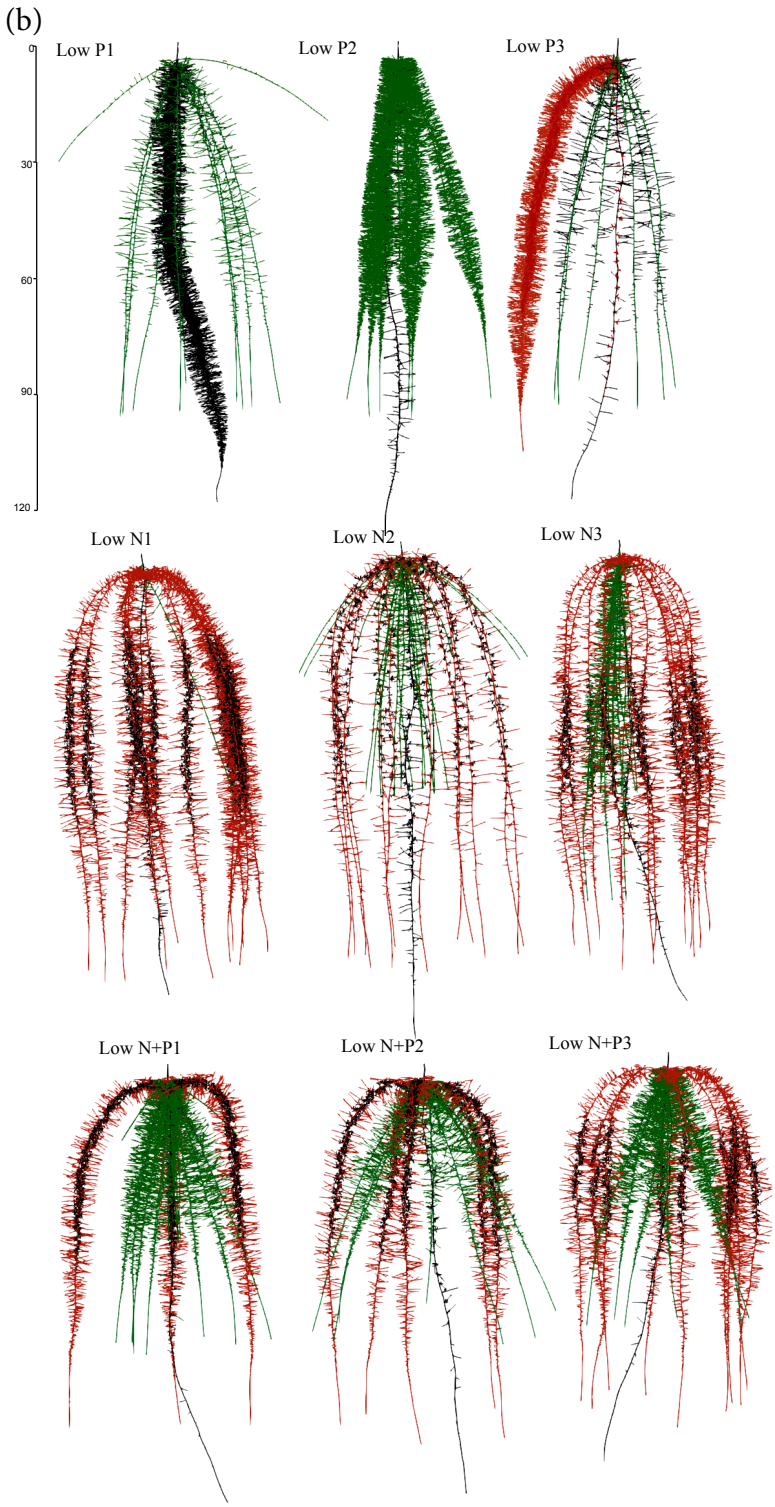

Figure 3-9: Heatmap showing the phene states of different phenes of optimal maize root system under low P, low N and low N+P (a). The distribution of the variables are represented color coded. White represents the absence of the particular class of roots and traits associated with that root class. PR- primary root; SR - Seminal roots; NR1-4 - Nodal roots 1-4. Lower values of the variable are in blue changing to yellow and red with increase in numerical value of the particular trait. The respective phenotypes are visualized in (b). #- Number of roots; Dia - Axial root diameter; LRBD - Lateral root branching density. Primary root is in black; Seminal roots are in red; Nodal roots are in green.

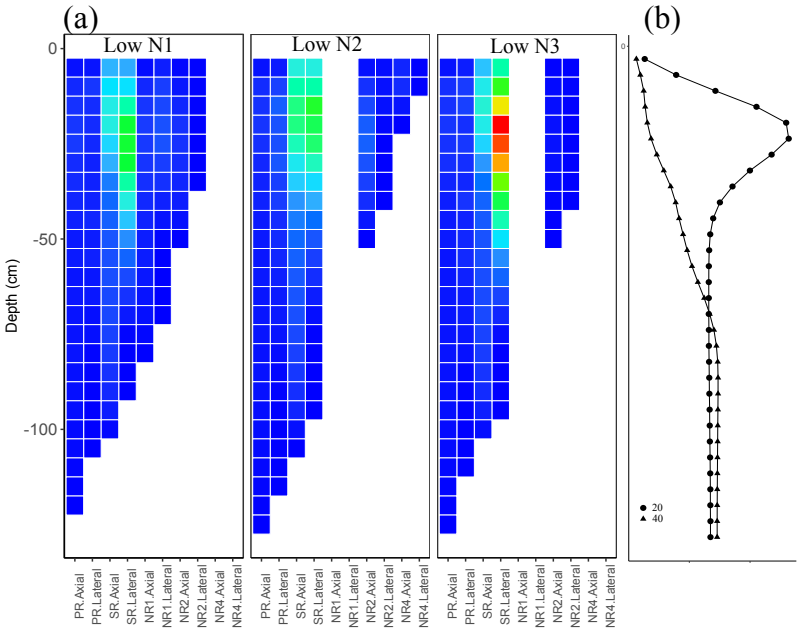
(a)
Low N1
Low N2
Low N3
0
-50
-100
Depth (cm)
PR.Axial
PR.Lateral
SR.Axial
SR.Lateral
NR1.Axial
NR1.Lateral
NR2.Axial
NR2.Lateral
NR4.Axial
NR4.Lateral
(b)
20
40

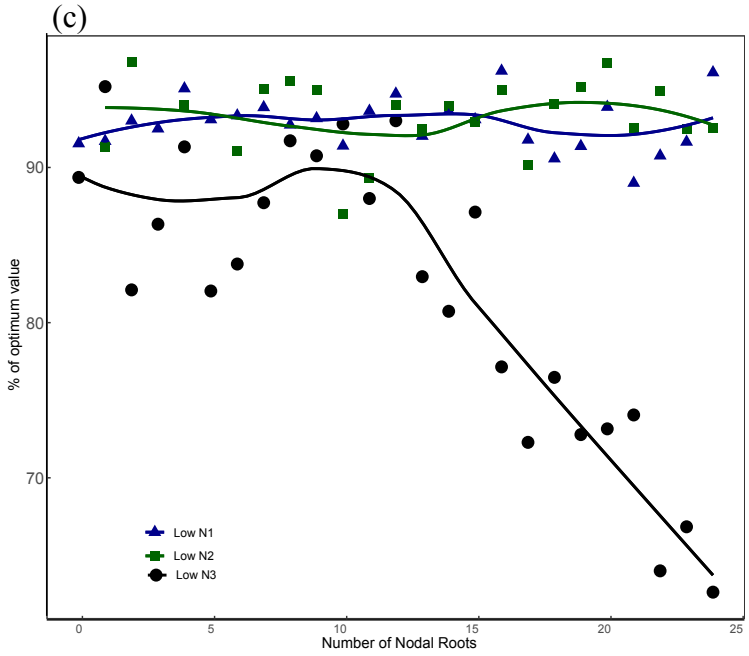
(c)
90
80
70
% of optimum value
Low N1
Low N2
Low N3
0
5
10
15
20
25
Number of Nodal Roots

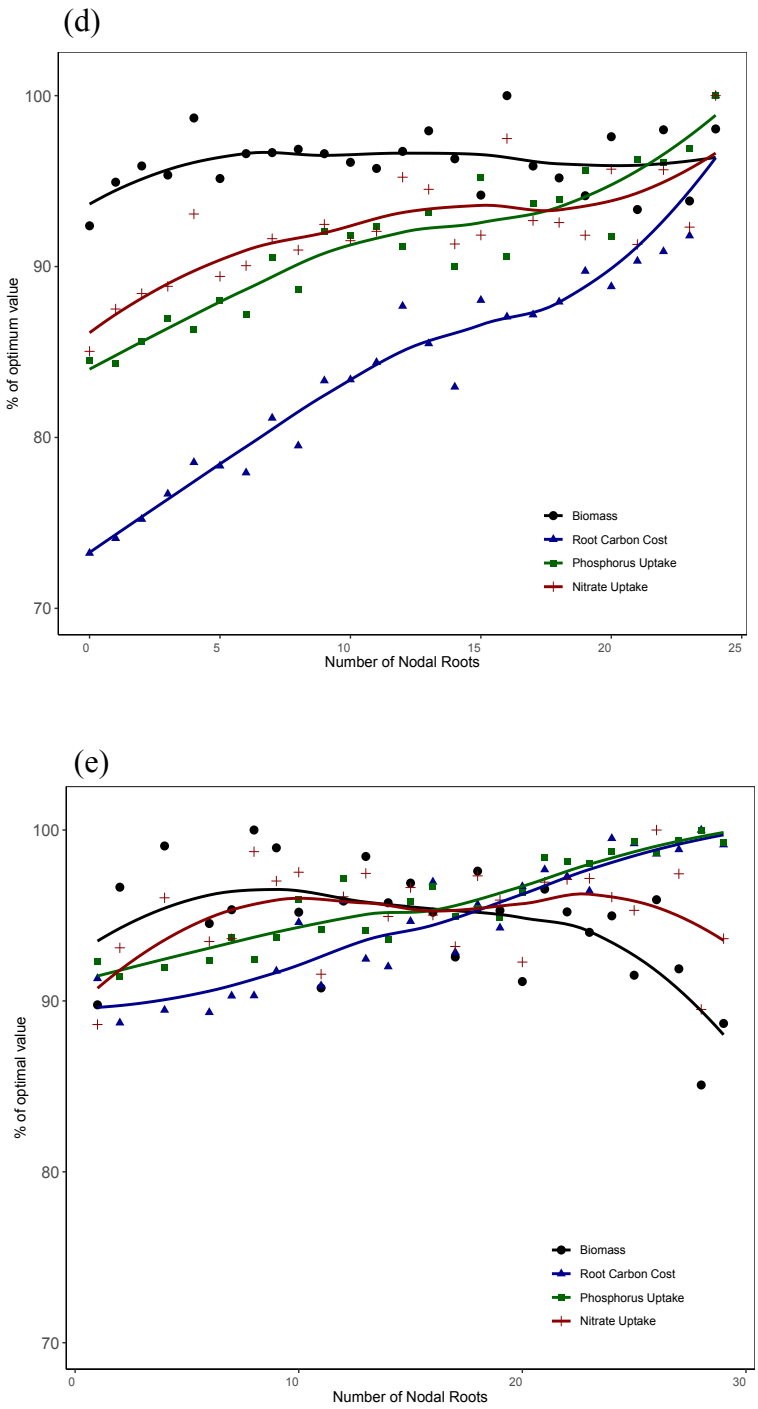

Figure 3-10: Root length distribution of maize root phenotypes Low N1, Low N2 and Low N3 (a). Color scale ranges from blue to red with blue being low values of root length. Regions in white depict absence of that root class in the phenotype. PR- Primary root; SR - Seminal root; NR - Nodal root. Nitrate availability in the soil profile at 20 days and 40 days (b). Performance of maize phenotypes Low N1, Low N2 and Low N3 with change in number of nodal roots (c). Performance of maize phenotype Low N1 in different objectives with change in NR number (d). Performance of maize phenotype Low N2 in different objectives with change in NR number (e).

Chapter 4

A comparative analysis of quantitative metrics of root architectural phenotypes

Harini Rangarajan and Jonathan Lynch

Published in *Plant Phenomics*

ABSTRACT

High throughput phenotyping is important to bridge the gap between genotype and phenotype. The methods used to describe the phenotype therefore should be robust to measurement errors, relatively stable over time, and most importantly, provide a reliable estimate of elementary phenotypic components. In this study, we use functional-structural modeling to evaluate quantitative phenotypic metrics used to describe root architecture to determine how they fit these criteria. Our results show that phenes such as root number, root diameter, lateral root branching density are stable, reliable measures and are not affected by imaging method or plane. Metrics aggregating multiple phenes such as *total length, total volume, convex hull volume, bushiness index* etc. estimate different subsets of the constituent phenes, they however do not provide any information regarding the underlying phene states. Estimates of phene aggregates are not unique representations of underlying constituent phenes: multiple phenotypes having phenes in different states could have similar aggregate metrics. Root growth angle is an important phene which is susceptible to measurement errors when 2D projection methods are used. Metrics that aggregate phenes which are complex functions of root growth angle and other phenes are also subject to measurement errors when 2D projection methods are used. These results support the hypothesis that estimates of phenes are more useful than metrics aggregating multiple phenes for phenotyping root architecture. We propose that these concepts are broadly applicable in phenotyping and phenomics.

INTRODUCTION

Crop production needs to double by 2050 to provide for the increasing global population (Tilman et al., 2011; Ray et al., 2013; Wise, 2013; FAO, 2017). A major challenge is the identification of efficient crops that cope with climate change and reduce the need for fertilizer and water inputs to make agriculture environmentally sustainable. Root architecture influences water and nutrient

uptake, so, selecting and developing efficient crops based on their root system architecture (RSA) has been proposed as a strategy towards a "second green revolution" (Lynch, 2007; Den Herder et al., 2010; Villordon et al., 2014; Lynch, 2019).

Development of powerful tools in genomic research has resulted in a deluge of genomic information. However, this genomic information cannot be fully exploited for crop improvement unless it is linked to the phenome (Lynch and Brown, 2012; Cobb et al., 2013; Tardieu et al., 2017). In the context of roots, the root phenome is the set of phenes manifested by roots of a plant, where phenes are elementary units of the phenotype; phenes are related to phenotypes as genes are to genotypes (Lynch and Brown, 2012; York et al., 2013). Phenotyping is a bottleneck for breeding and genetic analysis because it is species-specific, labor intensive and environmentally sensitive, unlike genotyping, which is uniform across organisms, highly automated, and increasingly inexpensive (Furbank and Tester, 2011; Lynch and Brown, 2012; Cobb et al., 2013; Atkinson et al., 2019). Phenotyping is especially challenging for roots because of their complexity, plasticity, and inaccessibility. Significant advances are being made in phenotyping methods and technology in an attempt to develop high-throughput platforms. In order to develop efficient strategies to explore the phenome, it is important to clarify what constitutes a phenotype, delineate the key components that comprise a phenotype, and determine the level of resolution at which phenotypic data must be collected. Although an essentially infinite number of measurements may be collected to describe each phenotype, a smaller number of more basic variables may explain most of the important phenotypic variation among genotypes. These basic variables, or *phenes* are the elementary units of the root phenotype and cannot be decomposed to more phenes at the same scale of organization (Lynch and Brown, 2012). Based on this definition, number of axial roots, lateral root branching density (LRBD), root growth angle, root diameter, root length of different root classes of the root system can be considered as phenes.

Current methods for developing high-throughput phenotyping platforms and identification of relevant quantitative trait loci (QTL) associated with traits of interest are largely based on non-elementary phenotypic metrics. Non-phenes, referred to as phene aggregates in this paper, are aggregate components of the root phenotype and describe the distribution of roots, shape of roots and/or size of the root system. Phene aggregates include several conventionally measured traits including *total root length, total area, total volume*, as well as novel phenotypic

metrics such as *convex hull volume, convex hull area, ellipse major axis, ellipse minor axis, ellipse aspect ratio, volume distribution, solidity, bushiness index* (Iyer-Pascuzzi et al., 2010; Clark et al., 2011; Cobb et al., 2013; Topp et al., 2013) and metrics which measure the geometry and complexity of root systems such as *fractal dimension* (FD), *fractal abundance* (FA), and *lacunarity* (Fitter and Stickland, 1992; Nielsen et al., 1999; Walk et al., 2004). Aggregate phenotypic metrics (referred to as aggregate metrics) are comprised of phenes, some of these can be measured as a simple aggregate of phenes (e.g. *total length*), some are represented as a function of other aggregates (e.g. *bushiness, solidity, volume distribution*), some measure shapes resulting from interaction of the constituent phenes (e.g. *Convex hull volume*), and some metrics are complex metrics which measure emergent properties of root architecture and cannot be described as a simple aggregate, shape aggregate or a function of other aggregates (*e.g. Fractal Dimension*).

Estimates of phene aggregates change over time and are phenotype specific. Some phene aggregates increase over time, some remain relatively static and some decrease in value over time (Iyer-Pascuzzi et al., 2010; Zurek et al., 2015). The magnitude of change in estimates of phene aggregates with time also vary greatly. This is because some of the phene aggregates are one-dimensional measurements while some measurements are a function of more than one dimension (Mairhofer et al., 2013). Many phene aggregates are estimates generated from the average values of the 2D projections in a rotational image series (Topp et al., 2013) and are thought to represent 3D root shape accurately. However, which traits can be measured accurately using estimates derived from 2D data and which require 3D representations is poorly understood. Depending on the phenotype, metrics derived from rotated 2D projections of the same 3D root system can vary significantly. This leads to a related question of how much should an aggregate phenotypic metric differ for two phenotypes to be considered distinctly different. Fractal analysis of corn roots have shown that the *FD* of two genotypes can be same but vary in *FA* (Eghball et al., 1993). Root systems with similar *FD* may vary functionally and genotypes can be distinguished when fractal analysis involves *FD, FA* and *lacunarity* (Walk et al., 2004). Aggregate phene metrics estimate the aggregate of multiple phenes. For example, greater rooting depth is an important trait for capture of subsoil N in maize. Greater rooting depth results from a combination of deeper axial root growth angle (Manschadi et al., 2006; Trachsel et al., 2013; Uga et al., 2013), root elongation rate (Manschadi et al., 2008), expression of fewer crown roots

(Saengwilai et al., 2014b; Gao and Lynch, 2016), reduced lateral branching density (Postma et al., 2014; Zhan et al., 2015), formation of root cortical aerenchyma (RCA) (Postma and Lynch, 2011; Saengwilai et al., 2014a), reduced cortical file number and increased cortical size (Jaramillo et al., 2013; Chimungu et al., 2014). Each of these phenes are under distinct genetic control and have important interactions with each other. Selection for combination of specific phenes will therefore be much simpler and precise than would selection for root depth itself (Lynch, 2019). Phenes are under more simple genetic control and permit more precise control over the root system architecture (RSA) and so, are more useful for selection for crop breeding (Lynch and Brown, 2012; Lynch, 2019).

In this study, we use the functional-structural plant model *SimRoot* to identify phenotyping metrics that are

- sensitive enough to provide information on the constituent root phenes and their states,
- stable over time and are independent of the time of phenotyping,
- robust to the imaging method *i.e.*, do not vary when measured in the intact 3D root system or when estimated using 2D rotational image series.

Our analysis shows that

- Phene aggregates can be explained by phenes. Different phene aggregates capture different combinations of subtending phenes. However, these metrics do not provide precise information or measures of subtending phene states.
- Several combinations of phenes in different states can produce phenotypes which have comparable estimates of phene aggregates. Estimates of phene aggregates are not unique representations of the state of the underlying phenes.
- As the number of phenes captured by an aggregate phenotypic metric increases, the stability of that metric becomes less stable over time.

METHODS

Simulation of phenotypes

The functional-structural plant model *SimRoot* (Lynch et al., 1997) was used to simulate bean (*Phaseolus vulgaris*) and maize (*Zea mays*) root phenotypes. In *SimRoot*, simulated root system

comprises of roots of distinct classes as specified by their root diameters, lateral root branching density, root growth rate and root growth angle in the input parameters. The root growth angle over time depends on the gravitropism. Stochasticity is included in all parameters. The roots are simulated as small connected root segments over time. Co-ordinates corresponding to the root being simulated as well as the root length, volume, area parameters are stored for the simulated root segments as the root grows at specified time points. The root length, area, volume of the root system is estimated by integrating the respective parameters over all root segments. The root image co-ordinates are used to visualize the simulated root system. The environment was considered to be uniform and plastic responses were not considered in this study.

The number of roots of different root classes, angle, diameter, lateral root branching density (LRBD) were varied to produce 1500 maize root phenotypes and 1500 bean root phenotypes. The range of values used for each of the root parameter used are given in Supplementary Material 2.

The data corresponding to the simulated root phenotypes were saved during the simulation runs. These data files contained the X, Y, Z co-ordinates of the simulated root system images used to simulate the root as well as data of root length, area, volume etc. of the simulated root segments with their corresponding root class. Roots were allowed to grow without any boundaries so that the growing roots did not touch any boundary surface and so no artifacts were introduced due to mirroring roots. Stochasticity was included in all the simulated parameters. Root growth angle was influenced by root gravitropism. The angle made by the root at 5 cm with the horizontal (soil surface) was calculated from the image co-ordinates and used as estimate of root angle. In order to obtain accurate estimates of all the phenotypic traits, elementary and aggregate phenotypic were extracted/calculated from the data of the simulated images.

Measurement of phene and aggregate phene metrics

Estimates of phene metrics were measured from the simulated images. Aggregate phenotypic trait metrics were calculated for intact 3D root systems as well as projections of the roots systems on a 2D plane. The root system was rotated by 20 degrees and the projections on a 2D plane were obtained (Figure **2-1** and Supplementary Figure S1). The average of the estimates of each metric in all the projected images for each phenotype was used in studies considering 2D projections. The average value was used also in 3D studies where 3D estimates were not

obtained including ellipse major axis, ellipse minor axis and ellipse aspect ratio. The phene aggregates estimated and considered in this study, the definitions of these traits and the method of obtaining those metrics from *SimRoot* output is given in Table 1. In order to evaluate how phene metrics and phenotypic trait metrics change over time, root images were obtained every 5 days starting 10 days after germination and metrics obtained for these root systems. This way phenotyping metrics were obtained for 3D root systems, 2D projections of the root systems, and root system images after different periods of growth.

Random forest analysis

Data obtained from 3D root systems were analyzed using Random Forest regression. For metrics where 3D metric data were not available (ellipse minor axis, ellipse major axis and ellipse aspect ratio), the average value of the aggregate phenotypic trait from 2D rotational series was used. Random Forest, is a nonparametric technique derived from classification and regression trees (CART). Random Forest consists of a combination of many trees, where each tree is generated by boot- strap samples, leaving about a third of the overall sample for validation (the out-of-bag predictions – OOB). Each split of the tree is determined using a randomized subset of the predictors at each node. The final outcome is the average of the results of all the trees (Breiman, 2001; Cutler et al., 2007). It uses the OOB samples (independent observations from those used to grow the tree) to calculate error rates and variable importance, no test data or cross-validation is required. However, this method does not calculate regression coefficients nor confidence intervals (Cutler et al., 2007). It allows the computation of variable importance measures that can be compared to other regression techniques. The R package Random Forest was employed for the data analyses, with ntree =1000 and mtry =8. Random forest regression was used with each aggregate phenotypic metric as the dependent variable and the input variables as the independent variables to identify the most important variables. The selection of the most relevant variables to include in the final model was done by ranking the variables according to their importance and excluding the least important variables. The variable importance measure, the mean decrease in accuracy (%IncMSE) was used for selecting the important variables. Variable importance is measured by mean squared error of a variable p, which is averaged increase in prediction error among all regression trees when the OOB data for variable p is randomly permuted. If variable p is important there will be an increase in prediction error. Random forest was conducted 50 times

and 90 percentile from distribution of mean squared error as the significance threshold of individual variables. The variables thus chosen were used to run a reduced variable model of the original random forest model for each aggregate metric. The reduced variable models were deemed acceptable if the Random Forest trained upon the most important descriptors gave a fit to the data set which was similar or better than that trained upon all variables.

Variation in estimates of phene aggregate metrics

One aspect of the study was to find if estimates of aggregate phenotypes were a unique representation of the phenes. To address this, a representative phenotype was chosen for the maize root system and phenotypes varying by less than 1 % of an aggregate phenotypic trait a shape phenotypic trait (Convex hull volume) and a complex phenotypic trait (FD) were chosen to find if the phenes constituting the phenotype varied when the aggregate phenotypic trait was similar. In an alternate approach, the estimates of convex hull volume and FD of bean root phenotypes with differences in basal root whorl number and root growth angles with distinct functional value (Rangarajan et al., 2018) were studied.

Estimates of phene and aggregate phene metrics obtained from 2D projections

In order to study the variation in metrics estimated in 2D rotational image series, the coefficient of variation for each phenotype for each phenotypic trait metric was calculated from 2D projections of the root system and the phenotypic metrics were compared.

Estimates of phene and aggregate phene metrics over time

Root system image data were saved every 5 days from day 10 to day 40 of growth and the 3D estimates of the phenes and phene aggregates were collected.

RESULTS

Different bean and maize phenotypes were simulated by varying input parameters in *SimRoot.*

Variation in simulated phenotypes

The estimates of all phenotypes were min-max scaled and the phenotypes were clustered by hierarchical cluster analysis of the phenotypes based on their phenes. The results of our study are based on a wide array of phenotypes. Phenotypes included in the study had vastly different phenotypes and differed in few or many phenes. The heatmap in Figure 4-2(a) shows a small subset of data: the relative values of the bean phenes in a few phenotypes (rows) and the corresponding phenotypes in Figure 4-2(b). Phenotype 1 had very shallow basal root growth angle compared to phenotype 2 while phenotypes 8 and 9 had deep basal root growth angles. Phenotype 7 had more basal roots than the other phenotypes. Phenotypes 5 and 6 differed in the basal root branching density as well as basal root angle. The heatmap in Figure 4-3(a) shows a small subset of data: the relative values of maize phenes in a few phenotypes (rows) and the corresponding phenotypes in Figure 4-3(b). Phenotypes 2 and 3 differed in the number of nodal roots with phenotype 2 having more nodal roots than phenotype 3. Phenotypes 4 and 6 had similar primary root lateral branching but phenotype 6 had no seminal roots while phenotypes 4 had 5 seminal roots. Phenotypes 8 and 9 differed in the number of seminal roots as well as seminal root LRBD and the number of nodal roots. The heatmap of all bean root phenotypes and representative phenotypes considered in this study is included in Supplementary Figure S2(a) and S2(b). A similar heatmap for maize root phenotypes are presented in Supplementary Figure S3(a) and S3(b) respectively.

Correlation among phenotypic metrics

Strong correlations were found among the phenes (Figure 4-4(a) and Figure 4-4(b)), in the bean root system as well as the maize root system. Axial root length was negatively correlated with diameter, number and LRBD of basal roots in bean and nodal roots in maize root system. The primary axial root length and seminal axial root length was negatively correlated with diameter of the primary root, seminal root axial root length was also negatively correlated with nodal root LRBD. Phenotypes with longer axial roots had greater *maximum width, maximum depth, convex hull area, convex hull volume, major ellipse axis, minor ellipse axis* but smaller values for *solidity* (Figure 4-4(b). *Solidity* was positively correlated with diameter and number of basal roots in bean. Strong correlations also exist between aggregate phenotypic trait metrics. *Major ellipse axis* positively correlated with *maximum depth*. *Convex hull area*, *convex hull volume*,

minor ellipse axis and *maximum width* are highly positively correlated with each other. but are negatively correlated with *solidity* (Figure 4-4).

Random forest analysis: Different phenes are important in determining the estimate of different aggregate phenes

The results of the random forest analysis are shown in Table 4-2. Reduced variable models created with Random Forest show proportion of explained variance (R^2) between 80 % and 99 % for models with all aggregate phenotypic metric except *bushiness*, which had 62 % in bean and 41% in maize; and *FD* which had R^2 of 67 % in bean and 20 % in maize. The most important variables for each aggregate phenotype for the bean and maize models are summarized in Table 4-3. The variables have been summarized based on the phene the variable represents.

Among the variables evaluated by the random forest analysis, axial root length and lateral root length were found to be important explanatory variables for all the phene aggregates in both bean as well as maize. Lateral Root Branching Density (LRBD) was found to be an important variable for *total length, total area, total volume, maximum number of roots, median number of roots bushiness*, *FD* and *FA* in bean as well as maize. LRBD was also important for *volume distribution* in maize root phenotypes and *ellipse aspect ratio* in bean root phenotypes. Number of roots and diameter played important roles in determining the *total area* in maize and bean root systems respectively. Root diameter was an important variable for *total volume, volume distribution, maximum depth, solidity* and *FD* in both bean and maize phenotypes. Diameter was also an important variable in *total area* and *ellipse aspect ratio* in bean and *bushiness* in maize root phenotypes. Angle was selected as an important variable by the random forest models for *maximum width, convex hull area, convex hull volume, ellipse minor axis, ellipse aspect ratio, solidity* and *FD* for both maize and bean. All the variables evaluated are important for the model with *FD* as the dependent variable.

Estimates of aggregate phene metrics can be similar for phenotypes with different phene states

Even in phenotypes with similar estimates for aggregate phenotypic metrics, the phene states of the constituent phenes varied greatly (Figure 4-5(a), Figure 4-5(b)). Phenotypes chosen based on the similarity of aggregate phenotypic metrics had different diameter, LRBD, and number of roots of different classes. Conversely, phenotypes in which phenes exist in different states have

similar aggregate phenotypic metrics (Figure 4-6). Four bean phenotypes that vary only in the number of basal roots and root growth angle were chosen and the estimate of total volume, convex hull volume and FD were compared (Figure 4-6). Phenotype 1 has one whorl of basal roots with shallow angles, phenotype 2 has one whorl of basal roots with deep angles, phenotype 3 has three whorls with fanned root growth angles. While phenotypes 1 and 2, which vary only in root growth angle, have different estimates for all the three metrics considered (total volume, convex hull volume and FD) phenotypes 1 and 3 have similar estimates for FD (varying by less than 2%) even though they vary in both in number of basal roots as well as root growth angles. Similarly, phenotype 4 has four whorls with fanned angles and differs from phenotype 3 and phenotype 1 in number of basal roots as well as root growth angle, but varies in the estimates of total volume by 1% and 16 % respectively; and in the estimate of convex hull volume by 1% and 4% respectively (Figure 4-6).

Variation in estimates of phene and phene aggregate metrics obtained from 2D projections

In order to study which metrics are not accurately represented by 2D projections, elementary and aggregate phenotypic metrics were estimated from 2D projections obtained by rotating the root system through 360 degrees at 20 degree intervals. It should be noted that *convex hull volume* and area of a 2D projection corresponds to surface area of a 2D hull and the length of the perimeter of a 2D hull respectively. Analysis with 2D image series shows that among phenes, estimates of root growth angle differ when projections are obtained at different rotations. Among aggregate phenotypic trait metrics, the metrics which have angle as one of the most important variables, including *convex hull volume, convex hull area, minor ellipse axis, major ellipse axis, ellipse aspect ratio, solidity, FD* and *FA*, as determined in the random forest analysis, are sensitive to projection. These phenotypic metrics had a coefficient of variation of 10-20 % but some had much greater CV depending on the phenotype in both the maize and bean (Figure 4-7(a) and Figure 4-7(b)). The differences in estimates inflated when an aggregate phenotypic trait was calculated as a function of two metrics which are already subject to lot of measurement variation (Figure 4-7(a) and Figure 4-7(b)).

Variation in estimates of phene and phene aggregate metrics over time

Some phene aggregates such increase substantially over 30 days, while some remained relatively static and estimates of some aggregate metric decreased with time (Figure 4-8(b), Figure 4-9(b)). Of the traits, *total length, total area, total volume, maximum depth, convex hull area, convex hull volume, major ellipse axis, minor ellipse axis* and *FA pro*gressively increased over time in both bean and maize (Figure 4-8(b), Figure 4-9(b), Supplementary Figure 4-S4(b), Supplementary Figure 4-S5(b)). There was only a small change in the *maximum number of roots* in bean over time but this value increased significantly in maize over time (Supplementary Figure S5(b)). The pattern of changes in *FD* over time was dependent on the phenotype. There was a small decrease in *bushiness* of bean over time (Figure 4-8(b)). In maize, the phenotypes showed a significant increase from day 10 to 20 followed by a drop from day 20 onwards (Figure 4-9(b)). The magnitude of increase was dependent on the phenotype. *Volume distribution* was either static or there was a slight increase in the bean phenotypes over time (Supplementary Figure 4-S4(b), Supplementary Figure 4-S5(b)). In maize the change in magnitude of *volume distribution* over time was dependent on the phenotype.

DISCUSSION

This study investigated the importance and utility of phenes and phene aggregate traits in phenotyping studies. Our results confirm that phenes are robust and stable over time and also sensitive enough to discriminate between highly similar root systems. In contrast, since phene aggregates capture combinations of subtending phenes, and several combinations of phenes in different states can produce phenotypes which have comparable estimates of phene aggregates, the estimates of phene aggregates are not unique representations of the state of the underlying phenes. Aggregate phene metrics are not stable over time, mostly because there is a rapid development of many elementary root phenes over time. When the number of phenes estimated by the aggregate metric increases, the complex interactions among phenes result in the same phenotype having vastly different estimates for the same aggregate metric at different time points.

Root models can aid exploration of root phenomics

In this study we use *SimRoot* to simulate root systems and use the simulated phenotypes to evaluate various root phenotyping metrics. We used modelling for this study due to constraints in obtaining empirical data caused by limitations in phenotyping methodologies and artifacts due to technicalities in image processing. Phenotyping efforts represent a compromise between throughput, precision and data processing. Many high-throughput phenotyping methodologies involve obtaining 2D metrics and depend on growing plants in controlled growth systems such as pouch, pots, gel plate systems, germination paper, etc. where root architecture is affected due to spatial growth constraints, in particular, branching angles. Not all 3D RSA estimates can be obtained by series of 2D image data; some phenotyping metrics such as volume of non-convex shapes cannot be obtained from 2D projections, especially from complex root systems. Occlusions in 2D images caused by crossing roots increase complexity of systems and reduce accuracy of many 2D estimates; this is especially true for mature root systems which are complex branched structures composed of overlapping and crossing segments (Lobet et al., 2017) ; 3D estimates are better for measuring these "traits" but are biased for other parameters such as surface area due to technicalities in image reconstructions. 3D imaging techniques such as x-ray computed tomography (μCT) and magnetic resonance imaging allow non-invasive studying of spatiotemporal dynamics of root growth (Mooney et al., 2012; Tracy et al., 2012; Schulz et al., 2013; Metzner et al., 2015), but require elaborate data processing and are suitable for relatively small and young root systems due to technical restrictions in container size (Bucksch et al., 2014; Landl et al., 2018) and are scanned at low throughput (Downie et al., 2015; Landl et al., 2018). Studies under controlled conditions enable study of growth of roots over time, however are generally used to assess less complex root structures on younger plants from germination to ca. 10 day after germination (Clark et al., 2011). This is a particular limitation for monocot roots which develop more axial roots over time. Destructive field sampling methods such as shovelomics (Trachsel et al., 2011; Burridge et al., 2016) allow the measurement of the root crown phenotype however is associated with loss and possible displacement of fine roots (Pagès and Pellerin, 1994; Pellerin and Pagès, 1994). Estimates of phenotyping metrics such as fractal dimension is sensitive to incompleteness of the excavated root network (Nielsen et al., 1999; Bucksch et al., 2014).

SimRoot, a functional-structural plant model has been used extensively for elucidating the functional value of one or more phenes, and to analyze phene interactions and root complexity

(Walk et al., 2004; Walk et al., 2006; Lynch, 2007; Postma and Lynch, 2011a; Postma and Lynch, 2011b; Postma et al., 2014; Dathe et al., 2016; Rangarajan et al., 2018). Simulations with *SimRoot* enable comparing genotypes that vary only in the phene of interest, i.e. near-isophenic lines, which are exceedingly difficult to obtain empirically (Lynch, 2011; York et al., 2013; Rangarajan et al., 2018). A significant advantage of using *SimRoot* is that root architecture over time is known in its entirety devoid of measurement and sampling error. Highly complex root systems can be simulated and resulting root images can be used without any requirement of cleaning images as there is no image noise. Root image co-ordinates are recorded as they grow in 3D space, and so root phenotyping traits can be measured at any time step without additional effort. One of the major hurdles in phenotyping roots is that artifacts may be present so that the representation of the root system may not be accurate.

Correlation among estimates of phenes and phene aggregates are an emergent property of SimRoot

Our studies with phenes and phene aggregates show that some phenes are highly correlated with each other. *SimRoot* is a mechanistic model and has no fixed relationships for the root architectural parameters. The phenotype is simulated based on a set of input parameters including number of roots of different root classes, root growth angles, root diameter, lateral root branching density with some stochasticity included in each of the parameters. Due to carbon feedbacks and restricted carbon availability, not all phenotypes are simulated. The root system develops based on carbon availability as determined by availability in the seed initially. Plant growth and development occurs as emerging from underlying processes such as photosynthesis, allocation of assimilates, uptake of nutrients and determine the growth of the plant root system (Walk et al., 2006; Postma et al., 2014; Rangarajan et al., 2018). There are no correlations built into the model and the correlations seen among the phenes in the phenotypes are a result of the mechanistic processes that are captured in the model. For example, larger diameter root axes result in larger carbon sinks leaving few resources for other roots. A set of carbon allocation rules determine carbon allocated to different root classes with axial roots having precedence over lateral roots. This is seen as a reduction in lateral root length when the number of roots is greater or when the root diameter is greater. Growth rates of the root tips are a function of carbon availability and if severe carbon limitations occur (as would occur if the phenotype being

simulated had many axial roots, greater branching density or large diameter roots or combination of these), axial root length is affected and in extreme cases may inhibit the emergence of roots emerging later. Attempts to factorially design phenotypes based on discrete values of the phene states resulted in some phenotypes not developing for more than few days due to carbon limitations. This is because *SimRoot* keeps track of resource allocation (C, N, P) and trade-offs in carbon allocation result in trade-offs among root traits, as occurs with real plants. The trade-offs include longer axial roots and longer lateral roots when number of axial roots/axial root diameter is reduced, which are seen as high correlations among those phenes. Only those phenotypes that supported plant growth for 40 days were used so that the metrics were dependent only on the phenotype. All metrics were recalculated/extracted from the simulated root system in order to get an accurate estimate of the phenotypic metric.

Correlations also exist among phene aggregates*; maximum depth* and *major ellipse axis* were highly correlated; *Convex hull area, convex hull volume, maximum width* and *minor ellipse axis* were also highly correlated as seen in several other studies *Major ellipse axis* and *maximum depth* are measures of rooting depth (Wedger et al., 2019) and were correlated with primary root length. *Maximum width, minor ellipse axis* and *convex hull* are phene aggregates which characterize expansion in sense of the outer shape of the root system (Paulus et al., 2014). *Maximum width* and *minor ellipse axis* estimates are one-dimensional metrics, *convex hull* is a function of all three dimensions (Mairhofer et al., 2013). These differences mean that as the root grows, estimates of the *convex hull* have a much greater increase in magnitude than does *maximum width*. *Solidity*, which is a ratio of the *total volume and convex hull,* could increase or decrease as *total volume* is dependent on number of roots, lengths of the roots of different root classes and diameters, however *convex hull* estimates the volumetric expansion of the outer shape of the root system.

Phene aggregate metrics are not an unique estimate of phenotype

Phene aggregate measures such as rooting depth are functionally useful traits, as has been demonstrated by several studies. Rooting depth however is influenced by several phenes including root angle, number of roots, LRBD , as shown by several studies (e.g. Manschadi et al., 2010; Trachsel et al., 2013; Saengwilai et al., 2014b; Zhan et al., 2015; Gao and Lynch, 2016). A measure of rooting depth however does not provide any information on the constituent

phenes such as rooting angle, number of roots etc. which all contribute to rooting depth. The same is true for other phene aggregate measures such as convex hull volume. Convex hull, defined as the shape of an object created by joining its outermost points, has been used as an indicator of the extent of soil exploration. Calculating convex hull from point clouds requires minimal preprocessing, making it a popularly used phenotyping metric. Although convex hull can provide interesting information about the overall root system shape (Ingram et al., 2012; Zurek et al., 2015), it was not found to be useful in discriminating between phenotypes of different populations (Iyer-Pascuzzi et al., 2010). In a study comparing roots in compacted and uncompacted soil where root geometry is severely affected by soil characteristics, convex hull volume differed by a factor of 3 (Tracy et al., 2012). Here we demonstrate that phenotypes with convex hull estimates within as low as 5% of each other can have phenes expressed in distinctly different states.

While the estimate of a single phene aggregate metric might not be useful in discriminating between phenotypes, using multiple phene aggregate metrics can probably be useful. Each phene aggregate trait gives an estimate of the phenotype by capturing different combinations of phenes. *Total length, area* and *volume* give an estimate of the size of the root system by indirectly measuring the number of roots, length of roots and the diameter of the roots. *Convex hull, minor ellipse axis, major ellipse axis, ellipse aspect ratio, maximum width* and *maximum depth* provide information of the extent of the shape by providing a measurement root angle and root length. Estimates of these phene aggregates, even though they distinguish features of the root system and complement one another in important ways (Topp et al., 2013), do not provide any information on the phene states that comprise the phenotype. Studies aimed at finding root traits which discriminate between populations / phenotypes have found that no single phene aggregate trait was important (Zurek et al., 2015). Which traits were key as well as the number of informative traits were highly dependent on differences between RSA and the imaging day (Zurek et al., 2015). Complexity of RSA over time reinforce the necessity of assessing a large number of traits to distinguish between different varieties as well as individual varieties at different ages (Iyer-Pascuzzi et al., 2010; Topp et al., 2013; Zurek et al., 2015). Accuracy of the different metrics is strongly linked to the root phenotypes analyzed as well as their size and complexity.

Variation in estimates from 2D projection images arise especially due to phenes that determine the geometry of the root system

Root angle is an important phene for soil resource capture; studies have shown that shallow root angles are important for capture of immobile soil nutrients and deep root angles for mobile soil nutrients as well as water capture(Zhu et al., 2005a; Omori and Mano, 2007; Uga et al., 2011; Dathe et al., 2013; Lynch, 2013; Miguel et al., 2013; Miguel et al., 2015; Dathe et al., 2016; Lynch, 2019) . Differences in root growth angle result in phenotypes with distinct differences due to trade-offs in the capture of mobile and immobile soil resources and resulting trade-offs in phenes leading to large effects in biomass production (Ge et al., 2000; Dathe et al., 2016; Rangarajan et al., 2018). Our results show that estimate of root angle is affected by the 2D projection of the root system. Root angle determines the geometry of the root system and was found to be an important variable in determining variations in *convex hull area, convex hull volume, maximum width* and *minor ellipse axis* (Table 2). Aggregate phene traits capturing the geometry or overall shape of the root cannot be measured accurately using estimates derived from 2D data. The variation in the estimates of root angle when measured using 2D projections affect the estimates of all phene aggregate traits in which they play an important role directly or indirectly; these include secondary phene aggregate traits such as solidity, ellipse aspect ratio as well as root complexity traits *FD* and *FA* (Figure 8 and Figure 9). Variation is greater in phene aggregates which are estimates of some function of more than one aggregate phene. Even though our root phenotypes are simulated, they are based on empirical parameters, and differences in number of roots, angles of each root class etc. were varied and as a result, our root phenotypes were not symmetrical, to replicate actual root system in fields. This is important because most roots found in nature are not symmetrical. We found that greater asymmetry was associated with greater variation in the aggregate phenotypic metrics estimated from 2D projections. Results from studies using 2D images from gel culture, growth pouches, narrow growth containers with a transparent face, etc., should be interpreted with caution.

Variation in phene aggregate metrics with time is species dependent

We analyzed root phenotypes of two species, maize and common bean, representing a monocot and a dicot root architecture. The main difference between bean, which is a dicot root system, and monocot root systems is that new roots (laterals) emerge from already existing roots in

dicots, whereas in monocots nodal roots continually emerge over time from shoot nodes near or above the soil surface (Rangarajan et al., 2018). Therefore, the vertical distribution of roots vary between maize and bean, with the bean root system having a relatively equal root distribution whereas maize has more proportion of roots in the topsoil (Postma and Lynch, 2012; Zhang et al., 2014). The number of roots as well as root diameter depends on the nodal position in maize. This is probably the reason for the great temporal variation in metrics such as *volume distribution* and *bushiness* which are related to root size. It has been suggested that metrics accurate for small dicot root systems might fail for large dicot or small monocot root systems (Lobet et al., 2017). Our study confirms that estimates of phene aggregates are not only dependent on phenotype and time but also on the plant species.

Metrics of root complexity

Fractal parameters are different from all the estimated phene aggregates in that they do not provide information on shape of the phenotype, extent of shape or size of the root system, but instead measure the geometric complexity of the root phenotype (Fitter and Stickland, 1992; Nielsen et al., 1997; Nielsen et al., 1999). All the phenes tested were important in determining fractal estimates. Fractal dimension was useful in differentiating between P inefficient and P efficient bean genotypes (Nielsen et al., 1999) as well study of roots fractal parameters with uptake of diffusion limited nutrients and between genotypic variation in wheat, study developmental responses in rice (Manschadi et al., 2008; Wang et al., 2009). It was found, however, that not a single but combinations of multiple fractal measurements provide useful information (Nielsen et al., 1999; Walk et al., 2004). Phenotypes with comparable aggregate phene trait estimates can be a result of different combinations of phenes in distinctly different phene states. This implies that estimates of phene aggregate traits measure the aggregate of multiple phenes (York et al., 2013). Studies have shown that complex phenotypic traits such as root complexity as measured by fractal analysis are determined by a multitude of genes with small effects (Grift et al., 2011). Even though several studies have resulted in identification of QTLs for aggregate phene traits (Topp et al., 2013; Atkinson et al., 2015; Zurek et al., 2015; Kenobi et al., 2017), only one gene directly controlling RSA has been cloned (Uga et al., 2011). Estimates of QTL locations or effects *per se* do not give us direct biological information regarding the product or function of each gene and the interactions among genes (Bernardo,

2008). Phenes are unique, meaning, are the product of only one set of genes and processes at a specified scale of resolution (Lynch and Brown, 2012; Lynch, 2019) and so, phene selection is more genetically tractable than selection for traits that aggregate multiple phenes, because axiomatically phenes are under simpler genetic control than any combination of phenes (Lynch, 2019).

Selection of phenotypes based on phenes are useful for breeding

Several phenes have been studied and their functional utility has been established including number of roots (crown roots in maize, basal roots in bean), root growth angle (shallow for phosphorus uptake and deep rooting angle for nitrogen capture), lateral root branching density and length for nitrate uptake(Zhu et al., 2005b; Lynch, 2013; Trachsel et al., 2013; Saengwilai et al., 2014; Miguel et al., 2015; Zhan and Lynch, 2015; Rangarajan et al., 2018; Sun et al., 2018). In the bean root system, basal roots emerge at the seedling stage and seedling root phenotypes have significant relationships with mature root phenotypes in the bean root system. Number of basal roots as well as basal root growth angle is stable over time as proven by the fact that studies selecting for basal root number and angle at different stages of growth from seedling to few weeks old plants (Liao et al., 2001; Vieira and Lynch, 2001; Vieira et al., 2008) have been consistent. Genetic factors explained 52% to 57 % of genetic variation of phenes in bean including basal root whorl number, basal root number, adventitious root number, and 52% of phenotypic variation in taproot length in seedlings (Strock et al., 2019). Crown root and brace root number , angle and LRBD were found to be genotype-specific and did not change across growth stages in maize (Trachsel et al., 2013). Basal diameter remains constant in maize while apical diameter varies; in dicots like bean, diameter increases with age due to secondary root growth (Strock et al., 2018). Root growth/ elongation rates determine the length of the root and are thought to be phenes (York et al., 2013; Strock et al., 2019). However, carbon limitations could result in delay of emergence of axial roots as well as play a role in determining the final number of axial roots. Demotes-Mainard and Pellerin (1992) have observed on maize that the emergence of axial roots was delayed, and the final number of axial roots was reduced, with increasing levels of competition for light between plants. Time of emergence of roots could also be an important phene, especially in maize where roots emerge from different nodes over time. Recent studies have shown that cellular anatomy varies among nodes providing evidence for

node-specific traits (Yang et al, 2019). Our approach using elemental phenes to discriminate between architecturally and anatomically distinct phenotypes based on phene states has been used successfully for selection of functionally superior phenotypes for different crop species (Burridge et al., 2017). We suggest that it is best to study the phenotypes at their elementary level of organization, namely phenes in order to get a better understanding of their functional value in terms of the interactions among the phenes and also to identify their genetic features.

CONCLUSIONS

These results demonstrate that phenes including number of roots, diameter of roots, lateral root branching density and root growth angle provide reliable descriptors of root phenotypes. Phenes are also stable over time and independent of time of phenotyping. Estimates of phenes provide a complete description of the resulting phenotype and also enable easier prediction of functional attributes the phenotype could potentially have. Data from our *in-silico* phenotyping environment provides access to complete information concerning root architectural phenotypes without measurement error, sampling limitations, or confounding factors such as phenotypic plasticity or root loss. Even under these conditions, estimates of aggregate phenotypic metrics are less reliable than those of phene states. Even though the estimates of aggregate phenotypic metrics are dependent on the phenotype, the estimates are not unique estimates of underlying states of the constituent phenes. Estimates of phene aggregates also vary in magnitude at different time points of growth, the magnitude of change being dependent on the aggregate phenotype metric used as well as the constituent phenes. Unlike methods used to estimate aggregate phenotypes, estimation of phenes involves simple, straightforward procedures and yield reliable results. We suggest that measurement of phenes provides data that are more robust, reliable and relevant than metrics that estimate the aggregation of multiple subtending phene states. We show this in the context of root architectural phenotypes but propose that these concepts apply to phenomic analysis of any organism.

ACKNOWLEDGEMENTS

This research was supported by the National Institute of Food and Agriculture, U.S Department of Agriculture Hatch project 4732 and the Foundation for Food and Agriculture Research 'Crops in Silico' project.

REFERENCES

Atkinson JA, Pound MP, Bennett MJ, Wells DM (2019) Uncovering the hidden half of plants using new advances in root phenotyping. *Current Opinion in Biotechnology* 55: 1–8

Atkinson JA, Wingen LU, Griffiths M, Pound MP, Gaju O, Foulkes MJ, Gouis JL, Griffiths S, Bennett MJ, King J, et al (2015) Phenotyping pipeline reveals major seedling root growth QTL in hexaploid wheat. *Journal of Experimental Botany* 66: 2283–2292

Bernardo R (2008) Molecular markers and selection for complex traits in plants: learning from the last 20 Years. *Crop Sci*ence 48: 1649

Breiman L. (2001) Random forests. *Machine Learning* 45: 5-32

Bucksch A, Burridge J, York LM, Das A, Nord E, Weitz JS, Lynch JP (2014) Image-Based High-Throughput Field Phenotyping of Crop Roots. *Plant Physiology* 166: 470–486

Burridge J, Jochua CN, Bucksch A, Lynch JP (2016) Legume shovelomics : High — Throughput phenotyping of common bean (Phaseolus vulgaris L .) and cowpea (*Vigna unguiculata subsp , unguiculata*) root architecture in the field. *Field Crop Res*earch 192: 21–32

Burridge JD, Schneider HM, Huynh BL, Roberts PA, Bucksch A, Lynch JP (2017) Genome-wide association mapping and agronomic impact of cowpea root architecture. *Theoretical and Applied Genetics* 130: 419–431

Chimungu JG, Brown KM, Lynch JP (2014) Large root cortical cell size improves drought tolerance in maize. *Plant Physiology* 166: 2166–2178

Clark RT, MacCurdy RB, Jung JK, Shaff JE, McCouch SR, Aneshansley DJ, Kochian LV. (2011) Three-dimensional root phenotyping with a novel imaging and software platform. *Plant Physiology* 156: 455–465

Cobb JN, DeClerck G, Greenberg A, Clark R, McCouch S (2013) Next-generation phenotyping: requirements and strategies for enhancing our understanding of genotype–phenotype relationships and its relevance to crop improvement. *Theoretical and Applied Genetics* 126: 867–887

Cutler DR, Edwards TC Jr, Beard KH, Cutler A, Hess KT, Gibson J, Lawler JJ (2007) Random forests for classification in ecology. *Ecology* 88: 2783–2792

Dathe A, Postma JA, Lynch JP. 2013. Modeling resource interactions under multiple edaphic stresses. In: Timlin D, Ahuja LR, eds. Enhancing understanding and quantification of soil-root interactions. Madison, WI: American Society of Agronomy, Crop Science Society of America, Soil Science Society of America, 273–294.

Dathe A, Postma JA, Postma-Blaauw MB, Lynch JP (2016) Impact of axial root growth angles on nitrogen acquisition in maize depends on environmental conditions. *Annals of Botany* 118: 401–414

Demotes-Mainard S, Pellerin S (1992) Effect of mutual shading on the emergence of nodal roots and the root/shoot ratio of maize. *Plant Soil* 147: 87- 93

Den Herder G, Van Isterdael G, Beeckman T, De Smet I (2010) The roots of a new green revolution. *Trends in Plant Science* 15: 600–607

Downie HF, Adu MO, Schmidt S, Otten W, Dupuy LX, White PJ, Valentine TA (2015) Challenges and opportunities for quantifying roots and rhizosphere interactions through imaging and image analysis. *Plant Cell & Environment* 38: 1213–1232

Eghball B, Settimi JR, Maranville JW, Parkhurst AM (1993) Fractal analysis for morphological description of corn roots under nitrogen stress. *Agronomy Journal* 85: 287-289

Fitter AH, Stickland TR (1992) Fractal characterization of root system architecture. *Functional Ecology* 6: 632-635

FAO (2015) The future of food and agriculture: Trends and challenges. Rome.

Furbank RT, Tester M (2011) Phenomics – technologies to relieve the phenotyping bottleneck. *Trends in Plant Science* 16: 635–644

Gao Y, Lynch JP (2016) Reduced crown root number improves water acquisition under water deficit stress in maize (*Zea mays* L.). *Journal of Experimental Botany* 67: 4545–4557

Ge Z, Rubio G, Lynch JP (2000) The importance of root gravitropism for inter-root competition and phosphorus acquisition efficiency: results from a geometric simulation model. *Plant Soil* 218: 159–171

Grift TE, Novais J, Bohn M (2011) High-throughput phenotyping technology for maize roots. *Biosystems Engineering* 110: 40–48

Ingram PA., Zhu J, Shariff A, Davis IW, Benfey PN, Elich T (2012) High-throughput imaging and analysis of root system architecture in *Brachypodium distachyon* under differential nutrient availability. *Philosophical Transactions of the Royal Society of London. Series B, Biological Sciences* 367: 1559–1569

Iyer-Pascuzzi AS, Symonova O, Mileyko Y, Hao Y, Belcher H, Harer J, Weitz JS, Benfey PN

(2010) Imaging and analysis platform for automatic phenotyping and trait ranking of plant root systems. *Plant Physiology* 152: 1148–57

Jaramillo RE, Nord EA, Chimungu JG, Brown KM, Lynch JP (2013) Root cortical burden influences drought tolerance in maize. *Annals of Botany* 112: 429–437

Kenobi K, Atkinson JA, Wells DM, Gaju O, De Silva JG, Foulkes MJ, Dryden IL, Wood ATA, Bennett MJ (2017) Linear discriminant analysis reveals differences in root architecture in wheat seedlings related to nitrogen uptake efficiency. *Journal of Experimental Botany* 68: 4969–4981

Landl M, Schnepf A, Vanderborght J, Bengough AG, Bauke SL, Lobet G, Bol R, Vereecken H (2018) Measuring root system traits of wheat in 2D images to parameterize 3D root architecture models. *Plant and Soil* 425: 457–477

Liao H, Rubio G, Yan X, Cao A, Brown KM, Lynch JP (2001) Effect of phosphorus availability on basal root shallowness in common bean. *Plant and Soil* 232: 69–79

Lobet G, Koevoets IT, Noll M, Meyer PE, Tocquin P, Pagès L, Périlleux C (2017) Using a structural root system model to evaluate and improve the accuracy of root image analysis pipelines. *Frontiers in Plant Science* 8: 447

Lynch JP, Nielsen KL, Davis RD, Jablokow AG (1997) *SimRoot* : Modelling and visualization of root systems. *Plant and Soil* 188: 139–151

Lynch JP (2007) Roots of the second green revolution. *Australian Journal of Botany* 55: 493-512

Lynch JP (2019) Root phenotypes for improved nutrient capture: an underexploited opportunity for global agriculture. *New Phytologist* 223: 548–564

Lynch JP (2013) Steep, cheap and deep: an ideotype to optimize water and N acquisition by maize root systems. *Annals of Botany* 112: 347–357

Lynch JP (2011) Root phenes for enhanced soil exploration and phosphorus acquisition: tools for future crops. *Plant Physiology* 156: 1041–1049

Lynch JP, Brown KM (2012) New roots for agriculture: exploiting the root phenome. *Philosophical Transactions of the Royal Society of London. Series B, Biological Sciences* 367: 1598–1604

Mairhofer S, Zappala S, Tracy S, Sturrock C, Bennett MJ, Mooney SJ, Pridmore TP (2013) Recovering complete plant root system architectures from soil via X-ray μ-computed tomography. *Plant Methods* 9: 8

Manschadi AM, Christopher J, deVoil P, Hammer GL (2006) The role of root architectural traits

in adaptation of wheat to water-limited environments. *Functional Plant Biology* 33: 823–837

Manschadi AM, Hammer GL, Christopher JT, deVoil P (2008) Genotypic variation in seedling root architectural traits and implications for drought adaptation in wheat (*Triticum aestivum* L.). *Plant and Soil* 303: 115–129

Metzner R, Eggert A, van Dusschoten D, Pflugfelder D, Gerth S, Schurr U, Uhlmann N, Jahnke S (2015) Direct comparison of MRI and X-ray CT technologies for 3D imaging of root systems in soil: potential and challenges for root trait quantification. *Plant Methods* 11: 17

Miguel MA, Postma JA, Lynch JP (2015) Phene synergism between root hair length and basal root growth angle for phosphorus acquisition. *Plant Physiology* 167: 1430–1439

Miguel MA, Widrig A, Vieira RF, Brown KM, Lynch JP (2013) Basal root whorl number: A modulator of phosphorus acquisition in common bean (*Phaseolus vulgaris*). *Annals of Botany* 112: 973–982

Mooney SJ, Pridmore TP, Helliwell J, Bennett MJ (2012) Developing X-ray computed tomography to non-invasively image 3-D root systems architecture in soil. *Plant and Soil* 352: 1–22

Nielsen KL, Lynch JP, Weiss HN (1997) Fractal geometry of bean root systems: field correlations between spatial and fractal dimension. *American Journal of Botany* 84: 26–33

Nielsen KL, Miller CR, Beck D, Lynch JP (1999) Fractal geometry of root systems: field observations of contrasting genotypes of common bean (*Phaseolus vulgaris* L.) grown under different phosphorus regimes. *Plant and Soil* 206: 181–190

Omori F, Mano Y (2007) QTL mapping of root angle in F_2 populations from maize 'B73' × teosinte '*Zea luxurians*'. *Plant Root* 1: 57–65

Pagès L, Pellerin S (1994) Evaluation of parameters describing the root system architecture of field grown maize plants (*Zea mays* L.). *Plant and aSoil* 164: 169–176

Paulus S, Schumann H, Kuhlmann H, Léon J (2014) High-precision laser scanning system for capturing 3D plant architecture and analysing growth of cereal plants. *Biosystems Engineering* 121: 1–11

Pellerin S, Pagès L (1994) Evaluation of parameters describing the root system architecture of field grown maize plants (*Zea mays* L.). *Plant and Soil* 164: 155–167

Rangarajan H, Postma JA, Lynch JP (2018) Co-optimization of axial root phenotypes for nitrogen and phosphorus acquisition in common bean. *Annals of Botany* 122: 1–15

Postma JA, Dathe A, Lynch JP (2014) The optimal lateral root branching density for maize depends on nitrogen and phosphorus availability. Plant Physiology 166: 1–13

Postma JA, Lynch JP (2012) Complementarity in root architecture for nutrient uptake in ancient maize/bean and maize/bean/squash polycultures. *Annals of Botany* 110: 521–534

Postma JA, Lynch JP (2011a) Theoretical evidence for the functional benefit of root cortical aerenchyma in soils with low phosphorus availability. *Annals of Botany* 107: 829–841

Postma JA, Lynch JP (2011b) Root cortical aerenchyma enhances the growth of maize on soils with suboptimal availability of nitrogen, phosphorus, and potassium. *Plant Physiology* 156: 1190–1201

Ray DK, Mueller ND, West PC, Foley JA (2013) Yield trends are insufficient to double global crop production by 2050. *PLoS One* 8: e66428

Saengwilai P, Tian X, Lynch JP (2014) Low crown root number enhances nitrogen acquisition from low nitrogen soils in maize (*Zea mays* L.). *Plant Physiology* 166: 581-589

Schulz H, Postma JA, van Dusschoten D, Scharr H, Behnke S (2013) Plant root system analysis from MRI images. *In* Computer Vision, Imaging and Computer Graphics: Theory and Application. Springer, Berlin, pp 411-425

Strock CF, Morrow de La Riva L, Lynch J (2018) Reduction in root secondary growth as a strategy for phosphorus acquisition. *Plant Physiology* 176: 691–703

Strock CF, Burridge J, Massas ASF, Beaver J, Beebe S, Camilo SA, Fourie D, Jochua C, Miguel M, Miklas PN, et al (2019) Seedling root architecture and its relationship with seed yield across diverse environments in *Phaseolus vulgaris*. *Field Crop Research* 237: 53–64

Sun B, Gao Y, Lynch JP (2018) Large crown root number improves topsoil foraging and phosphorus acquisition. *Plant Physiology* 177: 90-104

Tardieu F, Cabrera-Bosquet L, Pridmore T, Bennett M (2017) Plant phenomics, from sensors to knowledge. *Current Biology* 27: R770–R783

Tilman D, Balzer C, Hill J, Befort BL (2011) Global food demand and the sustainable intensification of agriculture. *Proceedings of the National Academy of Sciences USA* 108: 20260–20264

Topp CN, Iyer-Pascuzzi AS, Anderson JT, Lee CR, Zurek PR, Symonova O, Zheng Y, Bucksch A, Mileyko Y, Galkovskyi T, et al (2013) 3D phenotyping and quantitative trait locus mapping identify core regions of the rice genome controlling root architecture. *Proceedings of the National Academy of Sciences USA* 110: 1695–1704

Trachsel S, Kaeppler SM, Brown KM, Lynch JP (2013) Maize root growth angles become steeper under low N conditions. *Field Crop Research* 140: 18–31

Tracy SR, Black CR, Roberts JA, Sturrock C, Mairhofer S, Craigon J, Mooney SJ (2012) Quantifying the impact of soil compaction on root system architecture in tomato (*Solanum lycopersicum*) by X-ray micro-computed tomography. *Annals of Botany* 110: 511–9

Uga Y, Okuno K, Yano M (2011) Dro1, a major QTL involved in deep rooting of rice under upland field conditions. *Journal of Experimental Botany* 62: 2485–2494

Vieira RF, Carneiro JES, Lynch JP (2008) Root traits of common bean genotypes used in breeding programs for disease resistance. *Pesqui Agropecuária Bras* 43: 707–712

Vieira RF, Lynch JP (2001) Root gravitropism of genotypes of common beans used for breeding in brazil. 4899: 2–3

Villordon AQ, Ginzberg I, Firon N (2014) Root architecture and root and tuber crop productivity. *Trends in Plant Sciences* 19: 419–425

Walk TC, Van Erp E, Lynch JP (2004) Modelling applicability of fractal analysis to efficiency of soil exploration by roots. *Annals of Botany* 94: 119–128

Walk TC, Jaramillo R, Lynch JP (2006) Architectural tradeoffs between adventitious and basal roots for phosphorus acquisition. *Plant and Soil* 279: 347–366

Wang H, Siopongco J, Wade LJ, Yamauchi A (2009) Fractal analysis on root systems of rice plants in response to drought stress. *Environmental and Experimental Botany* 65: 338–344

Wedger MJ, Topp CN, Olsen KM (2019) Convergent evolution of root system architecture in two independently evolved lineages of weedy rice. *New Phytologist* 223: 1031-1042

Wise TA. (2013) Can we feed the world in 2050? A scoping paper to assess the evidence. GDAE Working paper Np.13-04. Global Development and Environment Institute, Tufts University, Medford, MA, USA. Available at http://www.ase.tufts.edu/gdae/Pubs/wp/113-04WiseFeedWorld2050.pdf

York LM, Nord EA, Lynch JP (2013) Integration of root phenes for soil resource acquisition. *Frontiers in Plant Science* 4: 355

Zhan A, Schneider H, Lynch JP (2015) Reduced lateral root branching density improves drought tolerance in maize. *Plant Physiology* 168: 1603–1615

Zhan A, Lynch JP (2015) Reduced frequency of lateral root branching improves N capture from low-N soils in maize. *Journal of Experimental Botany* 66: 2055–2065

Zhang C, Postma JA, York LM, Lynch JP (2014) Root foraging elicits niche complementarity-dependent yield advantage in the ancient "three sisters" (maize/bean/squash) polyculture. *Annals of Botany* 114: 1719–1733

Zhu J, Kaeppler SM, Lynch JP (2005a) Topsoil foraging and phosphorus acquisition efficiency in maize (*Zea mays*). *Functional Plant Biol*ogy 32: 749

Zhu J, Kaeppler SM, Lynch JP (2005b) Mapping of QTLs for lateral root branching and length in maize (*Zea mays* L.) under differential phosphorus supply. *Theoretical and Applied Genetics* 111: 688–695

Zurek PR, Topp CN, Benfey PN (2015) Quantitative trait locus mapping reveals regions of the maize genome controlling root system architecture. *Plant Physiology* 167: 1487–1496

Table 4-1: Aggregate phene metrics, definition and method of obtaining them from *SimRoot* output.

Parameter	3D	2D	Description	Measurement
Total Length	Y	Y	Summed length along the whole root system	Calculated from *SimRoot* output
Total Area	Y	Y	Summed surface area of the whole root system	Calculated from *SimRoot* output
Total Volume	Y	Y	Summed volume of the whole root system	Calculated from *SimRoot* output
Maximum width	Y	Y	Maximum horizontal width of the whole root system	Calculated using minimum enclosing circle algorithm in R
Maximum depth	Y	Y	Maximum vertical depth of the whole root system	Calculated from *SimRoot* output
Median no. of roots	Y	Y	Median no. of roots from root counts	Calculated from *SimRoot* output
Maximum no. of roots	Y	Y	No. of roots at the 84th percentile of a sorted list (smallest to largest) of root counts	Calculated from *SimRoot* output
Bushiness	Y	Y	Ratio of the maximum no. of roots to the median no. of roots	Calculated from *SimRoot* output
Volume distribution	Y	Y	Ratio of the volume of the root system contained above one-third depth of the root system to the volume of the root system contained below one-third depth of the root system	Calculated from *SimRoot* output
Convex hull volume	Y	Y	Volume of the convex hull that encompasses the whole root system	Obtained using Convhulln function in R
Convex hull area	Y	Y	Surface Area of the convex hull that encompasses the whole root system	Obtained using Convhulln function in R
Solidity	Y	Y	Ratio of volume to convex hull volume	Calculated
Major Ellipse axes	Y	N	Length of major axis of an ellipse best fit to overall shape and size of root system	Obtained using minimum volume enclosing ellipse algorithm in R
Minor Ellipse Axes	Y	N	Length of minor axis of an ellipse best fit to overall shape and size of root system	Obtained using minimum volume enclosing ellipse algorithm in R
Ellipse axis aspect ratio	Y	N	Ratio of major axis of ellipse to minor axis	Calculated from minor ellipse axes and major ellipse axes
Fractal Dimension (FD)	Y	Y	Measure of root complexity. Fractal dimension expresses the space filling properties of a structure (e.g. root system) and is associated with branching pattern	Obtained using box count code written in R
Fractal Abundance (FA)	Y	Y	Measure of root complexity. Fractal abundance is associated with the volume of space explored	Obtained using box count code written in R

Table 4-2: Results of regression models created with random forest. The R^2 values of Random Forest model with entire set of variables and those with only most important variables are presented for the bean and maize aggregate phene metrics.

Aggregate Phenotypic Metric	R^2 (% Variance Explained)			
	Bean		Maize	
	Model With All Variables	Model with Most Important Variables	Model with All Variables	Model with Most Important Variables
Total Length	89.5	91.6	82	85
Total Area	87	87	78	81
Total Volume	81.7	88.5	79	81.6
Volume Distribution	87	91	61	66
Max no. of roots	78.8	84	67	72.8
Median no. of roots	79.9	87	71	75
Bushiness	62	67	36	41
Max Depth	98.6	99.6	79	84
Max Width	91	90	95	99
Convex hull Area	97.8	97	90	93.4
Convex hull Volume	97.6	97.6	87	89.9
Ellipse Minor Axis	94.9	93.6	80	85
Ellipse Major Axis	96.7	97.3	95	98.6
Ellipse Aspect Ratio	85.9	87.4	51.9	62
Solidity	97.4	97.5	89	89
FD	67	68	16	20
FA	93.5	94.9	88	90

Note: Random Forest possesses its own reliable statistical characteristics, which could be used for validation and model selection. The major criterion for estimation of internal predictive ability of the Random Forest models and model selection is the value of R^2. R^2 in Random Forest is interpreted as a measure of predictive quality of Random Forest model on independent samples. Random Forest models were run with the aggregate phenotype as dependent variable and all the phenes as predictor variables. Most important variables were chosen based on the % increase in mean square and Random Forest models were run with only the most important variables.

Table 4-3: Summary of the most important variables selected by random forest model for phenotyping metric evaluated for bean root system and maize root system.

Phene aggregates	Phenes					
	Axial Root Length	No. of Roots	LRBD	Angle	Diameter	Lateral Root Length
Total Length	Maize Bean	Maize Bean	Maize Bean			Maize Bean
Total Area	Maize Bean	Maize	Maize Bean		Bean	Maize Bean
Total Volume	Maize Bean	Maize Bean	Maize Bean		Maize Bean	Maize Bean
Volume Distribution	Maize Bean	Maize Bean	Maize		Maize Bean	Maize Bean
Max # of Roots	Maize Bean	Maize	Maize Bean			Maize Bean
Median # of Roots	Maize Bean	Maize	Maize Bean			Maize Bean
Bushiness	Maize Bean	Maize	Maize Bean	Bean	Maize	Maize Bean
Max Depth	Maize Bean			Maize	Maize Bean	Maize Bean
Max Width	Maize Bean			Maize Bean		Maize Bean
Convex hull Area	Maize Bean			Maize Bean		Maize Bean
Convex hull Volume	Maize Bean			Maize Bean		Maize Bean
Ellipse Minor Axis	Maize Bean			Maize Bean		Maize Bean
Ellipse Major Axis	Maize Bean					Maize Bean
Ellipse Aspect Ratio	Maize Bean	Maize Bean	Bean	Maize Bean	Bean	Maize Bean
Solidity	Maize Bean	Maize		Maize Bean	Maize Bean	Maize Bean
FD	Maize Bean	Maize Bean	Maize Bean	Maize Bean	Maize Bean	Maize Bean
FA	Maize Bean	Maize	Maize Bean	Bean		Maize Bean

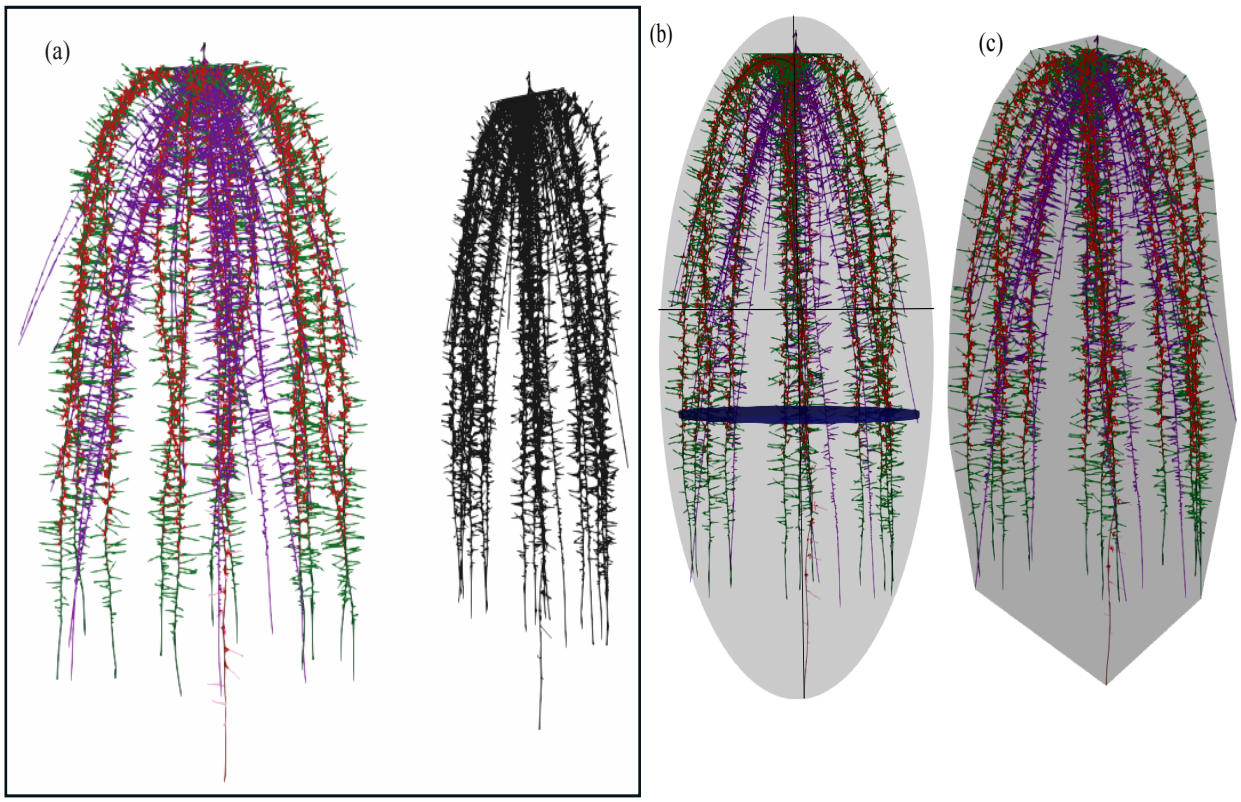

Figure 4-1: Representation of 2D projection of a 3D root system (a) Visualization of maximum width, major ellipse axis of a 2D root system (b) and convex hull volume of a 3D root system (c).

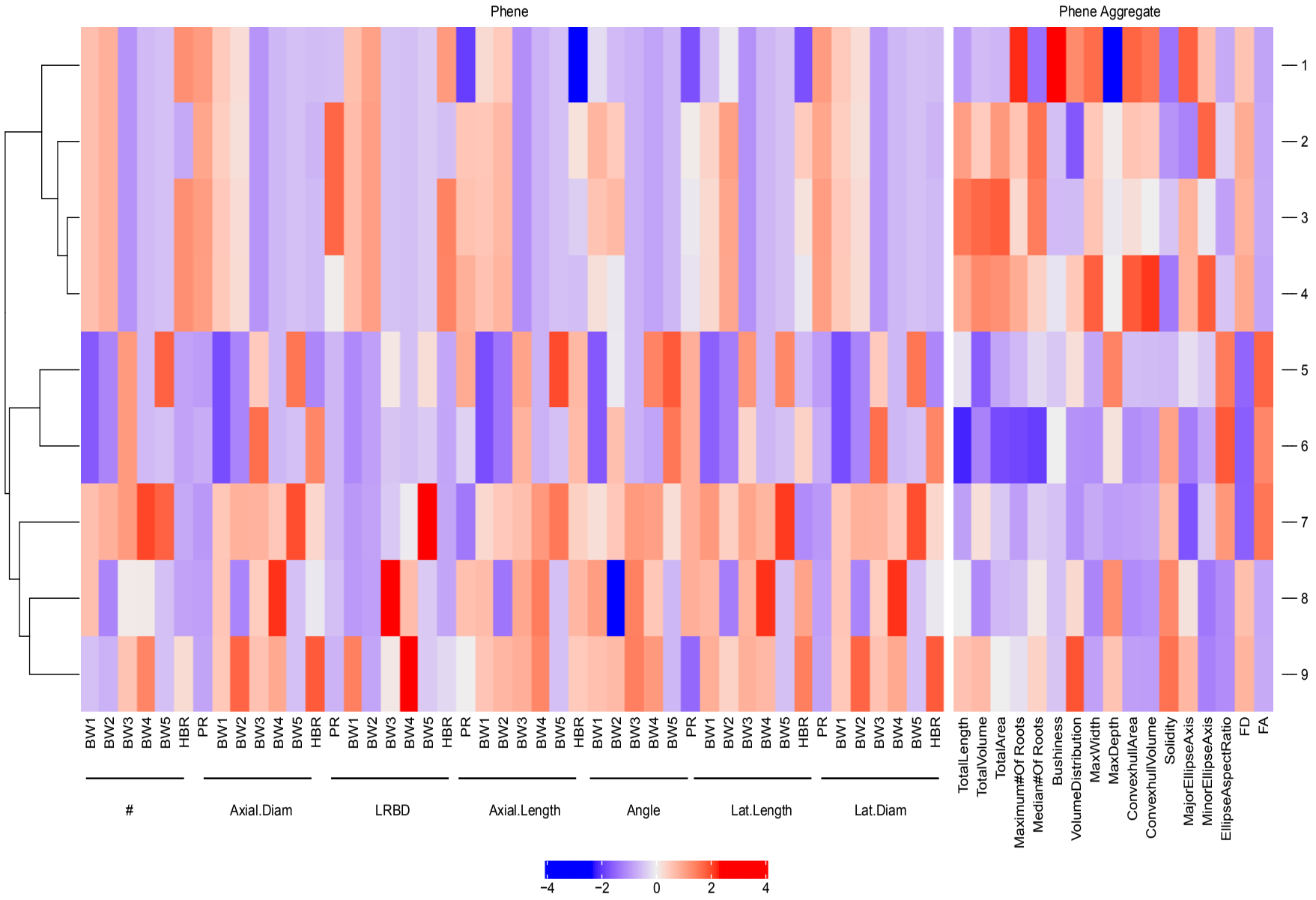
Phene
Phene Aggregate
1
2
3
4
5
6
7
8
9
BW1 BW2 BW3 BW4 BW5 HBR PR
#
Axial.Diam
LRBD
Axial.Length
Angle
Lat.Length
Lat.Diam
TotalLength
TotalVolume
TotalArea
Maximum#Of Roots
Median#Of Roots
Bushiness
VolumeDistribution
MaxWidth
MaxDepth
ConvexhullArea
ConvexhullVolume
Solidity
MajorEllipseAxis
MinorEllipseAxis
EllipseAspectRatio
FD
FA
−4
−2
0
2
4

(a)

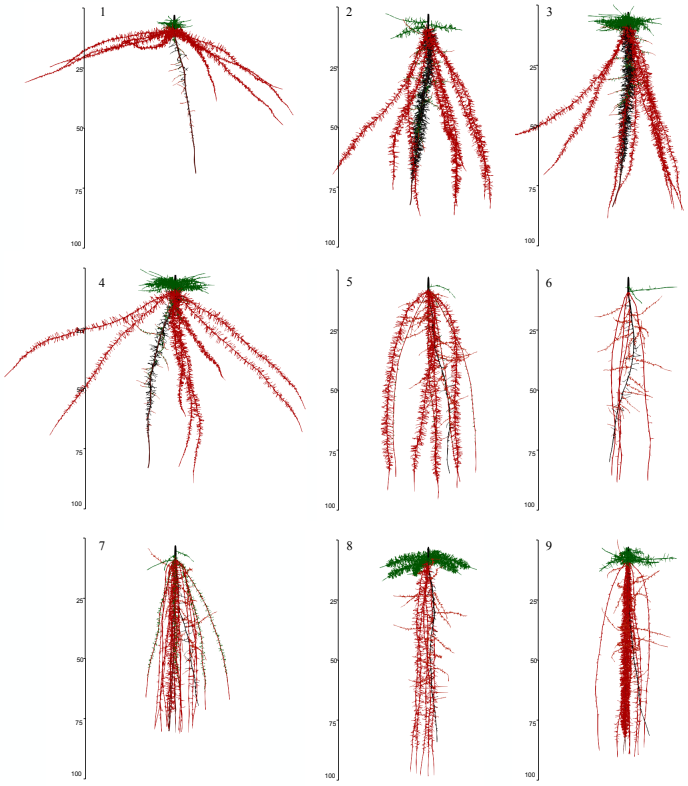

(b)

Figure 4-2: Cluster heatmap of phenotypic traits. Hierarchical clustering of a few phenotypes was generated using Spearman correlation of max-min scaled phene values of bean phenotypes at 40 days (a). The color scale indicates the magnitude of the trait values (blue, low value; red, high value). The numbers indicated on the heatmap refer to the phenotype in the specific row of the heatmap. The corresponding phenotypes are visualized in (b). Primary roots are in black; basal roots are in red; hypocotyl-borne roots are in green. # - number of axial roots; Axial.Diam – axial root diameter; LRBD – lateral root branching density; Lat.Length – lateral root length; Lat.Diam – lateral root diameter; BW1 – basal roots at whorl 1; BW2 – basal roots at whorl 2; BW3 – basal roots at whorl 3; BW4 – basal roots at whorl 4; BW5 – basal roots at whorl 5; HBR – hypocotyl-borne roots; PR – primary root.

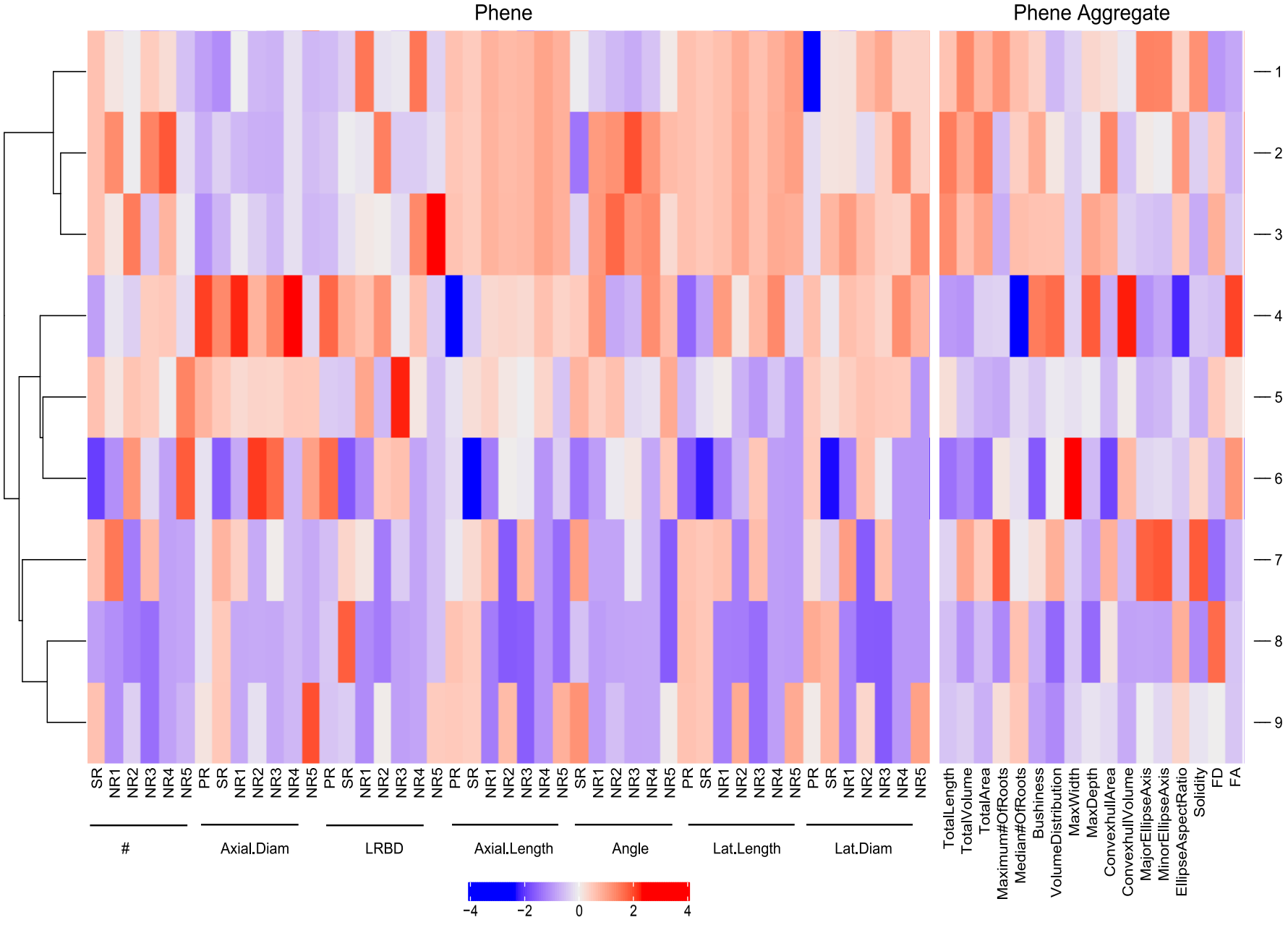
Phene
Phene Aggregate
SR NR1 NR2 NR3 NR4 NR5 PR
#
Axial.Diam
LRBD
Axial.Length
Angle
Lat.Length
Lat.Diam
TotalLength
TotalVolume
TotalArea
Maximum#OfRoots
Median#OfRoots
Bushiness
VolumeDistribution
MaxWidth
MaxDepth
ConvexhullArea
ConvexhullVolume
MajorEllipseAxis
MinorEllipseAxis
EllipseAspectRatio
Solidity
FD
FA
1
2
3
4
5
6
7
8
9
−4
−2
0
2
4

(a)

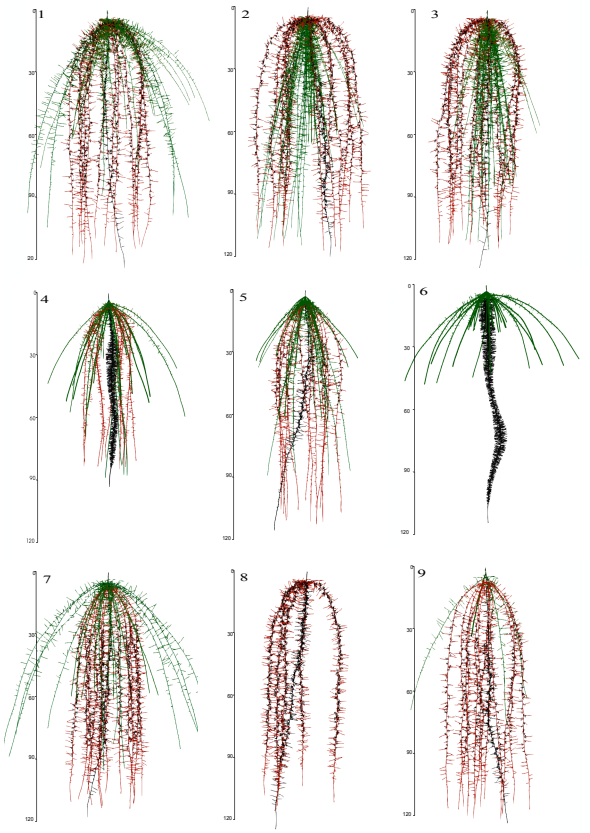

(b)

Figure 4-3: Cluster heatmap of phenotypic traits. Hierarchical clustering of a few phenotypes was generated using Spearman correlation of max-min scaled phene values of maize phenotypes at 40 days (a). The color scale indicates the magnitude of the trait values (blue, low value; red, high value). The numbers indicated on the heatmap refer to a phenotype in the specific row of the heatmap. The corresponding phenotypes are visualized in (b). Primary roots are in black; seminal roots are in red; nodal roots are in green. # - number of axial roots; Axial.Diam – axial root diameter; LRBD – lateral root branching density; Lat.Length – lateral root length; Lat.Diam – lateral root diameter; NR1 – nodal roots at position 1; NR2 – nodal roots at position 2; NR3 – nodal roots at position 3; NR4 – nodal roots at position 4; SR – seminal roots; PR – primary root.

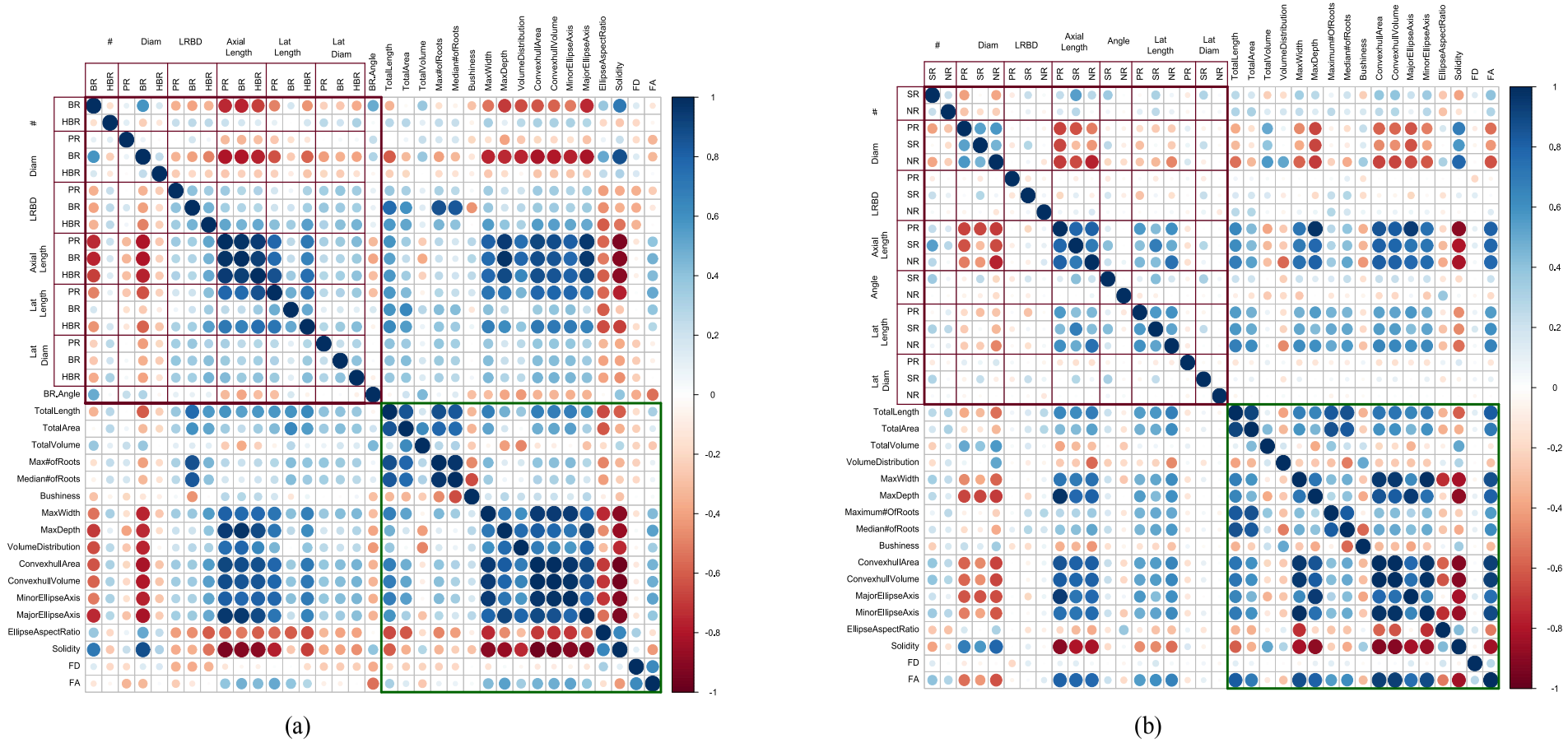

Figure 4-4: Phenotypic trait relationship. Correlation matrix of phenes and phene aggregates evaluated for bean root phenotypes (a). Correlation matrix of phenes and phene aggregates evaluated for maize root phenotypes (b). The color scale indicates Spearman correlation coefficient between traits (red, negative; blue, positive). Color intensity and size of the circle are proportional to the correlation coefficients between two traits. Correlations between phenes are indicated by the points in the red box, the green box contains the correlations between phene aggregates. BR – basal roots; HBR – hypocotyl-borne roots; PR – primary root; SR – seminal roots; NR – nodal roots; # - number of axial roots; Diam – axial root diameter; LRBD – lateral root branching density; Axial Length – axial root length; Lat Length – lateral root length; Lat Diam – lateral root diameter

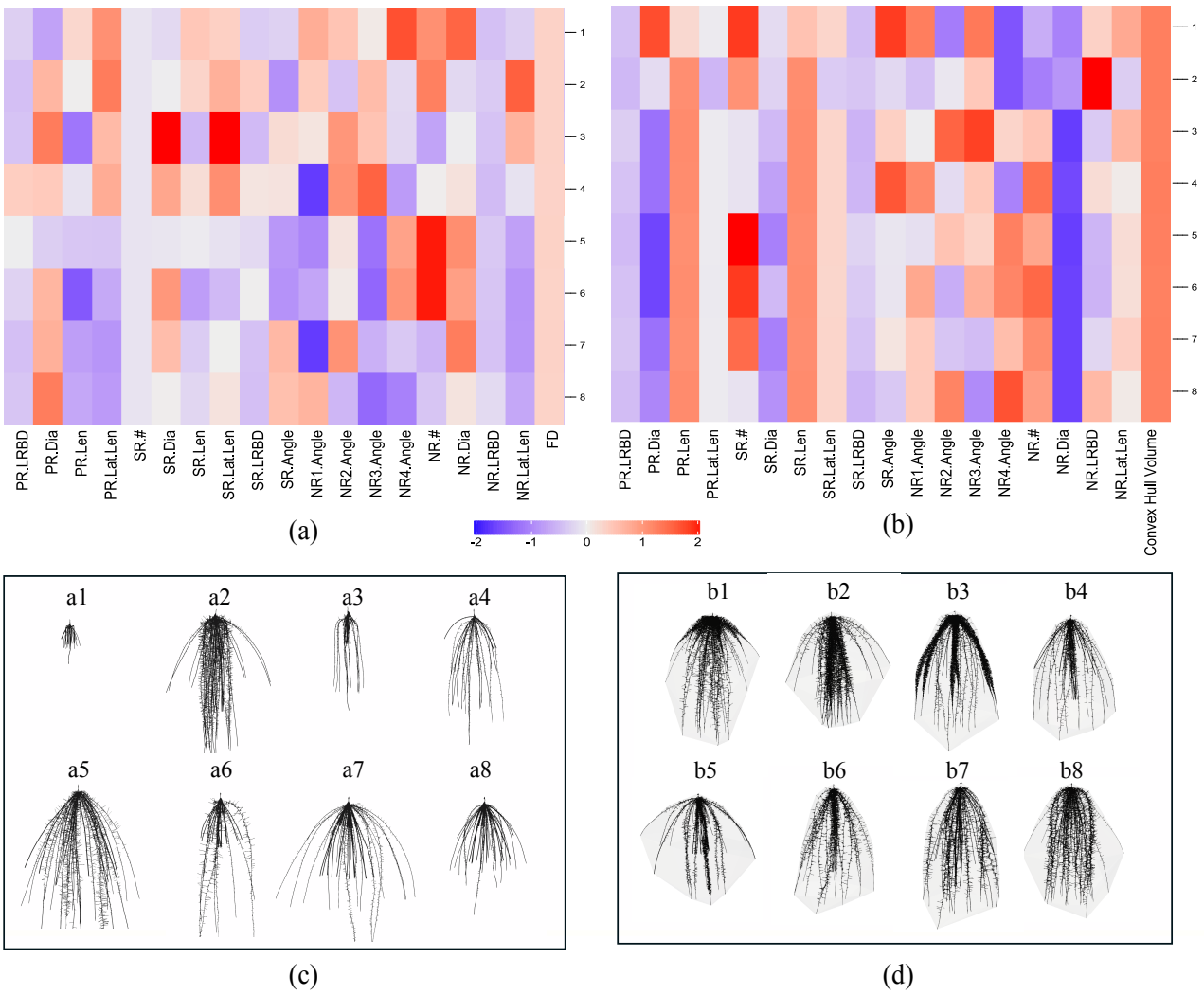

Figure 4-5: Phene values of maize root phenotypes with comparable FD (a) and convex hull volume (b). The heatmap shows values of the traits obtained by dividing the values with maximum values of respective traits. Phenotypes with similar FD and similar convex hull volume are visualized in (c) and (d) respectively Phenotypes a1 - a8 have similar FD; Phenotypes b1-b8 have similar convexhull volume; PR- Primary Root; SR -Seminal root; NR - Nodal root; LRBD- lateral root branching density; Len - axial root length; Lat.Len - lateral root length; # - number of axial roots; Dia - diameter; FD -Fractal Dimension.

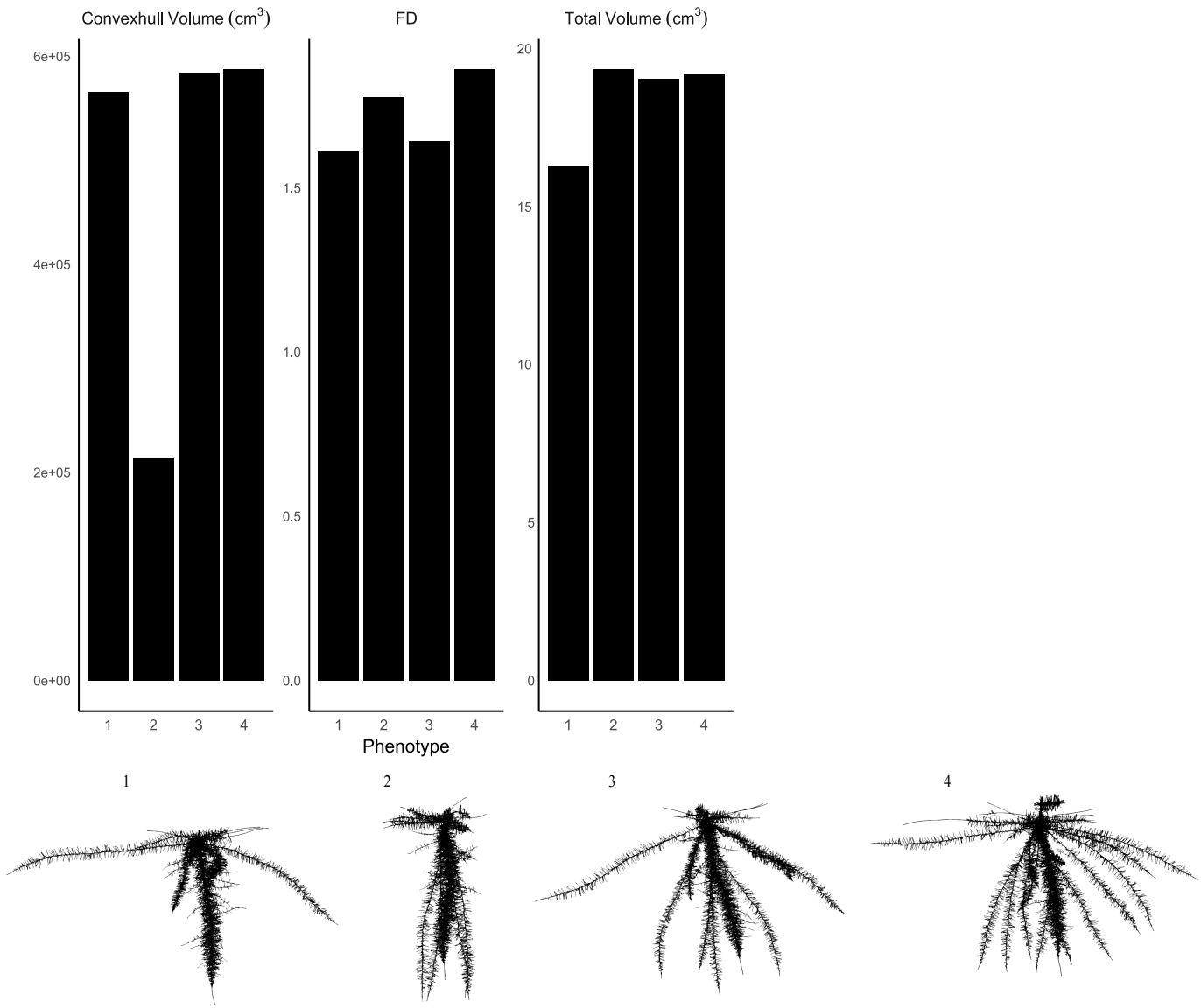

Figure 4-6: Convex hull volume, FD and total volume of bean root phenotypes with (a) one whorl and shallow angle, (b) one whorl and deep angle(c) two whorls and fanned angle (d) four whorls and fanned angles. The corresponding phenotypes are visualized in lower panel. FD – fractal dimension.

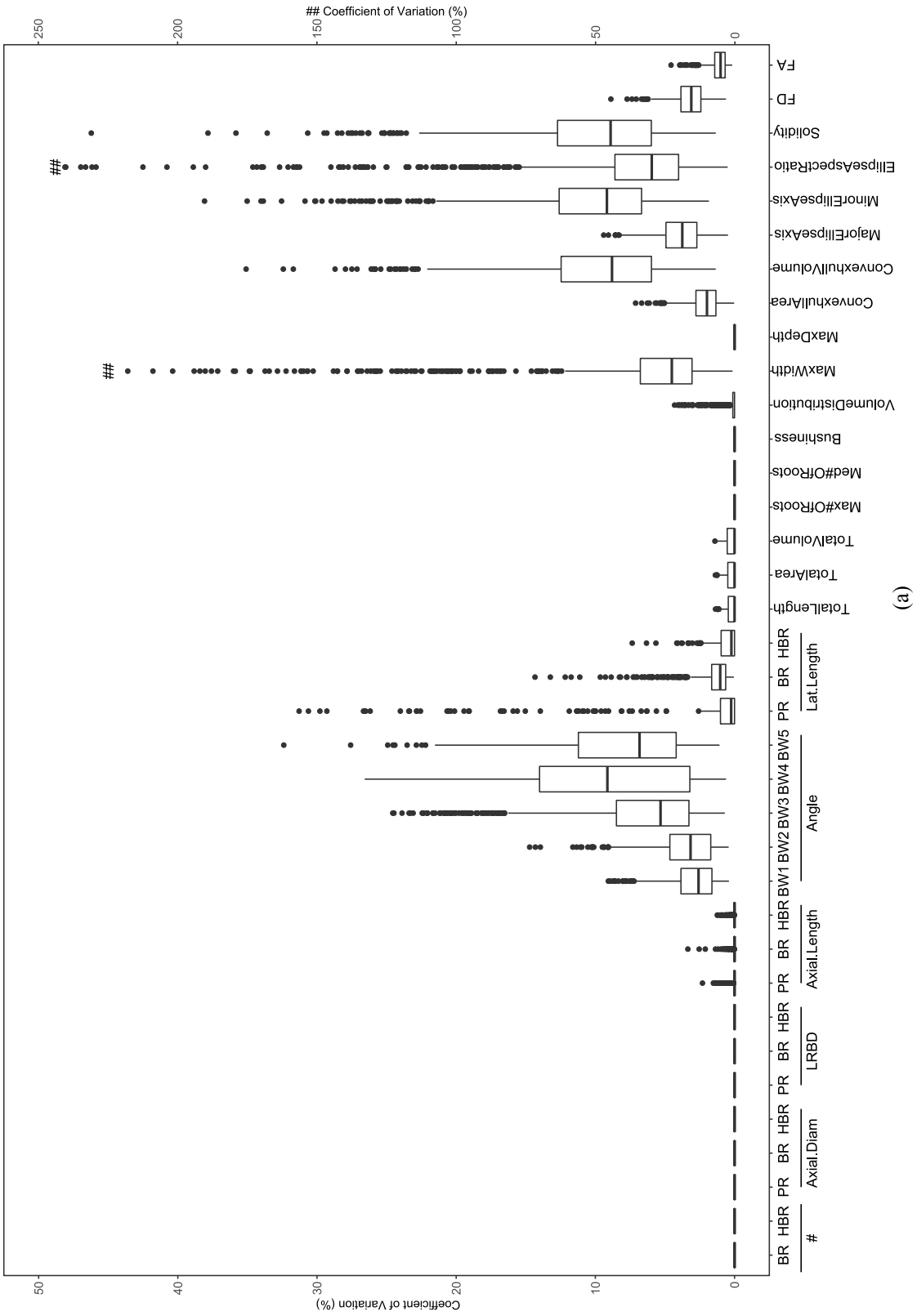
Coefficient of Variation (%)
Coefficient of Variation (%)
FA
FD
Solidity
EllipseAspectRatio
MinorEllipseAxis
MajorEllipseAxis
ConvexhullVolume
ConvexhullArea
MaxDepth
MaxWidth
VolumeDistribution
Bushiness
Med#OfRoots
Max#OfRoots
TotalVolume
TotalArea
TotalLength
BR HBR PR BR HBR PR BR HBR PR BR HBR PR BR HBR BW1 BW2 BW3 BW4 BW5 PR BR HBR
Axial.Diam LRBD Axial.Length Angle Lat.Length

(a)

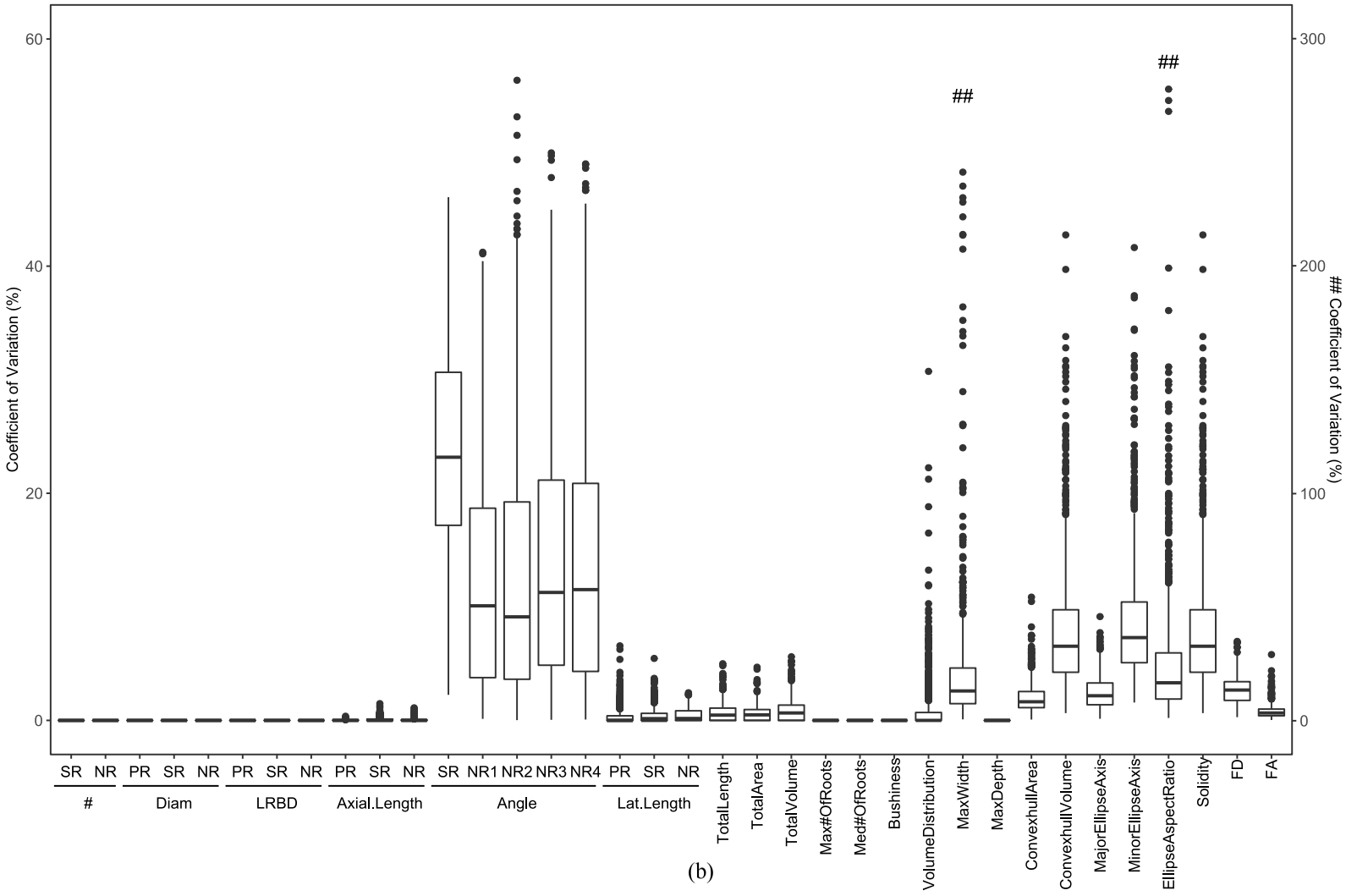

Figure 4-7: Variation in phene and phene aggregate metrics estimated from rotational series of 2D projected images of 3D bean root system (a) and 3D maize root system (b). BW -basal root; HBR-hypocotyl-borne root; PR- primary root; SR – seminal root; NR -nodal root; # - number of roots; Axial.Diam – axial root diameter; Axial.Length – axial root length; LRBD – lateral root branching density; Lat.Length – lateral root length; FD – fractal dimension; FA – fractal abundance

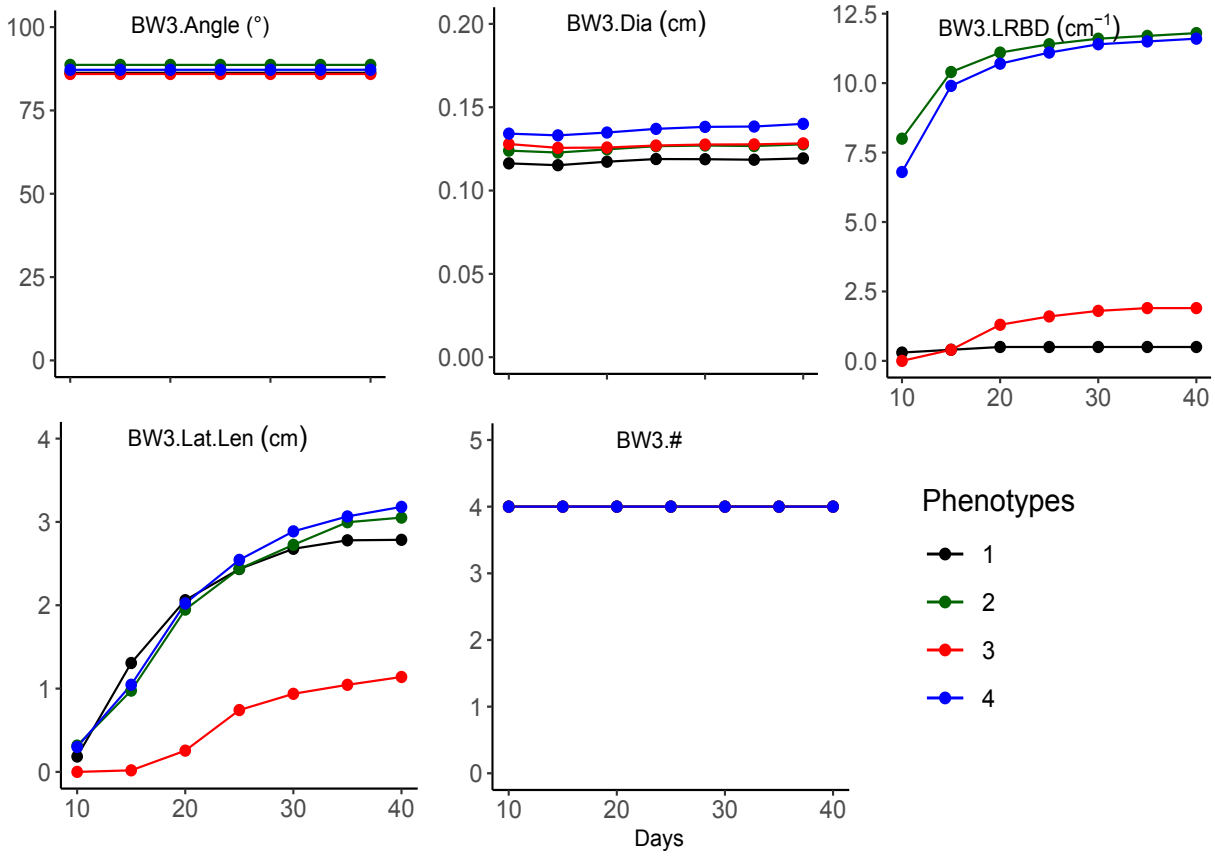
BW3.Angle (°)
BW3.Dia (cm)
BW3.LRBD (cm^{-1})
BW3.Lat.Len (cm)
BW3.#
Days
Phenotypes
1
2
3
4

(a)

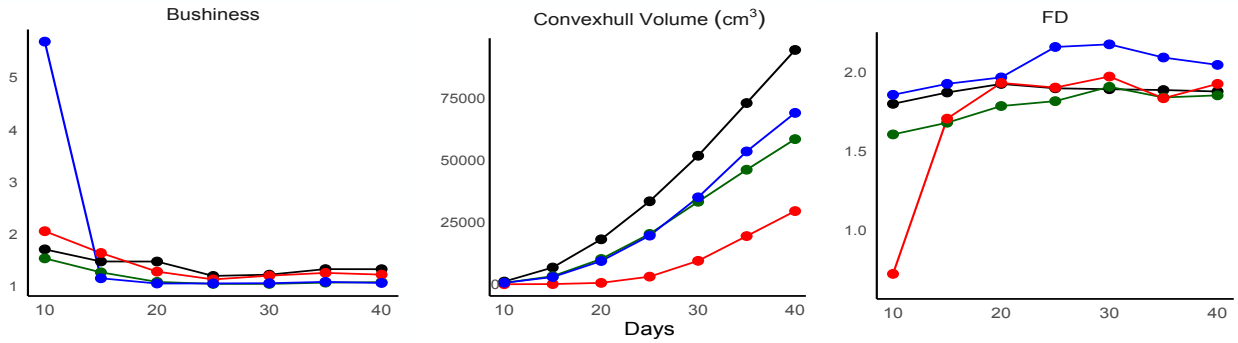
Bushiness
Convexhull Volume (cm^3)
FD
Days

(b)

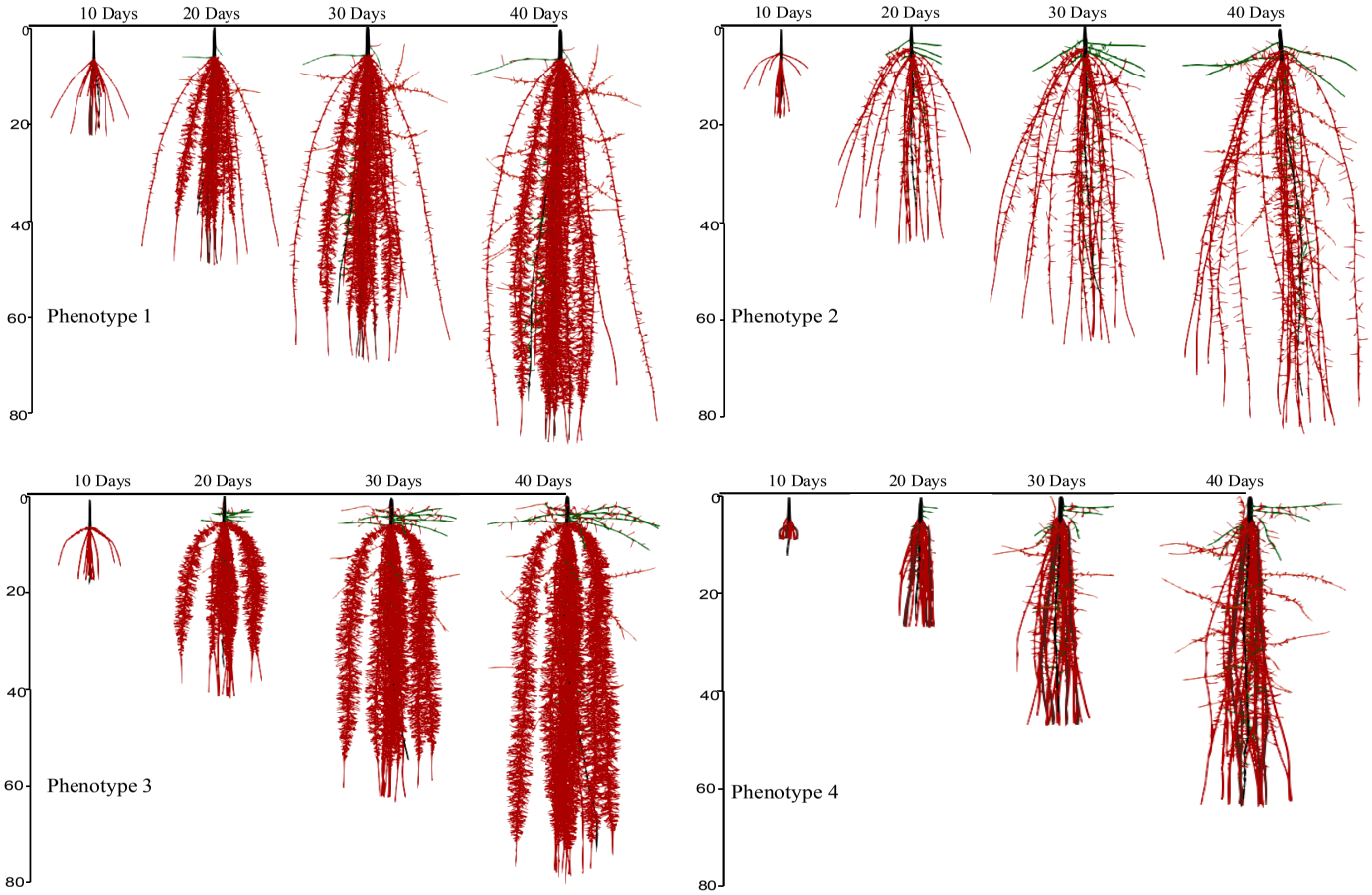

Figure 4-8: Trait dynamics of bean root phenotypes over 30 days of growth from day 10 to day 40. Change in estimates of phenes associated with basal whorl 3 (BW3) are shown in Figure 8(a). Similar trends were seen in other root classes (Supplementary Figure S4(a)). Change in estimates of the phene aggregates bushiness, convex hull volume and fractal dimension (FD) are shown in Figure 4-8(b). Trends in estimates of other phene aggregates included in this study are shown in Supplementary Figure S4(b). The phenotypes for which the metrics are presented in Figure 4- 8(a) and (b) are visualized in Figure 4-8(c). Primary roots are in black; basal root in red; hypocotyl-borne roots in green. BW3 – basal roots at whorl 3; Dia – axial root diameter; LRBD – lateral root branching density; Lat.Len – lateral root length; # - number of axial roots.

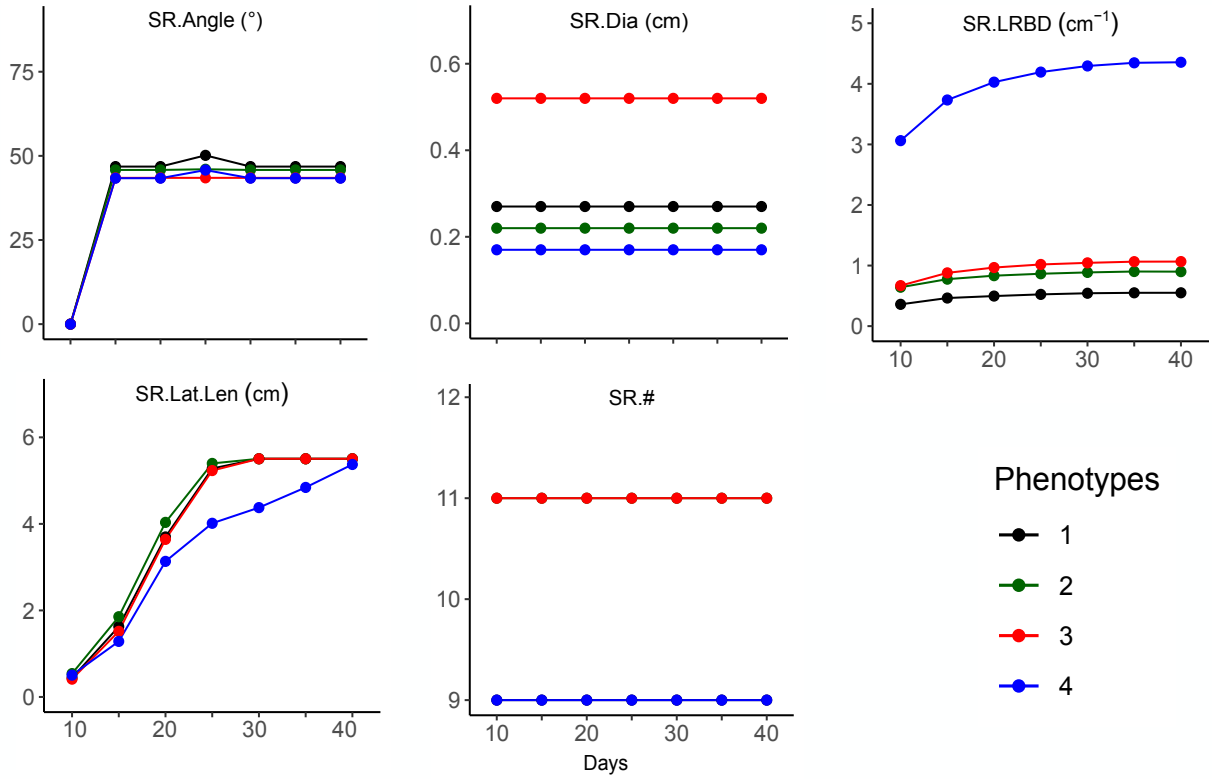
SR.Angle (°)
SR.Dia (cm)
SR.LRBD (cm^{-1})
SR.Lat.Len (cm)
SR.#
Days
Phenotypes
1
2
3
4

(a)

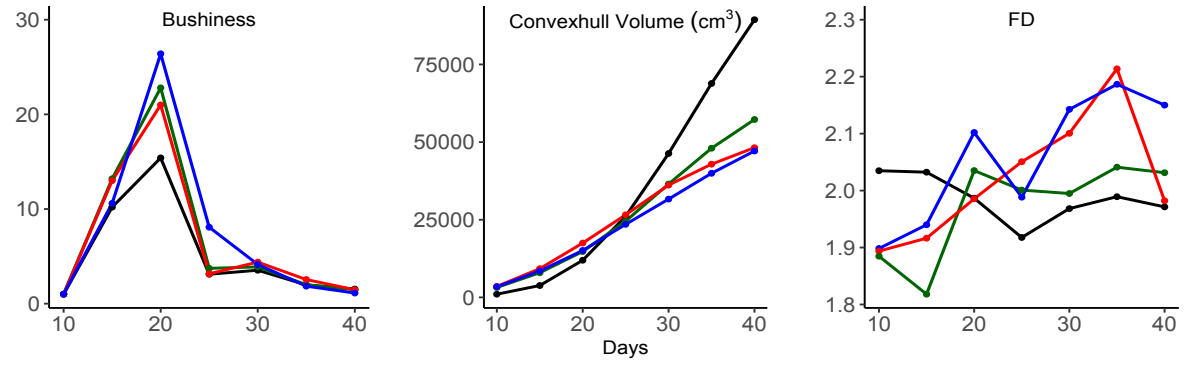
Bushiness
Convexhull Volume (cm^3)
FD
Days

(b)

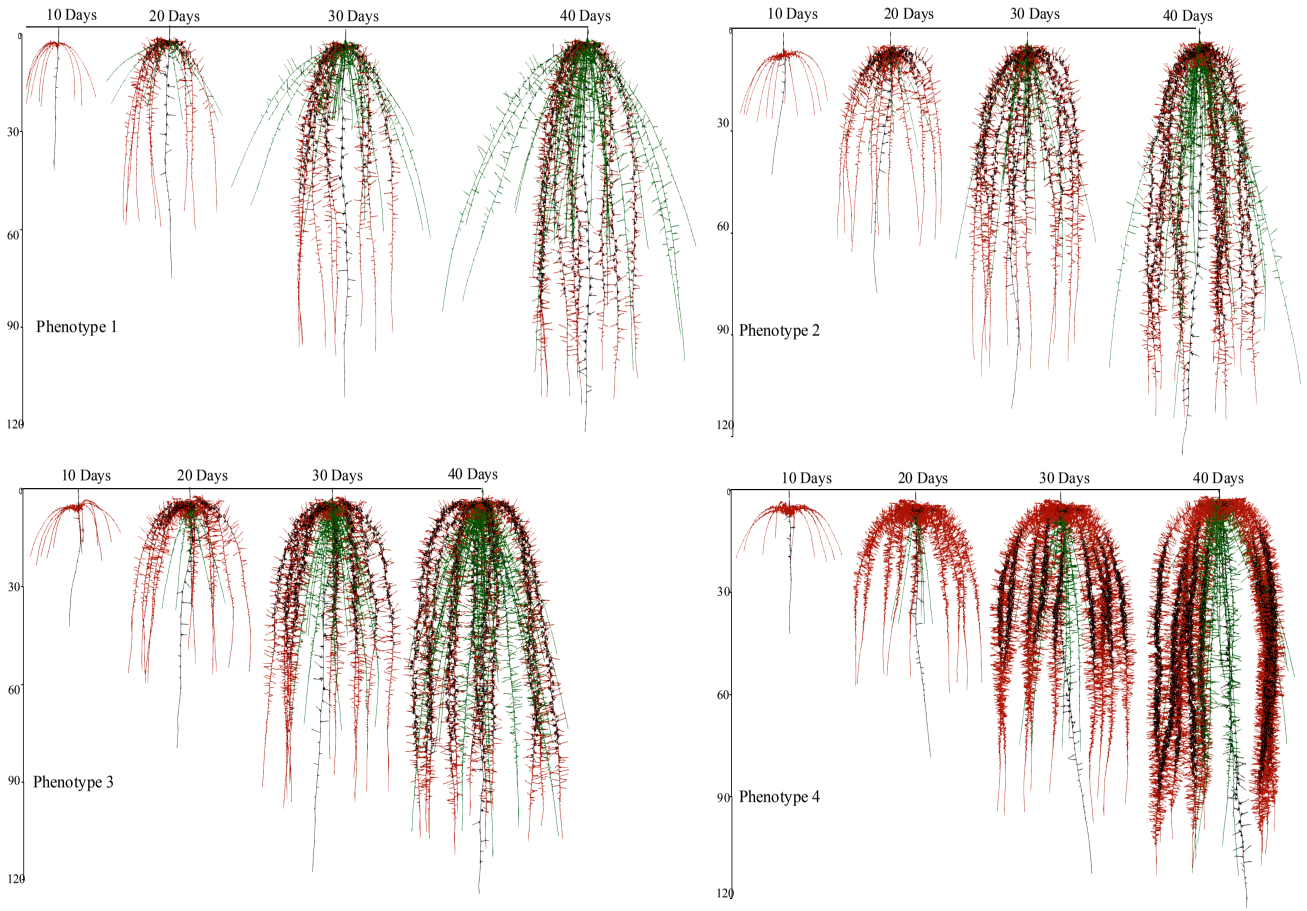

Figure 4-9: Trait dynamics of maize root phenotypes over 30 days of growth from day 10 to day 40. Change in estimates of phenes associated with seminal roots (SR) are shown in figure 4-9(a). Similar trends were seen in other root classes (Supplementary Figure S5(a)). Change in estimates of the phene aggregates bushiness, convex hull volume and fractal dimension (FD) are shown in Figure 4-9(b). Trends in estimates of other phene aggregates included in this study are shown in Supplementary Figure S5(b). The phenotypes for which the metrics are presented in Figure 4-9(a) and (b) are visualized in Figure 4-9(c). Primary roots are in black; seminal roots in red; nodal roots in green. SR – seminal roots; Dia – axial root diameter; LRBD – lateral root branching density; Lat.Len – lateral root length; # - number of axial roots.

Chapter 5

General conclusions

Exploring root phenomics *in situ* is challenging because it is labor intensive, time consuming and observation of root systems in 3 dimensions non-invasively through opaque soil is challenging. Root architectural models capture the interactions between the root components as well as the environment and are valuable to investigate the influence of various environmental factors on the growth of root system and plant productivity.

In the first chapter, I used the functional structural model *SimRoot* to study the interaction among axial root phenes in the bean root system to identify optimal root phenotypes in an environment with limited phosphorus, limited nitrate and an environment limited in both phosphorus and nitrate. The results from chapter 1 suggest that interactions among the phenes result in distinct phenotypes with similar performances in a given environment. The occurrence of several optimal phenotypes when just a few phenes were considered got us thinking about methods to identify the optimal phenotypes when all possible architectural phenes are considered. We realized that the large decision space presented by the numerous phenes needed alternate methods of evaluation and found that multiobjective evolutionary algorithms would be perfect to address the problem.

In chapter 2 we used *SimRoot* with a multiobjective evolutionary algorithm to identify several optimal bean and maize root systems in environments low in phosphorus or/and nitrate. While we have conducted the study in a specific soil and precipitation scenario, the study can be extended to several other scenarios. The optimal phenotypes identified in Chapter 2 have specific elements of ideotypes confirmed to have utility for improved P acquisition or N capture. So, our approach using multiobjective evolutionary algorithms can be a valuable tool to identify and select phenotypes specific for the target environment.

We recognize that the scenarios presented in our study are simplified compared to what plants experience in the field. However, models can be made to include processes of interest. Modelling a process stimulates new ideas and suggests priorities in the application of resources for research. Architectural models are, by themselves, computationally challenging because the various processes associated with root growth is explicitly calculated while also coupling the root processes with processes in the environment. So, the level of details that the modeler includes

(type of model, level of resolution) in any model depends on the purposes. It is important to make sure that model is simple enough to allow manipulation and understanding the process and sufficiently complex to simulate relevant processes and allow meaningful conclusions.

In chapter 3, we had a different utility for the functional structural model in which we did not consider the functional aspect of the model but utilized the capability of the model to generate explicit root architectures to estimate and compare various root phenotyping metrics. We found that estimates of phenes are more useful than metrics aggregating multiple phenes for phenotyping root architecture. Based on this finding, we suggest that selection for combination of specific phenes will be much simpler and more precise and more useful for selection for crop breeding.

The theme binding all the chapters of this dissertation is the utility of functional structural models in exploring various aspects of the root phenome. We have demonstrated the application of functional structural models specifically in root phenomics; however, the concepts and applications demonstrated in this research work is pertinent broadly in phenomic studies.

Appendix A

Supplementary figures for Chapter 2

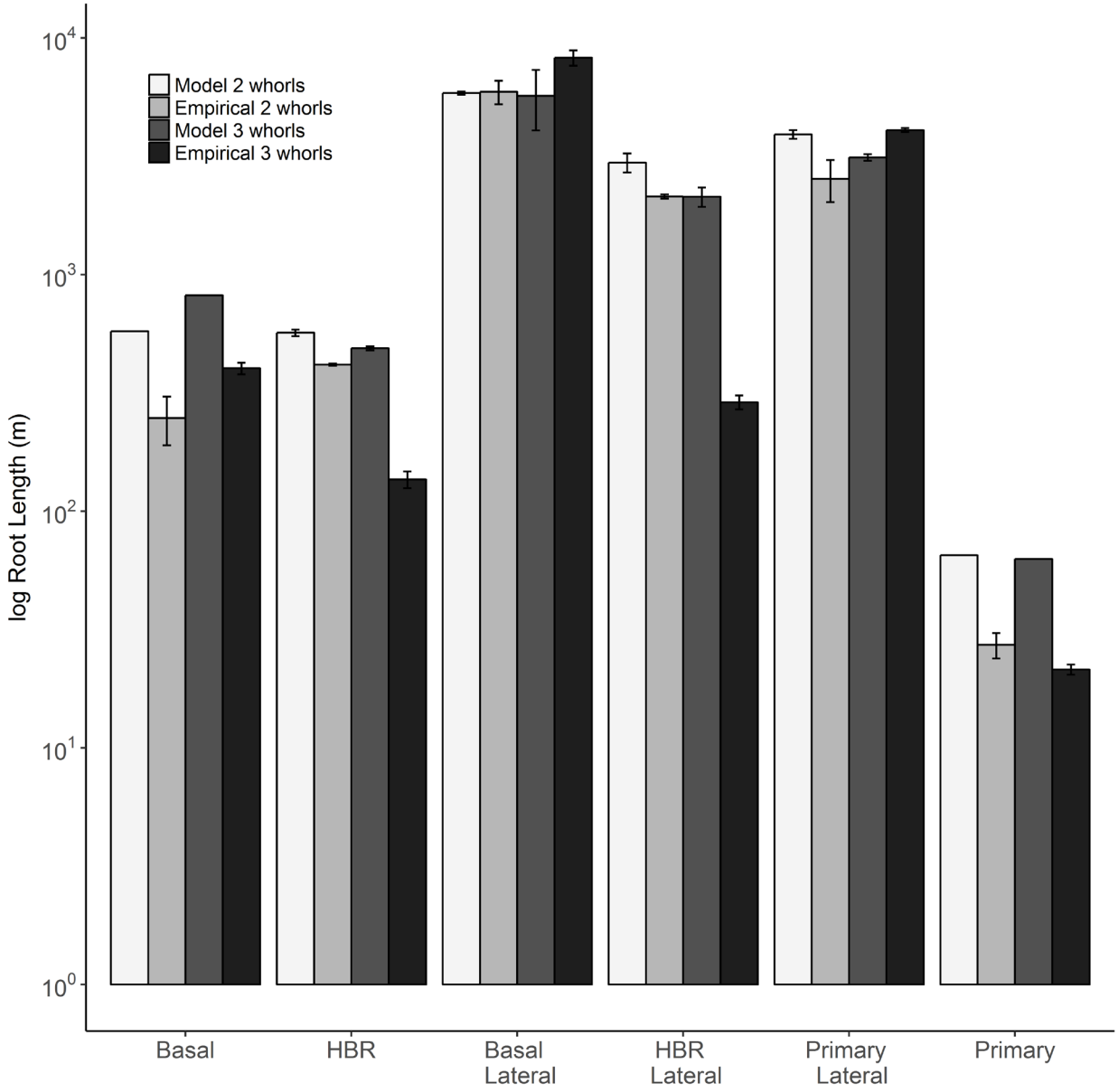

Supplementary Figure 2-S1: Validation of simulated data. Data of root lengths of different root classes from greenhouse experiments as reported in Walk *et al*., 2006 are represented along with simulated data. Error bars present SE for three repeated runs. Variation is caused by simulated stochasticity in root growth rates, growth direction and branching frequency.

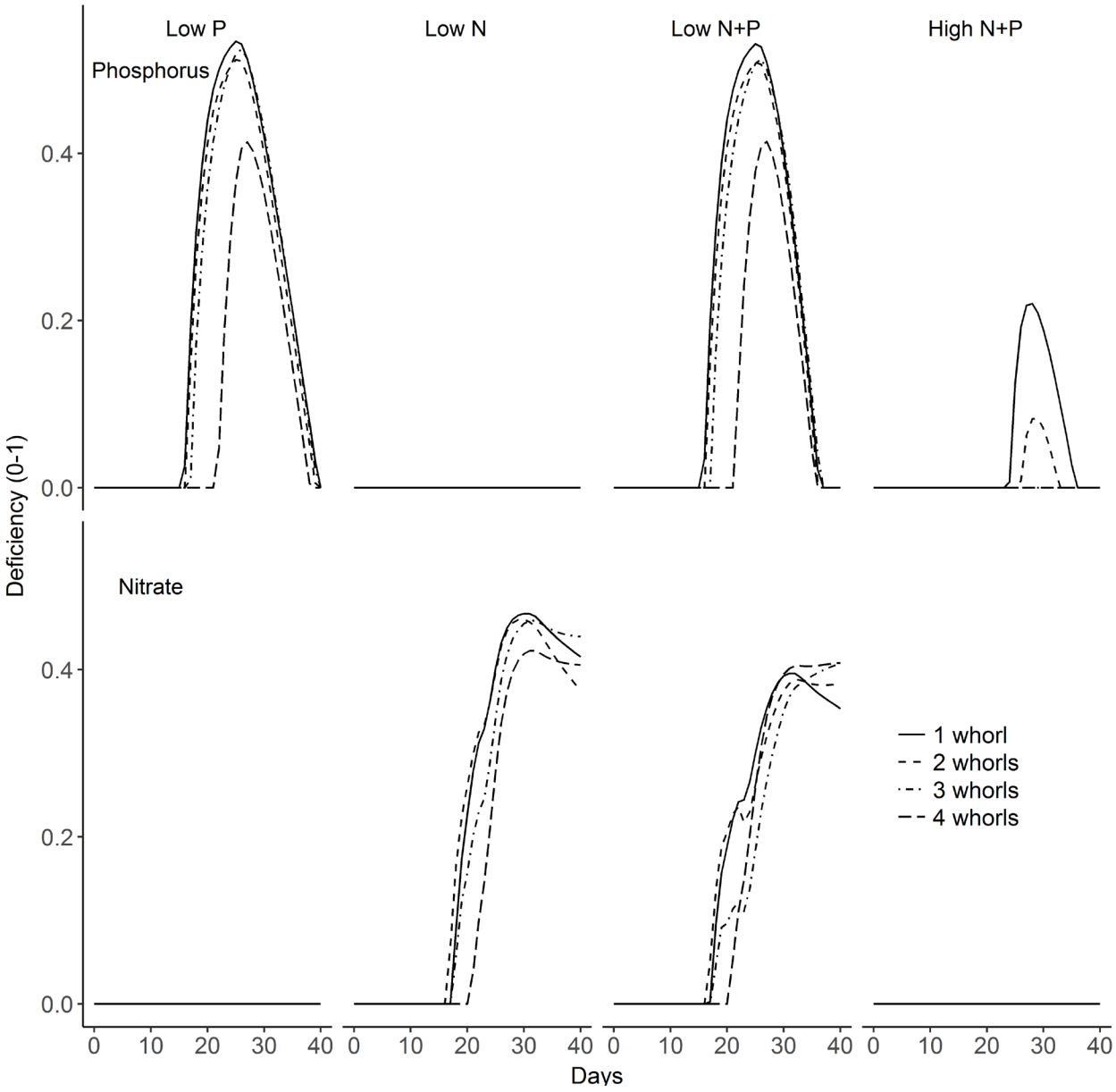

Supplementary Figure 2-S2: Nutrient stress as it develops over time. Stress is calculated as 1-(u-m)/(o-m), where u is the nutrient uptake (phosphorus or nitrate), o is the optimal nutrient content in the plant and m is the minimal nutrient content in the plant. 0 indicates no stress, 1 indicates severe stress. The plants are simulated in soil with low phosphorus and low nitrate, and default precipitation. The phenotypes are deep angled.

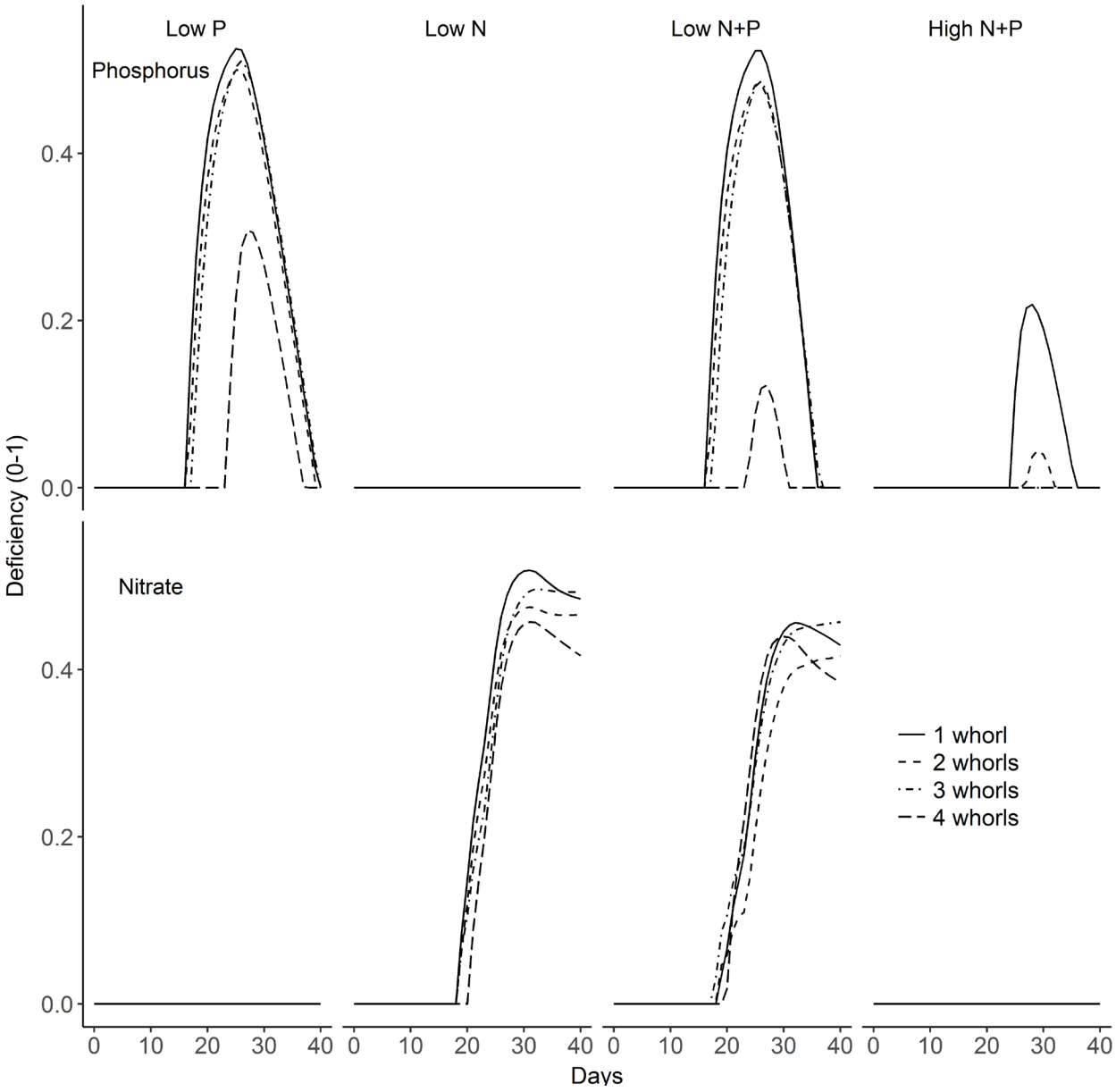

Supplementary Figure 2-S3: Nutrient stress as it develops over time. Stress is calculated as 1-(u-m)/(o-m), where u is the nutrient uptake (phosphorus or nitrate), o is the optimal nutrient content in the plant and m is the minimal nutrient content in the plant. 0 indicates no stress, 1 indicates severe stress. The plants are simulated in soil with low phosphorus and low nitrate, and default precipitation. The phenotypes are fanned angle.

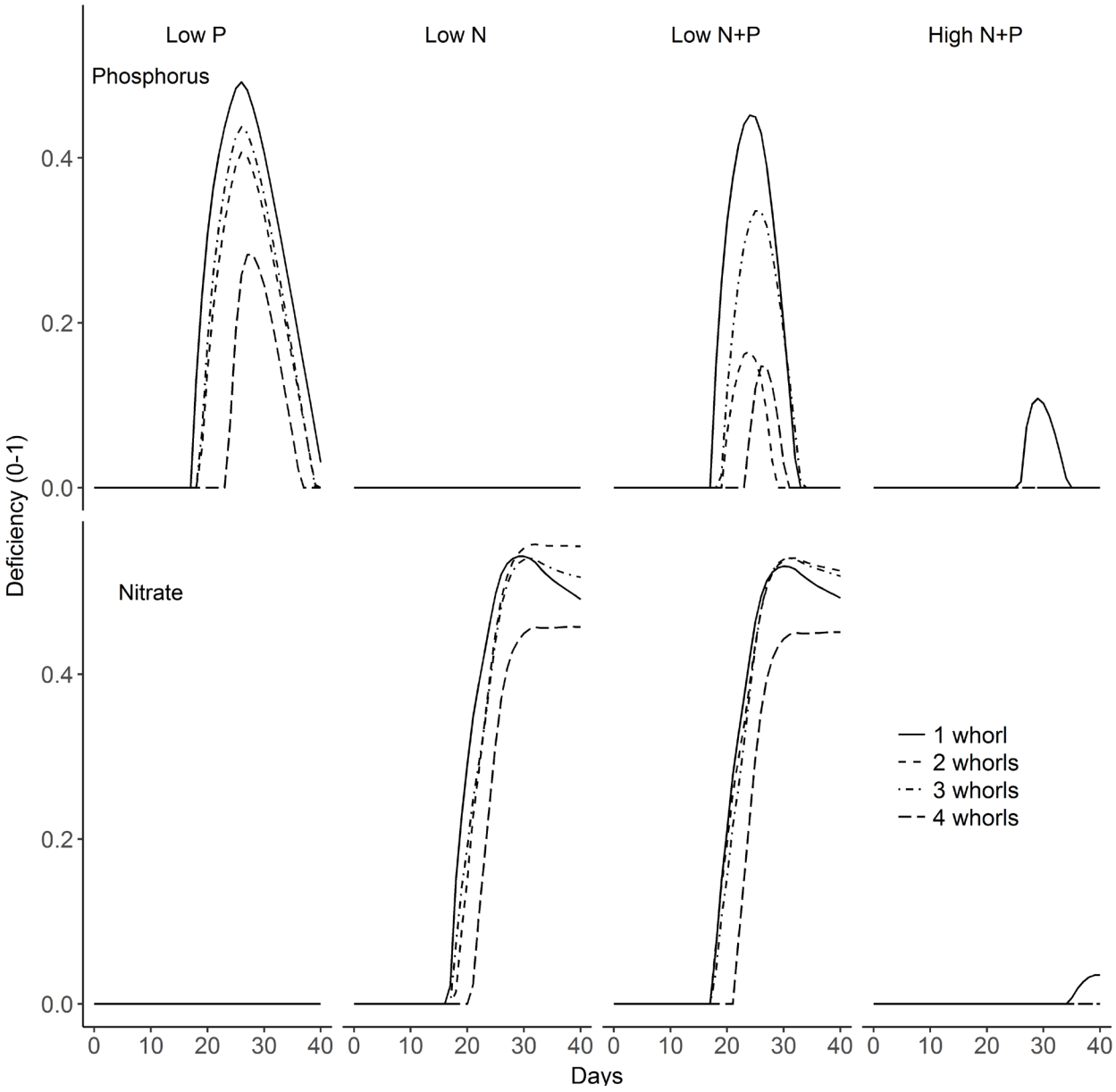

Supplementary Figure 2-S4: Nutrient stress as it develops over time. Stress is calculated as 1-(u-m)/(o-m), where u is the nutrient uptake (phosphorus or nitrate), o is the optimal nutrient content in the plant and m is the minimal nutrient content in the plant. 0 indicates no stress, 1 indicates severe stress. The plants are simulated in soil with low phosphorus and low nitrate, and default precipitation. The phenotypes are shallow angle.

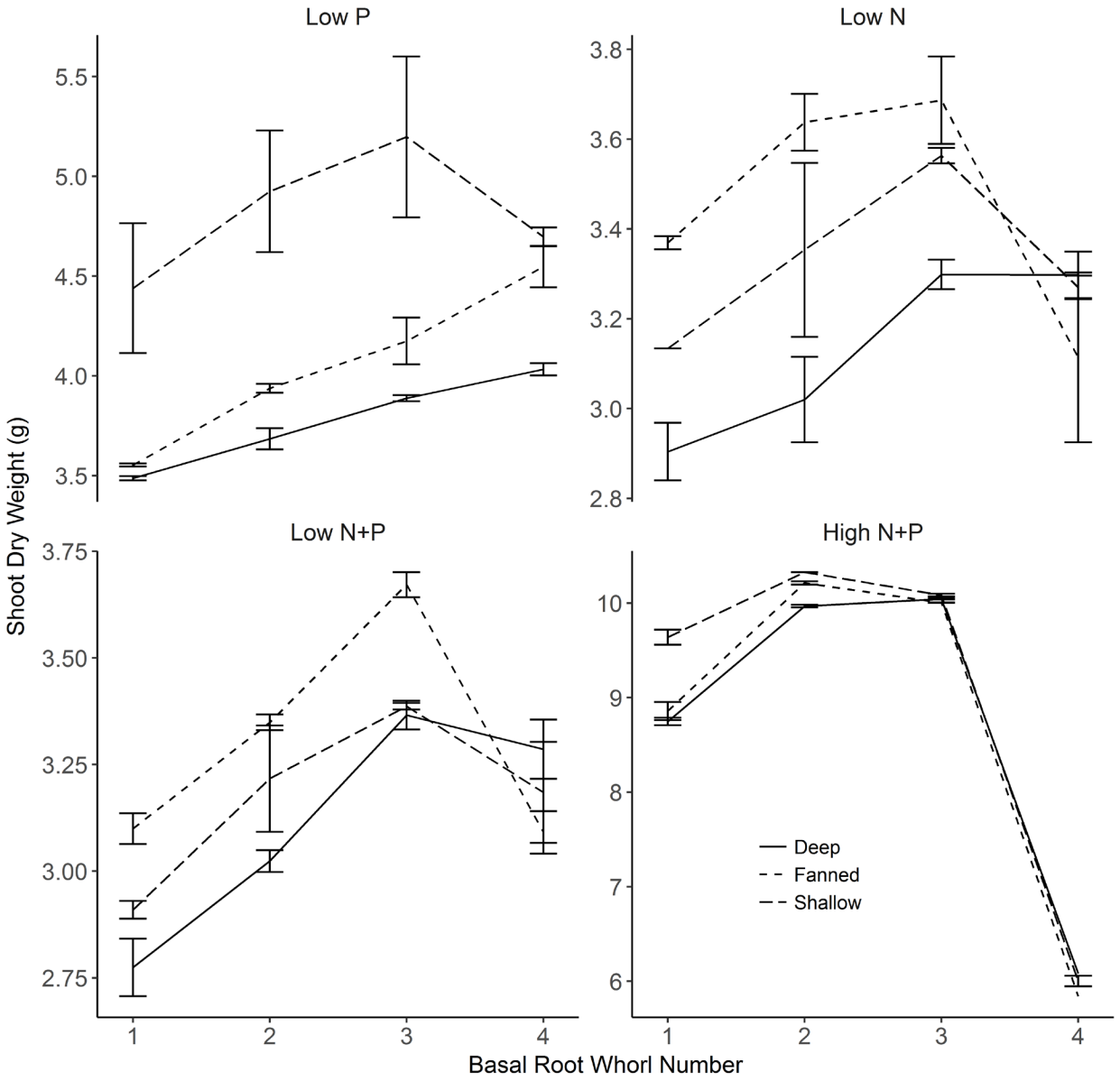

Supplementary Figure 2-S5: Shoot biomass 40 days after germination (d.a.g) at low phosphorus, low nitrogen, combined low phosphorus and low nitrogen, and non-limiting nitrogen and phosphorus availability. Lines show results for plants one, two, three and four whorls with shallow, fanned and deep root growth angles. Simulations were conducted with half the default precipitation. Error bars show the standard error for three repeated runs. Variation is caused by simulated stochasticity in root growth rates and branching frequency.

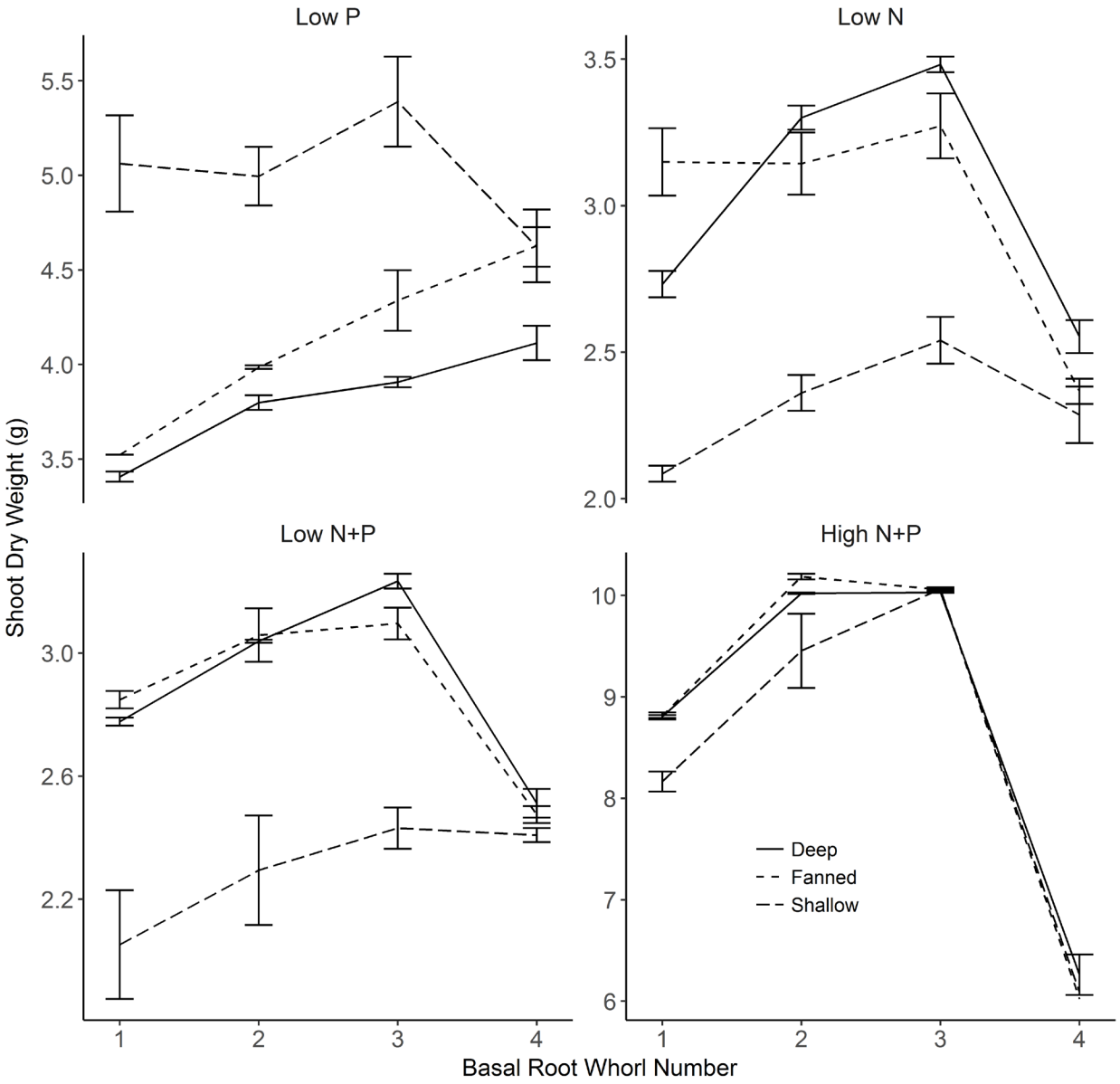

Supplementary Figure 2-S6: Shoot biomass 40 days after germination (d.a.g at low phosphorus, low nitrogen, combined low phosphorus and low nitrogen, and non-limiting nitrogen and phosphorus availability. Lines show results for plants one, two, three and four whorls with shallow, fanned and deep root growth angles. Simulations were conducted with 1.5 times the default precipitation. Error bars show the standard error for three repeated runs. Variation is caused by simulated stochasticity in root growth rates and branching frequency.

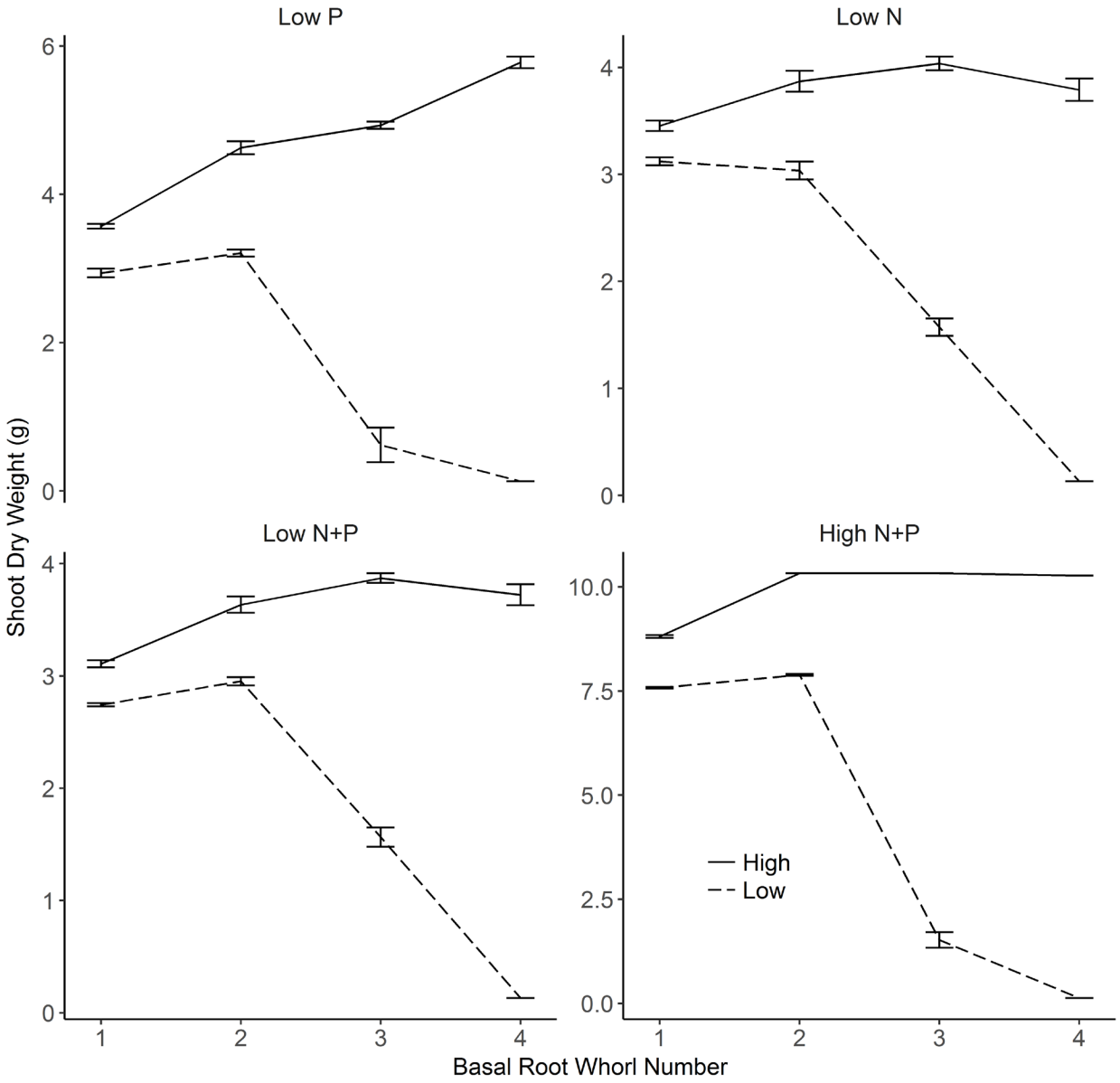

Supplementary Figure 2-S7: Shoot biomass 40 days after germination (d.a.g) at low phosphorus, low nitrogen, combined low phosphorus and low nitrogen, and non-limiting nitrogen and phosphorus availability under varying carbon fixation. Roots are fanned angled. Error bars show the standard error for three repeated runs. Variation is caused by simulated stochasticity in root growth rates and branching frequency.

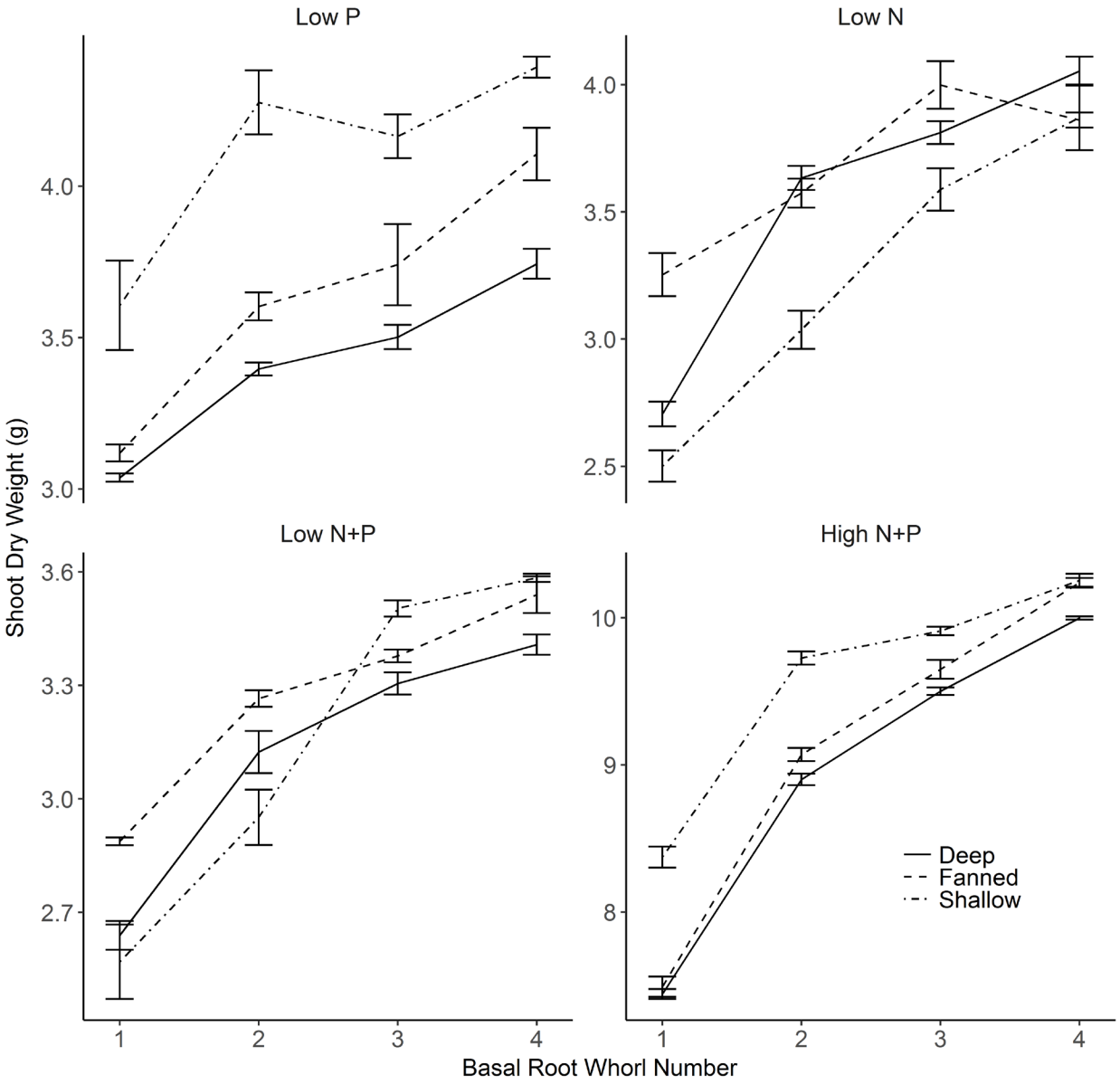

Supplementary Figure 2-S8: Shoot biomass, of plants with lower LRBD, 40 days after germination (d.a.g) at low phosphorus, low nitrogen, combined low phosphorus and low nitrogen, and non-limiting nitrogen and phosphorus availability. Lines show results for plants one, two, three and four whorls with shallow, fanned and deep root growth angles. Error bars show the standard error for three repeated runs. Variation is caused by simulated stochasticity in root growth rates.

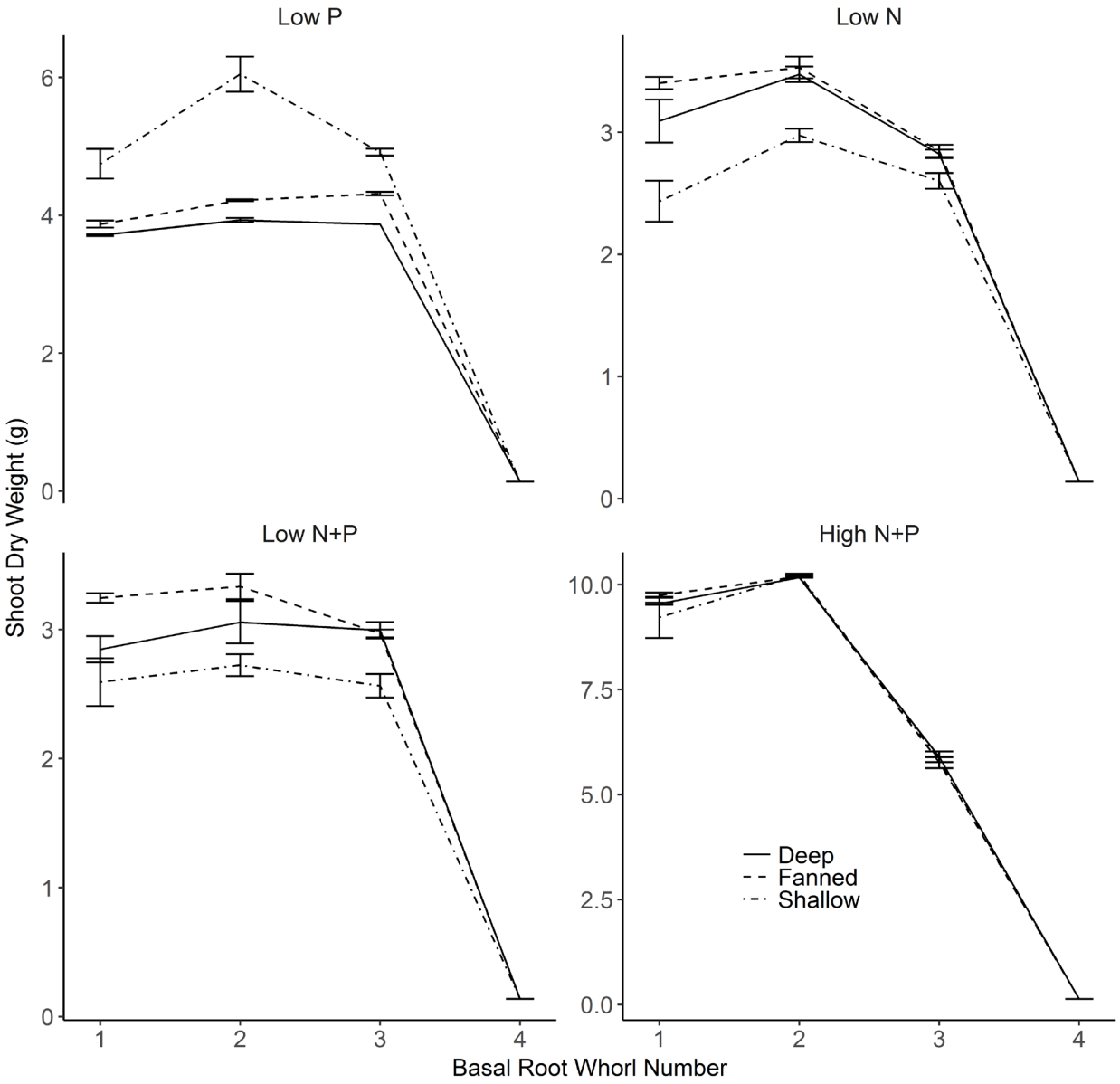

Supplementary Figure 2-S9: Shoot biomass of plants with greater LRBD, 40 d after germination (d.a.g) at low phosphorus, low nitrogen, combined low phosphorus and low nitrogen, and non-limiting nitrogen and phosphorus availability. Lines show results for plants one, two, three and four whorls with shallow, fanned and deep root growth angles. Error bars show the standard error for three repeated runs. Variation is caused by simulated stochasticity in root growth rates.

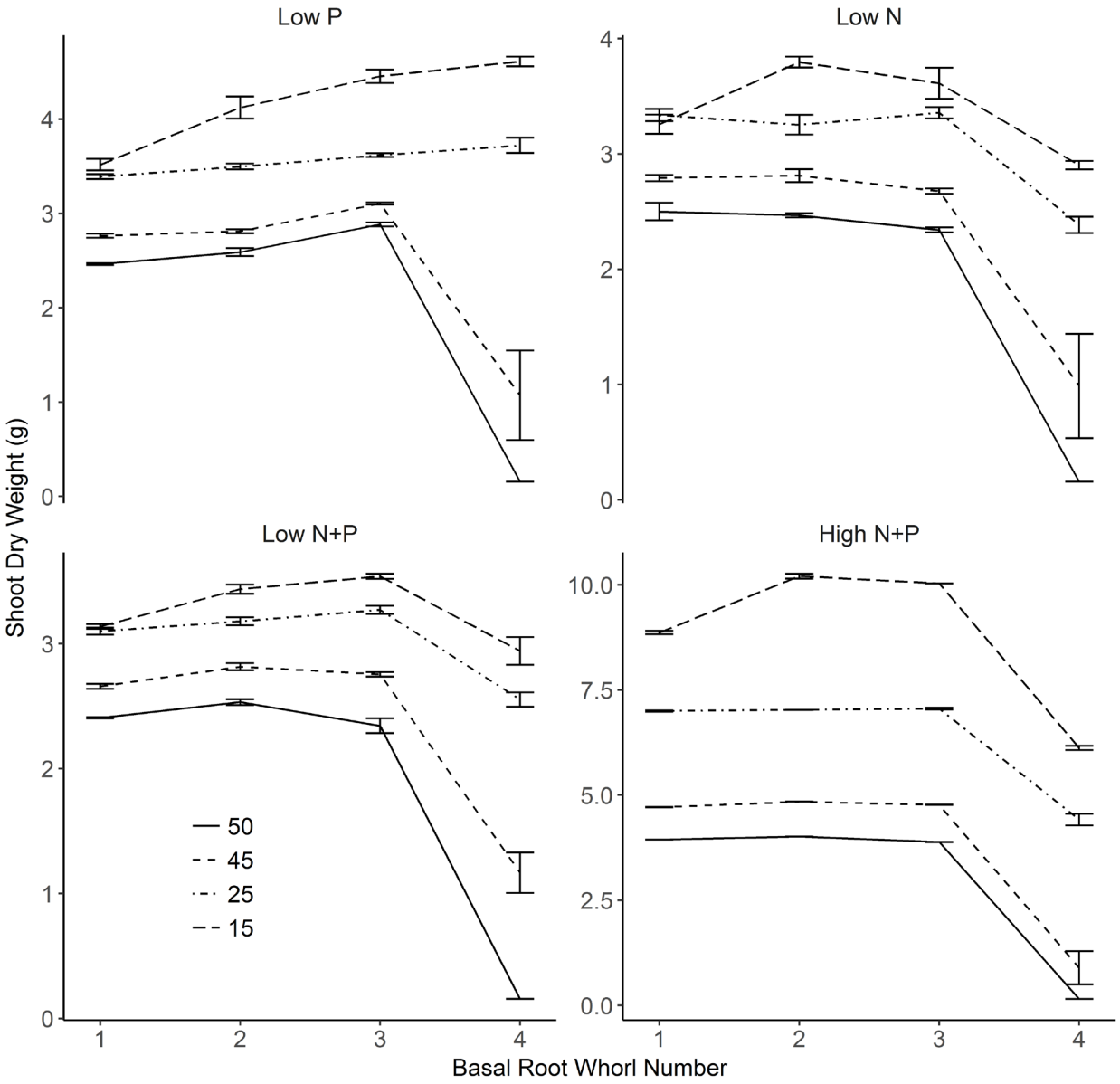

Supplementary Figure 2-S10: Shoot biomass 40 d after germination (d.a.g) at low phosphorus, low nitrogen, combined low phosphorus and low nitrogen, and non-limiting nitrogen and phosphorus availability, under varying planting densities given as plants per m^2. Roots are fanned angled. Error bars show the standard error for three repeated runs. Variation is caused by simulated stochasticity in root growth rates and branching frequency.

Appendix B

SimRoot parameterization

SimRoot uses a hierarchical xml formatted input file which is graphically presented below. The hierarchy gives the parameters context. For example, the parameter 'specific leaf area'belongs to the shoot of a specific plant. In SimRoot parameters can be a single value, a value drawn from a distribution, or the result of an interpolation table.

1 'environment'
    1.1 'atmosphere'
        1.1.1 'evaporation'(cm) =f{'time'} (day) x,y pairs :{ 0 0 1 0.05 2 0.1 3 0.1 4 0.05 5 0.05 6 0.1 7 0.05 8 0.05 9 0.1 10 0.1
        11 0.05 12 0.1 13 0.1 14 0.05 15 0.04 16 0.03 17 0.02 18 0.09 19 0.09 20 0.04 21 0.09 22 0.09 23 0.04 24 0.03 25 0.02 26
        0.02 27 0.08 28 0.03 29 0.08 30 0.03 31 0.08 32 0.07 33 0.07 34 0.07 35 0.03 36 0.02 37 0.01 38 0 39 0 40 0 41 0 42 0.06}
        1.1.2 'irradiation'= 4000 (uMol/cm2/day)
        1.1.3 'precipitation'(cm) =f{'time'} (day) x,y pairs :{ 0 0 1 0 2 1 3 0.29 4 0 5 0 6 0.61 7 0 8 0 9 0.25 10 0.03 11 0 12
        0.64 13 0.33 14 0 15 0 16 0 17 0 18 1.8 19 0.2 20 0 21 2.84 22 0.38 23 0 24 0 25 0 26 0 27 0.18 28 0 29 0.46 30 0 31 1.35
        32 0.13 33 0.23 34 0.25 35 0 36 0 37 0 38 0 39 0 40 0 41 0 42 1.42 }

    1.2 'dimensions'
        1.2.1 'max corner'= 30 0 34 (cm)
        1.2.2 'min corner'= -30 -150 -26 (cm)

    1.3 'soil'
        1.3.1 'bulk density'(g/cm3) =f{'depth'} (cm) x,y pairs :{ -200 1.51 -65 1.51 -47 1.4 -30 1.42 -16 1.29 -5 1.24 0 1.24 }
        1.3.2 'nitrate'
            1.3.2.1 'adsorption coefficient'= 0 (uMol/cm)
            1.3.2.2 'buffer power'(noUnit) =f{'depth'} (cm) x,y pairs :{ -1000 0.4 1000 0.4 }
            1.3.2.3 'concentration'(uMol/ml) =f{'depth'} (cm) x,y pairs :{ -1000 1.59 -55 1.59 -45 1.67 -35 2.17 -25 3.15 -15 4.02 -5
            2.36 0 2.8 0.01 0 100 0 }
            1.3.2.4 'diffusion coefficient'(cm2/day) =f{'depth'} (cm) x,y pairs :{ -1000 0.216 -0 0.216 1e-05 1e-08 1000 1e-08 }
            1.3.2.5 'longitudinal dispersivity'= 1 (cm)
            1.3.2.6 'r1-r0'= 4 (cm)
            1.3.2.7 'saturated diffusion coefficient'= 1.6416 (cm2/day)
            1.3.2.8 'transverse dispersivity'= 0.5 (cm)
        1.3.3 'organic'

1.3.3.1 'C/N ratio microbes'= 10 (g/g)
1.3.3.2 'C/N ratio'(g/g) =f{'depth'} (cm) x,y pairs :{ -10000 13 0 13 }
1.3.3.3 'assimilation efficiency microbes'= 1 (noUnit)
1.3.3.4 'carbon content'(g/g) =f{'depth'} (cm) x,y pairs :{ -200 0.005 -40 0.005 -30 0.01 -10 0.02 0 0.02 }
1.3.3.5 'initial relative mineralisation rate'(g/g/year) =f{'depth'} (cm) x,y pairs :{ -1000 0 -25 0 -10 0.037 0 0.037 }
1.3.3.6 'speed of aging'= 0.46 (noUnit)
1.3.3.7 'time offset'= 30 (day)
1.3.4 'phosphorus'
1.3.4.1 'adsorption coefficient'= 400 (uMol/cm)
1.3.4.2 'buffer power'(noUnit) =f{'depth'} (cm) x,y pairs :{ -1000 400 1000 400 }
1.3.4.3 'concentration'(uMol/ml) =f{'depth'} (cm) x,y pairs :{ -1000 0.00024 -30 0.00025 -29 0.00175 0 0.00175
0.0001 0 1000 0 }
1.3.4.4 'diffusion coefficient'(cm2/day) =f{'depth'} (cm) x,y pairs :{ -1000 0.00019872 -0 0.00019872 1000
0.00019872 }
1.3.4.5 'longitudinal dispersivity'= 1 (cm)
1.3.4.6 'r1-r0'= 0.3 (cm)
1.3.4.7 'saturated diffusion coefficient'= 0.094 (cm2/day)
1.3.4.8 'transverse dispersivity'= 0.5 (cm)
1.3.5 'potassium'
1.3.5.1 'adsorption coefficient'= 10 (uMol/cm)
1.3.5.2 'buffer power'(noUnit) =f{'depth'} (cm) x,y pairs :{ -1000 10 1000 10 }
1.3.5.3 'concentration'(uMol/ml) =f{'depth'} (cm) x,y pairs :{ -1000 0.05 -30 0.05 -29 0.15 0 0.15 1e-05 0 1000 0 }
1.3.5.4 'diffusion coefficient'(cm2/day) =f{'depth'} (cm) x,y pairs :{ -1000 0.0143 -0 0.0143 1000 0.0143 }
1.3.5.5 'longitudinal dispersivity'= 1 (cm)
1.3.5.6 'r1-r0'= 1.5 (cm)
1.3.5.7 'saturated diffusion coefficient'= 1.56 (cm2/day)
1.3.5.8 'transverse dispersivity'= 0.5 (cm)
1.3.6 'water'
1.3.6.1 'initial hydraulic head'(cm) =f{'depth'} (cm) x,y pairs :{ -200 0 -151 -50 -50 -150 -45 -155 -40 -160 -35 -165 -30
-170 -25 -175 -20 -180 -15 -190 -10 -200 -5 -220 -2 -240 -1 -300 -0 -400 }
1.3.6.2 'residual water content'(100%) =f{'depth'} (cm) x,y pairs :{ -300 0.067 0 0.067 }
1.3.6.3 'saturated conductivity'(cm/day) =f{'depth'} (cm) x,y pairs :{ -300 10.8 0 10.8 }
1.3.6.4 'saturated water content'(100%) =f{'depth'} (cm) x,y pairs :{ -300 0.39 -65 0.39 -35 0.39 -25 0.43 -15 0.45 0

0.46 }
1.3.6.5 'van genuchten:alpha'(noUnit/cm) =f{'depth'} (cm) x,y pairs :{ -300 0.02 0 0.02 }
1.3.6.6 'van genuchten:n'(noUnit) =f{'depth'} (cm) x,y pairs :{ -300 1.41 0 1.41 }
1.3.6.7 'volumetric water content in barber cushman'= 0.3 (cm3/cm3)

2 'root type parameters'
2.1 'bean- carioca- sim root4'
2.1.1 'basal whorl1'
2.1.1.1 'aerenchyma formation'(100%) =f{'time since creation'} (day) x,y pairs :{ 0 0 3 0 5 0.05 10 0.1 20 0.268 1000 0.268 }
2.1.1.2 'bottom boundary'= 1 (noUnit)
2.1.1.3 'bounce of the side'= 1 (noUnit)
2.1.1.4 'branch list'
2.1.1.4.1 'lateral basal roots'
2.1.1.4.1.1 'allow branches to form above ground'= 0 (noUnit)
2.1.1.4.1.2 'branching frequency'= 0.15 (cm)
2.1.1.4.1.3 'length root tip'= 8 (cm)
2.1.1.5 'branching angle'= 90 (degrees)
2.1.1.6 'density'= 0.094 (g/cm3)
2.1.1.7 'diameter'= 0.068 (cm)
2.1.1.8 'gravitropism'= 0.002 (noUnit)
2.1.1.9 'gravitropism.v2'(cm) =f{'uniform distribution'} minimum=-0.08 maximum=-0.04
2.1.1.10 'growth rate'(cm/day) =f{'time since creation'} (day) x,y pairs :{ 0 0.1 3 4 10 4 15 3 25 2.352 35 2.352 40 0 1000 0 }
2.1.1.11 'nitrate'
2.1.1.11.1 'Cmin'= 0.001 (uMol/ml)
2.1.1.11.2 'Imax'= 1.9 (uMol/cm2/day)
2.1.1.11.3 'Km'= 0.0161 (uMol/ml)
2.1.1.11.4 'minimal nutrient concentration'= 600 (uMol/g)
2.1.1.11.5 'optimal nutrient concentration'= 1200 (uMol/g)
2.1.1.12 'number of xylem poles'= 4 (noUnit)
2.1.1.13 'phosphorus'
2.1.1.13.1 'Cmin'= 0.0002 (uMol/ml)
2.1.1.13.2 'Imax'= 0.0555 (uMol/cm2/day)
2.1.1.13.3 'Km'= 0.00545 (uMol/ml)
2.1.1.13.4 'minimal nutrient concentration'= 30 (uMol/g)
2.1.1.13.5 'optimal nutrient concentration'= 60 (uMol/g)
2.1.1.14 'potassium'
2.1.1.14.1 'Cmin'= 0.002 (uMol/ml)
2.1.1.14.2 'Imax'= 0.467 (uMol/cm2/day)

2.1.1.14.3 'Km'= 0.039 (uMol/ml)
2.1.1.14.4 'minimal nutrient concentration'= 168 (uMol/g)
2.1.1.14.5 'optimal nutrient concentration'= 234 (uMol/g)
2.1.1.15 'reduction in respiration due to aerenchyma'(100%) =f{'aerenchymaFormation'} (100%) x,y pairs :{ 0 0 0.3 0.7 0.6 1 }
2.1.1.16 'regular topology'= 0 (noUnit)
2.1.1.17 'relative carbon cost of exudation'(g/cm/day) =f{'time since creation'} (day) x,y pairs :{ 0 1.915e-05 1.8 1.511e-05 3.1 1.699e-05 4.4 1.362e-05 100 1.362e-05 }
2.1.1.18 'relative respiration'(g/g/day) =f{'time since creation'} (day) x,y pairs :{ 0 0.09 2 0.04 6 0.04 1000 0.04 }
2.1.1.19 'root class ID'= 99 (noUnit)
2.1.1.20 'root hair density'(#/cm2) =f{'time since creation'} (day) x,y pairs :{ 0 2000 10 2000 30 2000 100 2000 }
2.1.1.21 'root hair diameter'= 0.0005 (cm)
2.1.1.22 'root hair length'(cm) =f{'time since creation'} (day) x,y pairs :{ 0 0 1 0 2 0.03 100 0.03 }
2.1.1.23 'secondary growth rate'(cm/day) =f{'root segment age'} (day) x,y pairs :{ 0 0 2 0 4 0.0005 5 0.001 7 0.0015 11 0.002 13 0.0023 18 0.0026 24 0.00285 29 0.003 100 0.003 }
2.1.1.24 'secondary growth scaling factor'(100%) =f{'distance to base of the root'} (cm) x,y pairs :{ 0 0.7 20 0.7 40 0.4 100 0.4 }
2.1.1.25 'soil impedence'= 0.008 (noUnit)
2.1.1.26 'soil impedence.v2'(cm) =f{'uniform distribution'} minimum=-0.04 maximum=0.04
2.1.1.27 'top boundary'= 1 (noUnit)

2.1.2 'basal whorl2'
2.1.2.1 'aerenchyma formation'(100%) =f{'time since creation'} (day) x,y pairs :{ 0 0 3 0 5 0.05 10 0.1 20 0.268 1000 0.268 }
2.1.2.2 'bottom boundary'= 1 (noUnit)
2.1.2.3 'bounce of the side'= 1 (noUnit)
2.1.2.4 'branch list'
2.1.2.4.1 'lateral basal roots'
2.1.2.4.1.1 'allow branches to form above ground'= 0 (noUnit)
2.1.2.4.1.2 'branching frequency'= 0.15 (cm)
2.1.2.4.1.3 'length root tip'= 10 (cm)
2.1.2.5 'branching angle'= 90 (degrees)
2.1.2.6 'density'= 0.094 (g/cm3)
2.1.2.7 'diameter'= 0.068 (cm)
2.1.2.8 'gravitropism'= 0.001 (noUnit)

2.1.2.9 'gravitropism.v2'(cm) =f{'uniform distribution'} minimum=-0.04 maximum=-0.02
2.1.2.10 'growth rate'(cm/day) =f{'time since creation'} (day) x,y pairs :{ 0 0.1 3 4 10 4 15 3 25 2.352 35 2.352 40 0
1000 0 }
2.1.2.11 'nitrate'
2.1.2.11.1 'Cmin'= 0.001 (uMol/ml)
2.1.2.11.2 'Imax'= 1.9 (uMol/cm2/day)
2.1.2.11.3 'Km'= 0.0161 (uMol/ml)
2.1.2.11.4 'minimal nutrient concentration'= 600 (uMol/g)
2.1.2.11.5 'optimal nutrient concentration'= 1200 (uMol/g)
2.1.2.12 'number of xylem poles'= 4 (noUnit)
2.1.2.13 'phosphorus'
2.1.2.13.1 'Cmin'= 0.0002 (uMol/ml)
2.1.2.13.2 'Imax'= 0.0555 (uMol/cm2/day)
2.1.2.13.3 'Km'= 0.00545 (uMol/ml)
2.1.2.13.4 'minimal nutrient concentration'= 30 (uMol/g)
2.1.2.13.5 'optimal nutrient concentration'= 60 (uMol/g)
2.1.2.14 'potassium'
2.1.2.14.1 'Cmin'= 0.002 (uMol/ml)
2.1.2.14.2 'Imax'= 0.467 (uMol/cm2/day)
2.1.2.14.3 'Km'= 0.039 (uMol/ml)
2.1.2.14.4 'minimal nutrient concentration'= 168 (uMol/g)
2.1.2.14.5 'optimal nutrient concentration'= 234 (uMol/g)
2.1.2.15 'reduction in respiration due to aerenchyma'(100%) =f{'aerenchymaFormation'} (100%) x,y pairs :{ 0 0 0.3
0.7 0.6 1 }
2.1.2.16 'regular topology'= 0 (noUnit)
2.1.2.17 'relative carbon cost of exudation'(g/cm/day) =f{'time since creation'} (day) x,y pairs :{ 0 1.915e-05 1.8
1.511e-05 3.1 1.699e-05 4.4 1.362e-05 100 1.362e-05 }
2.1.2.18 'relative respiration'(g/g/day) =f{'time since creation'} (day) x,y pairs :{ 0 0.09 2 0.04 6 0.04 1000 0.04 }
2.1.2.19 'root class ID'= 99 (noUnit)
2.1.2.20 'root hair density'(#/cm2) =f{'time since creation'} (day) x,y pairs :{ 0 2000 10 2000 30 2000 100 2000 }
2.1.2.21 'root hair diameter'= 0.0005 (cm)
2.1.2.22 'root hair length'(cm) =f{'time since creation'} (day) x,y pairs :{ 0 0 1 0 2 0.03 100 0.03 }
2.1.2.23 'secondary growth rate'(cm/day) =f{'root segment age'} (day) x,y pairs :{ 0 0 2 0 4 0.0005 5 0.001 7 0.0015
11 0.002 13 0.0023 18 0.0026 24 0.00285 29 0.003 100 0.003 }
2.1.2.24 'secondary growth scaling factor'(100%) =f{'distance to base of the root'} (cm) x,y pairs :{ 0 0.7 20 0.7 40
0.4 100 0.4 }
2.1.2.25 'soil impedence'= 0.008 (noUnit)

2.1.2.26 'soil impedence.v2'(cm) =f{'uniform distribution'} minimum=-0.04 maximum=0.04
2.1.2.27 'top boundary'= 1 (noUnit)

2.1.3 'basal whorl3'
2.1.3.1 'aerenchyma formation'(100%) =f{'time since creation'} (day) x,y pairs :{ 0 0 3 0 5 0.05 10 0.1 20 0.268 1000 0.268 }
2.1.3.2 'bottom boundary'= 1 (noUnit)
2.1.3.3 'bounce of the side'= 1 (noUnit)
2.1.3.4 'branch list'
2.1.3.4.1 'lateral basal roots'
2.1.3.4.1.1 'allow branches to form above ground'= 0 (noUnit)
2.1.3.4.1.2 'branching frequency'= 0.15 (cm)
2.1.3.4.1.3 'length root tip'= 10 (cm)
2.1.3.5 'branching angle'= 90 (degrees)
2.1.3.6 'density'= 0.094 (g/cm3)
2.1.3.7 'diameter'= 0.068 (cm)
2.1.3.8 'gravitropism'= 0.0005 (noUnit)
2.1.3.9 'gravitropism.v2'(cm) =f{'uniform distribution'} minimum=-0.02 maximum=-0.01
2.1.3.10 'growth rate'(cm/day) =f{'time since creation'} (day) x,y pairs :{ 0 0.1 2 4 10 4 15 3 25 2.352 35 2.352 40 0 1000 0 }
2.1.3.11 'nitrate'
2.1.3.11.1 'Cmin'= 0.001 (uMol/ml)
2.1.3.11.2 'Imax'= 1.9 (uMol/cm2/day)
2.1.3.11.3 'Km'= 0.0161 (uMol/ml)
2.1.3.11.4 'minimal nutrient concentration'= 600 (uMol/g)
2.1.3.11.5 'optimal nutrient concentration'= 1200 (uMol/g)
2.1.3.12 'number of xylem poles'= 4 (noUnit)
2.1.3.13 'phosphorus'
2.1.3.13.1 'Cmin'= 0.0002 (uMol/ml)
2.1.3.13.2 'Imax'= 0.0555 (uMol/cm2/day)
2.1.3.13.3 'Km'= 0.00545 (uMol/ml)
2.1.3.13.4 'minimal nutrient concentration'= 30 (uMol/g)
2.1.3.13.5 'optimal nutrient concentration'= 60 (uMol/g)
2.1.3.14 'potassium'
2.1.3.14.1 'Cmin'= 0.002 (uMol/ml)
2.1.3.14.2 'Imax'= 0.467 (uMol/cm2/day)
2.1.3.14.3 'Km'= 0.039 (uMol/ml)
2.1.3.14.4 'minimal nutrient concentration'= 168 (uMol/g)
2.1.3.14.5 'optimal nutrient concentration'= 234 (uMol/g)
2.1.3.15 'reduction in respiration due to aerenchyma'(100%) =f{'aerenchymaFormation'} (100%) x,y pairs :{ 0 0 0.3

0.7 0.6 1 }
2.1.3.16 'regular topology'= 0 (noUnit)
2.1.3.17 'relative carbon cost of exudation'(g/cm/day) =f{'time since creation'} (day) x,y pairs :{ 0 1.915e-05 1.8
1.511e-05 3.1 1.699e-05 4.4 1.362e-05 100 1.362e-05 }
2.1.3.18 'relative respiration'(g/g/day) =f{'time since creation'} (day) x,y pairs :{ 0 0.09 2 0.04 6 0.04 1000 0.04 }
2.1.3.19 'root class ID'= 99 (noUnit)
2.1.3.20 'root hair density'(#/cm2) =f{'time since creation'} (day) x,y pairs :{ 0 2000 10 2000 30 2000 100 2000 }
2.1.3.21 'root hair diameter'= 0.0005 (cm)
2.1.3.22 'root hair length'(cm) =f{'time since creation'} (day) x,y pairs :{ 0 0 1 0 2 0.03 100 0.03 }
2.1.3.23 'secondary growth rate'(cm/day) =f{'root segment age'} (day) x,y pairs :{ 0 0 4 0.0005 5 0.001 7 0.0015 11
0.002 13 0.0023 18 0.0026 24 0.00285 29 0.003 100 0.003 }
2.1.3.24 'secondary growth scaling factor'(100%) =f{'distance to base of the root'} (cm) x,y pairs :{ 0 0.7 20 0.7 40
0.4 100 0.4 }
2.1.3.25 'soil impedence'= 0.008 (noUnit)
2.1.3.26 'soil impedence.v2'(cm) =f{'uniform distribution'} minimum=-0.04 maximum=0.04
2.1.3.27 'top boundary'= 1 (noUnit)

2.1.4 'basal whorl4'
2.1.4.1 'aerenchyma formation'(100%) =f{'time since creation'} (day) x,y pairs :{ 0 0 3 0 5 0.05 10 0.1 20 0.268 1000
0.268 }
2.1.4.2 'bottom boundary'= 1 (noUnit)
2.1.4.3 'bounce of the side'= 1 (noUnit)
2.1.4.4 'branch list'
2.1.4.4.1 'lateral basal roots'
2.1.4.4.1.1 'allow branches to form above ground'= 0 (noUnit)
2.1.4.4.1.2 'branching frequency'= 0.15 (cm)
2.1.4.4.1.3 'length root tip'= 10 (cm)
2.1.4.5 'branching angle'= 90 (degrees)
2.1.4.6 'density'= 0.094 (g/cm3)
2.1.4.7 'diameter'= 0.068 (cm)
2.1.4.8 'gravitropism'= 0.0005 (noUnit)
2.1.4.9 'gravitropism.v2'(cm) =f{'uniform distribution'} minimum=-0.02 maximum=-0.01
2.1.4.10 'growth rate'(cm/day) =f{'time since creation'} (day) x,y pairs :{ 0 0.1 2 4 10 4 15 3 25 2.352 35 2.352 40 0
1000 0 }
2.1.4.11 'nitrate'

2.1.4.11.1 'Cmin'= 0.001 (uMol/ml)
2.1.4.11.2 'Imax'= 1.9 (uMol/cm2/day)
2.1.4.11.3 'Km'= 0.0161 (uMol/ml)
2.1.4.11.4 'minimal nutrient concentration'= 600 (uMol/g)
2.1.4.11.5 'optimal nutrient concentration'= 1200 (uMol/g)
2.1.4.12 'number of xylem poles'= 4 (noUnit)
2.1.4.13 'phosphorus'
2.1.4.13.1 'Cmin'= 0.0002 (uMol/ml)
2.1.4.13.2 'Imax'= 0.0555 (uMol/cm2/day)
2.1.4.13.3 'Km'= 0.00545 (uMol/ml)
2.1.4.13.4 'minimal nutrient concentration'= 30 (uMol/g)
2.1.4.13.5 'optimal nutrient concentration'= 60 (uMol/g)
2.1.4.14 'potassium'
2.1.4.14.1 'Cmin'= 0.002 (uMol/ml)
2.1.4.14.2 'Imax'= 0.467 (uMol/cm2/day)
2.1.4.14.3 'Km'= 0.039 (uMol/ml)
2.1.4.14.4 'minimal nutrient concentration'= 168 (uMol/g)
2.1.4.14.5 'optimal nutrient concentration'= 234 (uMol/g)
2.1.4.15 'reduction in respiration due to aerenchyma'(100%) =f{'aerenchymaFormation'} (100%) x,y pairs :{ 0 0 0.3 0.7 0.6 1 }
2.1.4.16 'regular topology'= 0 (noUnit)
2.1.4.17 'relative carbon cost of exudation'(g/cm/day) =f{'time since creation'} (day) x,y pairs :{ 0 1.915e-05 1.8 1.511e-05 3.1 1.699e-05 4.4 1.362e-05 100 1.362e-05 }
2.1.4.18 'relative respiration'(g/g/day) =f{'time since creation'} (day) x,y pairs :{ 0 0.09 2 0.04 6 0.04 1000 0.04 }
2.1.4.19 'root class ID'= 99 (noUnit)
2.1.4.20 'root hair density'(#/cm2) =f{'time since creation'} (day) x,y pairs :{ 0 2000 10 2000 30 2000 100 2000 }
2.1.4.21 'root hair diameter'= 0.0005 (cm)
2.1.4.22 'root hair length'(cm) =f{'time since creation'} (day) x,y pairs :{ 0 0 1 0 2 0.03 100 0.03 }
2.1.4.23 'secondary growth rate'(cm/day) =f{'root segment age'} (day) x,y pairs :{ 0 0 4 0.0005 5 0.001 7 0.0015 11 0.002 13 0.0023 18 0.0026 24 0.00285 29 0.003 100 0.003 }
2.1.4.24 'secondary growth scaling factor'(100%) =f{'distance to base of the root'} (cm) x,y pairs :{ 0 0.7 20 0.7 40 0.4 100 0.4 }
2.1.4.25 'soil impedence'= 0.008 (noUnit)
2.1.4.26 'soil impedence.v2'(cm) =f{'uniform distribution'} minimum=-0.04 maximum=0.04
2.1.4.27 'top boundary'= 1 (noUnit)

2.1.5 'finelateral'

2.1.5.1 'aerenchyma formation'(100%) =f{'time since creation'} (day) x,y pairs :{ 0 0 3 0 5 0.05 10 0.1 20 0.268 1000
0.268 }
2.1.5.2 'bottom boundary'= 1 (noUnit)
2.1.5.3 'bounce of the side'= 1 (noUnit)
2.1.5.4 'branch list'
2.1.5.5 'branching angle'= 75 (degrees)
2.1.5.6 'density'= 0.094 (g/cm3)
2.1.5.7 'diameter'= 0.01 (cm)
2.1.5.8 'gravitropism'= 0 (noUnit)
2.1.5.9 'gravitropism.v2'= 0 0 0 (cm)
2.1.5.10 'growth rate'(cm/day) =f{'time since creation'} (day) x,y pairs :{ 0 0.2 3 0.2 5 0 100 0 }
2.1.5.11 'longitudinal growth rate multiplier'(cm) minimum=0.3 maximum=1 mean=0.6 stdev=0.1
2.1.5.12 'nitrate'
2.1.5.12.1 'Cmin'= 0.001 (uMol/ml)
2.1.5.12.2 'Imax'= 1.9 (uMol/cm2/day)
2.1.5.12.3 'Km'= 0.0161 (uMol/ml)
2.1.5.12.4 'minimal nutrient concentration'= 600 (uMol/g)
2.1.5.12.5 'optimal nutrient concentration'= 1200 (uMol/g)
2.1.5.13 'number of xylem poles'= 4 (noUnit)
2.1.5.14 'phosphorus'
2.1.5.14.1 'Cmin'= 0.0002 (uMol/ml)
2.1.5.14.2 'Imax'= 0.0555 (uMol/cm2/day)
2.1.5.14.3 'Km'= 0.00545 (uMol/ml)
2.1.5.14.4 'minimal nutrient concentration'= 30 (uMol/g)
2.1.5.14.5 'optimal nutrient concentration'= 60 (uMol/g)
2.1.5.15 'potassium'
2.1.5.15.1 'Cmin'= 0.002 (uMol/ml)
2.1.5.15.2 'Imax'= 0.467 (uMol/cm2/day)
2.1.5.15.3 'Km'= 0.039 (uMol/ml)
2.1.5.15.4 'minimal nutrient concentration'= 168 (uMol/g)
2.1.5.15.5 'optimal nutrient concentration'= 234 (uMol/g)
2.1.5.16 'reduction in respiration due to aerenchyma'(100%) =f{'aerenchymaFormation'} (100%) x,y pairs :{ 0 0 0.3
0.7 0.6 1 }
2.1.5.17 'regular topology'= 0 (noUnit)
2.1.5.18 'relative carbon cost of exudation'(g/cm/day) =f{'time since creation'} (day) x,y pairs :{ 0 1.915e-05 1.8
1.511e-05 3.1 1.699e-05 4.4 1.362e-05 100 1.362e-05 }
2.1.5.19 'relative respiration'(g/g/day) =f{'time since creation'} (day) x,y pairs :{ 0 0.09 2 0.04 6 0.04 1000 0.04 }
2.1.5.20 'root class ID'= 97 (noUnit)
2.1.5.21 'root hair density'(#/cm2) =f{'time since creation'} (day) x,y pairs :{ 0 3000 100 3000 }

2.1.5.22 'root hair diameter'= 0.0005 (cm)
2.1.5.23 'root hair length'(cm) =f{'time since creation'} (day) x,y pairs :{ 0 0 1 0 2 0.03 100 0.03 }
2.1.5.24 'soil impedence'= 0.5 (noUnit)
2.1.5.25 'soil impedence.v2'(cm) =f{'uniform distribution'} minimum=-0.1 maximum=0.1
2.1.5.26 'top boundary'= 1 (noUnit)
2.1.5.27 'topology offset'= 0 (noUnit)

2.1.6 'finelateral fast growing'
2.1.6.1 'aerenchyma formation'(100%) =f{'time since creation'} (day) x,y pairs :{ 0 0 3 0 5 0.05 10 0.1 20 0.268 1000 0.268 }
2.1.6.2 'bottom boundary'= 1 (noUnit)
2.1.6.3 'bounce of the side'= 1 (noUnit)
2.1.6.4 'branch list'
2.1.6.5 'branching angle'= 75 (degrees)
2.1.6.6 'density'= 0.094 (g/cm3)
2.1.6.7 'diameter'= 0.015 (cm)
2.1.6.8 'gravitropism'= 0 (noUnit)
2.1.6.9 'gravitropism.v2'= 0 0 0 (cm)
2.1.6.10 'growth rate'(cm/day) =f{'time since creation'} (day) x,y pairs :{ 0 0.5 1 0.8 2 1 3 1 4 0 100 0 }
2.1.6.11 'longitudinal growth rate multiplier'(cm) minimum=0.3 maximum=1 mean=0.6 stdev=0.1
2.1.6.12 'nitrate'
2.1.6.12.1 'Cmin'= 0.001 (uMol/ml)
2.1.6.12.2 'Imax'= 1.9 (uMol/cm2/day)
2.1.6.12.3 'Km'= 0.0161 (uMol/ml)
2.1.6.12.4 'minimal nutrient concentration'= 600 (uMol/g)
2.1.6.12.5 'optimal nutrient concentration'= 1200 (uMol/g)
2.1.6.13 'number of xylem poles'= 4 (noUnit)
2.1.6.14 'phosphorus'
2.1.6.14.1 'Cmin'= 0.0002 (uMol/ml)
2.1.6.14.2 'Imax'= 0.0555 (uMol/cm2/day)
2.1.6.14.3 'Km'= 0.00545 (uMol/ml)
2.1.6.14.4 'minimal nutrient concentration'= 30 (uMol/g)
2.1.6.14.5 'optimal nutrient concentration'= 60 (uMol/g)
2.1.6.15 'potassium'
2.1.6.15.1 'Cmin'= 0.002 (uMol/ml)
2.1.6.15.2 'Imax'= 0.467 (uMol/cm2/day)
2.1.6.15.3 'Km'= 0.039 (uMol/ml)
2.1.6.15.4 'minimal nutrient concentration'= 168 (uMol/g)
2.1.6.15.5 'optimal nutrient concentration'= 234 (uMol/g)
2.1.6.16 'reduction in respiration due to aerenchyma'(100%) =f{'aerenchymaFormation'} (100%) x,y pairs :{ 0 0 0.3

0.7 0.6 1 }
2.1.6.17 'regular topology'= 0 (noUnit)
2.1.6.18 'relative carbon cost of exudation'(g/cm/day) =f{'time since creation'} (day) x,y pairs :{ 0 1.915e-05 1.8
1.511e-05 3.1 1.699e-05 4.4 1.362e-05 100 1.362e-05 }
2.1.6.19 'relative respiration'(g/g/day) =f{'time since creation'} (day) x,y pairs :{ 0 0.09 2 0.04 6 0.04 1000 0.04 }
2.1.6.20 'root class ID'= 97 (noUnit)
2.1.6.21 'root hair density'(#/cm2) =f{'time since creation'} (day) x,y pairs :{ 0 3000 100 3000 }
2.1.6.22 'root hair diameter'= 0.0005 (cm)
2.1.6.23 'root hair length'(cm) =f{'time since creation'} (day) x,y pairs :{ 0 0 1 0 2 0.03 100 0.03 }
2.1.6.24 'soil impedence'= 0.5 (noUnit)
2.1.6.25 'soil impedence.v2'(cm) =f{'uniform distribution'} minimum=-0.1 maximum=0.1
2.1.6.26 'top boundary'= 1 (noUnit)
2.1.6.27 'topology offset'= 0 (noUnit)

2.1.7 'hypocotyl'
2.1.7.1 'aerenchyma formation'(100%) =f{'time since creation'} (day) x,y pairs :{ 0 0 100 0 }
2.1.7.2 'bottom boundary'= 1 (noUnit)
2.1.7.3 'bounce of the side'= 1 (noUnit)
2.1.7.4 'branch list'
2.1.7.4.1 'basal whorl1'
2.1.7.4.1.1 'branching frequency'= 0.01 (cm)
2.1.7.4.1.2 'branching spatial offset'= 0.01 (cm)
2.1.7.4.1.3 'branching time offset'= 4.167 (day)
2.1.7.4.1.4 'max number of branches'= 4 (#)
2.1.7.4.1.5 'number of branches/whorl'= 4 (#)
2.1.7.4.2 'basal whorl2'
2.1.7.4.2.1 'branching frequency'= 0.5 (cm)
2.1.7.4.2.2 'branching spatial offset'= 0.3 (cm)
2.1.7.4.2.3 'branching time offset'= 6.25 (day)
2.1.7.4.2.4 'max number of branches'= 4 (#)
2.1.7.4.2.5 'number of branches/whorl'= 4 (#)
2.1.7.4.3 'hypocotyl born roots'
2.1.7.4.3.1 'allow branches to form above ground'= 0 (noUnit)
2.1.7.4.3.2 'branching delay'= 0 (day)
2.1.7.4.3.3 'branching frequency'= 0.4 (cm)
2.1.7.4.3.4 'branching spatial offset'= 0.4 (cm)
2.1.7.4.3.5 'branching time offset'= 10 (day)
2.1.7.4.3.6 'max number of branches'= 10 (#)
2.1.7.5 'density'= 0.094 (g/cm3)

2.1.7.6 'diameter'= 0.4 (cm)
2.1.7.7 'gravitropism.v2'(cm) =f{'uniform distribution'} minimum=0.5 maximum=0.6
2.1.7.8 'growth rate'(cm/day) =f{'time since creation'} (day) x,y pairs :{ 0 1 1 3 2 3 3 1 3.3 0.5 4 0.2 5 0 1000 0 }
2.1.7.9 'nitrate'
2.1.7.9.1 'Cmin'= 0.001 (uMol/ml)
2.1.7.9.2 'Imax'= 1.9 (uMol/cm2/day)
2.1.7.9.3 'Km'= 0.0161 (uMol/ml)
2.1.7.9.4 'minimal nutrient concentration'= 600 (uMol/g)
2.1.7.9.5 'optimal nutrient concentration'= 1200 (uMol/g)
2.1.7.10 'number of xylem poles'= 4 (noUnit)
2.1.7.11 'phosphorus'
2.1.7.11.1 'Cmin'= 0.0002 (uMol/ml)
2.1.7.11.2 'Imax'= 0.0555 (uMol/cm2/day)
2.1.7.11.3 'Km'= 0.00545 (uMol/ml)
2.1.7.11.4 'minimal nutrient concentration'= 30 (uMol/g)
2.1.7.11.5 'optimal nutrient concentration'= 60 (uMol/g)
2.1.7.12 'potassium'
2.1.7.12.1 'Cmin'= 0.002 (uMol/ml)
2.1.7.12.1 'Imax'= 0.467 (uMol/cm2/day)
2.1.7.12.3 'Km'= 0.039 (uMol/ml)
2.1.7.12.4 'minimal nutrient concentration'= 168 (uMol/g)
2.1.7.12.5 'optimal nutrient concentration'= 234 (uMol/g)
2.1.7.13 'reduction in respiration due to aerenchyma'(100%) =f{'aerenchymaFormation'} (100%) x,y pairs :{ 0 0 0.3
0.7 0.6 1 }
2.1.7.14 'relative carbon cost of exudation'(g/cm/day) =f{'time since creation'} (day) x,y pairs :{ 0 0 100 0 }
2.1.7.15 'relative respiration'(g/g/day) =f{'time since creation'} (day) x,y pairs :{ 0 0.09 2 0.04 6 0.04 1000 0.04 }
2.1.7.16 'root class ID'= 96 (noUnit)
2.1.7.17 'root hair density'(#/cm2) =f{'time since creation'} (day) x,y pairs :{ 0 0 100 0 }
2.1.7.18 'root hair diameter'= 0.0005 (cm)
2.1.7.19 'root hair length'(cm) =f{'time since creation'} (day) x,y pairs :{ 0 0 1 0 2 0.03 100 0.03 }
2.1.7.20 'secondary growth rate'(cm/day) =f{'root segment age'} (day) x,y pairs :{ 0 0 4 0.0005 5 0.001 7 0.0015 11
0.002 13 0.0023 18 0.0026 24 0.00285 29 0.003 100 0.003 }
2.1.7.21 'secondary growth scaling factor'(100%) =f{'distance to base of the root'} (cm) x,y pairs :{ 0 7 2 7 10 7 1000
7}
2.1.7.22 'soil impedence.v2'(cm) =f{'uniform distribution'} minimum=-0.01 maximum=0.01
2.1.7.23 'top boundary'= 0 (noUnit)

2.1.8 'hypocotyl born roots'
2.1.8.1 'aerenchyma formation'(100%) =f{'time since creation'} (day) x,y pairs :{ 0 0 3 0 5 0.05 10 0.1 20 0.268 1000 0.268 }
2.1.8.2 'bottom boundary'= 1 (noUnit)
2.1.8.3 'bounce of the side'= 1 (noUnit)
2.1.8.4 'branch list'
2.1.8.4.1 'lateral hypocotyl born roots'
2.1.8.4.1.1 'allow branches to form above ground'= 0 (noUnit)
2.1.8.4.1.2 'branching frequency'= 0.4 (cm)
2.1.8.4.1.3 'length root tip'= 10 (cm)
2.1.8.5 'branching angle'= 85 (degrees)
2.1.8.6 'density'= 0.094 (g/cm3)
2.1.8.7 'diameter'= 0.064 (cm)
2.1.8.8 'gravitropism'= 0 (noUnit)
2.1.8.9 'gravitropism.v2'(cm) =f{'uniform distribution'} minimum=-0.002 maximum=0
2.1.8.10 'growth rate'(cm/day) =f{'time since creation'} (day) x,y pairs :{ 0 1 25 0.8 35 0 60 0 }
2.1.8.11 'longitudinal growth rate multiplier'(cm) minimum=0.5 maximum=1.5 mean=1 stdev=0.1
2.1.8.12 'nitrate'
2.1.8.12.1 'Cmin'= 0.001 (uMol/ml)
2.1.8.12.2 'Imax'= 1.9 (uMol/cm2/day)
2.1.8.12.3 'Km'= 0.0161 (uMol/ml)
2.1.8.12.4 'minimal nutrient concentration'= 600 (uMol/g)
2.1.8.12.5 'optimal nutrient concentration'= 1200 (uMol/g)

2.1.8.13 'number of xylem poles'= 4 (noUnit)
2.1.8.14 'phosphorus'
2.1.8.14.1 'Cmin'= 0.0002 (uMol/ml)
2.1.8.14.2 'Imax'= 0.0555 (uMol/cm2/day)
2.1.8.14.3 'Km'= 0.00545 (uMol/ml)
2.1.8.14.4 'minimal nutrient concentration'= 30 (uMol/g)
2.1.8.14.5 'optimal nutrient concentration'= 60 (uMol/g)

2.1.8.15 'potassium'
2.1.8.15.1 'Cmin'= 0.002 (uMol/ml)
2.1.8.15.2 'Imax'= 0.467 (uMol/cm2/day)
2.1.8.15.3 'Km'= 0.039 (uMol/ml)
2.1.8.15.4 'minimal nutrient concentration'= 168 (uMol/g)
2.1.8.15.5 'optimal nutrient concentration'= 234 (uMol/g)
)
2.1.8.16 'reduction in respiration due to aerenchyma'(100%) =f{'aerenchymaFormation'} (100%) x,y pairs :{ 0 0 0.3

0.7 0.6 1 }
2.1.8.17 'regular topology'= 0 (noUnit)
2.1.8.18 'relative carbon cost of exudation'(g/cm/day) =f{'time since creation'} (day) x,y pairs :{ 0 1.915e-05 1.8
1.511e-05 3.1 1.699e-05 4.4 1.362e-05 100 1.362e-05 }
2.1.8.19 'relative respiration'(g/g/day) =f{'time since creation'} (day) x,y pairs :{ 0 0.09 2 0.04 6 0.04 1000 0.04 }
2.1.8.20 'root class ID'= 98 (noUnit)
2.1.8.21 'root hair density'(#/cm2) =f{'time since creation'} (day) x,y pairs :{ 0 3000 10 3000 30 3000 100 3000 }
2.1.8.22 'root hair diameter'= 0.0005 (cm)
2.1.8.23 'root hair length'(cm) =f{'time since creation'} (day) x,y pairs :{ 0 0 1 0 2 0.03 100 0.03 }
2.1.8.24 'secondary growth rate'(cm/day) =f{'root segment age'} (day) x,y pairs :{ 0 0 4 0.0005 5 0.001 7 0.0015 11
0.002 13 0.0023 18 0.0026 24 0.00285 29 0.003 100 0.003 }
2.1.8.25 'secondary growth scaling factor'(100%) =f{'distance to base of the root'} (cm) x,y pairs :{ 0 0.6 50 0.2 100
0.2 }
2.1.8.26 'soil impedence'= 0.003 (noUnit)
2.1.8.27 'soil impedence.v2'(cm) =f{'uniform distribution'} minimum=-0.04 maximum=0.04
2.1.9.28 'top boundary'= 1 (noUnit)

2.1.9 'lateral basal roots'
2.1.9.1 'aerenchyma formation'(100%) =f{'time since creation'} (day) x,y pairs :{ 0 0 3 0 5 0.05 10 0.1 20 0.268 1000
0.268 }
2.1.9.2 'bottom boundary'= 1 (noUnit)
2.1.9.3 'bounce of the side'= 1 (noUnit)
2.1.9.4 'branch list'
2.1.9.4.1 'finelateral'
2.1.9.4.1.1 'allow branches to form above ground'= 0 (noUnit)
2.1.9.4.1.2 'branching frequency'= 0.5 (cm)
2.1.9.4.1.3 'length root tip'= 4 (cm)
2.1.9.5 'branching angle'= 75 (degrees)
2.1.9.6 'density'= 0.094 (g/cm3)
2.1.9.7 'diameter'= 0.03 (cm)
2.1.9.8 'gravitropism'= 0 (noUnit)
2.1.9.9 'gravitropism.v2'= 0 0 0 (cm)
2.1.9.10 'growth rate'(cm/day) =f{'time since creation'} (day) x,y pairs :{ 0 0.768 2 0.768 4 0.768 6 0.2 10 0 1000 0 }
2.1.9.11 'longitudinal growth rate multiplier'(cm) minimum=0.6 maximum=1 mean=0.8 stdev=0.1
2.1.9.12 'nitrate'
2.1.9.12.1

2.1.9.12.2
2.1.9.12.3
2.1.9.12.4
2.1.9.12.5
'Cmin'= 0.001 (uMol/ml)
'Imax'= 1.9 (uMol/cm2/day)
'Km'= 0.0161 (uMol/ml)
'minimal nutrient concentration'= 600 (uMol/g)
'optimal nutrient concentration'= 1200 (uMol/g)
2.1.9.13 'number of xylem poles'= 4 (noUnit)
2.1.9.14 'phosphorus'
2.1.9.14.1 'Cmin'= 0.0002 (uMol/ml)
2.1.9.14.2 'Imax'= 0.0555 (uMol/cm2/day)
2.1.9.14.3 'Km'= 0.00545 (uMol/ml)
2.1.9.14.4 'minimal nutrient concentration'= 30 (uMol/g)
2.1.9.14.5 'optimal nutrient concentration'= 60 (uMol/g)
2.1.9.15 'potassium'
2.1.9.15.1 'Cmin'= 0.002 (uMol/ml)
2.1.9.15.2 'Imax'= 0.467 (uMol/cm2/day)
2.1.9.15.3 'Km'= 0.039 (uMol/ml)
2.1.9.15.4 'minimal nutrient concentration'= 168 (uMol/g)
2.1.9.15.5 'optimal nutrient concentration'= 234 (uMol/g)
2.1.9.16 'reduction in respiration due to aerenchyma'(100%) =f{'aerenchymaFormation'} (100%) x,y pairs :{ 0 0 0.3 0.7 0.6 1 }
2.1.9.17 'regular topology'= 0 (noUnit)
2.1.9.18 'relative carbon cost of exudation'(g/cm/day) =f{'time since creation'} (day) x,y pairs :{ 0 1.915e-05 1.8 1.511e-05 3.1 1.699e-05 4.4 1.362e-05 100 1.362e-05 }
2.1.9.19 'relative respiration'(g/g/day) =f{'time since creation'} (day) x,y pairs :{ 0 0.09 2 0.04 6 0.04 1000 0.04 }
2.1.9.20 'root class ID'= 97 (noUnit)
2.1.9.21 'root hair density'(#/cm2) =f{'time since creation'} (day) x,y pairs :{ 0 3000 100 3000 }
2.1.9.22 'root hair diameter'= 0.0005 (cm)
2.1.9.23 'root hair length'(cm) =f{'time since creation'} (day) x,y pairs :{ 0 0 1 0 2 0.03 100 0.03 }
2.1.9.24 'soil impedence'= 0.02 (noUnit)
2.1.9.25 'soil impedence.v2'(cm) =f{'uniform distribution'} minimum=-0.1 maximum=0.1
2.1.9.26 'top boundary'= 1 (noUnit)
2.1.9.27 'topology offset'= 0 (noUnit)

2.1.10 'lateral hypocotyl born roots'
2.1.10.1 'aerenchyma formation'(100%) =f{'time since creation'} (day) x,y pairs :{ 0 0 3 0 5 0.05 10 0.1 20 0.268 1000

0.268 }
2.1.10.2 'bottom boundary'= 1 (noUnit)
2.1.10.3 'bounce of the side'= 1 (noUnit)
2.1.10.4 'branch list'
2.1.10.5 'branching angle'= 75 (degrees)
2.1.10.6 'density'= 0.094 (g/cm3)
2.1.10.7 'diameter'= 0.03 (cm)
2.1.10.8 'gravitropism'= 0 (noUnit)
2.1.10.9 'gravitropism.v2'= 0 0 0 (cm)
2.1.10.10 'growth rate'(cm/day) =f{'time since creation'} (day) x,y pairs :{ 0 0.768 2 0.768 4 0.768 6 0.2 10 0 1000 0 }
2.1.10.11 'longitudinal growth rate multiplier'(cm) minimum=0.6 maximum=1 mean=0.8 stdev=0.1
2.1.10.12 'nitrate'
2.1.10.12.1 'Cmin'= 0.001 (uMol/ml)
2.1.10.12.2 'Imax'= 1.9 (uMol/cm2/day)
2.1.10.12.3 'Km'= 0.0161 (uMol/ml)
2.1.10.12.4 'minimal nutrient concentration'= 600 (uMol/g)
2.1.10.12.5 'optimal nutrient concentration'= 1200 (uMol/g)
2.1.10.13 'number of xylem poles'= 4 (noUnit)
2.1.10.14 'phosphorus'
2.1.10.14.1 'Cmin'= 0.0002 (uMol/ml)
2.1.10.14.2 'Imax'= 0.0555 (uMol/cm2/day)
2.1.10.14.3 'Km'= 0.00545 (uMol/ml)
2.1.10.14.4 'minimal nutrient concentration'= 30 (uMol/g)
2.1.10.14.5 'optimal nutrient concentration'= 60 (uMol/g)
2.1.10.15 'potassium'
2.1.10.15.1 'Cmin'= 0.002 (uMol/ml)
2.1.10.15.2 'Imax'= 0.467 (uMol/cm2/day)
2.1.10.15.3 'Km'= 0.039 (uMol/ml)
2.1.10.15.4 'minimal nutrient concentration'= 168 (uMol/g)
2.1.10.15.5 'optimal nutrient concentration'= 234 (uMol/g)
2.1.10.16 'reduction in respiration due to aerenchyma'(100%) =f{'aerenchymaFormation'} (100%) x,y pairs :{ 0 0 0.3
0.7 0.6 1 }
2.1.10.17 'regular topology'= 0 (noUnit)
2.1.10.18 'relative carbon cost of exudation'(g/cm/day) =f{'time since creation'} (day) x,y pairs :{ 0 1.915e-05 1.8
1.511e-05 3.1 1.699e-05 4.4 1.362e-05 100 1.362e-05 }
2.1.10.19 'relative respiration'(g/g/day) =f{'time since creation'} (day) x,y pairs :{ 0 0.09 2 0.04 6 0.04 1000 0.04 }
2.1.10.20 'root class ID'= 97 (noUnit)
2.1.10.21 'root hair density'(#/cm2) =f{'time since creation'} (day) x,y pairs :{ 0 3000 100 3000 }
2.1.10.22 'root hair diameter'= 0.0005 (cm)

2.1.10.23 'root hair length'(cm) =f{'time since creation'} (day) x,y pairs :{ 0 0 1 0 2 0.03 100 0.03 }
2.1.10.24 'soil impedence'= 0.015 (noUnit)
2.1.10.25 'soil impedence.v2'(cm) =f{'uniform distribution'} minimum=-0.1 maximum=0.1
2.1.10.26 'top boundary'= 1 (noUnit)
2.1.10.27 'topology offset'= 0 (noUnit)

2.1.11 'lateral primary root'
2.1.11.1 'aerenchyma formation'(100%) =f{'time since creation'} (day) x,y pairs :{ 0 0 3 0 5 0.05 10 0.1 20 0.268
1000 0.268 }
2.1.11.2 'bottom boundary'= 1 (noUnit)
2.1.11.3 'bounce of the side'= 1 (noUnit)
2.1.11.4 'branch list'
2.1.11.4.1 'finelateral'
2.1.11.4.1.1 'allow branches to form above ground'= 0 (noUnit)
2.1.11.4.1.2 'branching frequency'= 0.5 (cm)
2.1.11.4.1.3 'length root tip'= 4 (cm)
2.1.11.5 'branching angle'= 75 (degrees)
2.1.11.6 'density'= 0.094 (g/cm3)
2.1.11.7 'diameter'= 0.03 (cm)
2.1.11.8 'gravitropism'= 0 (noUnit)
2.1.11.9 'gravitropism.v2'= 0 0 0 (cm)
2.1.11.10 'growth rate'(cm/day) =f{'time since creation'} (day) x,y pairs :{ 0 0.768 2 0.768 4 0.768 6 0.768 10 0 1000
0}
2.1.11.11 'longitudinal growth rate multiplier'(cm) minimum=0.8 maximum=1.2 mean=1 stdev=0.1
2.1.11.12 'nitrate'
2.1.11.12.1 'Cmin'= 0.001 (uMol/ml)
2.1.11.12.1 'Imax'= 1.9 (uMol/cm2/day)
2.1.11.12.3 'Km'= 0.0161 (uMol/ml)
2.1.11.12.4 'minimal nutrient concentration'= 600 (uMol/g)
2.1.11.12.5 'optimal nutrient concentration'= 1200 (uMol/g)
2.1.11.13 'number of xylem poles'= 4 (noUnit)
2.1.11.14 'phosphorus'
2.1.11.14.1 'Cmin'= 0.0002 (uMol/ml)
2.1.11.14.2 'Imax'= 0.0555 (uMol/cm2/day)
2.1.11.14.3 'Km'= 0.00545 (uMol/ml)
2.1.11.14.4 'minimal nutrient concentration'= 30 (uMol/g)
2.1.11.14.5 'optimal nutrient concentration'= 60 (uMol/g)
2.1.11.15 'potassium'
2.1.11.15.1 'Cmin'= 0.002 (uMol/ml)
2.1.11.15.2 'Imax'= 0.467 (uMol/cm2/day)
2.1.11.15.3 'Km'= 0.039 (uMol/ml)

2.1.11.15.4 'minimal nutrient concentration'= 168 (uMol/g)
2.1.11.15.5 'optimal nutrient concentration'= 234 (uMol/g)
2.1.11.16 'reduction in respiration due to aerenchyma'(100%) =f{'aerenchymaFormation'} (100%) x,y pairs :{ 0 0 0.3 0.7 0.6 1 }
2.1.11.17 'regular topology'= 0 (noUnit)
2.1.11.18 'relative carbon cost of exudation'(g/cm/day) =f{'time since creation'} (day) x,y pairs :{ 0 1.915e-05 1.8 1.511e-05 3.1 1.699e-05 4.4 1.362e-05 100 1.362e-05 }
2.1.11.19 'relative respiration'(g/g/day) =f{'time since creation'} (day) x,y pairs :{ 0 0.09 2 0.04 6 0.04 1000 0.04 }
2.1.11.20 'root class ID'= 97 (noUnit)
2.1.11.21 'root hair density'(#/cm2) =f{'time since creation'} (day) x,y pairs :{ 0 2000 10 2000 30 2000 100 2000 }
2.1.11.22 'root hair diameter'= 0.0005 (cm)
2.1.11.23 'root hair length'(cm) =f{'time since creation'} (day) x,y pairs :{ 0 0 1 0 2 0.03 100 0.03 }
2.1.11.24 'secondary growth rate'(cm/day) =f{'root segment age'} (day) x,y pairs :{ 0 0 4 0.0005 5 0.001 7 0.0015 11 0.002 13 0.0023 18 0.0026 24 0.00285 29 0.003 100 0.003 }
2.1.11.25 'secondary growth scaling factor'(100%) =f{'distance to base of the root'} (cm) x,y pairs :{ 0 0.1 50 0.1 100 0.1 }
2.1.11.26 'soil impedence'= 0.02 (noUnit)
2.1.11.27 'soil impedence.v2'(cm) =f{'uniform distribution'} minimum=-0.2 maximum=0.2
2.1.11.28 'top boundary'= 1 (noUnit)
2.1.11.29 'topology offset'= 0 (noUnit)

2.1.12 'lateral primary root fast growing'
2.1.12.1 'aerenchyma formation'(100%) =f{'time since creation'} (day) x,y pairs :{ 0 0 3 0 5 0.05 10 0.1 20 0.268 1000 0.268 }
2.1.12.2 'bottom boundary'= 1 (noUnit)
2.1.12.3 'bounce of the side'= 1 (noUnit)
2.1.12.4 'branch list'
2.1.12.4.1 'finelateral fast growing'
2.1.12.4.1.1 'allow branches to form above ground'= 0 (noUnit)
2.1.12.4.1.2 'branching frequency'= 0.55 (cm)
2.1.12.4.1.3 'length root tip'= 4 (cm)
2.1.12.5 'branching angle'= 75 (degrees)
2.1.12.6 'density'= 0.094 (g/cm3)
2.1.12.7 'diameter'= 0.03 (cm)
2.1.12.8 'gravitropism'= 0 (noUnit)
2.1.12.9 'gravitropism.v2'= 0 0 0 (cm)

2.1.12.10 'growth rate'(cm/day) =f{'time since creation'} (day) x,y pairs :{ 0 0.768 2 0.768 15 0.768 20 0 1000 0 }

2.1.12.11 'longitudinal growth rate multiplier'(cm) minimum=1.4 maximum=1.8 mean=1.6 stdev=0.2

2.1.12.12 'nitrate'

2.1.12.12.1 'Cmin'= 0.001 (uMol/ml)

2.1.12.12.2 'Imax'= 1.9 (uMol/cm2/day)

2.1.12.12.3 'Km'= 0.0161 (uMol/ml)

2.1.12.12.4 'minimal nutrient concentration'= 600 (uMol/g)

2.1.12.12.5 'optimal nutrient concentration'= 1200 (uMol/g)

2.1.12.13 'number of xylem poles'= 4 (noUnit)

2.1.12.14 'phosphorus'

2.1.12.14.1 'Cmin'= 0.0002 (uMol/ml)

2.1.12.14.2 'Imax'= 0.0555 (uMol/cm2/day)

2.1.12.14.3 'Km'= 0.00545 (uMol/ml)

2.1.12.14.4 'minimal nutrient concentration'= 30 (uMol/g)

2.1.12.14.5 'optimal nutrient concentration'= 60 (uMol/g)

2.1.12.15 'potassium'

2.1.12.15.1 'Cmin'= 0.002 (uMol/ml)

2.1.12.15.2 'Imax'= 0.467 (uMol/cm2/day)

2.1.12.15.3 'Km'= 0.039 (uMol/ml)

2.1.12.15.4 'minimal nutrient concentration'= 168 (uMol/g)

2.1.12.15.5 'optimal nutrient concentration'= 234 (uMol/g)

2.1.12.16 'reduction in respiration due to aerenchyma'(100%) =f{'aerenchymaFormation'} (100%) x,y pairs :{ 0 0 0.3 0.7 0.6 1 }

2.1.12.17 'regular topology'= 0 (noUnit)

2.1.12.18 'relative carbon cost of exudation'(g/cm/day) =f{'time since creation'} (day) x,y pairs :{ 0 1.915e-05 1.8 1.511e-05 3.1 1.699e-05 4.4 1.362e-05 100 1.362e-05 }

2.1.12.19 'relative respiration'(g/g/day) =f{'time since creation'} (day) x,y pairs :{ 0 0.09 2 0.04 6 0.04 1000 0.04 }

2.1.12.20 'root class ID'= 97 (noUnit)

2.1.12.21 'root hair density'(#/cm2) =f{'time since creation'} (day) x,y pairs :{ 0 3000 100 3000 }

2.1.12.22 'root hair diameter'= 0.0005 (cm)

2.1.12.23 'root hair length'(cm) =f{'time since creation'} (day) x,y pairs :{ 0 0 1 0 2 0.03 100 0.03 }

2.1.12.24 'secondary growth rate'(cm/day) =f{'root segment age'} (day) x,y pairs :{ 0 0 4 0.0005 5 0.001 7 0.0015 11 0.002 13 0.0023 18 0.0026 24 0.00285 29 0.003 100 0.003 }

2.1.12.25 'secondary growth scaling factor'(100%) =f{'distance to base of the root'} (cm) x,y pairs :{ 0 0.3 50 0.2 100 0.2 }

2.1.12.26 'soil impedence'= 0.02 (noUnit)

2.1.12.27 'soil impedence.v2'(cm) =f{'uniform distribution'} minimum=-0.1 maximum=0.1
2.1.12.28 'top boundary'= 1 (noUnit)
2.1.12.29 'topology offset'= 0 (noUnit)

2.1.13 'primary root'
2.1.13.1 'aerenchyma formation'(100%) =f{'time since creation'} (day) x,y pairs :{ 0 0 3 0 5 0.05 10 0.1 20 0.268 1000 0.268 }
2.1.13.2 'bottom boundary'= 1 (noUnit)
2.1.13.3 'bounce of the side'= 1 (noUnit)
2.1.13.4 'branch list'
2.1.13.4.1 'lateral primary root'
2.1.13.4.1.1 'allow branches to form above ground'= 0 (noUnit)
2.1.13.4.1.2 'branching frequency'= 0.1 (cm)
2.1.13.4.1.3 'length root tip'= 10 (cm)
2.1.13.4.1.4 'number of branches/whorl'= 1 (#)
2.1.13.4.2 'lateral primary root fast growing'
2.1.13.4.2.1 'allow branches to form above ground'= 0 (noUnit)
2.1.13.4.2.2 'branching frequency'(cm) minimum=1 maximum=5
2.1.13.4.2.3 'length root tip'= 10 (cm)
2.1.13.4.2.4 'number of branches/whorl'= 1 (#)
2.1.13.5 'branching angle'= 0 (degrees)
2.1.13.6 'density'= 0.094 (g/cm3)
2.1.13.7 'diameter'= 0.09 (cm)
2.1.13.8 'gravitropism'= 0.011 (noUnit)
2.1.13.9 'gravitropism.v2'(cm) =f{'uniform distribution'} minimum=-0.015 maximum=-0.005
2.1.13.10 'growth rate'(cm/day) =f{'time since creation'} (day) x,y pairs :{ 0 2.357 10 2.357 15 2.357 250 2.357 }
2.1.13.11 'nitrate'
2.1.13.11.1 'Cmin'= 0.001 (uMol/ml)
2.1.13.11.2 'Imax'= 1.9 (uMol/cm2/day)
2.1.13.11.3 'Km'= 0.0161 (uMol/ml)
2.1.13.11.4 'minimal nutrient concentration'= 600 (uMol/g)
2.1.13.11.5 'optimal nutrient concentration'= 1200 (uMol/g)

2.1.13.12 'number of xylem poles'= 16 (noUnit)
2.1.13.13 'phosphorus'
2.1.13.13.1 'Cmin'= 0.0002 (uMol/ml)
2.1.13.13.2 'Imax'= 0.0555 (uMol/cm2/day)
2.1.13.13.3 'Km'= 0.00545 (uMol/ml)
2.1.13.13.4 'minimal nutrient concentration'= 30 (uMol/g)
2.1.13.13.5 'optimal nutrient concentration'= 60 (uMol/g)
2.1.13.14 'potassium'
2.1.13.14.1 'Cmin'= 0.002 (uMol/ml)

2.1.13.14.2 'Imax'= 0.467 (uMol/cm2/day)
2.1.13.14.3 'Km'= 0.039 (uMol/ml)
2.1.13.14.4 'minimal nutrient concentration'= 168 (uMol/g)
2.1.13.14.5 'optimal nutrient concentration'= 234 (uMol/g)

2.1.13.15 'reduction in respiration due to aerenchyma'(100%) =f{'aerenchymaFormation'} (100%) x,y pairs :{ 0 0 0.3
0.7 0.6 1 }
2.1.13.16 'relative carbon cost of exudation'(g/cm/day) =f{'time since creation'} (day) x,y pairs :{ 0 1.915e-05 1.8
1.511e-05 3.1 1.699e-05 4.4 1.362e-05 100 1.362e-05 }
2.1.13.17 'relative respiration'(g/g/day) =f{'time since creation'} (day) x,y pairs :{ 0 0.09 2 0.04 6 0.04 1000 0.04 }
2.1.13.18 'root class ID'= 100 (noUnit)
2.1.13.19 'root hair density'(#/cm2) =f{'time since creation'} (day) x,y pairs :{ 0 2000 10 2000 30 2000 100 2000 }
2.1.13.20 'root hair diameter'= 0.0005 (cm)
2.1.13.21 'root hair length'(cm) =f{'time since creation'} (day) x,y pairs :{ 0 0 1 0 2 0.03 100 0.03 }
2.1.13.22 'secondary growth rate'(cm/day) =f{'root segment age'} (day) x,y pairs :{ 0 0 4 0.0005 5 0.001 7 0.0015 11
0.002 13 0.0023 18 0.0026 24 0.00285 29 0.003 100 0.003 }
2.1.13.23 'secondary growth scaling factor'(100%) =f{'distance to base of the root'} (cm) x,y pairs :{ 0 4 0.5 4 1 4 20
4 40 2 100 2 }
2.1.13.24 'soil impedence'= 0.01 (noUnit)
2.1.13.25 'soil impedence.v2'(cm) =f{'uniform distribution'} minimum=-0.05 maximum=0.05
2.1.13.26 'top boundary'= 1 (noUnit)

2.1.14 'resources'
2.1.14.1 'cto dry weight ratio'= 0.45 (100%)
2.1.14.2 'carbon allocation2 leafs factor'(100%) =f{'time since creation'} (day) x,y pairs :{ 0 0.7 10 0.65 30 0.65 40
0.65 60 0.4 }
2.1.14.3 'carbon allocation2 roots factor'(100%) =f{'time since creation'} (day) x,y pairs :{ 0 1 1 0.5 5 0.2 1000 0.2 }
2.1.14.4 'carbon cost of biologcial nitrogen fixation'= 3.95e-05 (g/uMol)
2.1.14.5 'carbon cost of nitrate uptake'= 1.392e-05 (g/uMol)
2.1.14.6 'max carbon allocation2 secondary growth'= 0.7 (100%)
2.1.14.7 'max carbon allocation2 shoot'= 0.85 (100%)
2.1.14.8 'nitrate'
2.1.14.8.1 'initial nutrient uptake'= 714 (uMol)
2.1.14.9 'phosphorus'
2.1.14.9.1 'initial nutrient uptake'= 39 (uMol)
2.1.14.10 'potassium'

2.1.14.10.1 'initial nutrient uptake'= 45 (uMol)
2.1.14.11 'relative reliance on b n f'= 30 (100%)
2.1.14.12 'reserve allocation rate'(100%/day) =f{'time since creation'} (day) x,y pairs :{ 0 0.4 2 0.4 3 0.4 4 0.4 1000 0.4 }
2.1.14.13 'seed size'= 0.2 (g)

2.1.15 'shoot'
2.1.15.1 'aerenchyma photosynthesis mitigation'= 0.5 (100%)
2.1.15.2 'area per plant'= 660 (cm2)
2.1.15.3 'extinction coefficient'= 0.9 (noUnit)
2.1.15.4 'leaf area expantion rate'(cm2/day) =f{'time'} (day) x,y pairs :{ 0 0 2 0 3 3 4 5 6 5 7.04 3.91 7.29 4.21 7.55
4.52 7.8 4.85 8.05 5.19 8.3 5.54 8.56 5.92 8.81 6.31 9.06 6.72 9.31 7.14 9.57 7.59 9.82 8.06 10.07 8.55 10.32 9.06 10.58
9.59 10.83 10.15 11.08 10.74 11.33 11.35 11.59 11.99 11.84 12.66 12.09 13.36 12.34 14.09 12.6 14.85 12.85 15.65 13.1
16.49 13.35 17.37 13.61 18.28 13.86 19.24 14.11 20.24 14.36 21.29 14.62 22.39 14.87 23.53 15.12 24.73 15.37 25.98
15.63 27.3 15.88 28.67 16.13 30.1 16.38 31.6 16.64 33.17 16.89 34.81 17.14 36.53 17.39 38.32 17.65 40.2 17.9 42.16
18.15 44.21 18.4 46.36 18.66 48.61 18.91 50.96 19.16 53.41 19.41 55.98 19.67 58.67 19.92 61.48 20.17 64.42 20.42
67.49 20.68 70.71 20.93 74.07 21.18 77.59 21.43 81.27 21.69 85.12 21.94 89.14 22.19 93.35 22.44 97.75 22.7 102.35
22.95 107.17 23.2 112.2 23.45 117.47 23.71 122.98 23.96 128.74 24.21 134.76 24.46 141.06 24.72 147.65 24.97 154.55
25.29 156.06 25.66 154.09 26.02 152.11 26.38 150.11 26.74 148.1 27.1 146.08 27.46 144.05 27.83 142.02 28.19 139.98
28.55 137.94 28.91 135.9 29.27 133.85 29.63 131.81 29.99 129.77 30.36 127.73 30.72 125.7 31.08 123.67 31.44 121.65
31.8 119.64 32.16 117.64 32.52 115.65 32.89 113.67 33.25 111.71 33.61 109.75 33.97 107.81 34.33 105.89 34.69
103.98 35.06 102.09 35.42 100.21 35.78 98.36 36.14 96.52 36.5 94.7 36.86 92.9 37.22 91.12 37.59 89.36 37.95 87.62
38.31 85.9 38.67 84.2 39.03 82.53 39.39 80.87 39.76 79.24 40.12 77.63 40.48 76.05 40.84 74.49 41.2 72.95 41.56 71.43
41.92 69.94 42.29 68.47 42.65 67.02 43.01 65.59 43.37 64.19 43.73 62.82 44.09 61.46 44.45 60.13 44.82 58.82 45.18
57.53 45.54 56.27 45.9 55.03 46.26 53.81 46.62 52.61 46.99 51.44 47.35 50.29 47.71 49.16 48.07 48.05 48.43 46.96
48.79 45.89 49.15 44.84 49.52 43.82 49.88 42.81 50.24 41.83 50.6 40.86 50.96 39.91 51.32 38.99 51.69 38.08 52.05
37.19 52.41 36.32 52.77 35.47 53.13 34.63 53.49 33.82 53.85 33.02 54.22 32.23 54.58 31.47 54.94 30.72 55.3 29.99

55.66 29.27 56.02 28.57 56.38 27.88 56.75 27.21 57.11 26.56 57.47 25.92 57.83 25.29 58.19 24.68 58.55 24.08 58.92
23.49 59.28 22.92 59.64 22.36 }
2.1.15.5 'light use efficiency'= 3.8e-07 (g/uMol)
2.1.15.6 'nitrate'
2.1.15.6.1 'leaf minimal nutrient concentration'= 1300 (uMol/g)
2.1.15.6.2 'leaf optimal nutrient concentration'= 2600 (uMol/g)
2.1.15.6.3 'stem minimal nutrient concentration'= 700 (uMol/g)
2.1.15.6.4 'stem optimal nutrient concentration'= 1300 (uMol/g)
2.1.15.7 'phosphorus'
2.1.15.7.1 'leaf minimal nutrient concentration'= 50 (uMol/g)
2.1.15.7.2 'leaf optimal nutrient concentration'= 100 (uMol/g)
2.1.15.7.3 'stem minimal nutrient concentration'= 25 (uMol/g)
2.1.15.7.4 'stem optimal nutrient concentration'= 50 (uMol/g)
2.1.15.8 'potassium'
2.1.15.8.1 'leaf minimal nutrient concentration'= 273 (uMol/g)
2.1.15.8.2 'leaf optimal nutrient concentration'= 430 (uMol/g)
2.1.15.8.3 'stem minimal nutrient concentration'= 273 (uMol/g)
2.1.15.8.4 'stem optimal nutrient concentration'= 215 (uMol/g)
2.1.15.9 'relative potential transpiration'= 100 (cm3/g)
2.1.15.10 'relative respiration rate leafs'= 0.04 (g/g/day)
2.1.15.11 'relative respiration rate stems'= 0.02 (g/g/day)
2.1.15.12 'specific leaf area'(g/cm2) =f{'time'} (day) x,y pairs :{ 0 0.0015 24 0.0025 40 0.003 60 0.003 }

2.1.16 'stress impact factors'
2.1.16.1 'impact on:leaf area expantion rate'
2.1.16.1.1 'impact by:nitrate'(noUnit) =f{'nitrate stress factor'} (noUnit) x,y pairs :{ 0 0 0.3 0.1 1 1 }
2.1.16.1.2 'impact by:phosphorus'(noUnit) =f{'phosphorus stress factor'} (noUnit) x,y pairs :{ 0 0 1 1 }
2.1.16.1.3 'impact by:potassium'(noUnit) =f{'potassium stress factor'} (noUnit) x,y pairs :{ 0 1 1 1 }
2.1.16.2 'impact on:photosynthesis'
2.1.16.2.1 'impact by:nitrate'(noUnit) =f{'nitrate stress factor'} (noUnit) x,y pairs :{ 0 0 0.4 0.5 1 1 }
2.1.16.2.1 'impact by:phosphorus'(noUnit) =f{'phosphorus stress factor'} (noUnit) x,y pairs :{ 0 0.5 1 1 }
2.1.16.2.3 'impact by:potassium'(noUnit) =f{'potassium stress factor'} (noUnit) x,y pairs :{ 0 0 1 1 }
2.1.16.3 'impact on:root segment carbon cost of exudates'
2.1.16.3.1 'impact by:nitrate'(noUnit) =f{'nitrate stress factor'} (noUnit) x,y pairs :{ 0 1 1 1 }
2.1.16.3.2 'impact by:phosphorus'(noUnit) =f{'phosphorus stress factor'} (noUnit) x,y pairs :{ 0 1 1 1 }

2.1.16.3.3 'impact by:potassium'(noUnit) =f{'potassium stress factor'} (noUnit) x,y pairs :{ 0 1 1 1 }
2.1.16.4 'impact on:root segment respiration'
2.1.16.4.1 'impact by:nitrate'(noUnit) =f{'nitrate stress factor'} (noUnit) x,y pairs :{ 0 1 1 1 }
2.1.16.4.2 'impact by:phosphorus'(noUnit) =f{'phosphorus stress factor'} (noUnit) x,y pairs :{ 0 1 1 1 }
2.1.16.4.3 'impact by:potassium'(noUnit) =f{'potassium stress factor'} (noUnit) x,y pairs :{ 0 1 1 1 }
2.1.16.5 'impact on:root segment secondary growth'
2.1.16.5.1 'impact by:nitrate'(noUnit) =f{'nitrate stress factor'} (noUnit) x,y pairs :{ 0 0 1 1 }
2.1.16.5.2 'impact by:phosphorus'(noUnit) =f{'phosphorus stress factor'} (noUnit) x,y pairs :{ 0 0 1 1 }
2.1.16.5.3 'impact by:potassium'(noUnit) =f{'potassium stress factor'} (noUnit) x,y pairs :{ 0 0 1 1 }

Appendix C

Supplementary figures for Chapter 3

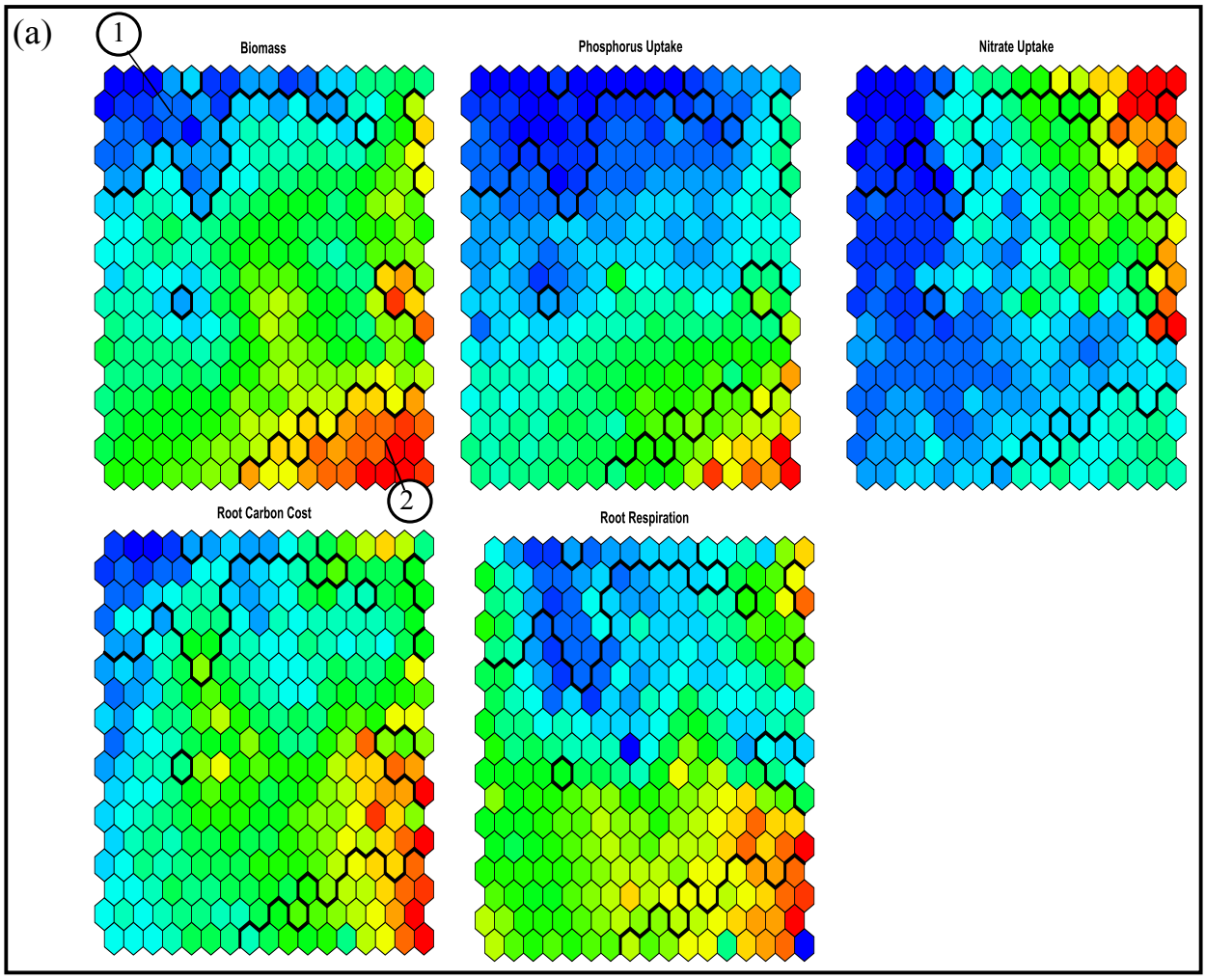

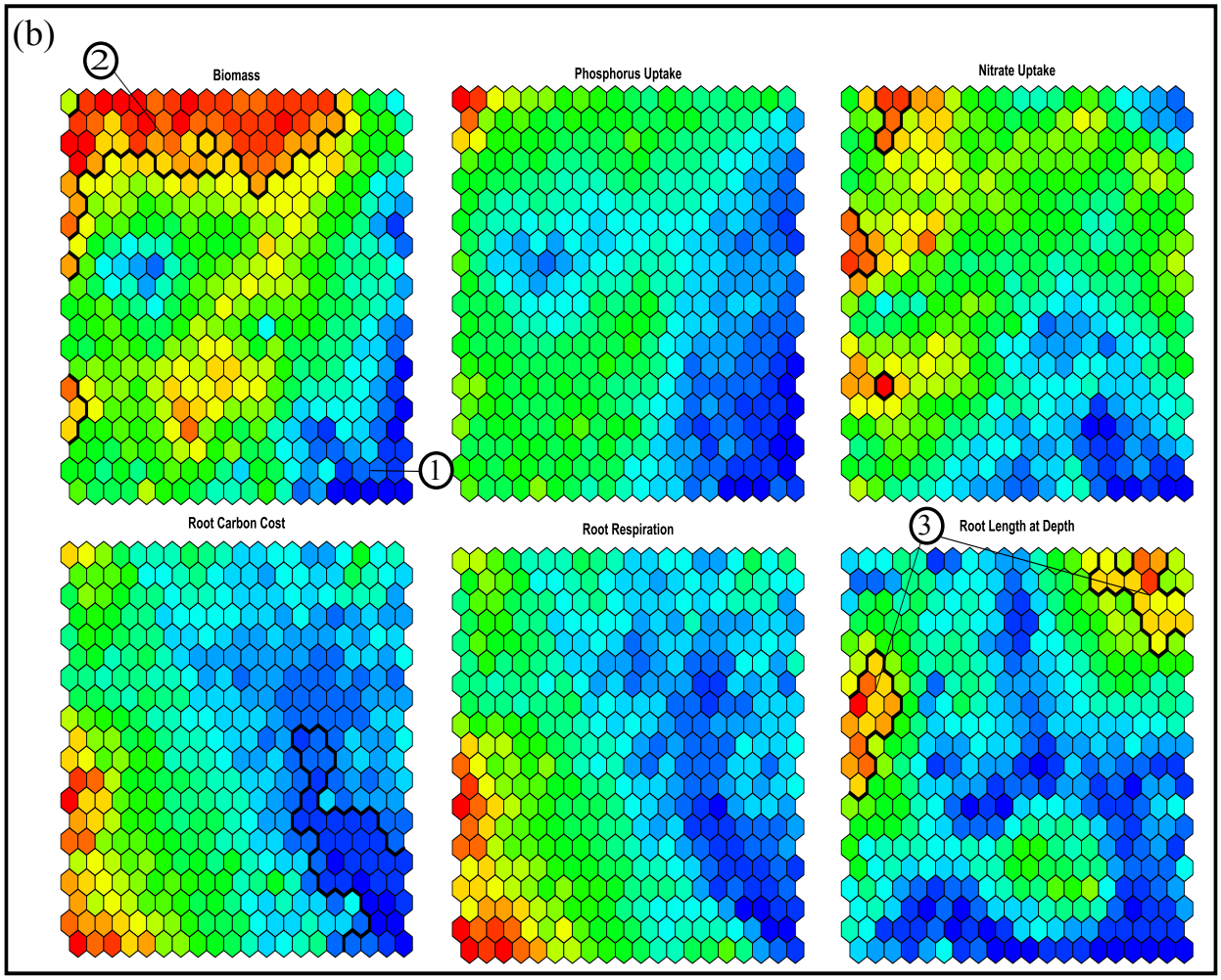

Supplementary Figure 3-S1: Distribution of each objective in bean SOM map (a). Distribution of each objective in maize SOM map (b). Region 1 corresponds to nodes with phenotypes with low carbon cost and root respiration. Region 2 corresponds to nodes with greatest biomass. Region 3 corresponds to nodes with greatest root length at depth. The mean of the objective in each node is represented. The change in color from blue to red show a change in magnitude of the value with red representing greatest values.

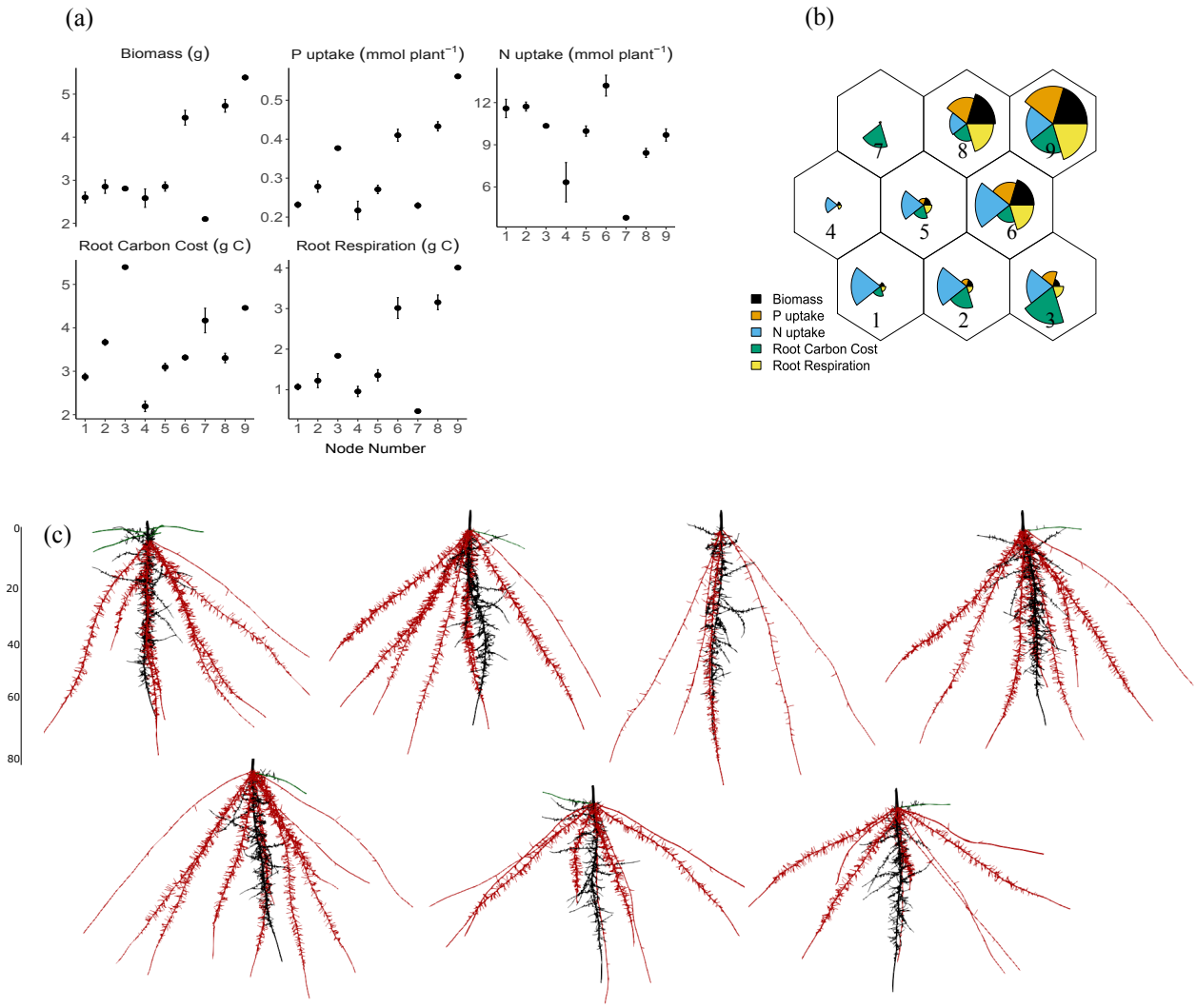

Supplementary Figure 3-S2: Mean value of objective in each node for bean optimal phenotypes in a region with sub-optimal N and P (a). The relative performance of the phenotypes in different objective in each node (b). Nodes 6, 8 and 9 have comparable biomass but vary in performance in other objectives. Some representative bean phenotypes with comparable biomass from nodes 6, 8 and 9 (c). Primary root is in black; Basal roots in red; Hypocotyl-borne roots in green.

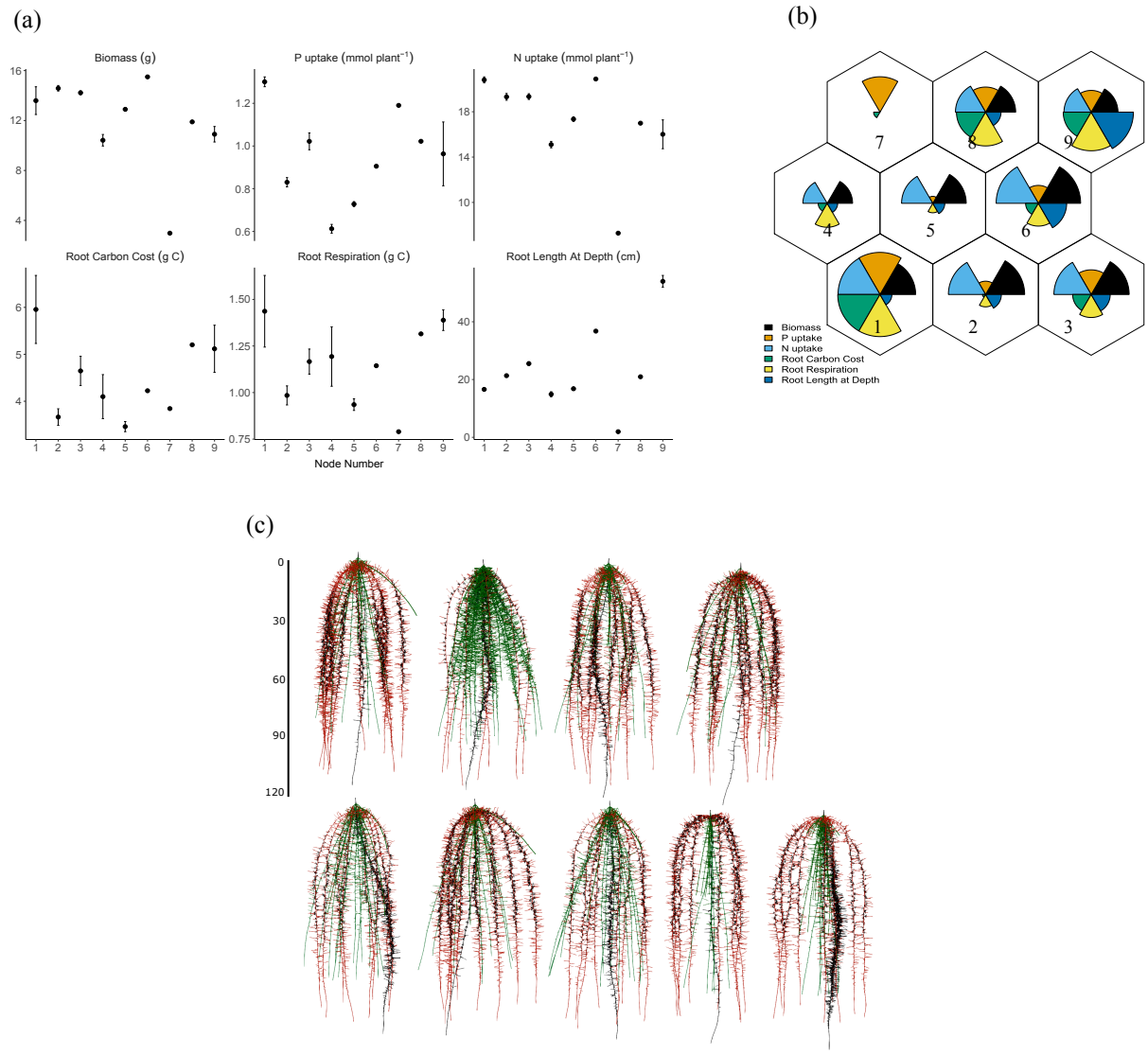

Supplementary Figure 3-S3: Mean value of objective in each node for maize optimal phenotypes in a region with sub-optimal N and P (a). The relative performance of the phenotypes in different objective in each node (b). Nodes 1, 2, 3, 5 and 6 have comparable biomass but vary in performance in other objectives. Some representative phenotypes with comparable biomass from nodes 1, 2, 3, 5 and 6 (c). Primary root is in black; Nodal roots in red; Nodal roots in green.

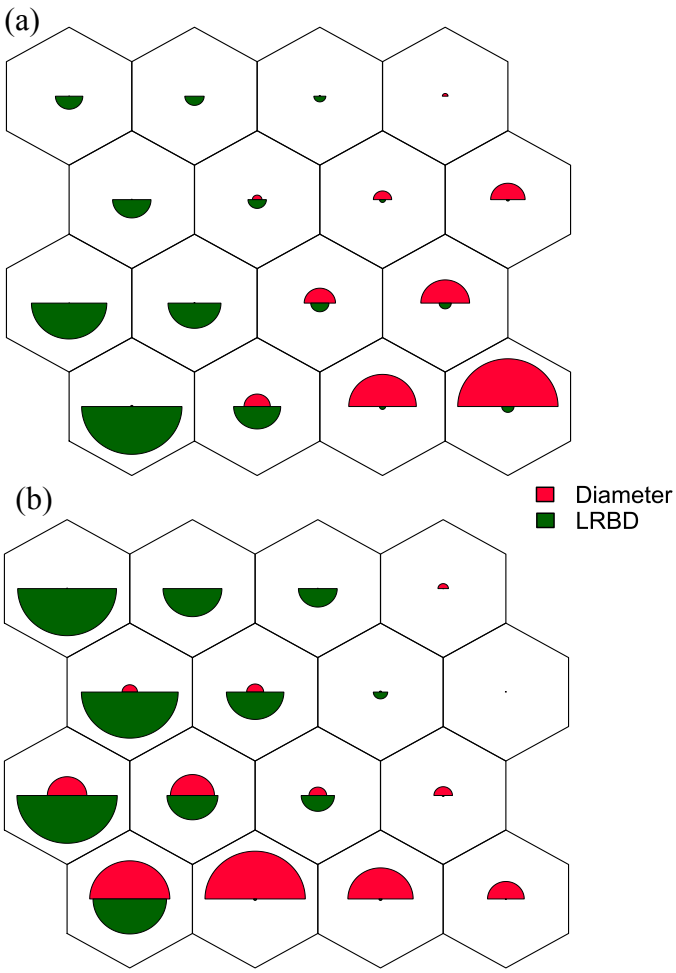

Supplementary Figure 3-S4: Different primary root phenotypes found in optimal bean phenotypes (a) and optimal maize phenotypes (b).

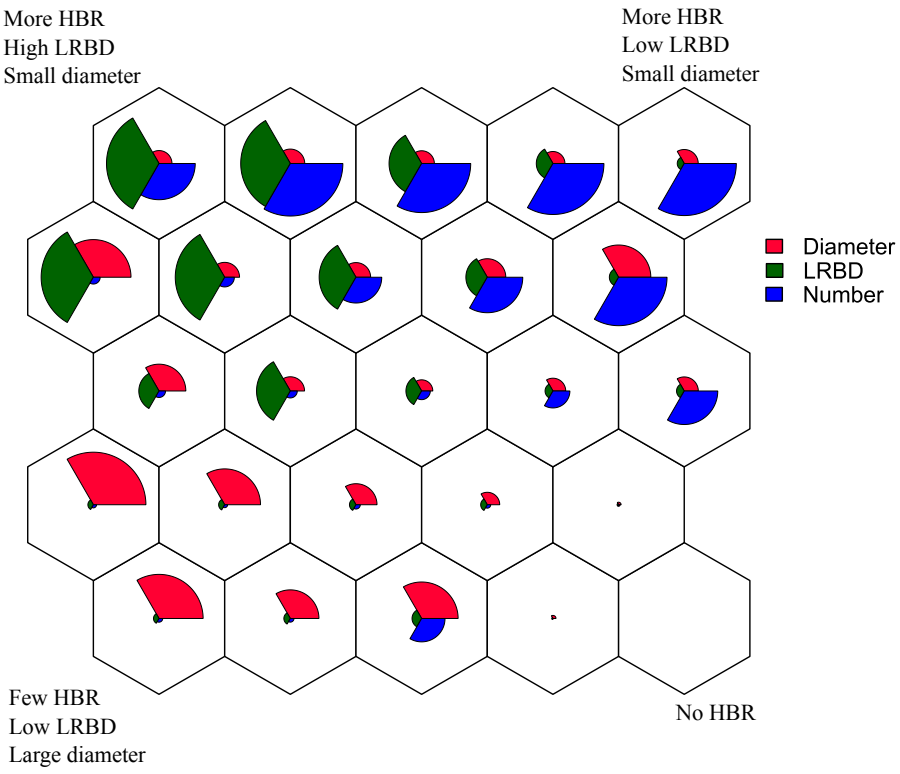

Supplementary Figure 3-S5: Different hypocotyl-borne root phenotypes found in optimal bean phenotypes.

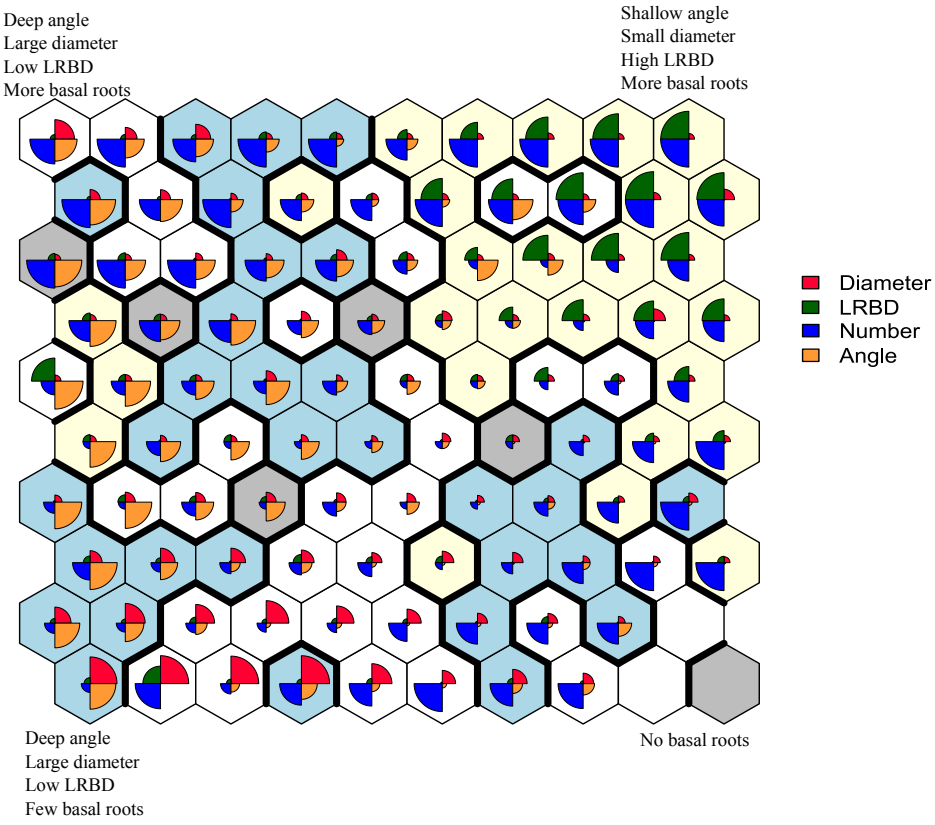

Supplementary Figure 3-S6: Different basal root phenotypes found in optimal bean phenotypes. Nodes in blue have phenotypes found in low N regions. Nodes in yellow have phenotypes found in low P regions. Nodes in grey have phenotypes found in low P as well as low N.

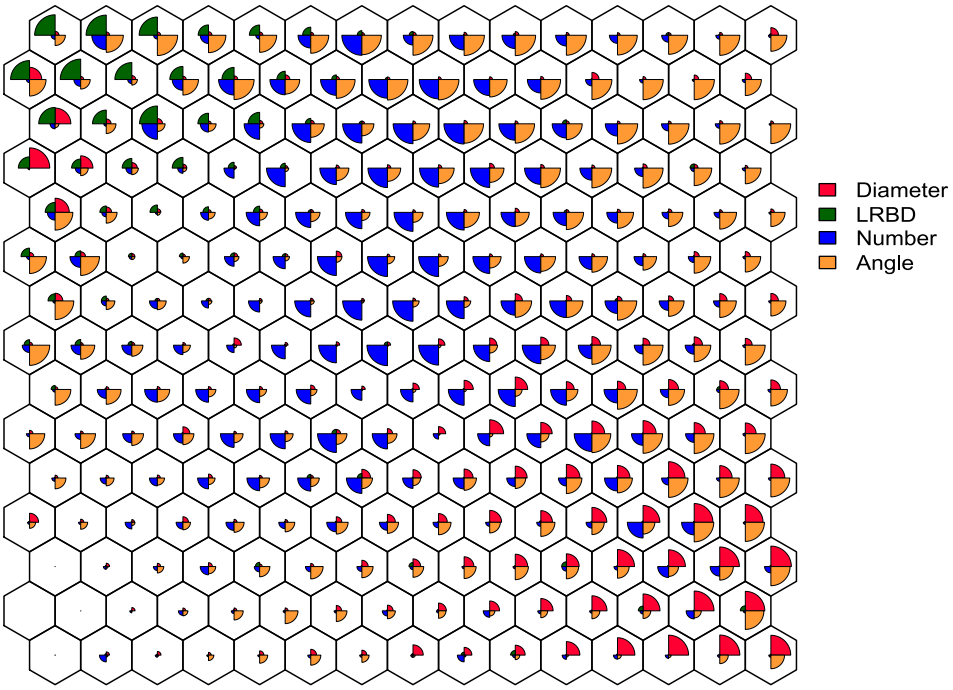

Supplementary Figure 3-S7: Different nodal root phenotypes found in optimal maize phenotypes.

Appendix D

Supplementary figures and tables for Chapter 4

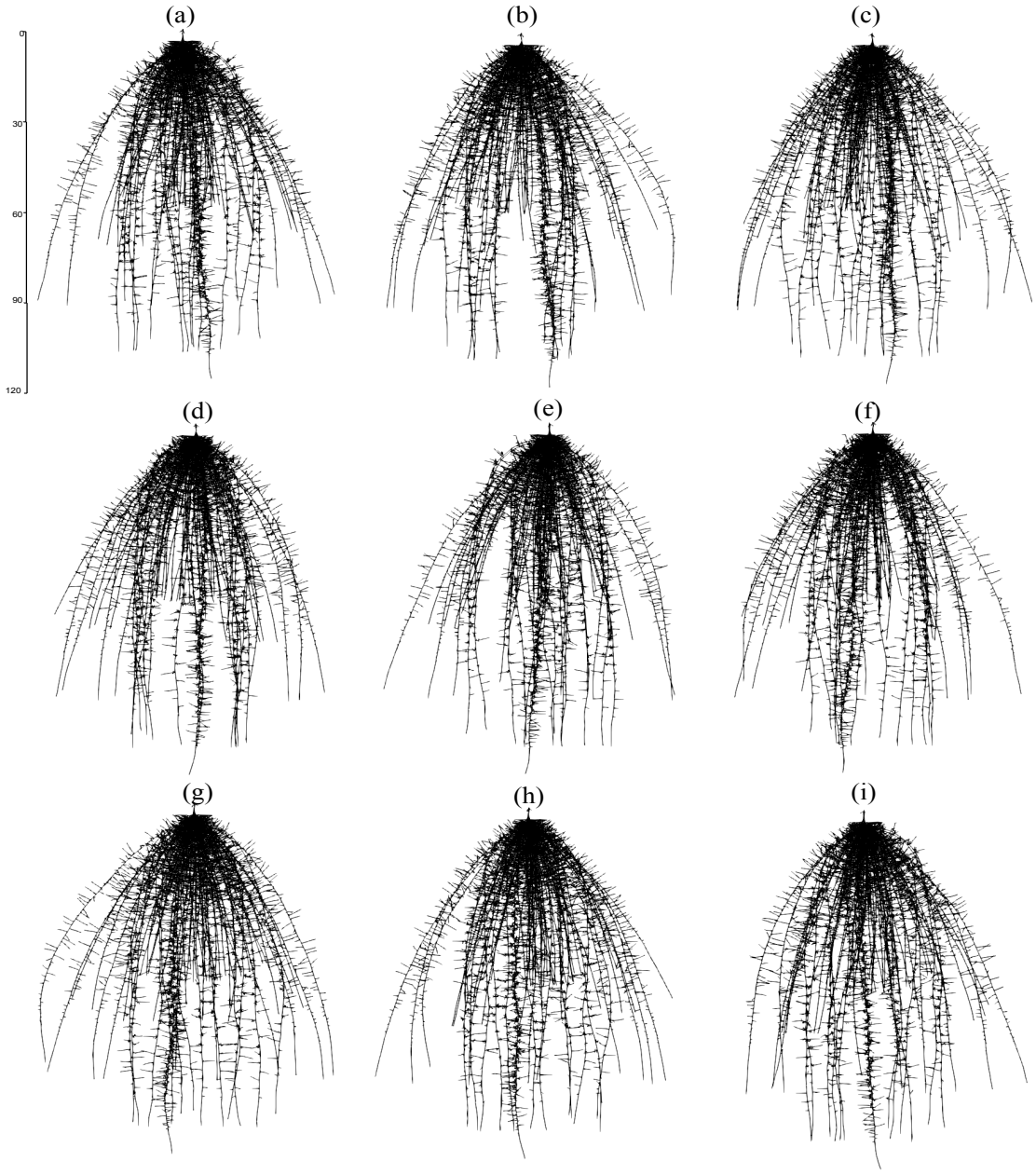

Supplementary Figure 4-S1(a)-S1(i): Representative images of 2D projections of a maize root system rotated by 20°, 60°, 100°, 140°, 180°, 220°, 260°, 300°, 340°.

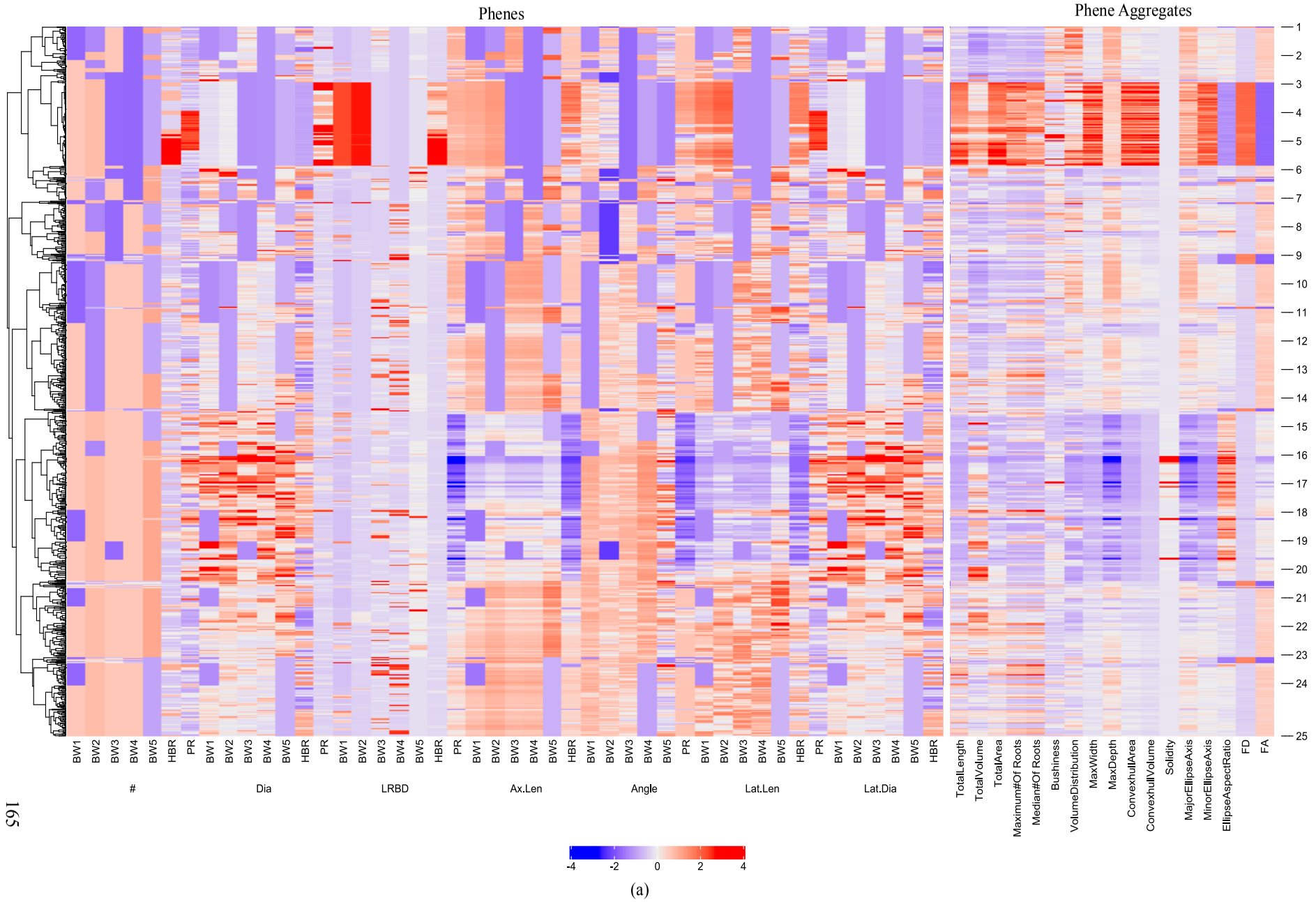
Phenes
Phene Aggregates
BW1 BW2 BW3 BW4 BW5 HBR PR
#
Dia
LRBD
Ax.Len
Angle
Lat.Len
Lat.Dia
TotalLength
TotalVolume
TotalArea
Maximum#Of Roots
Median#Of Roots
Bushiness
VolumeDistribution
MaxWidth
MaxDepth
ConvexhullArea
ConvexhullVolume
Solidity
MajorEllipseAxis
MinorEllipseAxis
EllipseAspectRatio
FD
FA
1 2 3 4 5 6 7 8 9 10 11 12 13 14 15 16 17 18 19 20 21 22 23 24 25
-4 -2 0 2 4

(a)

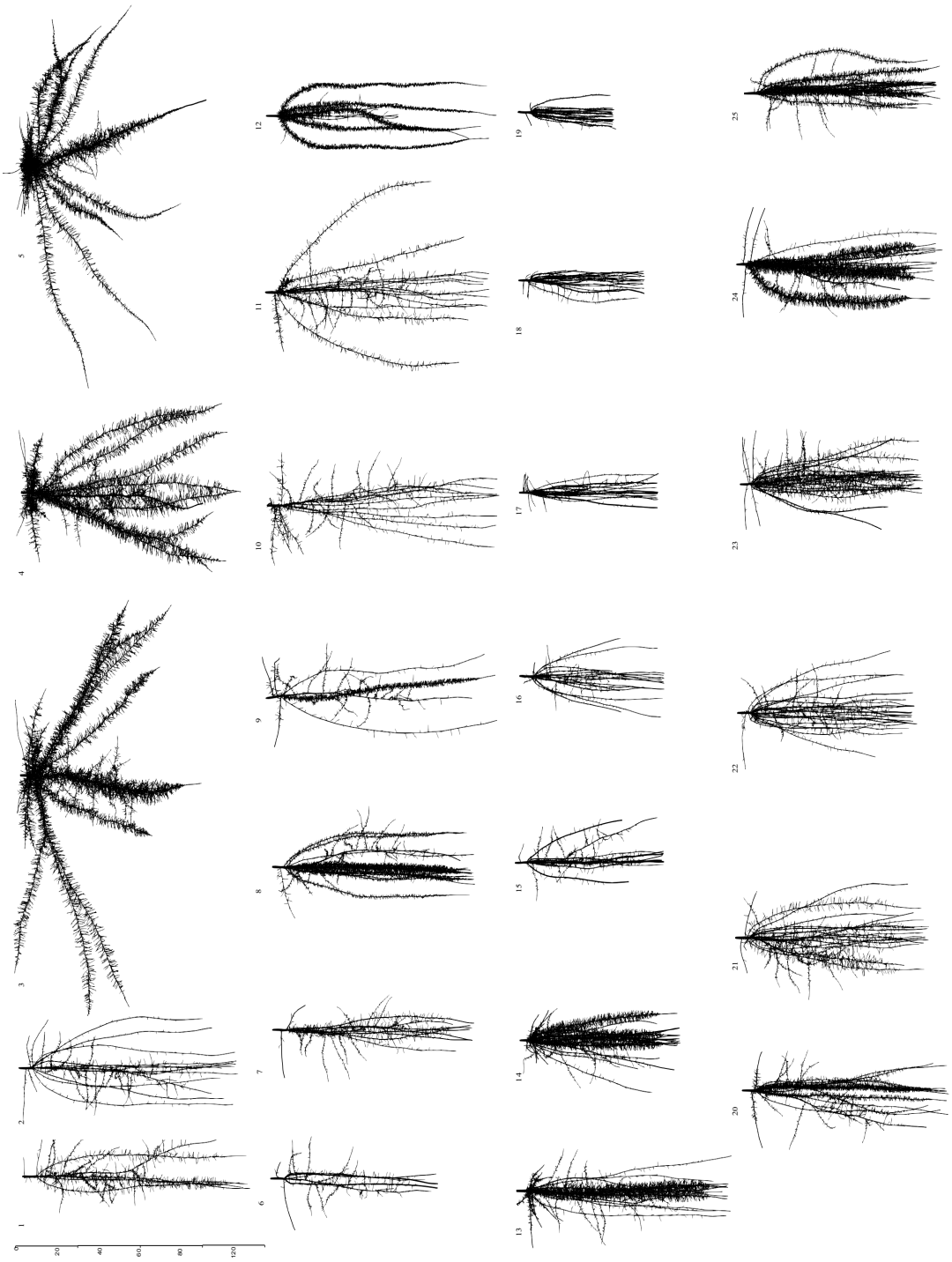
1
2
3
4
5
6
7
8
9
10
11
12
13
14
15
16
17
18
19
20
21
22
23
24
25
0
20
40
60
80
120

Supplementary Figure 4-S2: Cluster heatmap of phenotypic traits. Hierarchical clustering of all bean phenotypes was generated using Spearman correlation coefficient of max-min scaled phene values at 40 days (a). The color scale indicates the magnitude of the trait values (blue, low value; red, high value). The numbers indicated on the heatmap refer to a representative phenotype in the specific region of the heatmap. The corresponding phenotypes are visualized in (b). # - Number of roots; Axial.Diam - axial root diameter; LRBD - lateral root branching density; Axial.Length - axial root length; Lat.Length- lateral root length; Lat.Diam - lateral root diameter; BW1 - basal roots at whorl 1; BW2 - basal roots at whorl 2; BW3 - basal roots at whorl 3; BW4 - basal roots at whorl 4; BW5 - basal roots at whorl 5; HBR - hypocotyl-borne roots; PR - primary root.

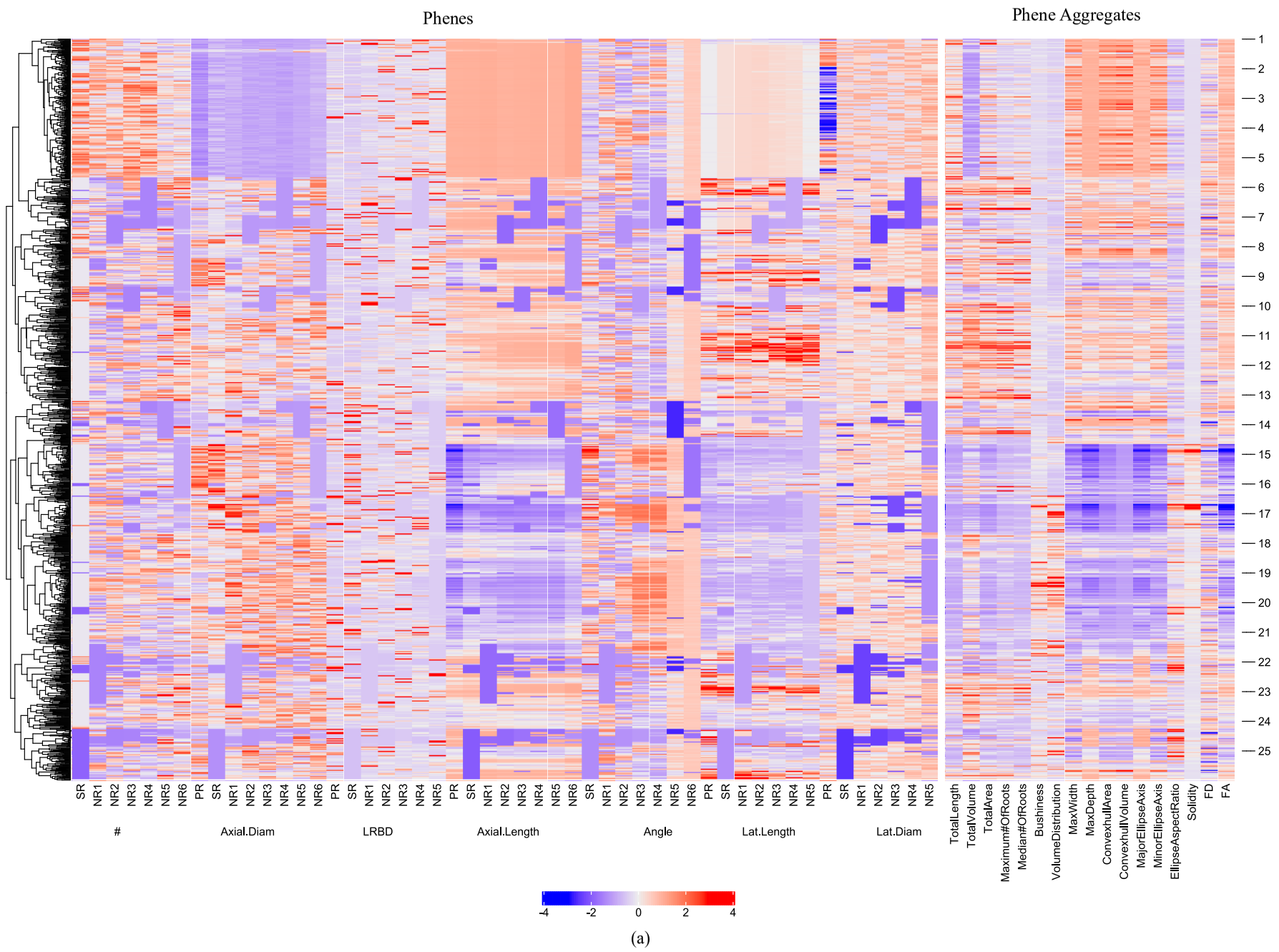
Phenes
Phene Aggregates
SR NR1 NR2 NR3 NR4 NR5 NR6 PR
#
Axial.Diam
LRBD
Axial.Length
Angle
Lat.Length
Lat.Diam
TotalLength
TotalVolume
TotalArea
Maximum#OfRoots
Median#OfRoots
Bushiness
VolumeDistribution
MaxWidth
MaxDepth
ConvexhullArea
ConvexhullVolume
MajorEllipseAxis
MinorEllipseAxis
EllipseAspectRatio
Solidity
FD
FA
1 2 3 4 5 6 7 8 9 10 11 12 13 14 15 16 17 18 19 20 21 22 23 24 25
-4 -2 0 2 4

(a)

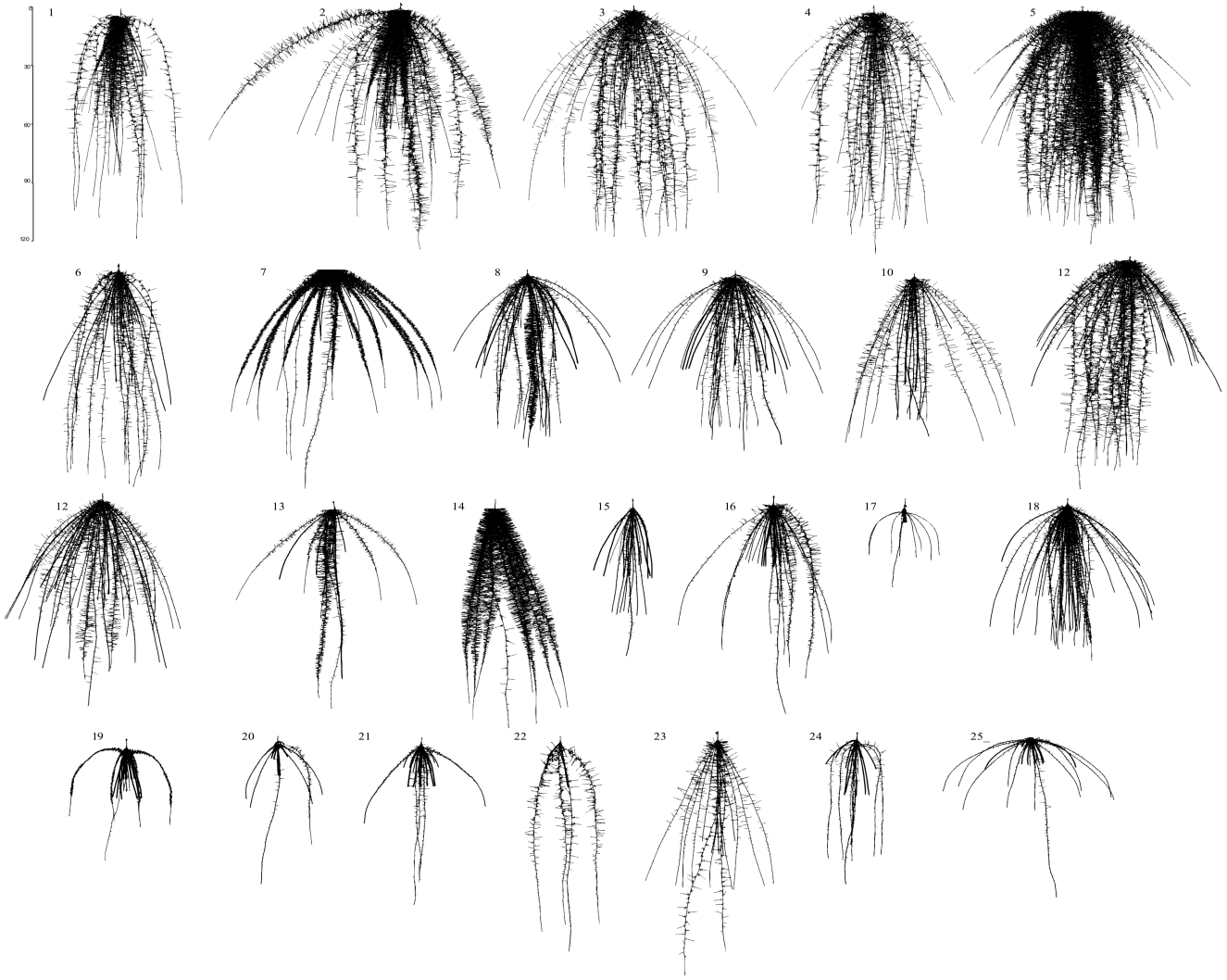
1
2
3
4
5
6
7
8
9
10
12
12
13
14
15
16
17
18
19
20
21
22
23
24
25

Supplementary Figure 4-S3: Cluster heatmap of phenotypic traits. Hierarchical clustering of all maize phenotypes was generated using Spearman correlation coefficient of max-min scaled phene values at 40 days (a). The color scale indicates the magnitude of the trait values (blue, low value; red, high value). The numbers indicated on the heatmap refer to a representative phenotype in the specific region of the heatmap. The corresponding phenotypes are visualized in (b). # - Number of roots; Axial.Diam - axial root diameter; LRBD - lateral root branching density; Axial.Length - axial root length; Lat.Length- lateral root length; Lat.Diam - lateral root diameter; NR1 - nodal roots at position 1; NR2 - nodal roots at position 2; NR3 - nodal roots at position 3; NR4 - nodal roots at position 4 ; SR - seminal roots; PR - primary root.

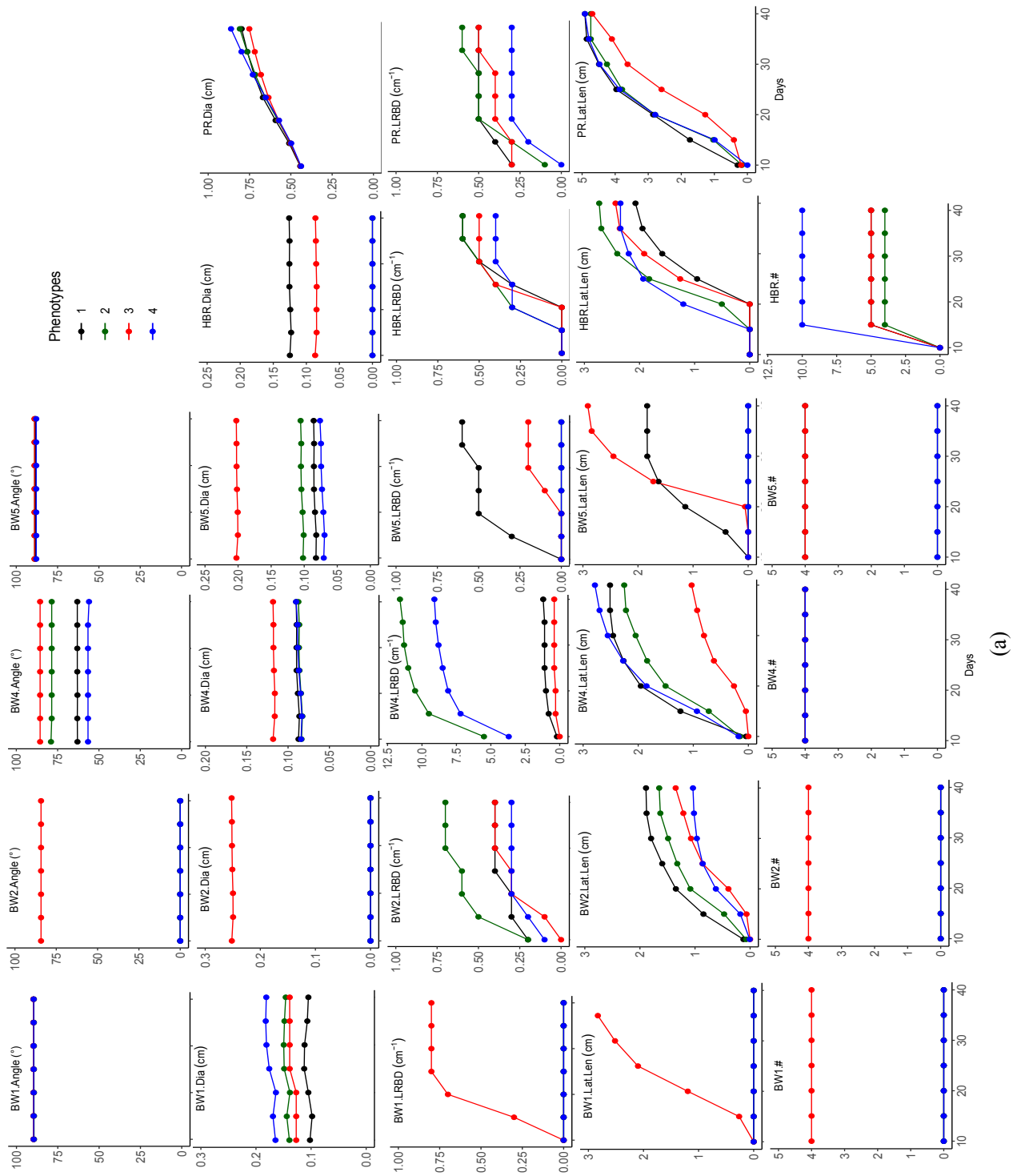
Phenotypes
1
2
3
4
BW1.Angle (°)
BW1.Dia (cm)
BW1.LRBD (cm⁻¹)
BW1.Lat.Len (cm)
BW1.#
BW2.Angle (°)
BW2.Dia (cm)
BW2.LRBD (cm⁻¹)
BW2.Lat.Len (cm)
BW2.#
BW4.Angle (°)
BW4.Dia (cm)
BW4.LRBD (cm⁻¹)
BW4.Lat.Len (cm)
BW4.#
BW5.Angle (°)
BW5.Dia (cm)
BW5.LRBD (cm⁻¹)
BW5.Lat.Len (cm)
BW5.#
HBR.Dia (cm)
HBR.LRBD (cm⁻¹)
HBR.Lat.Len (cm)
HBR.#
PR.Dia (cm)
PR.LRBD (cm⁻¹)
PR.Lat.Len (cm)
Days

(a)

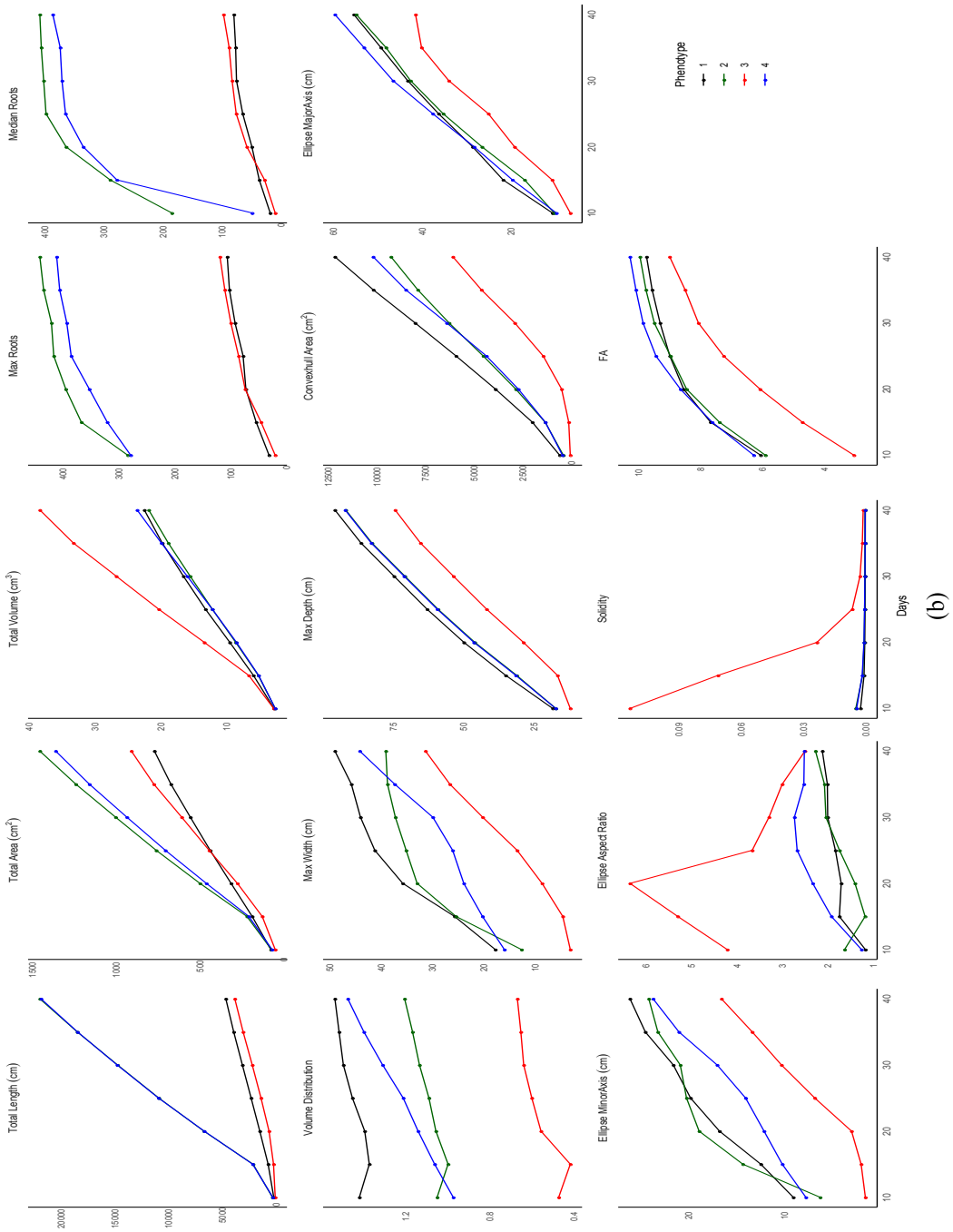
Median Roots
Max Roots
Ellipse MajorAxis (cm)
Convexhull Area (cm²)
FA
Total Volume (cm³)
Max Depth (cm)
Solidity
Total Area (cm²)
Max Width (cm)
Ellipse Aspect Ratio
Total Length (cm)
Volume Distribution
Ellipse MinorAxis (cm)
Days
Phenotype
1
2
3
4

(b)

Supplementary Figure 4-S4: Trait dynamics of bean root phenotypes over 30 days of growth from day 10 to day 40. Change in estimates of phenes (a). Change in estimates of the phene aggregates (b). BW1 - basal roots at whorl 1; BW2 - basal roots at whorl BW4 - basal roots at whorl 4; BW5 - basal roots at whorl 5; HBR - hypocotyl-borne roots; PR - primary root; Dia - axial root diameter; LRBD - lateral root branching density; Lat.Len - lateral root length; # - number of axial roots; FA - fractal abundance.

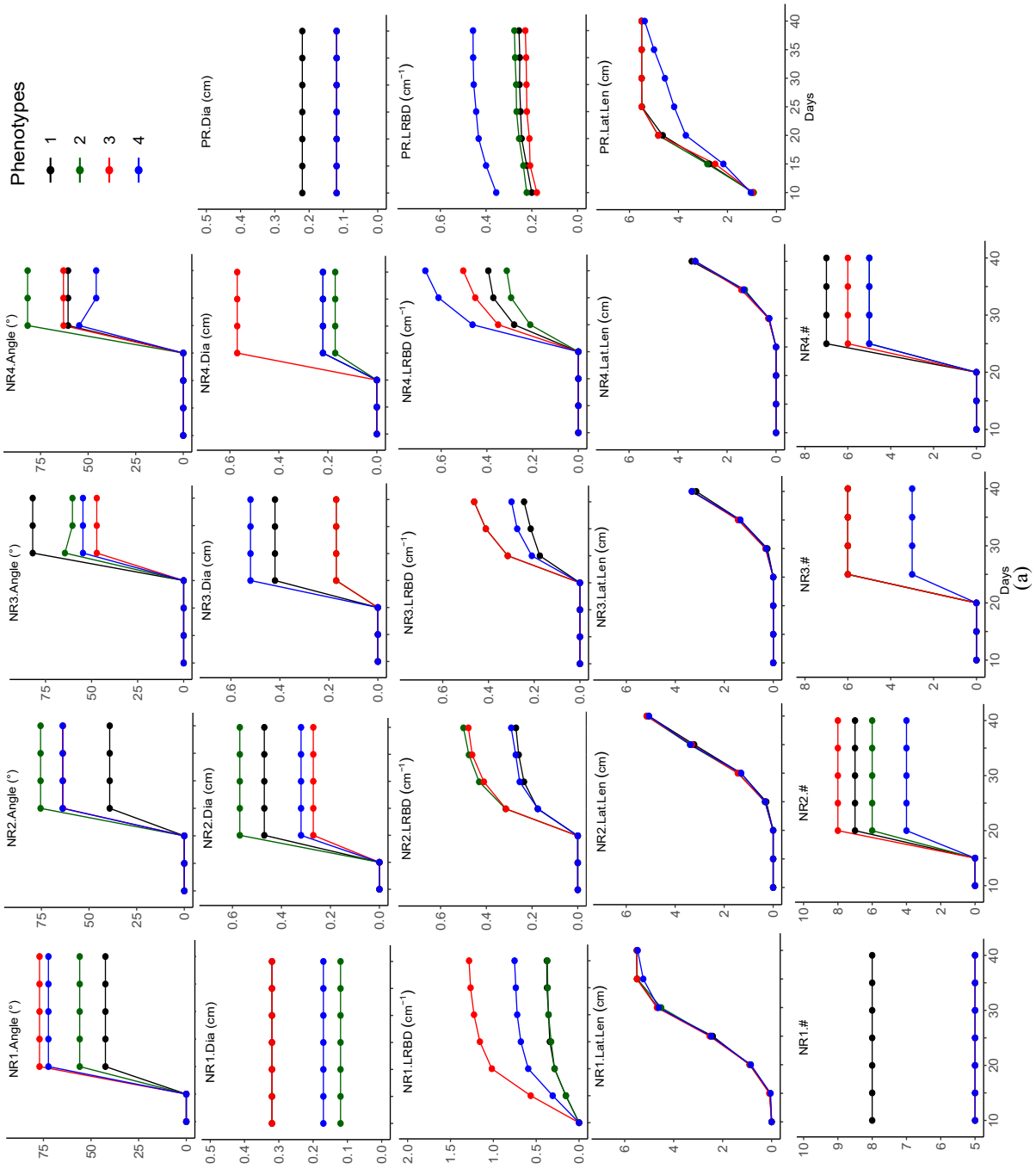
Phenotypes
1
2
3
4
NR1.Angle (°)
NR2.Angle (°)
NR3.Angle (°)
NR4.Angle (°)
NR1.Dia (cm)
NR2.Dia (cm)
NR3.Dia (cm)
NR4.Dia (cm)
NR1.LRBD (cm⁻¹)
NR2.LRBD (cm⁻¹)
NR3.LRBD (cm⁻¹)
NR4.LRBD (cm⁻¹)
NR1.Lat.Len (cm)
NR2.Lat.Len (cm)
NR3.Lat.Len (cm)
NR4.Lat.Len (cm)
NR1.#
NR2.#
NR3.#
NR4.#
PR.Dia (cm)
PR.LRBD (cm⁻¹)
PR.Lat.Len (cm)
Days
(a)

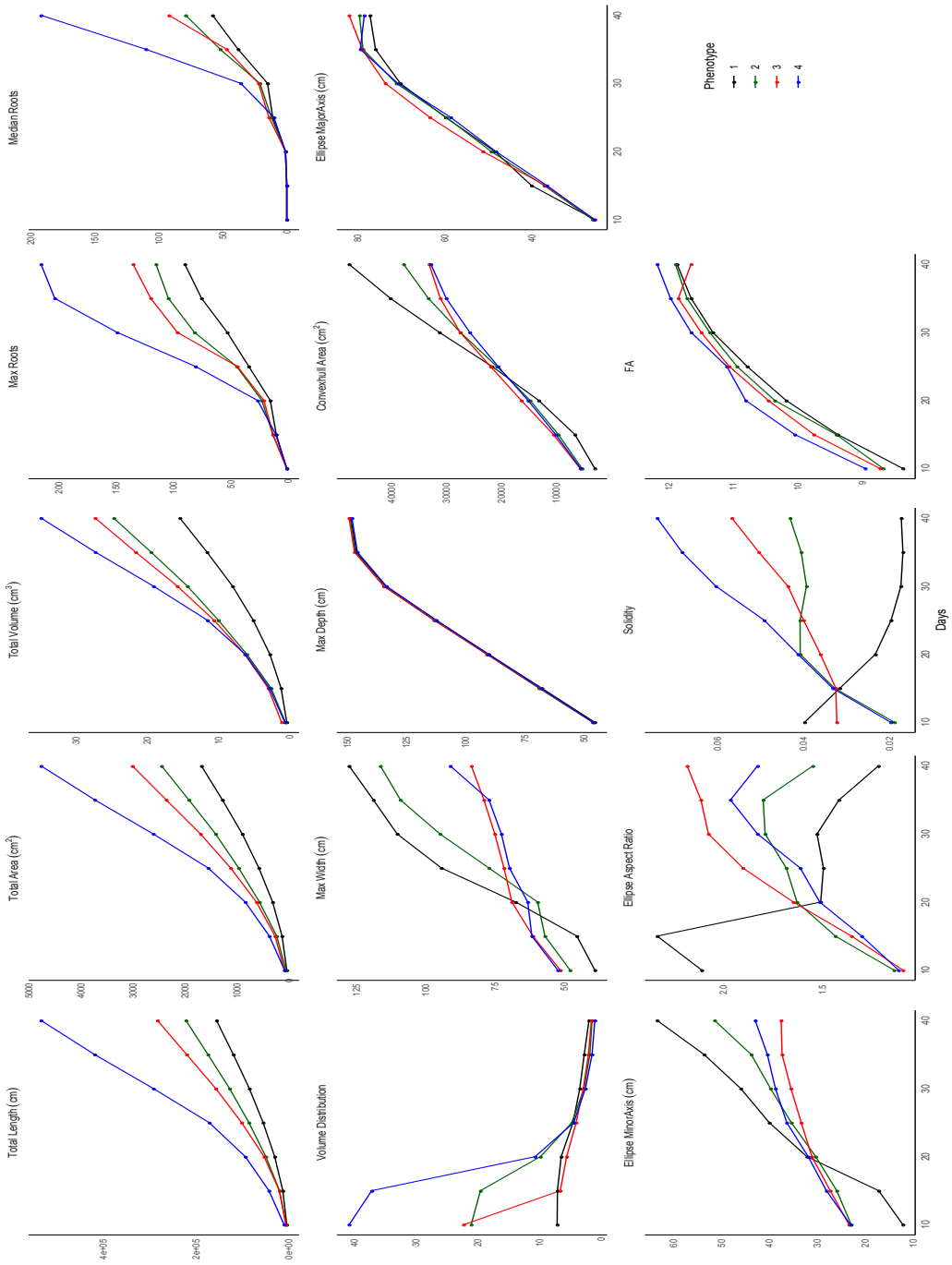
Median Roots
Ellipse MajorAxis (cm)
Phenotype
1
2
3
4
Max Roots
Convexhull Area (cm²)
FA
Total Volume (cm³)
Max Depth (cm)
Solidity
Days
Total Area (cm²)
Max Width (cm)
Ellipse Aspect Ratio
Total Length (cm)
Volume Distribution
Ellipse MinorAxis (cm)

(b)

Supplementary Figure 4-S5: Trait dynamics of maize root phenotypes over 30 days of growth from day 10 to day 40. Change in estimates of phenes (a). Change in estimates of the phene aggregates (b). NR1 - nodal roots at position 1; NR2 - nodal roots at position 2; NR3 - nodal roots at position 3; NR4 - nodal roots at position 4; PR - primary root; Dia - axial root diameter; LRBD - lateral root branching density; Lat.Len - lateral root length; # - number of axial roots; FA - fractal abundance.

Supplementary Table 4-S1: Range of input values for generating bean root phenotypes. PR – primary root; HBR- Hypocotyl-Borne-Root; BW – Basal Whorl; BW1, BW2, BW3, BW4, BW5 refer to the position of the basal whorl counted from basipetal to acropetal position; Dia – axial root diameter; Lat.Dia – lateral root diameter; LRBD – lateral root branching density.

	Units	Min	Max	References
Number.BW1	NA	0	4	Miguel et al., 2013
Number.BW2	NA	0	4	
Number.BW3	NA	0	4	
Number.BW4	NA	0	4	
Number.BW5	NA	0	4	
Number.HBR	NA	0	30	Miller et al., 2003
PR.Dia	cm	0.08	0.45	Henry et al., 2009
BW1.Dia	cm	0	0.45	
BW2.Dia	cm	0	0.45	
BW3.Dia	cm	0	0.45	
BW4.Dia	cm	0	0.45	
BW5.Dia	cm	0	0.45	
HBR.Dia	cm	0	0.45	
BW1.Lat.Dia	cm	0	0.03	
BW2.Lat.Dia	cm	0	0.03	
BW3.Lat.Dia	cm	0	0.03	
BW4.Lat.Dia	cm	0	0.03	
BW5.Lat.Dia	cm	0	0.03	
HBR.Lat.Dia	cm	0	0.03	
PR.Lat.Dia	cm	0	0.03	
BW1.LRBD	cm^{-1}	0	40	Miller et al., 2003
BW2.LRBD	cm^{-1}	0	40	
BW3.LRBD	cm^{-1}	0	40	
BW4.LRBD	cm^{-1}	0	40	
BW5.LRBD	cm^{-1}	0	40	
PR.LRBD	cm^{-1}	0	40	
HBR.LRBD	cm^{-1}	0	40	
BW1.Angle	degree	0	90	Miguel et al., 2013
BW2.Angle	degree	0	90	
BW3.Angle	degree	0	90	
BW4.Angle	degree	0	90	
BW5.Angle	degree	0	90	

Supplementary Table 4-S2: Range of input values for generating maize root phenotypes. PR - Primary Root; SR -Seminal Root; NR-Nodal Root; NR1, NR2, NR3, NR4 refer to the nodal root position; Dia – axial root diameter; Lat.Dia – lateral root diameter; LRBD – lateral root branching density. *NR at different positions were considered to have similar parameters.

	Units	Min	Max	References
Number.SR	NA	0	12	Hochholdinger and Tuberosa, 2009
Number.NR1	NA	0	12	Burton et al., 2013; York and Lynch, 2015
Number.NR2	NA	0	12	
Number.NR3	NA	0	12	
Number.NR4	NA	0	12	
PR.Dia	cm	0.08	0.6	Burton et al., 2013; Burton et al., 2014; York and Lynch, 2015
SR.Dia	cm	0	0.6	
NR1.Dia	cm	0	0.6	
NR2.Dia	cm	0	0.6	
NR3.Dia	cm	0	0.6	
NR4.Dia	cm	0	0.6	
PR.Lat.Dia	cm	0	0.05	
SR.Lat.Dia	cm	0	0.05	
NR1.Lat.Dia	cm	0	0.05	
NR2.Lat.Dia	cm	0	0.05	
NR3.Lat.Dia	cm	0	0.05	
NR4.Lat.Dia	cm	0	0.05	
PR.LRBD	cm^{-1}	0	40	Postma et al., 2014; York and Lynch, 2015
SR.LRBD	cm^{-1}	0	40	
NR1.LRBD	cm^{-1}	0	40	
NR2.LRBD	cm^{-1}	0	40	
NR3.LRBD	cm^{-1}	0	40	
NR4.LRBD	cm^{-1}	0	40	
SR.Angle	degree	0	90	Liao et al., 2004; Zhu et al., 2005
NR1.Angle	degree	0	90	
NR2.Angle	degree	0	90	
NR3.Angle	degree	0	90	
NR4.Angle	degree	0	90	

REFERENCES

Burton AL, Brown KM, Lynch JP (2013) Phenotypic Diversity of Root Anatomical and Architectural Traits in Species. *Crop Science* 53: 1042-1055

Burton AL, Johnson JM, Foerster JM, Hirsch CN, Buell CR, Hanlon MT, Kaeppler SM, Brown KM, Lynch JP (2014) QTL mapping and phenotypic variation for root architectural traits in maize (Zea mays L.). *Theoretical and Applied Genetics* 127: 2293-2311

Henry A, Kleinman PJA, Lynch JP (2009) Phosphorus runoff from a phosphorus deficient soil under common bean (Phaseolus vulgaris L.) and soybean (Glycine max L.) genotypes with contrasting root architecture. *Plant and Soil* 317: 1–16

Hochholdinger F, Tuberosa R (2009) Genetic and genomic dissection of maize root development and architecture. *Current Opinion in Plant Biology* 12: 172–177

Liao H, Yan X, Rubio G, Beebe SE, Blair MW, Lynch JP (2004) Genetic mapping of basal root gravitropism and phosphorus acquisition efficiency in common bean. *Functional Plant Biology* 31: 959–970

Miguel MA, Widrig A, Vieira RF, Brown KM, Lynch JP (2013) Basal root whorl number: A modulator of phosphorus acquisition in common bean (Phaseolus vulgaris). *Annals of Botany* 112: 973–982

Miller CR, Ochoa I, Nielsen KL, Beck D, Lynch JP (2003) Genetic variation for adventitious rooting in response to low phosphorus availability: Potential utility for phosphorus acquisition from stratified soils. *Functional Plant Biology* 30: 973–985

Postma JA, Dathe A, Lynch JP (2014) The optimal lateral root branching density for maize depends on nitrogen and phosphorus availability. *Plant Physiology* 166: 590-602

York LM, Lynch JP (2015) Intensive field phenotyping of maize (Zea mays L.) root crowns identifies phenes and phene integration associated with plant growth and nitrogen acquisition. *Journal of Experimental Botany* 66: 5493–5505

Zhu J, Kaeppler SM, Lynch JP (2005) Topsoil foraging and phosphorus acquisition efficiency in maize (Zea mays). *Functional Plant Biology* 32: 749

VITA

Harini Rangarajan

EDUCATION

May 2021	Ph.D.	Pennsylvania State University	Horticulture
2005-2009	Ph.D. Candidate (discontinued)	NIMHANS, Bangalore	Biophysics
2005	M.Phil	NIMHANS, Bangalore	Biophysics
2003	Advanced Diploma	Madurai Kamaraj University	Bioinformatics
2002	M.Sc.	Bangalore University	Biochemistry
2000	B.Sc.	Bangalore University	Biotechnology

PUBLICATIONS

- **Rangarajan H,** Lynch JP (2021) A Comparative Analysis of Quantitative Metrics of Root Architecture. Plant Phenomics. https://doi.org/10.34133/2021/6953197
- Burridge J**, Rangarajan H**, Lynch J. (2020). Comparative phenomics of annual grain legume root architecture. Crop Science**.**
- **Rangarajan H,** Postma JA, Lynch JP (2018) Co-optimization of axial root phenotypes for nitrogen and phosphorus acquisition in common bean. Ann Bot ;122(3):485-499

SCHOLARSHIPS AND AWARDS

- Walter Thomas memorial scholarship (Aug 2011 – May 2017)
- Council for Scientific and Industrial Research (CSIR), India, Senior Research Fellow (Feb 2009 – June 2009).
- Council for Scientific and Industrial Research, Junior Research Fellow (Jan 2007 – Jan 2009).
- Indian Council for Medical Research, Junior Research Fellow (2006).
- Lady TATA Memorial Trust Senior Research Fellow (2006).
- Graduate Aptitude Test for Engineers Qualified (2005).
- Award for scoring highest marks in M.Phil biophysics.
- M. Phil Biophysics, NIMHANS fellowship sponsored by NIMHANS (2003-2005).
- Advanced diploma in Bioinformatics scholarship sponsored by Department of Biotechnology, Government of India (2002 – 2003).

APPOINTMENTS

2019-2021	Research Support, Root biology lab, Pennsylvania State University
2011-2017	Graduate Assistant, Department of Plant Sciences, Pennsylvania State University
2005-2009	Research Fellow, Department of Biophysics, NIMHANS, Bangalore, India

TEACHING EXPERIENCE

Teaching Assistant and guest lecturer, Plant Nutrition, Hort 402W, Pennsylvania State University, 2012 to 2016